UNIVERSIDADE FEDERAL DE SANTA CATARINA
PROGRAMA DE PÓS-GRADUAÇÃO EM
ENGENHARIA MECÂNICA

LIMITES PARA A APLICAÇÃO DA TEORIA DE MATRIZES RANDÔMICAS NA ANÁLISE DE SISTEMAS DINÂMICOS

Tese submetida à

UNIVERSIDADE FEDERAL DE SANTA CATARINA

para a obtenção do grau de

DOUTOR EM ENGENHARIA MECÂNICA

JÚLIO APOLINÁRIO CORDIOLI

Florianópolis, março de 2006.

UNIVERSIDADE FEDERAL DE SANTA CATARINA
PROGRAMA DE PÓS-GRADUAÇÃO EM ENGENHARIA MECÂNICA

LIMITES PARA A APLICAÇÃO DA TEORIA DE MATRIZES RANDÔMICAS NA ANÁLISE DE SISTEMAS DINÂMICOS

JÚLIO APOLINÁRIO CORDIOLI

Esta tese foi julgada adequada para a obtenção do título de

DOUTOR EM ENGENHARIA
ESPECIALIDADE ENGENHARIA MECÂNICA

sendo aprovada em sua forma final.

_____
Samir N. Y. Gerges, Ph.D. - Orientador

_____
Robin S. Langley, Ph.D. – Co-orientador

_____
José Antônio Bellini da Cunha Neto, Dr. – Coordenador do Curso

BANCA EXAMINADORA

_____
Robin S. Langley, Ph.D. - Presidente

_____
Valder Steffen Junior, Ph.D.

_____
Jose Roberto de Franca Arruda, Dr.

_____
Marcelo Krajnc Alves, Ph.D.

_____
Arcanjo Lenzi, Ph.D.

_____
Roberto Jordan, Dr.Eng.

FEDERAL UNIVERSITY OF SANTA CATARINA
POSTGRADUATE PROGRAM IN
MECHANICAL ENGINEERING

LIMITS OF THE APPLICABILITY OF RANDOM MATRIX THEORY TO THE DYNAMICS OF STRUCTURES WITH UNCERTAINTIES

A thesis submitted to the

FEDERAL UNIVERSITY OF SANTA CATARINA

for the degree of

DOCTOR IN MECHANICAL ENGINEERING

JÚLIO APOLINÁRIO CORDIOLI

Florianópolis, March 2006.

Engineering is the art of moulding materials we do not wholly understand, into shapes we cannot precisely analyse, so as to withstand forces we cannot really assess, in such a way that the community at large has no reason to suspect the extent of our ignorance.

Anonymous

ACKNOWLEDGEMENTS

First of all, I would like to thank Professor Samir Gerges for introducing me to the acoustic and vibration field when I was only an undergraduate student and for all his support during the development of this Doctorate.

I am highly in-debited to Professor Robin Langley for accepting me for a six-month period at the University of Cambridge. Without his support, many of the developments of this thesis would not have been possible. I would like to thank him, not only for his patience and willingness to explain to me his points of view, but also for his friendship and the talks we had about all kinds of subjects.

I am grateful to the other professors of the LVA/UFSC: Professor Arcanjo Lenzi and Professor Roberto Jordan, for all the lessons and discussion on sound and vibration and for the insights into the direction of this thesis. I also would like to thank Mr. Adilto (Paru) for his support in all the issues concerning the experimental part of this work and for the coffee that was always available.

I would also like to acknowledge the financial support provided by CNPq and to thank the Federal University of Santa Catarina (UFSC) and the University of Cambridge for accepting me as a graduate student and a visiting fellow, respectively.

Thanks also to my friends at the LVA Mario (Sapo), Marcelo (Bilu), Fabiano (Bibi) and Thiago (Zmi) for the technical discussions and many projects we undertook together, but especially for their company and friendship during the years at the LVA, which I will always remember. Special thanks to Thiago for his reading of the manuscript. For providing an excellent working environment, I also thank all the other students and colleagues at LVA.

For receiving me so openly and making my stay in Cambridge an enjoyable experience, I would like to thank my friends at the DVRO Rolf, Andrew, Asan, Srikantha and my Brazilian friends in Cambridge Juliano and Ronaldo. Special thanks to Rolf and Srikantha for the technical discussions on and insights into the issues of this thesis.

I would like to thank my friends in Florianópolis Alexandre (Leco), Andre (Dedé), my cousins Thiago and Matheus (Feio), and, more recently, Humberto (Sacola) and others for not calling me during the last six months of the Doctorate whenever there were good waves, otherwise, working and concentrating on this thesis would have been much more difficult. Thanks also to my friends of the old LIRA swimming team. Although none of us swim together any more, I am thankful for the time we spent together rock climbing.

For their fortitude and support throughout my education, I would like to thank my parents Celito and Cristina, who also provided me with opportunities that they themselves did

not have. I am also thankful to my sisters Carolina, Ana Betriz and Maria Luiza, my niece Maria Carolina and all my relatives for all the encouragement and support they gave me not only in this Doctorate but also in all the projects I have undertaken.

I am particularly thankful to Regina for her friendship, support, and encouragement during this project and for opening her house to me at many lunch times.

Finally, I have no words to express my gratitude to a person that has been part of my life during the past 6 years and who I hope will be part of it until the end. Bel, thank you for your support, inspiration and all the moments we spent together.

TABLE OF CONTENTS

LIST OF FIGURES

LIST OF TABLES

LIST OF SYMBOLS

A	Area
A_t^n	Transfer inertance between the excitation point and the *n*th point
A	Random matrix
$\mathbf{A_0}$	Deterministic part of **A**
$\mathbf{A_{ran}}$	Random part of **A**
$b(\theta)$	Fourier transform of Y_2
c_f	Sound speed in the fluid
c_L'	Longitudinal wave speed
C	Matrix of coupling and damping loss factors
$\mathbf{D_i}$, **D**	Matrix with the realization of the *i*th eigenvector
E	Energy
E_{ym}	Young's modulus
$\hat{\mathbf{E}}$	Vector of modal energy
f	Force vector
F	Force amplitude
$F(\theta)$	Fourier transform of the function $g(\Omega)$
$g(\Omega)$	Function defined by Equation (4.4)
g_1	First cumulant of the random process
g_2	Second cumulant of the random process
g	Excitation vector
$G_2(\theta)$	Fourier transform of the second cumulant
h	Plate thickness
H	Perturbation analysis parameter
I	Identity matrix
J	Trace of the matrix **S**
K	Mode shape statistics factor
K	Stiffness matrix
m, $m(\omega)$	Modal overlap factor
M	Total mass
M	Mass matrix
$p(\lambda_1,\ldots,\lambda_N)$	jpdf of the eigenvalues

P	Parameter for the eigenvalue mixing
$\mathbf{q}$	Response vector in modal coordinates
$\mathbf{q_R}$	Response vector in random modal coordinates
Q	Parameter for the eigenvector mixing
r_T^2	Relative energy density variance
R	Random level constant
R_k	*k*th correlation function
R_2	Two-level correlation function
s_i	Statistical overlap factor of the *i*th eigenvalue
$S_T(\theta)$	Spectral density of the energy density
$S_\xi(\theta)$	Spectral density of the random function $\xi(\omega)$
$\mathbf{S}$	Matrix from the SVD with singular values
T	Kinetic energy density
$\boldsymbol{u_i}$	*i*th eigenvector
$\mathbf{U}$	Matrix with eigenvectors
v, $v(\omega)$	Modal density
$\overline{v^2}$	Time-mean square velocity
V	Kinetic energy
V_a	Volume of an acoustic subsystem
$\mathbf{V}$	Matrix from the SVD
x, y, z	Cartesian coordinates
$\mathbf{x}$	Response vector in generalized coordinates
X	Transfer function
$Y(\omega)$	Mobility
Y_2	Two-level cluster function
$\mathbf{W}$	Matrix from the SVD with basis functions
Z	Parameter defined in Equation (6.8)
α	Spatial factor
$\delta(x)$	Dirac delta function
Δ	Frequency band
Δ_3	Delta 3 function
$\Delta\lambda$	Interval in the eigenvalue domain
ϕ_n	Mode shape function of the *n*th mode

η	Loss factor, damping loss factor
κ	Bending radius of gyration
λ_B	Bending wave length
λ_I	*i*th eigenvalue
$\mathbf{\Lambda}$	Matrix of eigenvalues
μ_i	Mean spacing between the *i*th and *i+1*th natural frequency
μ_T	Mean energy density
$\boldsymbol{\mu}$	Random variable mean
Π_j	Power dissipated by the *j*th subsystem
Π_{ij}	Power transmitted by the *i*th subsystem to the *j*th subsystem
$\Pi_{in,j}$	Power input to the *j*th subsystem
$\mathbf{\Pi_{in}}$	Vector of input subsystems
ρ	Density
$\rho'(x)$	Mass distribution function
ρ_f	Fluid density
σ_T^2	Energy density variance
σ_{ω_i}	Standard deviation of the *i*th natural frequency
$\boldsymbol{\sigma}$	Random variable standard deviation
υ	Poisson's coefficient
Σ^2	Number variance
ω	Frequency
ω_n	Natural frequency of the *n*th mode
$\xi(\omega)$	Random function given by Equation (4.14)

Notation and Abbreviations

$Tr(\ )$	Trace of matrix
$\mathrm{E}[\ ]$	Ensemble average
$\langle\ \rangle$	Space average
$\mathrm{Re}(\ )$	Real part
BE	Boundary Element
CPP	Coupling power proportionality
FE	Finite Element

FRF	Frequency Response Function
jpdf	Joint probability density function
LANL	Los Alamos National Laboratories
pdf	Probability density function
GOE	Gaussian Orthogonal Ensemble
GSE	Gaussian Symplectic Ensemble
GUE	Gaussian Unitary Ensemble
RMT	Random Matrix Theory
SEA	Statistical Energy Analysis
SVD	Singular Value Decomposition
TBL	Turbulent Boundary Layer

ABSTRACT

Engineering structures are always subject to uncertainties arising from the manufacturing process. In a welding process or in the cutting of a plate, differences between the produced item and its design will always be present. If the performance of the structure may be affected by these uncertainties, they must be taken into account in the design. However, this may be a complex task if the performance is determined by the vibro-acoustic characteristics of the structure. One approach would be the adoption of a numerical deterministic method like the Finite Element Method, together with a statistical description of the structure parameters. Through a Monte Carlo analysis, an ensemble of structures is created and the response calculated for each member of the ensemble. However, increasing the frequency range requires larger models and more information on the statistics of the input parameters, and the analysis becomes unfeasible. The Statistical Energy Analysis (SEA) is a vibro-acoustic method where the concept of uncertainty is built-in the method and, together with a recently presented variance theory, may be used to predict the response statistics. The variance formulation was derived based on the assumption that the eigenvalue statistics may be predicted by means of the Random Matrix Theory for a special ensemble of matrices known as the Gaussian Orthogonal Ensemble (GOE). In this thesis, a literature review of the method used to estimate the response statistics of structures with uncertainty properties is presented. The variance theory is reviewed and the results compared with numerical and experimental data. The conditions for the assumption of the GOE model to be valid are discussed and verified through numerical analysis. A new approach is presented for the study of the response statistics of random dynamic systems and a new parameter is proposed with the aim of verifying the agreement between the eigenvalue statistics and the GOE model. Finally, a perturbation analysis is used to derive a new parameter and allow its calculation based on the statistics of the input parameters. The applicability of the new parameter is verified using numerical models and promising results are observed.

RESUMO

Estruturas aeroespaciais, automotivas, navais ou de outras áreas estão sempre sujeitas às imperfeições e incertezas advindas dos diferentes processos de fabricação. Seja na confecção de uma solda ou no corte de uma placa, diferenças entre a estrutura produzida e aquela projetada sempre existirão. Estas incertezas tornam-se importantes quando existe a possibilidade de comprometimento do desempenho da estrutura. Neste caso, o projeto da estrutura deve levar em consideração as incertezas quanto ao processo de fabricação. Isto se torna difícil quando a performance da estrutura é determinada por seu comportamento vibro-acústico. Uma possibilidade seria modelar a estrutura utilizando métodos numéricos como o Método de Elementos Finitos ou o Método de Elementos de Contorno, juntamente com uma descrição probabilística das propriedades da estrutura. Através do Método de Monte Carlo, um conjunto de estruturas é gerado, a resposta dinâmica de cada membro do conjunto é calculada e dados estatísticos são obtidos. Entretanto, o aumento da faixa de freqüência de interesse requer uma maior discretização do modelo, o que inviabiliza computacionalmente tal abordagem. A Análise Estatística Energética (SEA – *Statistical Energy Analysis*) é um método vibro-acústico que considera as incertezas das propriedades da estrutura, mas até recentemente era capaz de predizer apenas o comportamento médio. Recentemente, uma nova formulação foi apresentada que permite predizer o comportamento estatístico da resposta vibratória de estruturas aleatórias e estimar a variância dos resultados de SEA. Esta formulação foi derivada com base na Teoria de Processo Estocástico e na hipótese de as freqüências naturais da estrutura seguirem o comportamento estatístico previsto na Teoria de Matrizes Randômicas para uma matriz do tipo GOE (*Gaussian Orthogonal Ensemble*). Nesta tese de doutorado, uma revisão dos métodos existentes para a determinação das características estatísticas da resposta de estruturas aleatórias é apresentada. A formulação recentemente proposta para o cálculo da variância é revisada e os resultados comparados com dados numéricos e experimentais. As condições para que o modelo estatístico GOE seja válido são discutidas e uma nova abordagem é apresentada para o estudo das características estatísticas de sistemas dinâmicos. Um parâmetro é proposto com o objetivo de verificar a aplicabilidade do modelo GOE. Finalmente, uma análise perturbacional é realizada, permitindo a determinação do novo parâmetro com base nas características estatísticas dos parâmetros da estrutura. Resultados promissores para a aplicação do novo parâmetro são verificados através de análises numéricas.

CHAPTER 1

INTRODUCTION

1.1 UNCERTAINTIES IN NOISE AND VIBRATION

The manufacturing process of any structure or article is always subject to uncertainties from the material properties, fabrication techniques and assembly process. No matter how strict the tolerance limits are, there will be always differences between the nominal parameters of the article (the dimensions, material properties, etc, defined in the project) and the parameters of the produced item. The level of uncertainty varies from one designed structure to another and is dependent on many variables from the manufacturing process. Whenever the performance of the structure is sensitive to these uncertainties, the design process should account for them in order to produce a safe and successful project. This may be the case when the performance is defined by the vibro-acoustic characteristics of a structure.

The last decade has seen a growing concern for the effects of uncertainty in the dynamic response of engineering structures. In the past, use was made of safety factors. However, the demand for an optimal design which should ensure a great efficiency with reduced cost and minimized risk has required improved computational methods. Two recent examples give an idea of the importance that has been given to the problem of uncertainties in structural dynamics. In 2000, the Los Alamos National Laboratories (LANL) in the US ran an unprecedented calculation on one of the most powerful computers at that time—the platform *Blue Mountain*. The aim was to quantify the propagation of uncertainty through a nonlinear finite element (FE) model of a weapon component under blast loading. The specific objective of the exercise was to determine the model sensitivity to certain input parameters. The calculation made use of 3968 processors from the available 6000 and used concurrently nearly 4000 ABAQUS/Explicit licences. The analysis took over 72 h and would have required 17.8 years of equivalent single-processor time [1].

More recently, Mace *et al.* [2] wrote a preface for the Journal of Sound and Vibration regarding uncertainty in structural dynamics. The authors discuss some current research work in the area by means of 14 recently published papers. The significant activity in the area is highlighted, together with the substantial challenges that still remain.

Experimental results regarding the effect of uncertainties in noise and vibration

response are usually not available. This is due to the large costs related to constructing an ensemble of structures and then evaluating the vibro-acoustic characteristics for each member of the ensemble. However, some examples can be found in the literature for automotive structures. In [3], Kompela and Bernhard measured the FRFs (Frequency Response Functions) for both structure-borne and airborne paths on two large ensembles of nominally identical vehicles. Care was taken to ensure that the observed variability would occur primarily due to the manufacturing and assembly processes. In Figure 1.1, it is possible to observe the structure-borne FRFs measured by Kompela and Bernhard for 99 identical cars. A variation of above 10 dB can be noted at some frequencies. A similar behaviour was also obtained for the airborne FRFs.

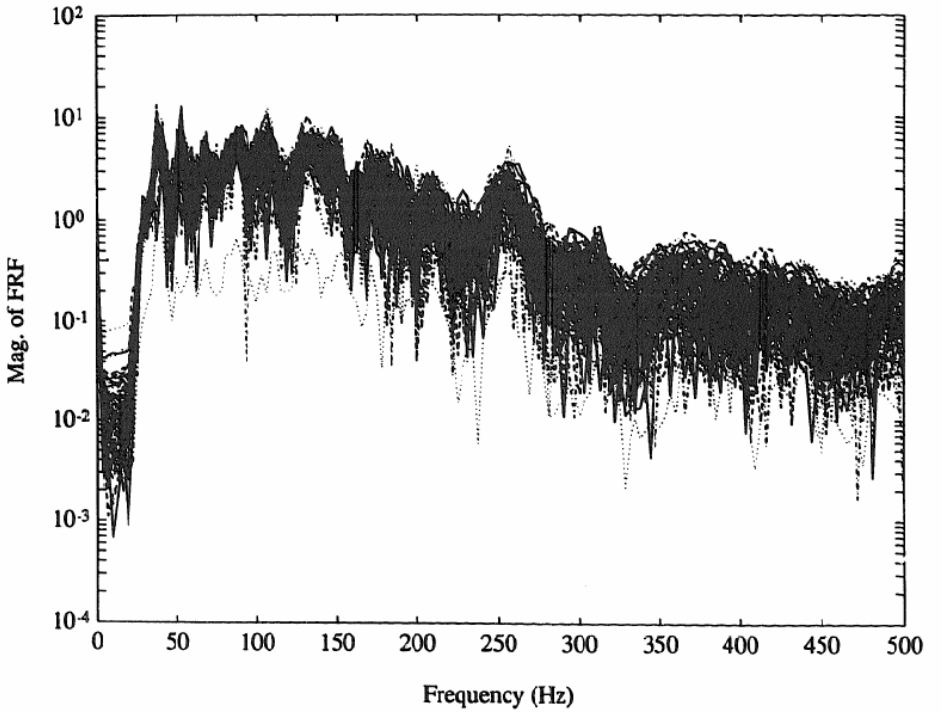

Figure 1.1 – Measured structure-borne FRFs for 99 nominally identical cars [3].

A similar study was developed by Cornish in [4]. Figure 1.2 shows six FRFs measured for nominally identical cars. Again, a large difference can be observed between the FRFs.

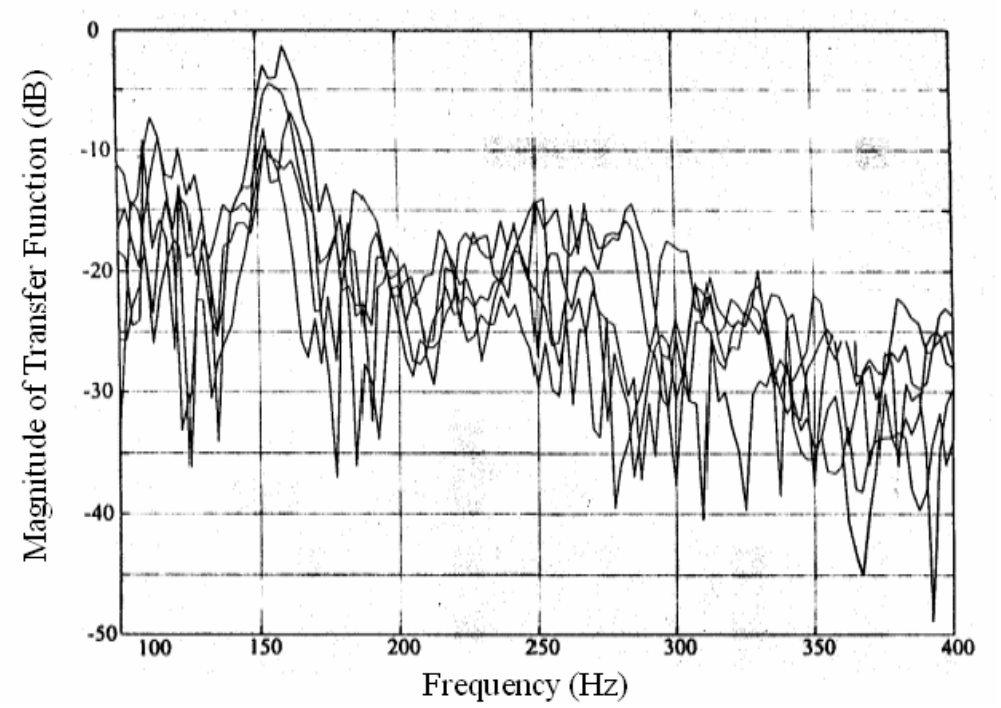

Figure 1.2 – Measured force-pressure FRFs for six nominally identical vehicles [4].

The two examples consider a low to mid frequency range and it would be expected that the FRFs would differ even more for higher frequencies, since the response becomes more sensitive to the uncertainties with the reduction in the wavelength. If an engineer is developing a new sound package for the car considered in Figure 1.1 or the one in Figure 1.2, it becomes difficult to decide which curve of the response should be used. Should it be a curve for one of the realizations? Or should it be the mean curve? The engineer may also have access to the curve from a deterministic model which adopted the nominal properties of the car. However, if it is necessary to control the risk of failure of the sound package (in this case, the risk of achieving noise levels above the maximum acceptable), the ideal data to work with would be the statistics of the response, allowing the calculation of confidence limits. Unfortunately, accessing the statistics of the response of a random dynamic system may be a complex task, depending on the frequency range of interest and the level of uncertainty. By a random dynamic system one should understand an ensemble of structures produced based on the same nominal specification (like the cars or airplanes from a production line). The definition may be also extended to the structures that “may be” produced from its specifications (like satellites, off-shore platforms, etc). In what follows, a review is given of the effects of uncertainties over the vibro-acoustic behaviour of structures.

1.2 THE PHYSICS OF UNCERTAINTY IN STRUCTURAL DYNAMICS

It is common to represent the response of a dynamic system as a summation of modes [5,6]. A mode can be defined as a standing wave created by interference between the waves travelling in different directions in the structure. Each mode is characterized by a peak in the response in the frequency domain called “natural frequency” and by a particular spatial distribution termed “mode shape”. Each mode is also associated with a certain level of damping which represents its energy dissipation. The modes are characteristics of each system and its boundary conditions, and are allocated in “order” which denotes the place of each mode in the modal sequence. Mathematically, the modes are considered as independent basis functions, which allow the expression of the response as a linear superposition of each mode’s response.

The first modes of the modal sequence, also called low order modes, are usually less sensitive to small variations in the system parameters [7]. A minor deviation of the real system from its mathematical model generally produces no serious discrepancy between the predicted and observed response. However, the strength of reflections and scattering (redistribution of incident wave energy in many directions) of vibrational waves by structural non-uniformities, inhomogeneities, or discontinuity of material or geometrical properties, usually increase as wavelength is reduced (or as the frequency increases). Hence, higher order modes are generally more sensitive to uncertainties in geometric and material properties of a structure.

Another common feature of the response of many structures is the presence of two regions in the frequency spectrum: one characterized by the dominance of individual modes and another by multimodal response [7]. This is due to the fact that structures composed of plates or cavities usually display an increasing half power bandwidth (the product of the natural frequency and the loss factor and can be viewed as the peak width in the frequency response), together with a constant or increasing modal density (number of modes per frequency unit, usually in [modes/rad/s]), with increasing frequency. Therefore, at higher frequency, the response usually comprises substantial contributions from several modes. A slight modification in one of the modes contributing to the response may result in a significant change in the response of the system. This characteristic emphasises the larger response sensitivity of the system at high frequencies. This behaviour can be observed in Figure 1.1. For the first resonance frequency the dispersion of the results is not as significant as the dispersion for the modes of higher order. The modal overlap factor is a parameter commonly used to quantify the number of modes contributing to the response at a given frequency and it

is given by

$$m(\omega) = \omega \eta v(\omega), \tag{1.1}$$

where ω is the frequency in rad/s, η is the loss factor and $v(\omega)$ is the modal density in modes/rad/s. It will be seen that the modal overlap factor is directly related with the response variance predictions.

It is common to find in the literature the term “high frequencies”. However, this term has a relative connotation and it is necessary to define it in relation to what is the frequency high. In this study, the term should be interpreted as the frequency range where the response involves high order modes. Therefore, the definition of low and mid frequency is also structure dependent. What may be low frequency for a specific structure may be high frequency for another.

Whenever a system displays uncertainties, its response should be thought of as being random and associated with an ensemble of structures. In the automotive example, as seen in Figure 1.1 and Figure 1.2, the ensemble can be interpreted as the collection of vehicles leaving the production line [8]. The aim of a dynamic analysis of an uncertain structure should then be to obtain the statistics of the response for a given ensemble, with the ensemble being defined based on the statistics of the structure input parameters. One possibility would be to adopt a deterministic method and calculate the response for a representative sample of the ensemble. Post-processing would allow access to the statistics of the response. It will be seen in what follows that this approach is applicable in many cases but becomes extremely computationally expensive as the frequency increases (and consequently the level of uncertainty increases). Another point is related with the increasing sensitivity of the modes to the uncertainties. As higher order modes are considered in the analysis, it becomes necessary to include more and more details about the system uncertainties. At higher frequencies, a large amount of data related to the statistics of the input parameters is required. For example, in the analysis of a plate, the plate thickness may be assumed to be a random variable for the first modes, however, as higher modes are considered in the response, it becomes necessary to include the distribution of plate thickness over the plate area and assume the thickness to be a spatially random process with increasing discretization as the frequency increases. This kind of information may be expensive to obtain and is not usually available [9]. At this point, one may be thinking that the determination of the response statistics would be feasible for the first modes, but would be very difficult with increasing mode order and almost impossible for the high frequency range. However, an interesting phenomenon occurs with increasing frequency

(and increasing uncertainty): the response statistics become independent of the details of the uncertainty, providing the ensemble is random enough. This behaviour can be observed in an example given by Langley in [8] and described below.

In [8], simulations were performed for three different ensembles of the same plate, but each ensemble considering a different randomization approach (different sources of uncertainty): random edge springs, 10 random located masses (corresponding to 20% of the bare plate mass) and 5 random located masses (corresponding to 5% of the bare plate mass). The randomization approaches, the individual responses and the ensemble mean are shown in Figure 1.3. An ensemble of 200 members was considered for each case.

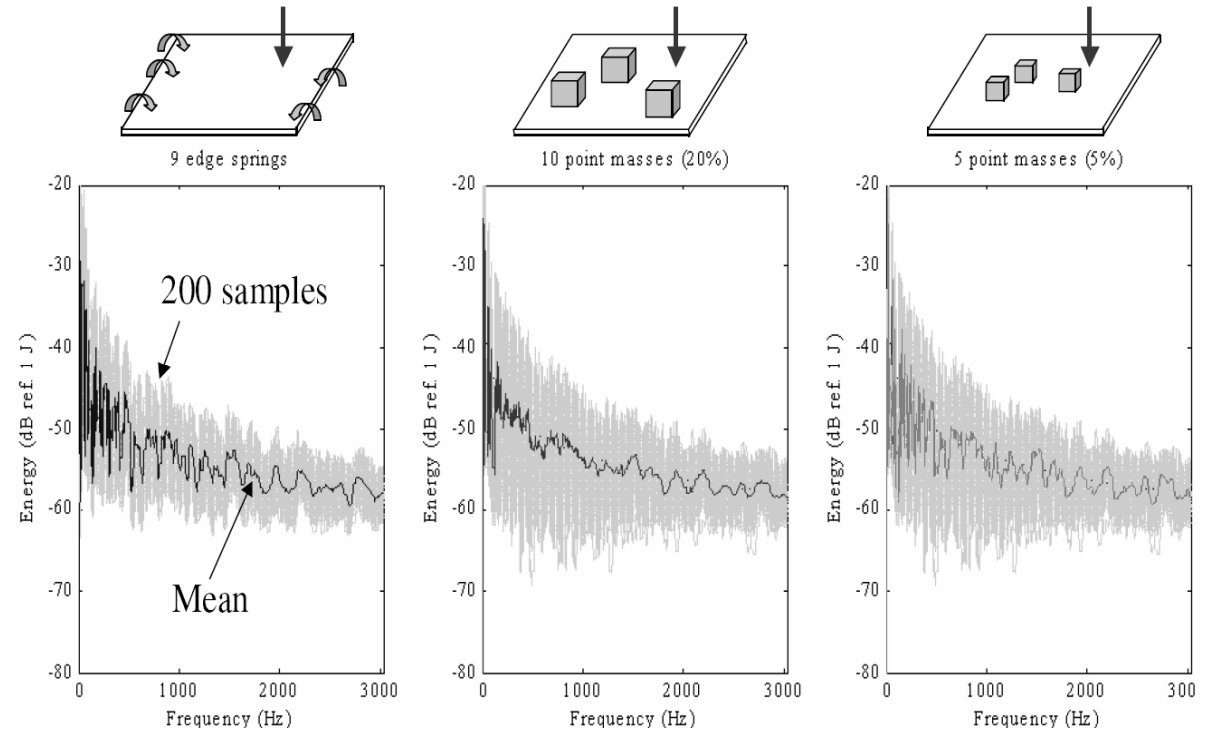

Figure 1.3 – Energy response of random plates (200 member ensemble) – different randomization approaches [8].

It can be observed that the mean response, although displaying distinct behaviours in low frequency, tends towards the same value at high frequency. This behaviour is not found exclusively for the mean but can also be seen for the variance, as shown in Figure 1.4. At low frequency, where the uncertainty is low, the variance is dependent on the randomization approach adopted, but as the level of uncertainty increases, the results tend towards the same value. In other words, the statistics of the response become independent of the source of uncertainty. It will be seen that it is possible to predict the statistics when the system is sufficiently random by considering the Random Matrix Theory (RMT) [8,10].

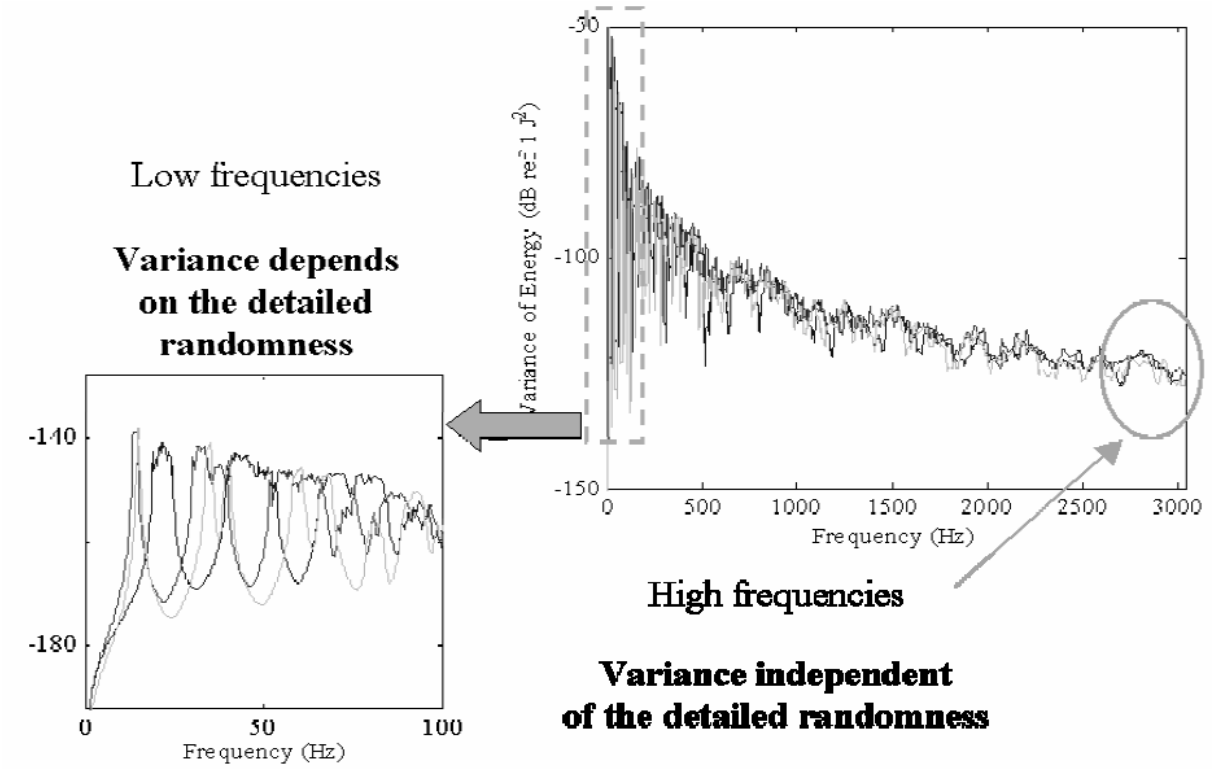

Figure 1.4 – Energy variance for the different randomization approaches (Figure 1.3) [8].

In what follows, a brief review of the methods used to access the response of random dynamic systems is given. The review covers approaches based on deterministic methods, with the statistics of the input parameters being treated in different ways, and the popular Statistical Energy Analysis (SEA). Special attention is given to the basic assumptions of SEA and the determination of SEA input parameters since many statistical concepts regarding structural dynamics are involved. The literature review proceeds with the studies related to the variance problem in SEA. The studies are divided in two groups: the numerical studies and the studies based on the point process approach. Finally, a discussion about the prediction of the response of structures with uncertain properties is given and the aims and scope of this thesis are presented.

1.3 METHODS FOR VIBRATION AND NOISE PREDICTION WITH UNCERTANTIES

The challenge of modelling the dynamic response of a structure with uncertainties in its parameters has been the subject of study of many authors for at least 30 years. During this time, several methods have been proposed with different backgrounds and their popularity has displayed considerable oscillation. The terminology used in the literature has also varied with time and authors and can lead to some confusion.

As in deterministic analysis, the methods for the prediction of the response of

random structures may also be grouped into low and high frequency methods. Typically, at low frequencies, an ensemble of structures is generated using a statistical description of the structure parameters and a deterministic method (FE method, BE method, Rayleigh-Ritz method, etc) is used to calculate the dynamic response of each member of the ensemble and then determine the response statistics. In some low frequency problems, expressions for the statistical moments of the response may be obtained analytically, either by integration or by considering the inverse function of a random variable, but these approaches are usually restricted to very simple problems [9]. On the other hand, high frequency methods are usually based on an energy flow approach and statistical concepts may be built into the method. The main method of this category is the Statistical Energy Analysis (SEA). In what follows, a brief description of the methods commonly used to analyse the dynamics of random structures is presented.

A first review of low frequency methods pertaining to structural dynamics with uncertainty parameters is given by Ibrahim in [11]. The problem of random eigenvalues is discussed for lumped parameter and continuous systems. The methods used to address the problem are summarized, including the perturbation methods. In the perturbation methods the input parameters are varied in order to access the rates of changes in the response. The response can then be approximately calculated through a Taylor expansion and the response statistics obtained for a given set of input parameter statistics. The application of the perturbation method to verify the effects of random parameters on the eigenvalues is reviewed by Manohar and Ibrahim in [12]. A more recent study on the rates of change in the eigenvalues and eigenvectors in the case of dynamic systems with nonproportional viscous damping was presented by Adhikari in [13]. Ibrahim also observe in [11] the progress made towards the use of the stochastic FE method and Monte Carlo simulations [14] for the calculation of the response statistics.

Before proceeding with the discussion on the stochastic FE method, it would be interesting to give a brief review on the FE method itself. The FE method is by far the most common analysis technique adopted for the prediction of the vibration and acoustic response of a complex structure [6]. In the FE method, the structure under analysis is split into relatively small regions called elements. An approximate response is obtained through the linear combination of trial functions defined over the element. The trial functions, also known as shape or interpolation functions, are interpolated over reference points defined on the elements. These points are termed nodes and may posses a prescribed number of degrees of freedom. The FE method may be seen as a variant of the Rayleigh-Ritz method with the basic difference between the two lying in the nature of the trial functions. Whereas in the classical

Rayleigh-Ritz method the trial functions are defined globally, in the FE method they are limited to each element [5]. Once the mesh of elements and their nodes are defined it is possible to obtained the mass and stiffness matrices by enforcing continuity of the response field. The FE method popularity is due mainly to its capacity for modelling structures with complex shapes in a relatively straightforward manner. More information on the FE method for structural dynamics can be found in [15].

The stochastic FE method is a numerical method for analysis of stochastic structures and has been the subject of many publications, including some books [16,17]. In its current version, the method represents the combination of a determinist FE method and a statistical analysis [18]. It establishes a system of recursive equations to obtain approximate first or higher order moments of the response, by expanding the random stiffness matrix with respect to the random variables involved through different techniques, such as series expansion or perturbation methods. The main sources of error for the technique are in the discretization associated with the FE method and the truncation of the expansion of the random stiffness matrix. Ren and Elishakoff proposed in [18] new approaches for the expansion of the stiffness matrix in order to reduce or eliminate the truncation error. A detailed review of the application of the FE method in probabilistic structural dynamics is also presented by Benaroya and Rehak in [19].

In a probabilistic analysis, the first step is related to the identification of the random variables and/or process associated with the structure. To perform the analysis it is thus necessary to define the statistics of these variables in the form of the joint probability density functions (jpdf). However, information concerning the statistics of the input parameters is not generally available. In fact, obtaining the jpdf of the random variables involved is almost impossible. Therefore, it is common in a probabilistic analysis that the statistical data of the random variables be assumed based on the designer experience instead of obtained experimentally. Elishakoff gives in [9] a detailed discussion on this issue. It is demonstrated that small errors in the input statistical data for a probabilistic analysis can lead to significant discrepancy in the predicted response statistics. Elishakoff then review some methods that he calls non-probabilistic methods, which are not based on a precise description of the probabilistic nature of the random variables but rather on possible scenarios for the random variables. The author names these methods as non-probabilistic methods but they are also known as possibilistic methods. The possible scenarios include the definition of intervals or envelope boundaries for the random variables without considering a specific probabilistic behaviour within the specified limits. Examples of possibilistic methods are interval analysis and convex modelling.

A more recent discussion on non-probabilistic methods is presented by Moens *et al.* in [20]. An attempt is made to give more uniformity to the terms used in non-deterministic methods. The authors review the basic concepts associated with probabilistic analysis and possibilistic methods like the interval analysis and fuzzy variables. The discussion is then extended to the application of possibilistic methods in a numerical context, including the interval FE method, the fuzzy FE method and their variations. The application of possibilistic methods in an absolute reliability analysis was also reviewed and it was concluded that it is rather limited. It is suggested that absolute reliability analysis should always be carried out based on objectively available data in order to prevent a misjudgement on the actual reliability of the design.

All the methods described above are primarily based on a deterministic method (in most cases on the FE method). However, although in a statistical context, the methods still suffer from the same problem displayed by the deterministic methods, mainly the increasing computational power required and an increasing sensitivity to uncertainties as the frequency increases [21]. Therefore, these methods are restricted to low frequency problems. One alternative to solve problems in the high frequency range relies on the statistical method known as Statistical Energy Analysis (SEA) together with a theory that allows the calculation of the variance of its results. This method is summarized in what follows.

1.4 STATISTICAL ENERGY ANALYSIS

1.4.1 Overview of SEA

SEA is the main alternative for the prediction of the response of dynamic systems at high frequency. An SEA model represents an ensemble of similar structures and its results give the response average within the ensemble. The concept of uncertainty is built into the method. An SEA model is usually many times smaller than a conventional equivalent model (an FE model for example) and can be solved in a much reduced time. The time required to construct an SEA model is also considerably shorter than a conventional approach and requires only rough information concerning the structure. As a consequence of these characteristics, SEA is probably the principal vibro-acoustic technique applied in the aerospace, automotive and naval industries and has been the subject of a great number of publications over the recent decades. General introductions to SEA can be obtained in [7,25-28] among others. SEA has also been implemented in some commercial computer packages and a list of the software codes can be found in [28]. It is not the aim of this thesis to

give a detailed review of SEA as this information can be found in the mentioned literature. In what follows a brief review of the method is presented. The basic concepts and assumptions regarding SEA are discussed and the main equations are given. The principal methods used to determine the SEA parameters are also presented and discussed.

1.4.2 SEA basic concepts

The first studies related to SEA date from the early 60's and were published by Lyon and Maidanik [29] and Smith [30], among others, and were initially related to the energy exchange between coupled oscillators. Since then, the basic assumptions and concepts of SEA have been extensively discussed in the literature, sometimes with disagreements between authors.

A complex structure is modelled in SEA as a network of subsystems. Each subsystem represents a set of similar modes and different wave types (flexural, longitudinal, etc) are considered in the model as different subsystems. The boundaries between subsystems should be characterized by significant changes in the dynamic properties (changes in wave impedance) in order to provide a weak coupling between subsystems [28]. A reverberant field is assumed in each subsystem, so elements with high damping should not be represented as subsystems but rather included in the damping of the other subsystems.

All the input parameters and the results in SEA are treated in frequency bands. It is assumed that the frequency bands are broad enough to encompass a minimum number of modes. Of course, enlarging the frequency bands to fulfil this requirement would result in less resolution of the response in the frequency domain.

The vibrational or acoustic state of a subsystem is given by its total energy E, which represents the sum of the time-averaged kinetic energy and potential energy of each mode at a given frequency. SEA assumes that the modes within a frequency bands possess the same energy. The main aim in SEA is the calculation of the subsystem energies. A subsystem j is characterized by the following parameters:

- Modal density ν_j – the number of modes per frequency unit (usually rad/s). The modal density is related to the capacity of the subsystem to store energy.
- Damping loss factor η_j – is the arithmetic mean of the loss factor of the modes within a frequency band. It represents the subsystem capacity to dissipate energy. Through the damping loss factor it is possible to calculate the dissipated power in the subsystem by

$$\Pi_j = \omega \eta_j E_j , \tag{1.2}$$

where E_j is the subsystem energy.

- Coupling loss factor η_{jk} – is the coupling loss factor between subsystem *j* and subsystem *k*. It relates the power flow between subsystems to the difference between their modal energies (energy divided by the modal density) by

$$\Pi_{jk} = \omega n_j \eta_{jk} \left(\frac{E_j}{n_j} - \frac{E_k}{n_k} \right). \tag{1.3}$$

The assumption made in Equation (1.3) that the coupling power between subsystems is proportional to the difference between their modal energies is known in the literature as the coupling power proportionality (CPP) [31]. The coupling loss factor for *j* to *k* is not equal to the coupling loss factor for *k* to *j*. However, they are related by the concept of reciprocity, which is given by

$$n_j \eta_{jk} = n_k \eta_{kj} . \tag{1.4}$$

- Power input Π_{in} – the external excitations are represented as power inputs to some subsystems. It is assumed that the power inputs in different subsystems are statistically independent.

The energy that enters a subsystem by means of an external excitation (power input) or is transmitted from another subsystem is assumed to be either dissipated within the subsystem or transmitted to other subsystems. By performing a power balance in a model composed of *N* subsystems it is possible to obtain a set of equations relating the subsystem energies given by

$$\Pi_{in,j} = \omega n_j E_j + \sum_{j \neq k} \omega n_j \eta_{jk} \left(\frac{E_j}{n_j} - \frac{E_k}{n_k} \right) \qquad j = 1, \ldots, N . \tag{1.5}$$

This system of equations can be also written in a matrix form

$$\mathbf{\Pi_{in}} = \mathbf{C}\hat{\mathbf{E}}, \tag{1.6}$$

where $\mathbf{\Pi_{in}}$ is a vector with the power inputs, $\hat{\mathbf{E}}$ is a vector with modal energies and the elements of matrix **C** are given by

$$\begin{aligned} C_{jk} &= \omega v_j \left(\eta_j + \sum_{j \neq k} \eta_{jk} \right) \qquad j = k \\ C_{jk} &= -\omega v_j \eta_{jk} \qquad\qquad\quad j \neq k \end{aligned}. \tag{1.7}$$

The energy of the subsystems is then obtained by solving the system of equations given by Equation (1.5) or Equation (1.6). The SEA results should be interpreted as average values in time, space (along the subsystem), frequency and an ensemble of similar structures, unless differently defined. From the vibrational or acoustic energy it is also possible to obtain other response variables. In the case of a structural subsystem, the mean-squared velocity and the energy are usually related by

$$E = M\left\langle \overline{v^2} \right\rangle, \tag{1.8}$$

where M is the total mass of the subsystem and a uniform distribution of the mass is assumed. For an acoustic subsystem with volume V_a, the relation between the mean-squared sound pressure and the subsystem energy is given by

$$E = \frac{V_a \left\langle \overline{p^2} \right\rangle}{\rho_f c_f}, \tag{1.9}$$

where ρ_f is the fluid density and c_f is the sound velocity in the fluid.

The CPP is one of the main assumptions in SEA and was first verified by Lyon and Mandanik [29] in the case of two weakly coupled linear oscillators excited by white noise. Since then, CPP has been found to hold for multiple oscillators and continuous systems under different conditions [27,32,33]. In these studies, in order for the CPP assumption to hold, a weak coupling between the subsystems is usually assumed. However, the quantification of

weak coupling has been shown to be a complex task. In [34], Langley derives the equations for the power flow between generic subsystems under random uncorrelated excitations. It is also demonstrated that the classical SEA equations can be recovered by assuming weak coupling. Langley defines in [35] weak coupling as the condition where the Green functions of each subsystem are not considerably affected by the presence of the other subsystems.

In [31], Mace defines the coupling as being weak if the power flow between subsystems is small compared with the dissipated power in each subsystem. For two subsystems, Mace demonstrates that the coupling loss factor can be negative or infinite. It is also shown that, in the case of more than two subsystems, the coupling power may not be uniquely defined due to the phenomenon named by Mace as power circulation. Mace and Rosemberg [36] extended the work by considering the case of two plates coupled by one side. It was observed that the power flow can be considerably affected by varying the shapes of the plates and the loss factor. A parameter is proposed for quantifying the strength of the coupling.

1.4.3 Input parameters

After the division of the structure into subsystems following the recommendations described above, the next step in the development of an SEA model is the definition of the input parameters: modal density, damping loss factor, coupling loss factor and power inputs. In fact, most of the SEA literature is related to methods for the determination of the input parameters, covering analytical, experimental and numerical approaches.

The modal density is mainly determined by means of three analytical methods. In [25], the modal density is calculated by means of a wavenumber diagram (Courant Method). In the wavenumber diagram the natural frequencies are considered as equally spaced and are represented as dots in the wavenumber domain. By integrating in the frequency band, it is possible to obtain the modal density. The method is limited to symmetric systems and it is extended in [37] for the calculation of the modal density of anisotropic structures. A more general approach is also presented in [25], where it is shown that the modal density is proportional to the space average of the real part of the point mobility. Cremmer *et al.* give in [38] asymptotic expressions for the point mobility of different types of systems. A more precise expression for the modal density of plates is shown in [39]. The derivation is made based on a Weyl expansion.

The analytical prediction of the coupling loss factor can be found by either a wave or modal approach [25,35]. In the modal approach it is considered that the responses of the modes within the same system are statistically independent and that the energy equipartition

between modes in a frequency band holds. On the other hand, the wave method is based on the determination of the wave transmission coefficient through the boundary between the subsystems. It is usually assumed that the transmission coefficient is small, that the effects of correlation between incident and reflected waves can be neglected and that an incident diffuse field exists. Expressions for the coupling loss factor for generic junctions between plates and beams with different angles are given by Langley and Heron in [40]. The expressions are extended by Langley in [41] to curved panels. More recently, Heron in [42,43] derived equations for the coupling loss factor for junctions between beams and plates based on the concept of linewave impedance.

Analytical predictions are also available for different types of power inputs. Equations for point excitations and distributed excitations are given in [25]. The power input due to more complex sources like an incident acoustic wave or the Turbulent Boundary Layer (TBL) can also be found in the literature [44,45].

Experimental methods are also commonly used for the determination of the input parameters. Review papers on experimental methods used in SEA can be found in [46-48]. One of the most popular methods is the Power Injection Method, first introduced by Bies and Hamid in [49] and used to measure the damping loss factor and coupling loss factor. The method can be quite time consuming as it includes the excitation of each subsystem while measuring the response in all the subsystems. An approach for obtaining the variance of the damping loss factor and coupling loss factor obtained through the Power Injection Method is given by De Langue in [50]. Other methods for the determination of SEA inputs are the Point Mobility method for the modal density [51-54] and the Decay method used to obtain the damping loss factor[55,56].

With the growing capacity of computers, some studies have verified the applicability of numerical methods for the determination of SEA inputs, in particular the FE method. In most cases, the studies were interested in the calculation of the coupling loss factor or the modal density. The determination of the damping loss factor by means of numerical or analytical methods is usually not applicable due to the complexity involved in the dissipation mechanisms. Two distinct approaches can be observed in these studies. In the first, each subsystem is entirely modelled with the FE method (sometimes using substructure approaches) and a procedure similar to the experimental Power Injection Method is used [57-59]. In the second case, only the boundary between subsystems is modelled and a wave approach is used to calculate the coupling loss factor [48].

The analytical methods used to calculate the SEA inputs usually adopt a statistical definition for the structure and the results are normally associated with an average for an

ensemble of structures. However, this is usually not the case for the experimental and numerical approaches, where evaluating more than one structure can be prohibitive. As a consequence, it is assumed that an average in the frequency band would lead to the same results as the ensemble average. In other words, an ergodic behaviour for the frequency domain and the ensemble domain is considered. This assumption has been shown to be valid for frequency bands with many modes, but usually does not hold when there is a reduced number of modes [60,61]. In this situation, care should be taken in the use of numerical and experimental data.

1.4.4 Some final comments on SEA

No doubt the development of SEA commercial software can be viewed as an important improvement for the SEA users and it was partially responsible for the increase in the method popularity. Many of the methods previously described for the determination of the SEA input parameters are implemented in the SEA codes for different types of subsystems. The programs usually also offer visualization tools, which can be quite important in a model with many subsystems. Some codes may also include more advanced features to calculate the effects of acoustic treatments or complex sound and vibration transmission paths. However, the great facility of modelling a structure using a commercial SEA program has also allowed non-experts in SEA (or even in noise and vibration) to perform a SEA analysis and obtain "results". The SEA codes usually do not warn users when their model is likely to break some of the SEA assumptions or the hypotheses assumed in the calculation of the SEA input parameters (e.g., when the model displays an inadequate number of modes in a frequency band or incorporates strong coupling). In fact, the implementation of such features may be a complex task in view of the theories involved and the possibility for many different approaches in SEA. Still, it is likely that the results obtained by a non-expert would display a large discrepancy with reality and, in some cases, may result in a loss in the SEA credibility as an important vibro-acoustic analysis technique.

1.5 HYBRID METHODS

Although the FE method and SEA cover a wide range of applications, there are still certain types of structures which are difficult to model using one of these techniques. These structures are composed of elements with both low and high frequency behaviour. The response of the low frequency elements is given by a few modes, while the high frequency elements are characterized by wavelengths much smaller than their dimensions (thus having a

large number of modes). This issue is also known as the mid frequency problem. An example is given by an aircraft structure where the frame has a deterministic behaviour while the skin panels have many modes and a high degree of uncertainty. It is not difficult to find out other examples of structures composed of both stiff parts and more flexible items. In such cases, it would be a considerable improvement if the FE method and SEA could be combined in a single method, taking advantage of the positive points of both methods depending on the part of the structure being modelled.

There have been many efforts in the literature to combine a deterministic and a statistical method in a single modelling technique. In [62], Soize proposed a method based on fuzzy concepts to model a structure in the mid frequency range. The system was divided into a master structure, which represents the deterministic part, and a structural fuzzy, which consists of secondary dynamic elements attached to the master structure with unknown properties. The master structure is modelled by conventional deterministic methods and the structural fuzzy is taken into account by setting probabilistic boundary impedances between the structural fuzzy and the master structure. The method allows the fuzzy constitutive laws to be defined for different probabilistic scenarios. Numerical tests were inconclusive about the validity of the method.

Combining the FE method and SEA is investigated by Shorter in [63]. Component mode synthesis is used to reduce the computational costs of a FE model and to allow the definition of a deterministic energy flow model. A stochastic flow model was then obtained by defining the statistics of the natural frequencies as being jointly Gaussian and combining a Taylor series expansion of the global modes with Monte Carlo simulations. The results were compared with full Monte Carlo simulations for different probabilistic models of the system input parameters. A good agreement and a significant reduction in the computational expense were observed.

Another method for the mid frequency problem is proposed in [64] by Langley and Bremner. The long wavelength elements are modelled deterministically, while the short wavelength elements are modelled using SEA. This is done by dividing the system degrees of freedom into a set of global modes and a set of local modes. The global modes can be found using a deterministic approach based on the FE method before the local response, although the presence of the local set of modes is taken into account. The local modes are then solved using SEA, including an input power term related to the presence of the global modes. It was observed that, although the global modes were treated deterministically, the effects of uncertainties could also be included in the analysis by using a stochastic FE approach. Good results were found for the case of a simple system comprised of two coupled rods.

Although they represent important improvements, the methods described above are limited to simple cases and become difficult to implement for more complex structures. More recently, a method, named the hybrid FE-SEA method, was proposed by Langley and Shorter [65] which seems to overcome this problem. The method is based on the concept of reciprocity between the diffuse field excitation of a connection and its radiation impedance. This diffuse field reciprocity relationship is shown to hold by Langley and Shorter [66] when describing uncertainty boundaries between subsystems and may possess an arbitrary number of degrees of freedom. The relation is used to derive a non-iterative method that includes both equations for the dynamic equilibrium and power balance. The derivation did not include references to SEA and it was argued that the SEA wave approach can be viewed as a special case of the method. Therefore, no assumptions were made regarding the coupling strength, the type of excitation or the number of modes contributing to the response and instead replaced by the consideration that certain subsystems were sufficiently random. Numerical tests showed a good agreement between the method and full FE Monte Carlo simulations. The great potential of the method is also demonstrated in more recent publications where numerical and experimental validation of the method are given [67,68]. Although an important improvement, the Langley and Shorter hybrid method in its current form still does not allow the calculation of the response statistics. Some studies are underway to extend the method's capacity to also predict the response statistics. These studies are based on a variance theory for SEA results that is described below [69].

1.6 SEA VARIANCE

1.6.1 Overview

In its original form, SEA is only capable of predicting the mean response (ensemble average). However, for a statistical method, it is somehow surprising that higher order statistics cannot be estimated. Without this information, accessing the confidence limits of the response or the worst case performance of a structure with uncertainties is not possible. This problem has been pointed out by many authors as an important drawback of the technique [7,25,28]. Indeed, Lyon and DeJong [25] state in the introduction of their book: *"A major piece of unfinished business in SEA is determining how these statistics depend on manufacturing procedures, and second, how the population statistics are to be used in computational response statistics."* The interest in extending the SEA capability to the prediction of the response statistics has resulted in many publications over the last few years

and two distinct approaches can be observed. In the first approach, numerical investigations were performed by adopting a probabilistic model for the structure parameters and calculating the response for an ensemble of structures. The response statistics are then obtained and analyzed. These studies are reviewed in section 1.6.2. The second approach is based on the Point Process Theory [70] and on the assumption of a statistical model for the natural frequencies and mode shapes, allowing the derivation of equations for some response statistics. The studies related to this approach are reviewed in section 1.6.3.

1.6.2 Numerical investigations

One of the first studies regarding the SEA variance based on a numerical approach was performed by Davies and Wahab in [70]. Equations for the power flow between two coupled beams were derived considering a rain-on-the-roof excitation (distributed random excitation with random phase). An ensemble of structures was generated by considering the ratio of the lengths L_1 / L_2 of the beams as a random variable with a uniform distribution given by $1 < L_1 / L_2 < 2$. It was observed that the power flow variance was highly sensitive to the modal overlap factor *m*, displaying a reduction with increasing *m*. Applying the wave approach to obtain the coupling loss factor, Davies and Wahab also observed that the numerical results conform well to the SEA predictions for high values of *m*. The study was extended by Davies and Khandoker in [72], where a point excitation was considered. The mean power flow showed the same behaviour as that for the rain-on-the-roof excitation, while the variance increased for the case of a point load.

In [73], Fahy and Mohammed considered structures composed of coupled beams or coupled plates to investigate the variance of the power flow. Following Davies and Wahab, the ratio of the lengths was considered as a random variable, but now with a Gaussian distribution and a standard deviation of 10%. The size of the ensemble analysed was limited to 32 members in view of the computer capacity available. The power flow was averaged for ten input force positions for each structure. The results showed that the modal overlap factor is, together with the number of coupled modes in the frequency band, the main factor which controls the power flow variance. The wave approach for the calculation of the coupling loss factor was considered to overestimate its value. An attempt was made to correlate the variance of responses (power flow and the coupling loss factor) with the variance of the input random parameters, but it was observed that both variances exceed the input variance. Fahy and Mohammed also observed that for $m > 1$, the power flow distribution tends to be normal. It was concluded that the common procedure in SEA of considering the frequency average as

representative of an ensemble average can lead to significant errors.

This problem was also studied by Keane in [61]. Different approaches were considered for the calculation of the power flow statistics for coupled beams under axial vibration and rain-on-the-roof excitation. The first approach included Monte Carlo simulations with the mass as a Gaussian random variable with 20% standard deviation. Alternatively, Keane calculated the power flow adopting a statistical model for the eigenvalues (uniform distribution). It was concluded that the second approach did not allow the calculation of the power flow statistics with confidence. Keane also showed concern regarding the procedure of averaging in frequency in order to obtain ensemble statistics.

Manohar and Keane investigated in [74] the statistical behaviour of the Green functions and the input receptance functions for the case of a single rod under axial vibration considering different probabilistic models. The probabilistic models included the cross-section area, Elasticity modulus and density as both random variables and random processes along the rod axes. Equations for the eigenvalues and eigenvectors were obtained based on the probabilistic model adopted, while numerical techniques were used for the pdf of the Green functions and receptance functions. The study was extended by Keane and Manohar in [75] by considering the power flow between two random rods with the probabilistic models cited above. It was observed that receptance functions displayed a statistically stationary behaviour beyond a cut-off frequency. However, this cut-off frequency was shown to be dependent on the type of excitation and the probabilistic model adopted. It was also noted that the measured dispersion associated with the response did not reduce with increasing frequency. Keane and Manohar identified the individual members of the ensemble which deviate considerably from the average and it was verified that even small variation on the input parameter may result in extreme responses.

Manohar and Keane continued their research on the reliability of SEA in [76]. The variability of the dissipated power spectra in a system composed of coupled beams or rods was investigated. The energy flow was calculated based on an exact formulation for the Green functions of the uncoupled subsystems for both point load and rain-on-the-roof excitation. The effects of different damping models, type of loading, type of subsystems and probabilistic model over the response statistics were investigated. It was found that the damping model may be determinant to the convergence of the mean with increasing frequency. When analysing the pdf of the eigenvalues, it was observed that there was an increasing overlap as frequency becomes higher or when the system randomness was increased. A greater overlap of pdfs was interpreted as an increase in the number of modes contributing to the response statistics, which would result in a smoother mean curve. Manohar and Keane proposed a

parameter to quantify the level of randomness of the system and so identify the cut-off frequency beyond which the response statistics are no longer dominated by individual modes. This parameter was named statistical overlap factor and, for the *i*th natural frequency, is given by

$$s_i = \frac{2\sigma_{\omega_i}}{\mu_i}, \tag{1.10}$$

where σ_{ω_i} is the standard deviation of the *i*th natural frequency and μ_i is the mean spacing (ensemble average) between the *i*th natural frequency and the *(i+1)*th natural frequency. For the cases considered, the statistical overlap factor was shown to be a good indicator of the cut-off frequency. Preliminary investigations by Manohar and Keane also showed that the lognormal and gamma pdfs may be adopted as the pdf of the response for the estimation of confidence limits.

More recently, Manohar and Adhikari [77] also considered the statistics of the response for an ensemble of structures composed of trusses with the mass, elasticity, damping and length of their elements as random variables. The analysis employed the dynamic stiffness matrix method and the Monte Carlo method to generated and solve an ensemble of systems. The authors were especially interested in the effects of a system comprised of many subsystems and of different damping models. Five damping models were considered: a) velocity dependent viscous damping, b) velocity hysteretic damping, c) strain rate dependent viscous damping, d) strain rate dependent hysteretic damping and e) four previous models applied to different members of the trusses. It was found that for the models with an increasing bandwidth with frequency (models c and d) the results converge for the SEA predictions. For the other models, an oscillatory behaviour was observed. It was also noted that the energy spectra were non-Gaussian and, for the majority of cases, a lognormal distribution was found to fit the numerical data over a wide range of system parameters. Manohar and Adhikari concluded that frequency averages may be representative of ensemble averages for the mean but that this is not the case for higher order statistics as the variance.

Some other studies can be found in the literature where an ensemble of structures is numerically generated in order to study the SEA assumptions [78-80]. However, these studies were mainly interested only in mean results.

1.6.3 Point process approach

The initial studies aiming at the development of a formulation for the response statistics of a dynamic system were performed in the field of room acoustics. Predicting the acoustic response of a room in the audio frequency range can be a complex task and usually involves thousand or even millions of modes. The development of a deterministic model becomes unfeasible and it is necessary to rely on a statistical description of the response. In [81], Schroeder considered the statistics of the frequency response between two points in an acoustic room where the ensemble consists of frequency responses measured for different source and receiver positions. By assuming that the direct sound transmission between source and receiver can be neglected and using concepts from the Random Process Theory [70], equations for the statistics of the real and imaginary part of the frequency response were derived. Schroeder concluded that the real and imaginary part become uncorrelated Gaussian variables of equal variance at sufficiently high frequency, which implies an exponential pdf for the squared modulus of the frequency response and a variance equal to the squared mean.

Considering the Poisson Point Process theory given by Rice in [82], Lyon [83] derived equations for the real and imaginary part of the point mobility and for the modulus squared of the velocity transfer function. The Poisson Point Process assumes an exponential distribution and a statistical independence between the natural frequencies. Lyon was especially interested in the real part of the point mobility, which defines the power injected by a point force, and found that the mean tends towards the result for infinite systems. It was observed that the variance of the modulus squared transfer function was greater than Schroeder's prediction, but tends towards Schroeder's results at high frequencies. A non-Poisson model for the natural frequencies was also considered by assuming a "nearest neighbour" distribution. Lyon observed that the variance was reduced by considering this pdf.

In a series of papers [84-86] Davy extended Lyon's equations to the case of multiple source and receiver positions. Davy's formulation still considered a Poisson model for the system natural frequencies and for the case of one source and one receiver reduced to Lyon's expressions. A non-Poisson model based on the "nearest neighbour" distribution was also considered. Davy compared his theoretical predictions with experimental data. However, his experimental results were based on an average across third octave bands, instead of an ensemble of structures. A good agreement was observed, although the predictions based on the non-Poisson model displayed a better match. A discussion about the mode shape statistics factor K was also given and it was observed that experimental results were considerably lower than the predictions based on sinusoidal mode shapes.

In [87] Weaver investigated the applicability of Random Matrix Theory (RMT)

[10] to the description of the statistics of the natural frequencies. It was found that the natural frequencies of small aluminium blocks experimentally obtained conform well to the predictions of RMT for a specific type of ensemble know as the Gaussian Orthogonal Ensemble (GOE). The GOE model predicts a Rayleigh distribution for the natural frequencies and correlations given by the "two-level cluster function", while the Poisson model assumes the natural frequencies are independent. In [88], Weaver applied the GOE model to Davy's equations of the relative variance of the transfer functions. The new formulation was found to be a significant improvement over the previous equations and displayed a better agreement with the experimental data. Weaver considered in the derivation that the two-level cluster function could be approximated by a delta function for large values of the modal overlap factor *m*, which results in zero variance in the case of a rain-on-the-roof excitation. This result was shown to be an important drawback of the formulation since rain-on-the-roof excitation is commonly found in many applications.

Figure 1.5 shows the pdfs used in the literature for the natural frequencies of a random dynamic system.

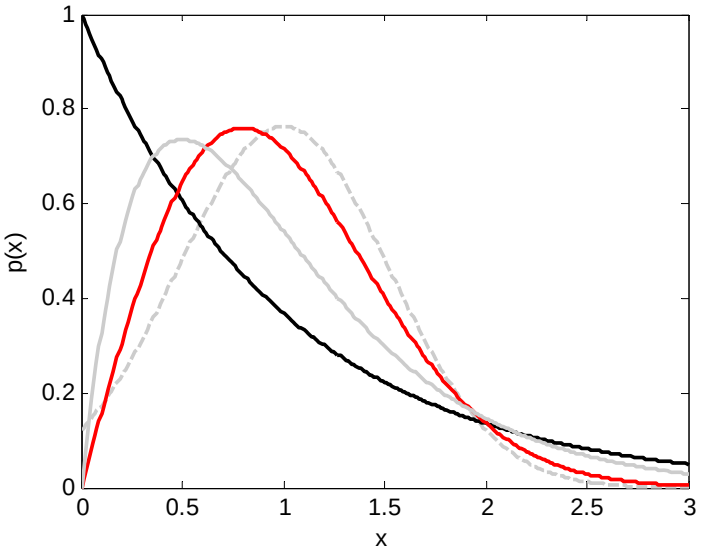

Figure 1.5 – Probability distributions considered in the literature for the natural frequencies. Exponential distribution, Rayleigh distribution, Nearest-neighbour distribution and Gaussian distribution.

Weaver's initial study was extended in [89] by Burkhardt and Weaver. The GOE model for the natural frequencies was still assumed but the effects of the variability on the modal decay rate of modes were also considered. The new formulation suggests an increase in the power input and power transmission variability as a result of the varying modal decay rate. The comparison of the new formulation with numerical results displayed an

improvement in the predicted results.

The problem was reconsidered in [90] by Lobkis *et al.* Both GOE statistics and a variable modal decay rate were assumed. The approximation for high modal overlap factor *m* of the GOE correlations adopted in [88,89] was removed. The resulting formulation was found to display a worsened agreement with experimental results. It was speculated that the poor agreement was caused by the modes being complex.

Langley and Brown gave a review of the problem in [91]. Equations were derived for the variance of the energy density considering three models for the natural frequency statistics: the Poisson model, the Rayleigh distribution with independent natural frequencies and the full GOE model. The restriction displayed by Weaver's formulation for the case of rain-on-the-roof excitation was removed. Numerical and experimental validation was carried out for the case of a plate loaded with masses in random positions. The formulation based on the full GOE model displayed a very good agreement with the numerical and experimental data. A Gaussian distribution for the pdf of the energy density was found for the case of rain-on-the-roof excitation, while the case of a point force displayed a lognormal behaviour. It was also observed that the numerical mode shape statistics factor *K* was less than the theoretical Gaussian value of 3. The numerical model was based on the proportional damping model, which does not allow complex modes and thus invalidates Lobkis *et al.*'s speculation that complex modes could be the cause of a *K* less than 3. Langley and Brown stated that the precise value of *K* remains an open question.

The work is extended in [92] by Langley and Brown for the case of frequency-band average results. Equations of the variance for the frequency-band average energy density were derived and reduce to the equations found in [91] for the case of the bandwidth tending towards zero. Again, the predictions are compared with numerical results for the case of a plate loaded with masses with a good match. However, it was observed that the numerical results become sensitive to small deviations from the GOE model at high values of *m*. In fact, as the level of randomness of the system was reduced (by reducing the number of random masses), the prediction deviated from the numerical data.

The above references considered the response statistics of a system comprised of a single subsystem. However, in order to allow the prediction of the SEA results variance it is necessary to extend the equations for the case of a built-up system. In [93], based on the previous results for the energy density variance, Langley and Cotoni derive the formulation for the variance of energy levels of a system composed of many subsystems. The expressions for the variance were obtained in terms of the standard SEA parameters and an additional set of parameters describing the nature of the power input and coupling between two subsystems.

The theoretical predictions showed a good agreement with numerical simulations carried out for different systems. It was pointed out that the analysis considered that the assumptions behind SEA were fulfilled and that errors in the prediction of the mean due to not respecting these hypotheses (for example, the presence of strong coupling or wave filtering) would not be included in the theory. More recently, an experimental analysis carried out for a structure composed of plates attached to a cylinder also demonstrated the good quality of the theoretical predictions [69]. A procedure for the calculation of confidence intervals based on a log-normal distribution was also proposed with good agreement with numerical and experimental data.

1.6.4 Random Matrix Theory

Random Matrix Theory (RMT) plays an important role in the derivation of a variance theory for the response of dynamic systems. The mathematical approach adopted in the variance theory requires the definition of the statistics of the eigenvalues of the random dynamic system. At first, it seems that the statistics would be directly related to the statistics of the input parameters and this is true for the low frequency range. However, increasing the frequency (and consequently the level of randomness), it has been noted by several authors that the statistics of the eigenvalues are independent of the input parameter statistics and conform well to the RMT predictions [87,91].

The RMT was mainly developed in the late fifties and early sixties by Wigner, Dyson, Mehta and others as an attempt to represent the statistical pattern of the energy levels of nuclei. A review article in the field is presented by Brody *et al.* in [94], while Mehta's textbook [10] presents the topic in a more detailed form.

The average behaviour of the energy level is important information in the study of nuclear reactions. 'Nuclear energy level' is the denomination used in the physics literature for the peaks that arise in the energy excitation spectra of any nucleus. For low levels of energy excitation the peaks can be predicted based on independent particle models. But as the energy level increases, the peaks become too dense and, beyond a certain value, a statistical model becomes necessary. The particle models are based on quantum mechanics and the energy levels can be described by the eigenvalues of a Hermitian matrix operator called Hamiltonian. As for a continuum elastic system, the Hamiltonian of a nuclear system should have an infinite number of eigenvalues. An approximation is performed through a truncation, limiting the size of the system, but still considering a large number of eigenvalues. Based on the statistical properties of the Hamiltonian and adopting some hypotheses on its structure, the aim of the RMT is to derive the statistical pattern of its eigenvalues.

In a more general form, the problem can be stated as follows. The eigenvalue problem associated with an *NxN* matrix **A** can be given as

$$\mathbf{A}\mathbf{u}_j = \lambda_j \mathbf{u}_j, \quad \mathbf{A} = \mathbf{U}\ \mathbf{\Lambda}\ \mathbf{U}^T, \quad \mathbf{U}\mathbf{U}^T = \mathbf{I}, \tag{1.11}$$

where λ_j is the *j*th eigenvalue of matrix **A** and $\mathbf{u}_j$ is the *j*th eigenvector. The columns of the matrix **U** correspond to the eigenvectors, while $\mathbf{\Lambda}$ is a diagonal matrix containing the eigenvalues. RMT deals with the problem of deriving expressions for the joint probability density functions (jpdf) of the eigenvalues of **A**, whose entries are random numbers and have a given jpdf. Obtaining the jpdf of the eigenvalues of a random matrix can be quite a complex task and closed-form solutions are only available for special types of random matrices. These special types of random matrices are known as Gaussian Ensembles and are discussed further in this thesis.

More recently, some authors have conjectured that the application of RMT is not restricted to the statistics of the nuclear energy levels, but can be applied to a wider range of cases [10,87,95]. In [10] Mehta mentioned some areas where recent results showed an agreement with RMT predictions, like the electromagnetic properties of small metallic particles and the zeros of the Riemann zeta function. In [96] Stockmann presents a detailed review of RMT and applies its results to quantum chaos. Much more important for this study are the results presented by Weaver in [87], where the statistics of resonance frequencies of aluminium blocks were found to conform well to the predictions from the RMT.

It is not yet clear the reasons why the results from RMT are so widely applicable, as the matrices from the problems mentioned are considerably different. Insights in this direction are given by some studies dealing with the concept of ‘universality’ [95,97], where the minimum requirements for a matrix to display RMT results are discussed. However, many questions regarding the GOE application for random dynamic systems remain to be investigated.

1.7 DISCUSSIONS, AIMS AND SCOPE

The above review has shown the great importance that the uncertainty issue has been given by the noise and vibration community in recent years. The requirements for greater efficiency, improved performance and reduced costs suggest that the problem will be the subject of many publications in the future.

It has been seen that the effects of uncertainties on the response of dynamic

systems vary with frequency and this must be considered in deciding about the method of analysis to be used. In low frequencies, a deterministic method (usually the FE method) is used to calculate the response of each member of an ensemble of structures defined based on a statistical description of the structure parameters. Information on the statistics of structure properties is rarely available and possibilistic approaches were developed in an attempt to overcome this restriction. In these approaches the input parameters are assumed to lie within certain ranges. As the frequency increases, the computational costs and the requirements for even more statistical data on the input parameters make the above methods unfeasible. However, the increase in the frequency of analysis has also led to the observation of a curious phenomenon: the response statistics become independent of the exact nature of the system uncertainties. It has been observed that the statistics of the system natural frequencies conform to the GOE statistics if the system is sufficiently random, which allows the prediction of the response statistics without knowing the precise sources of uncertainty. This behaviour has been observed by many numerical investigations for different structures and considering different definitions of the ensemble of structures. In fact, a formulation for the energy density variance has been derived based on the GOE assumption and then extended to predict the variance of SEA results. It is also expected that the assumption of a GOE model will allow the calculation of the variance associated with the new hybrid method results. However, the reasons for the agreement between the natural frequency statistics and the statistics of the GOE model remain unclear. A recent publication by Langley in [97] where the conditions for the universality of the eigenvalue statistics is investigated shed some light on the problem but some questions are still unanswered. For example, in the past the main statistics used to verify the agreement with GOE statistics was the pdf of the spacing between natural frequencies, but one may question whether the pdf comparison would be sufficient to ensure the agreement with other higher order statistics. If the answer is negative, then the question turns to which statistics should be used. It is not clear for real engineering structures to what extent the full agreement with the GOE model is valid or required. Of course, the effects of a low level of agreement will depend on the application. In this case, further investigation is required in order to estimate the errors in the variance prediction when the system does not display a perfect match with the GOE statistics.

From the above discussion, another important question also arises: what is the meaning of “sufficiently random”? A system being sufficiently random is the requirement for the GOE model to be applicable and, as a consequence, it is a requirement for the variance theory to be valid. However, there is currently no robust way of estimating the level of randomness of a system and therefore verifying its agreement with the GOE model. The

statistical overlap factor has been used in the past to verify the level of randomness of a system. Langley and Brown [91] suggested that a value greater than unity would be enough for the GOE model to apply. Mace *et al.* [2] also indicate a similar parameter called the stochastic factor (by the definition given, it would be half the value of the statistical overlap factor) to evaluate the randomness level of a system. However, some results obtained by Brown in [39] and by Kessissoglou and Langley in [98] have shown that these parameters would fail in many situations. The determination of the statistical overlap factor also requires the solution of the eigenproblem for each member of the ensemble which can be quite complex in many situations. Therefore, defining a new parameter with the required characteristics would be an important step towards providing a greater confidence in the GOE model and the variance predictions.

In view of the above discussion, this thesis will be centred on the following aims:

- A better understanding of the relation between the GOE ensemble and ensemble of real structures and how to verify the discrepancies in the statistics;
- The effects of discrepancies between the GOE statistics and the statistics of ensembles of real structures on the variance prediction;
- The derivation of a single parameter to allow the estimation of the agreement between a real ensemble of structures and the GOE model.

In order to undertake this task, this thesis is subdivided into the following Chapters:

Chapter 2 – A numerical approach based on the FE method and a probabilistic analysis is proposed in order to generate and solve an ensemble of structures. The numerical approach is verified through the comparison with experimental results for the statistics of the energy density of an ensemble of structures formed by plates loaded with masses in random positions. The results are also compared with some SEA predictions. The approach is then adopted in the studies carried out in the following Chapters.

Chapter 3 – A detailed review of the Random Matrix Theory is given in Chapter 3. The different Gaussian ensembles are described and the statistics used in the physics literature to verify the agreement between real systems and the RMT predictions are presented. The application of RMT to the statistics of random dynamic systems is also reviewed. The ergodicity and the presence of symmetries are two important concepts in RMT regarding its application to dynamic systems and therefore are discussed in detail. Numerical cases are studied using the approach given in Chapter 2 and the effects of different randomization

approaches on the eigenvalue statistics are investigated.

Chapter 4 – The variance theory given by Langley and Brown in [91] is reviewed and the predictions are compared with numerical results. Some of the cases described in Chapter 3 are considered and the energy density mean and variance are calculated using the approach described in Chapter 2. The study allows the verification of the effects of different randomization approaches on the energy density variance and the errors associated with the variance theory. The assumptions adopted by Langley and Brown regarding the mode shape statistics are also verified through numerical analysis.

Chapter 5 – In view of the computational costs of the numerical method given in Chapter 2, a new approach is proposed for the study of random dynamic systems. The new approach is based on a general random dynamic system where the stiffness matrix is the only source of randomness. Different randomization scenarios are investigated and the new approach seems to display the same behaviour observed for the eigenvalue statistics and the energy density variance for the real systems considered in Chapter 3 and 4.

Chapter 6 – A new parameter is proposed for the estimation of the system level of randomness based on the eigenvector mixing. The approach developed in Chapter 5 is used to verify the parameter behaviour in different situations. A perturbation analysis is performed in order to derive equations for the new parameter based on the statistics of the input data, which would allow the determination of the level of randomness of a system and the checking of its agreement with the GOE model before performing the complete analysis.

Chapter 7 – A summary of the work is presented. The original objectives of the research are reviewed and the extent to which they have been met is discussed. The main conclusions drawn from the thesis are summarized and recommendations are made for future work.

CHAPTER 2

ENERGY DENSITY STATISTICS USING THE FE METHOD

2.1 INTRODUCTION

In the development of this study, the Finite Elements (FE) Method will be used to access the statistics of the response of random dynamic systems, in particular, the statistics of the energy density. Applications of the FE method to vibro-acoustic problems are widely documented in the literature [12]. The method is adopted here in view of its capacity to model complex systems. However, some questions may arise about the capacity of the FE method for addressing the proposed problem (response statistics). As a mathematical model, the FE method is based on idealizations and assumptions that may affect the results obtained for the statistics of natural frequencies or the mean and variance of the energy density, especially at higher frequencies. The modelling process can also be affected by errors in the definition of element types, material properties, boundary conditions, etc. In order to verify these points, a validation approach based on the statistics of the energy density was adopted following Langley and Brown in [91]. A structure composed of a plate loaded by point masses and subject to a harmonic point excitation was considered. This type of structure allows the physical generation of an ensemble of random structures by randomly varying the position of the point masses. Frequency response functions (FRF) were measured for each member of the ensemble and the statistics of the energy density for the ensemble could be accessed. The same problem was then modelled using the FE method to determine the natural frequencies and mode shapes. Through a mode expansion the energy density was calculated for a similar ensemble of structures, allowing the calculation of its statistics. In what follows, the equipment used and the measurement procedure of the FRFs are described. The equations adopted to calculate the energy density are reviewed and the results are shown. The numerical procedure using the FE method is also described and discussed. The experimental and numerical results for the energy density are compared with SEA predictions. Finally, the statistics of the energy density obtained experimentally and numerically are compared in order to validate the modelling approach.

2.2 EXPERIMENTAL APPROACH

2.2.1 Structure and support

Figure 2.1 gives the dimensions of the plate used for the experimental and numerical investigation, together with the position of the point force. The bare plate was composed of an aluminium plate with 0.002 m thickness. Table 2.1 presents the properties of the aluminium used in the numerical analysis.

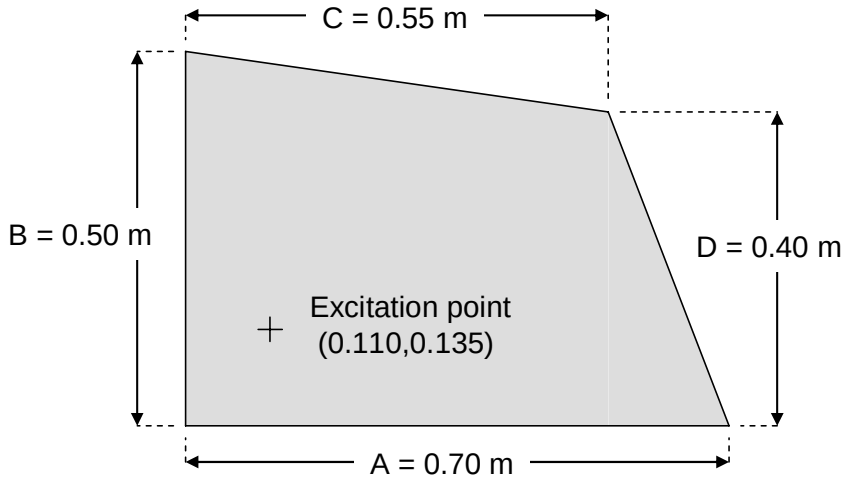

Figure 2.1 – Dimensions of the structure used in the experimental procedure.

Table 2.1 – Aluminium properties.

Property	Value
Young's Modulus	71 GPa
Poisson Ratio	0.33
Density	2800 Kg/m^3

Ten point masses were attached to the plate in random positions. Each point mass was composed of a lead cylinder with a diameter of 0.01 m and mass of around 0.00915 kg (±0.0002 kg). The mass of the bare plate was of 1.554 kg and the 10 point masses represent approximately 5.9% of the plate mass. Damping material (3M® damping foil 2552) was added to the plate in order to increase its loss factor and facilitate the measurement of the FRFs by reducing the dynamic range required. The damping material was added to one side of the plate, while the random masses were attached to the other side. The masses were attached to the plate using a super glue type of adhesive, which allows a reasonably fast removal and re-

attachment of the masses when changing their position. Care was taken in order to prevent the accumulation of glue material on the plate after the repositioning of the masses. The mass positions were generated using the Monte Carlo method considering a spatial uniform distribution of the positions. An ensemble of 35 structures was considered.

The structure was suspended by elastic cords from a rigid structure as can be seen in Figure 2.2, which allows the assumption of free-free boundary conditions. Figure 2.3 shows the masses attached to the structure.

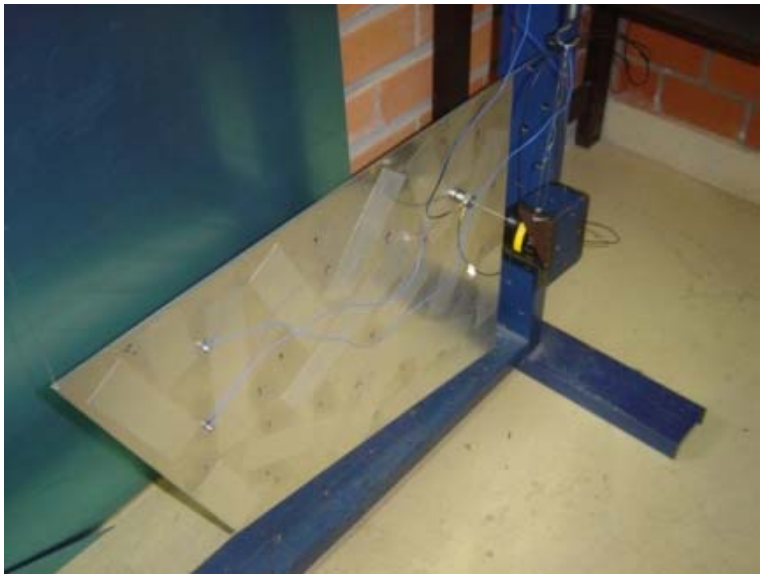

Figure 2.2 – Test structure and support.

Figure 2.3 – Plate with random masses.

2.2.2 Apparatus

The experimental procedures included basically the measurement of punctual and transfer FRFs. The excitation was provided by an electrodynamic mini-shaker B&K type 4180 attached to an impedance head transducer PCB 288D01 which was responsible for measuring the input force and the response at the excitation point. The shaker was also suspended using elastic cords and mechanically connected to the impedance head by means of a stringer which should work as a mechanical protection for the impedance head in case of a fall of the shaker or the structure. The impedance head was screwed to the structure using a small bolt. The excitation mounting can be observed in Figure 2.4. The response at other points of the structure was measured using two small PCB 352B10 accelerometers. The small accelerometers were chosen in order to reduce the errors in the measured FRFs caused by their masses (0.0007 kg each). The effects of the impedance head mass and the mass of the screw were corrected as later explained. The accelerometers were attached to the structure using wax. The mounting resonance of the accelerometer was verified and lay outside the frequency range of interest. It was observed that the measurements were significantly sensitive to deviations in the alignment of the shaker, the stringer and the impedance head. However, it was possible to control the quality of the alignment, and consequently the quality of the measurement, by analysing the coherence curve prior to each measurement.

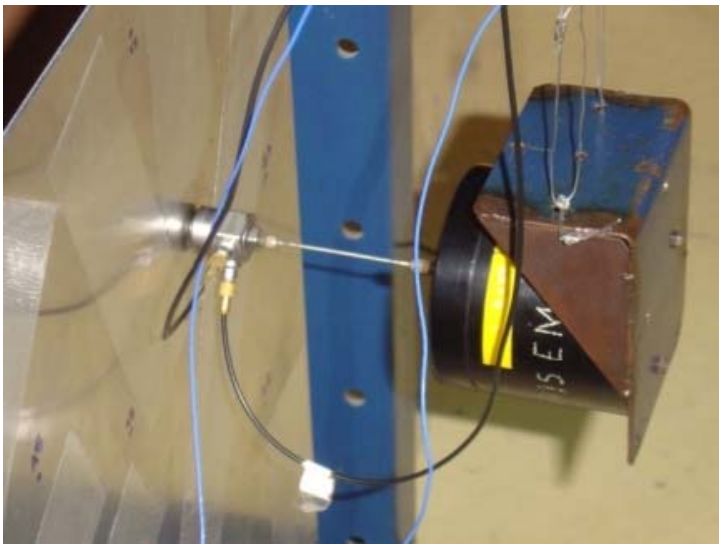

Figure 2.4 – Details of the excitation assembly.

A B&K Pulse® system with a notebook was used to generate the input signal to the shaker and to process the data from the transducers. A white noise with a frequency range of 0 – 3200 Hz was adopted as an input signal to the shaker. The signal was amplified using a B&K Power Amplifier type 2706. Once adjusted, the input signal level was kept the same for

all the measurements, although its modification should not affect the results. Other input signals were investigated (sweep sine with different parameters), but no improvement was observed in the quality of the measurements in comparison with the white noise signal.

An FFT analyser was set inside the Pulse software. A frequency range of 0-3200 Hz was chosen with 3200 lines, which gives a discretization of the FRFs of 1 Hz. A linear averaging was adopted and included 100 samples with a maximum overlap (default). A hanning window was adopted for the measurements. Inertances (acceleration/force FRFs) were measured for the excitation point and the accelerometer positions. The coherence curves were used to evaluate the leakage errors or verify other errors in the measurement procedure.

The assembly adopted for the measurement of the FRF is shown on Figure 2.5. A detailed description of the excitation assembly is also shown in Figure 2.5.

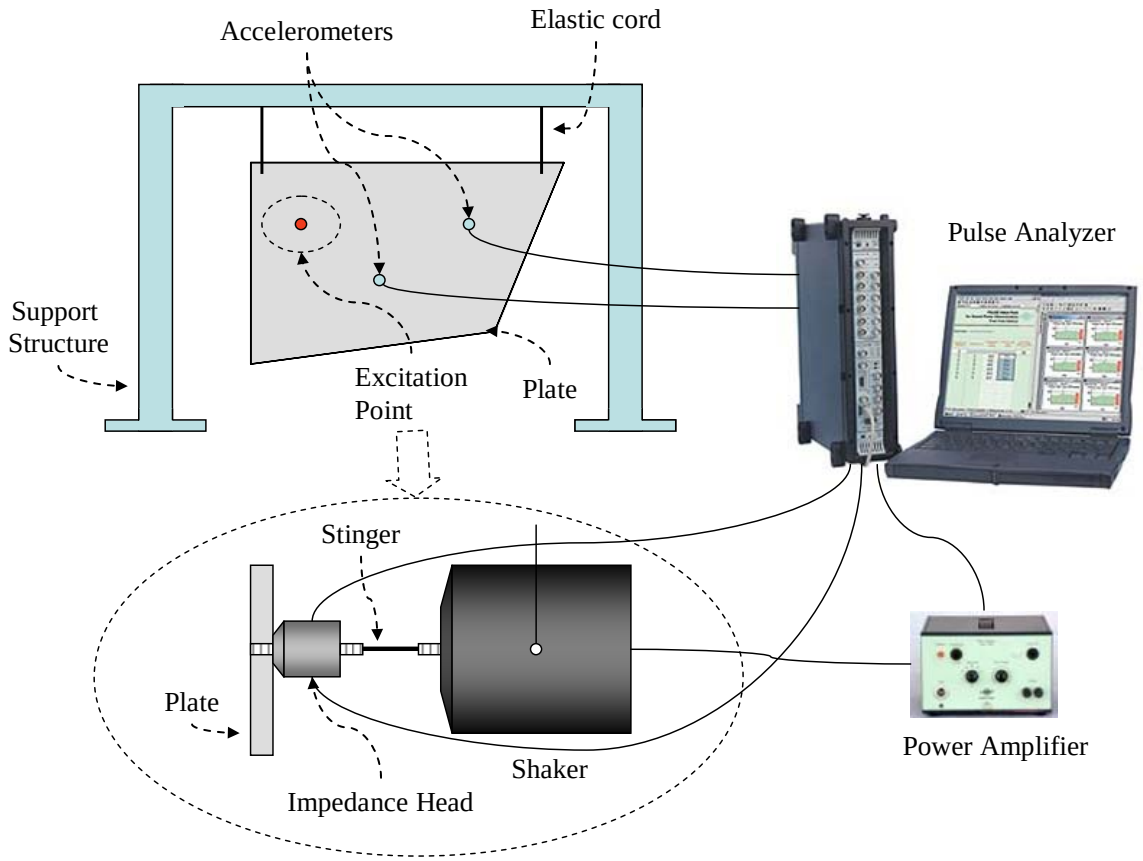

Figure 2.5 – Schematic representation of the equipment assembly.

A list of the equipment used in the experimental procedure can be observed in Table 2.2 , together with comments about some items.

Table 2.2 – Equipment used in the experiments.

Item	Description	Comment
1	Notebook Dell Latitude	With the Pulse® software installed
2	Pulse® Front-end B&K type 3109 and 7533	Digital analyzer with six channels (four inputs and two outputs)
3	Impedance head PCB® 288D01	
4	Two accelerometers PCB® 352B10	
5	Shaker B&K type 4810	
6	Power amplifier B&K type 2706	
7	Vibration Calibrator PCB® 394C06	

2.2.3 Procedure

The first step in the experimental procedure was the calibration of the measuring system. This was performed using a PCB 394C06 vibration calibrator and the calibration tool available in the Pulse software. The calibration procedure is described in Appendix A.1. After the calibration of the measuring system, some measurements were also performed to verify the attachments of the transducers and the shaker. Examples of measured inertances and coherence functions are given in Figure 2.6 and Figure 2.7.

Figure 2.6 shows a point inertance and the associated coherence. A coherence level close to unity is an indication of low levels of leakage or external noises. The observed coherence indicates a high quality measurement for the whole frequency range. Some low levels of coherence can be seen at low frequency and around 2250 Hz. At low frequency, the low coherence is caused by the great difference between resonances and anti-resonances and the limited dynamic range of the measuring system. The low coherence at 2250 Hz was associated with the fundamental natural frequency of the stringer. A similar behaviour can be seen in Figure 2.7 for a transfer inertance.

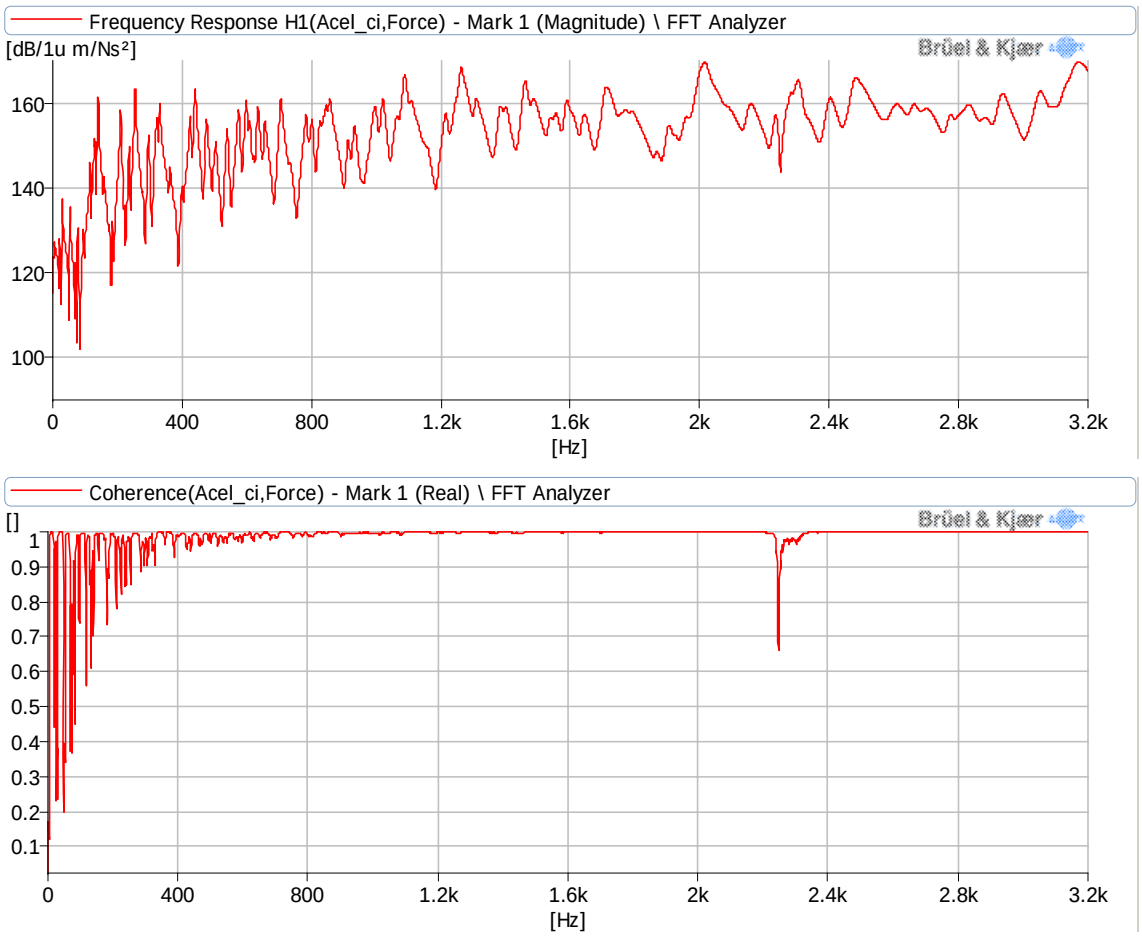

Figure 2.6 – Example of measured point inertance and associated coherence.

For each member of the ensemble, the measuring procedure was repeated 13 times, varying the position of the two accelerometers in order to allow the measurements of 26 transfer inertances. The number of FRFs measured is considerably larger than the usual number used to estimate the energy of a plate [46,47]. Errors from external noise are likely to be averaged out when considering a large number of points. The effects on the mean of extreme responses that may happen close to the point masses are also reduced.

The measured inertances were saved in TXT files and exported to MATLAB® in order to be analysed and the energy and loss factor calculated. The procedure was repeated for each configuration of mass positions, in other words, for each member of the ensemble of structures considered.

The mass added to the structure by the impedance head and the bolt used to attach the impedance head to the structure cause significant errors in the measured FRFs. However, it is possible to correct the measured FRFs if the added mass is known. The procedure given in [99] was adopted to correct the mass errors during the measurements and it is described in Appendix A.2.

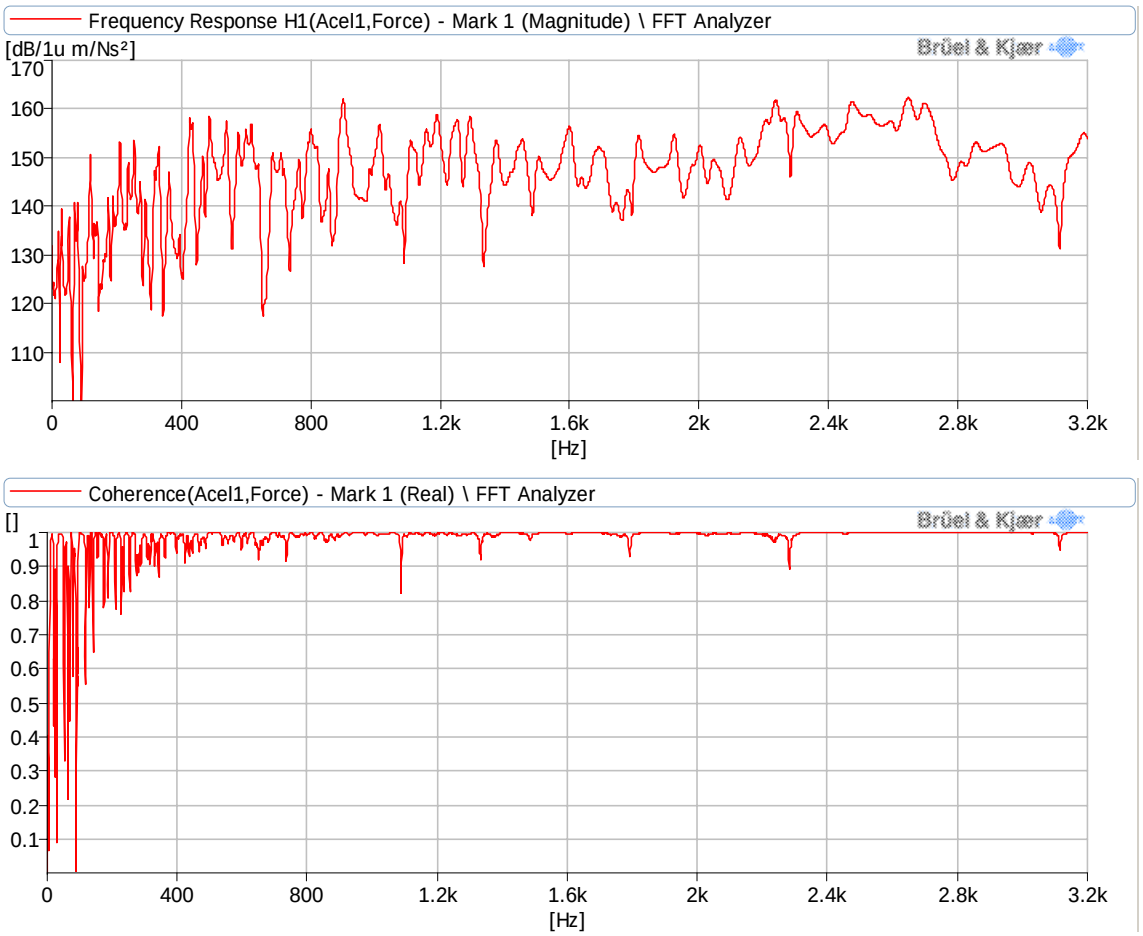

Figure 2.7 – Examples of measured transfer inertance and associated coherence.

2.2.4 Kinetic Energy Density

The mass corrected inertances may then be used to calculate the energy density of the plate. The total time-averaged vibration energy of a structure E is approximately twice the time-averaged kinetic energy V and in the case of a uniform spatial distribution of the mass can be given by

$$E = 2V = M\left\langle \overline{v^2} \right\rangle, \tag{2.1}$$

where $\left\langle \overline{v^2} \right\rangle$ is the spatial average of the time-averaged square velocity and M is the total mass of the structure. For a plate subjected to a point force of amplitude F, with area A and N_p measured transfer inertances, the kinetic energy density can then be calculated by

$$T(\omega) = \frac{V(\omega)}{A} = \frac{MF^2}{2AN_p} \sum_{n=1}^{Np} \left| \frac{A_t^{\,n}(\omega)}{i\omega} \right|^2 . \tag{2.2}$$

In SEA, it is common to carry out the analysis in frequency bands. In this case, the energy is averaged over each frequency band. Band-averaged energy density was also considered and obtained through

$$T_\Delta(\omega_\Delta) = \frac{1}{\Delta} \sum_{\omega=\omega_1}^{\omega_2} T(\omega), \tag{2.3}$$

with Δ being the frequency-band limited by the frequencies ω_1 and ω_2 and with central frequency ω_Δ. One-third octave bands were adopted in the current analysis.

Applying Equation (2.2), the energy density of each member of the ensemble of structures was calculated, allowing the determination of the statistics of the energy density. The energy density of 20 members of the ensemble is shown in Figure 2.8 together with the mean energy density for the 35 member ensemble. The peak around 2250 Hz is associated with one of the stringer natural frequencies and can be observed in all the following results. It can be seen that the mean response becomes smoother with increase frequency, while the resonances can still be observed at low frequency.

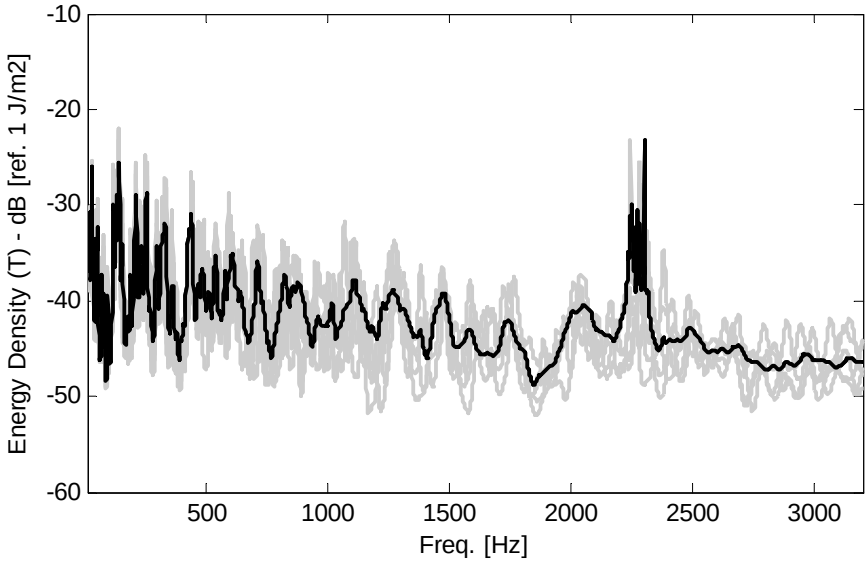

Figure 2.8 – Experimental energy density. ——— ensemble mean, ——— typical ensemble members.

Figure 2.9 shows the band-average energy density for 20 members of the ensemble and the mean curve for the whole ensemble. As expected the dispersion of the results is lower for the band-frequency average results than for the narrow-band curve, since some differences are averaged out in band-frequency averaging. The peak associated with the stringer fundamental natural frequencies can also be observed in the band-averaged data and causes a higher dispersion of the results in the closest frequency bands.

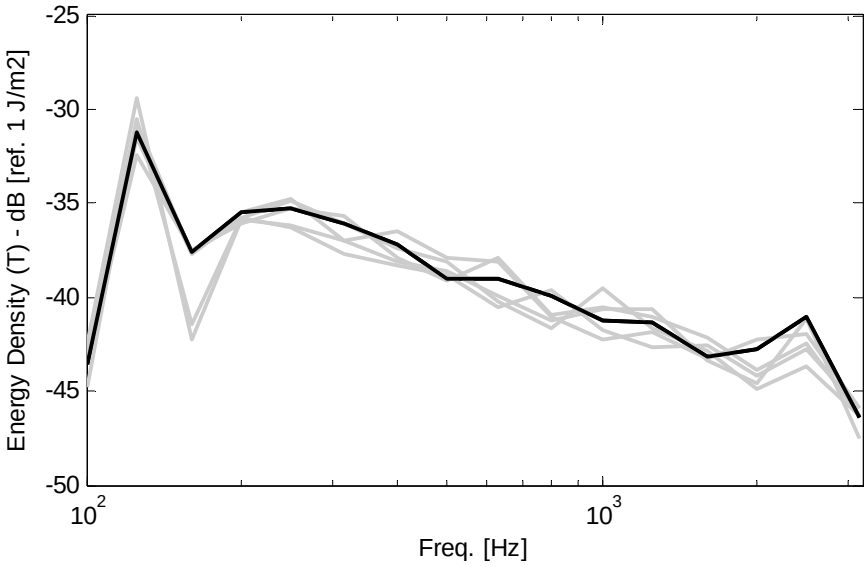

Figure 2.9 – Experimental band-averaged energy density. ——— ensemble mean, ——— typical ensemble members.

The convergence issue is investigated in Figure 2.10 which gives the mean energy density in narrow bands for three ensemble sizes. The ensemble size adopted seems to be sufficient to achieve the convergence of the mean and only small differences can be observed between the curves associated with 20 and 35 ensemble sizes. This behaviour is confirmed by Figure 2.11 where the mean energy density is plotted against the ensemble size for six discrete frequencies. The ensemble size seems to be just enough for the mean convergence. However, the limited ensemble size makes it difficult to draw more definitive conclusions about the convergence and this subject is later investigated using the numerical procedure.

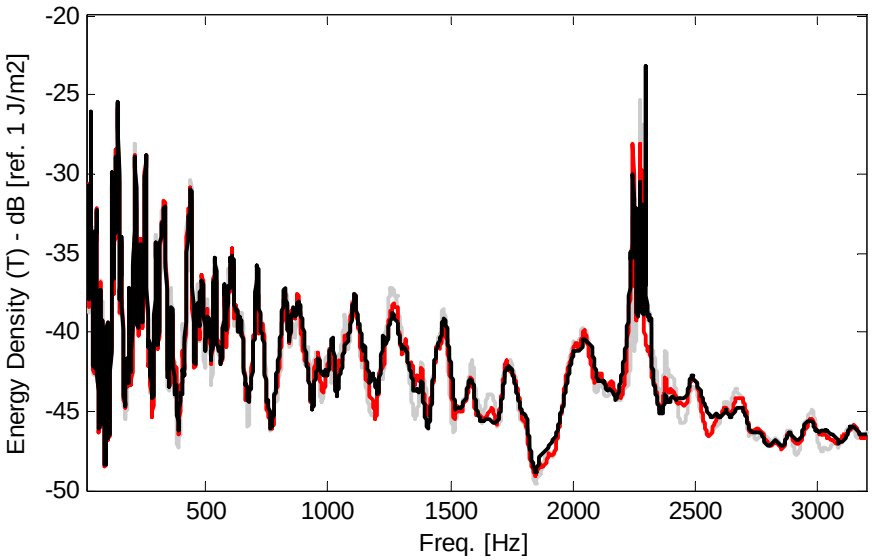

Figure 2.10 – Experimental mean energy density – Spectra convergence of the mean. 10 member ensemble, 20 member ensemble, 35 member ensemble.

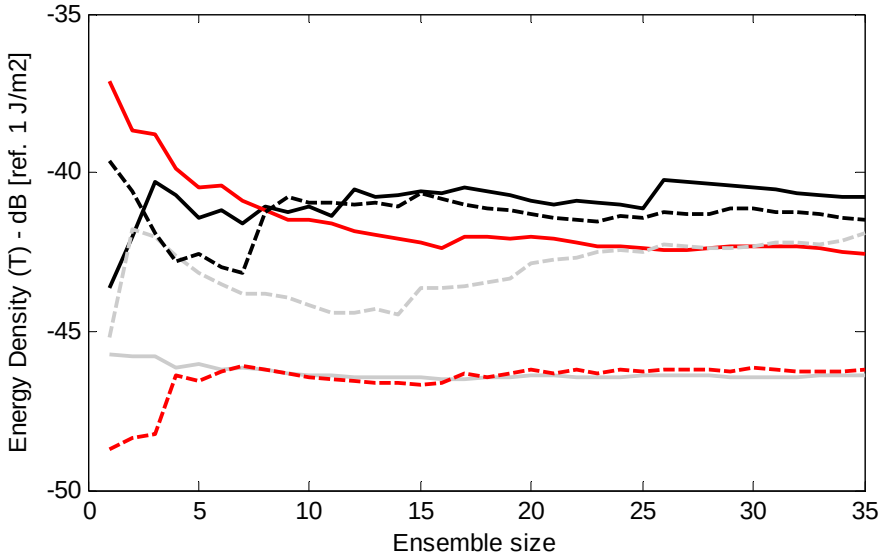

Figure 2.11 – Experimental mean energy density – Discrete frequency convergence of the mean. 100 Hz, 500 Hz, 1000 Hz, 1500 Hz, 2000 Hz, 3000 Hz.

The convergence of the mean band-average energy density is investigated in Figure 2.12 and Figure 2.13. As expected, the band-average results display a faster convergence of the mean. An ensemble size of 20 members would be enough to ensure a difference of less than one dB in the mean curve for all the frequencies.

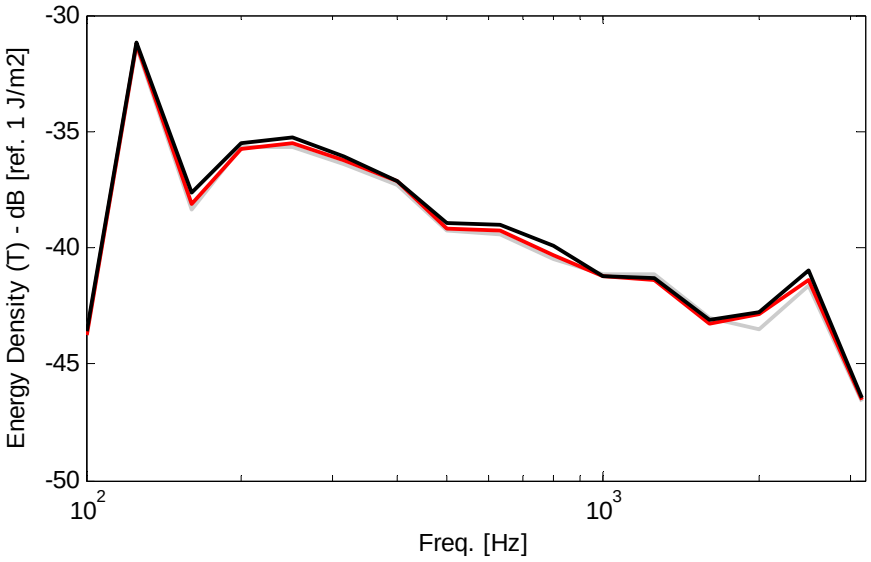

Figure 2.12 – Experimental mean band-averaged energy density – Spectra convergence of the mean. 10 member ensemble, 20 member ensemble, 35 member ensemble.

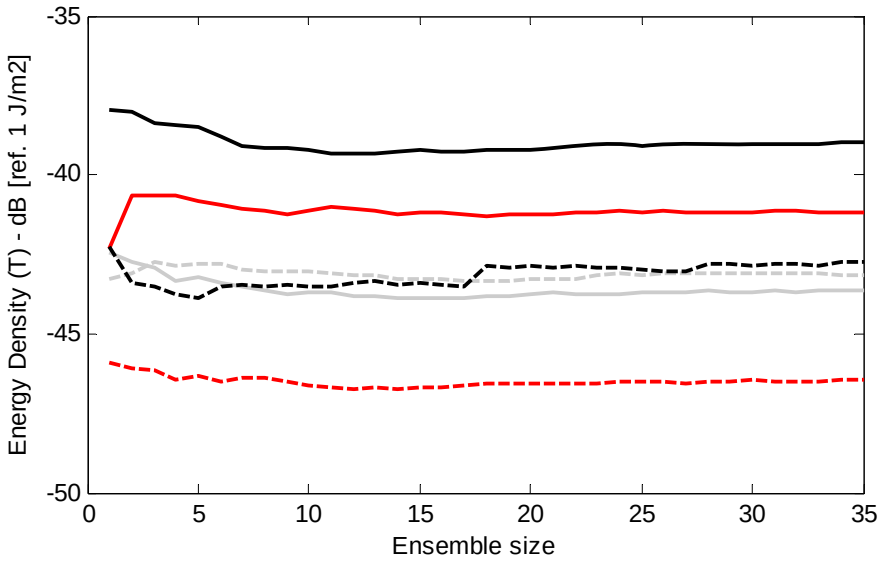

Figure 2.13 – Experimental mean band-averaged energy density – Frequency-band convergence of the mean. 100 Hz, 500 Hz, 1000 Hz, 1600 Hz, 2000 Hz, 3150 Hz.

A similar analysis was carried out for the energy density variance. Three curves considering different ensemble sizes can be observed in Figure 2.14. As could be anticipated, the variance displays a slower convergence than the mean and a larger difference between the curves can be observed. However, it may be noted that all the curves seem to display the same tendency and should converge to a smoother curve with a similar trend if a larger ensemble size were used. In agreement with the higher dispersion observed in Figure 2.10, a higher

variance can be noted in the frequencies around the stringer natural frequency. Of a little more concern are the results given in Figure 2.15. Although five of the six curves considered display a reasonably flat behaviour for an ensemble size larger than 25, the curve for the narrow-band of 500 Hz shows a significant variation. This may be caused by a resonance falling close to the narrow-band being considered, increasing its variance. This type of behaviour is expected particularly for structures with low damping.

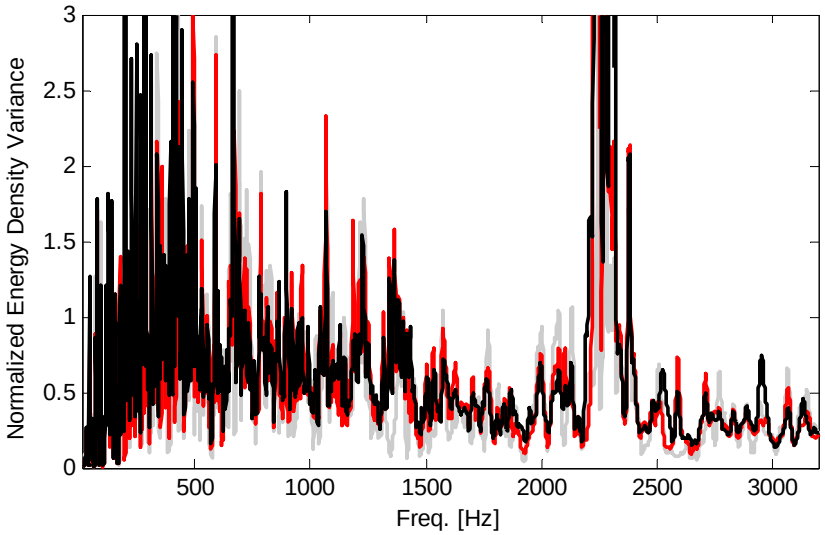

Figure 2.14 – Experimental normalized energy density variance – Spectra convergence of the normalized variance. 10 member ensemble, 20 member ensemble, 35 member ensemble.

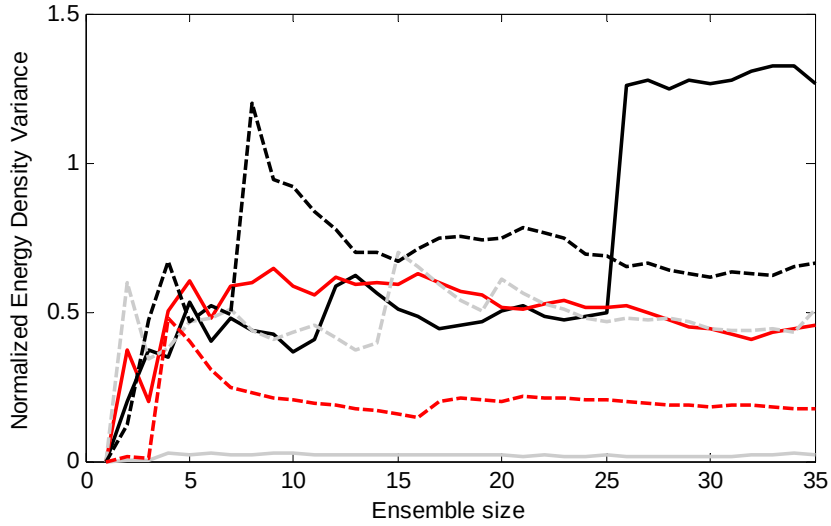

Figure 2.15 – Experimental normalized energy density variance – Discrete frequency convergence of the normalized variance. 100 Hz, 500 Hz, 1000 Hz, 1500 Hz, 2000 Hz, 3000 Hz.

The same results are shown in Figure 2.16 and Figure 2.17 for the variance of the band-average energy density. The large variance values for the frequency-bands above 2000 Hz were caused by the stringer natural frequency and they are also responsible for the large variation observed for the 2000 Hz band observed in Figure 2.17. In view of the limited size of the ensemble, care should be taken when using the variance results obtained.

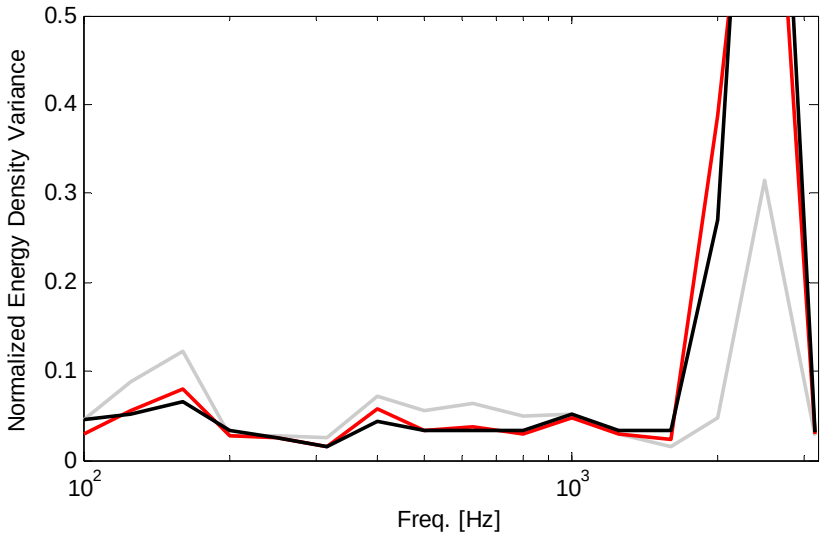

Figure 2.16 – Experimental normalized variance of the band-averaged energy density – Spectra convergence of the normalized variance. 10 member ensemble, 20 member ensemble, 35 member ensemble.

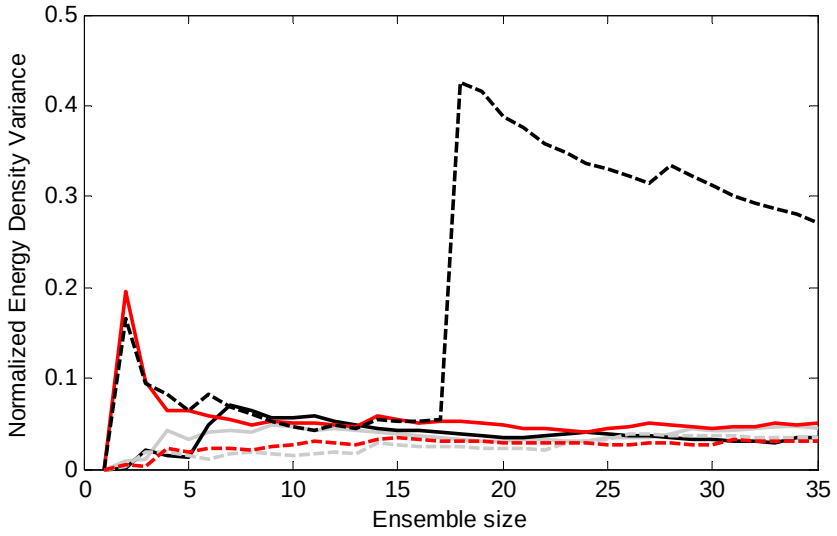

Figure 2.17 – Experimental normalized variance of the band-averaged energy density – Frequency-band convergence of the normalized variance. 100 Hz, 500 Hz, 1000 Hz, 1600 Hz, 2000 Hz, 3150 Hz.

2.2.5 Loss factor

For a single subsystem like the case considered, the SEA power balance states that the power input to the structure is equal to the dissipated power given in Equation (1.2) or as in [25]:

$$\eta = \frac{\Pi_{in}}{\omega E}. \tag{2.4}$$

In SEA analysis, the variables in Equation (2.4) are usually taken as band-average variables and the frequency ω is the frequency-band central frequency. An experimental approach known as the Power Balance Method is proposed in [25] for the determination of the SEA damping loss factor. In that case, the energy of the system is obtained by averaging the response of a single system over the space and in the frequency band. Considering a point force excitation, the power input in Equation (2.4) may be given by

$$\Pi_{in} = \frac{1}{2} F^2 \left\langle \mathrm{Re}\left(Y(\omega)\right) \right\rangle, \tag{2.5}$$

where $\langle\ \rangle$ denotes spatial average and $Y(\omega)$ is the input mobility. The spatial average is an attempt to estimate the input mobility of an infinite system, since this is the assumption usually adopted in the analytical SEA. An ergodic nature of the response for the frequency and ensemble domains is also assumed. However, the present analysis has a different aim. In fact, the interest is in the damping loss factor associated with each structure for a specific excitation point. Therefore, the power input was calculate as given by Cremer *et al.* [38] for a point force

$$\Pi_{in} = \frac{1}{2} F^2 \,\mathrm{Re}\left(Y(\omega)\right). \tag{2.6}$$

The energy for each structure can be obtained using Equation (2.2) and the loss factor calculated using Equation (2.4). The damping loss factor to be used in the numerical analysis was determined by averaging the loss factor over the ensemble and over the frequency since a single value was adopted. Figure 2.18 shows the damping loss factor for three realizations together with the mean loss factor for the 35 member ensemble and the value used in the numerical simulations. It can be observed that the damping loss factor is

relatively flat over the frequency and becomes smoother with increasing frequency. This behaviour is a result of the damping material used.

The damping loss factor in one-third octave bands was also calculated for each member of the ensemble and then averaged over the ensemble. The results are shown in Figure 2.19 and display a similar behaviour to the narrow-band results.

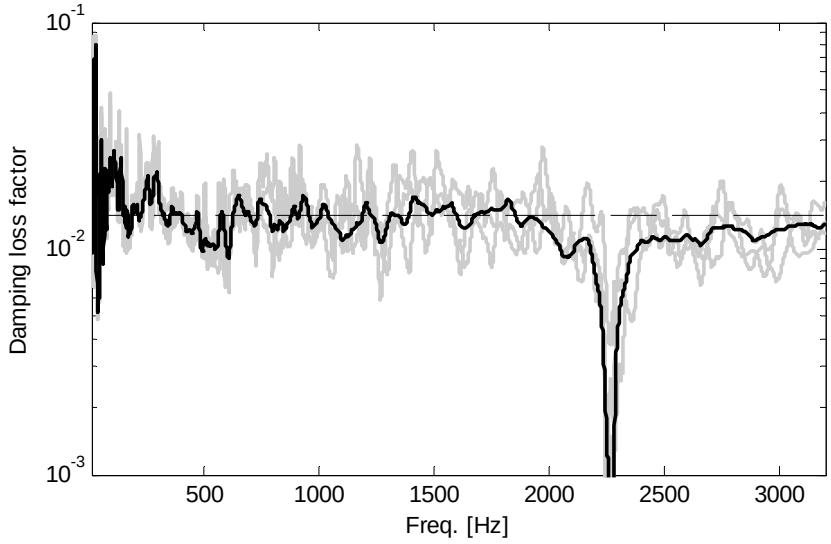

Figure 2.18 – Experimental damping loss factor – Narrow-band. ——— ensemble mean, ——— typical ensemble members, – – – value used in the numerical calculations.

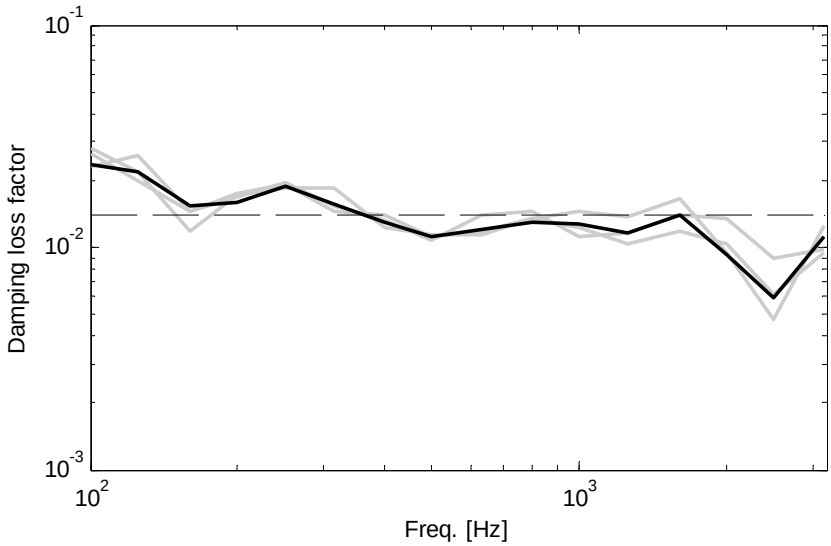

Figure 2.19 – Experimental damping loss factor – 1/3 octave bands. ——— ensemble mean, ——— typical ensemble members, – – – value used in the numerical calculations.

2.3 NUMERICAL PROCEDURE

2.3.1 Overview

The same problem analyzed experimentally was modelled using the FE method. A FE mesh was created using the commercial software ANSYS® and the model solved to obtain the natural frequencies and mode shapes at the excitation point. A modal summation was then performed using MATLAB® to obtain the energy density of each member of the ensemble. A post process of the data allowed the calculation of the energy density statistics. There was the option to perform a full analysis using the FE method with Direct or Modal methods of solution. In this case, the response would be calculated for several points and the spatial average response determined in an approach similar to the experimental procedure. However, tests were carried out and it was observed that the time necessary to solve the full analysis was considerably larger than performing the external modal summation. This is due to the internal procedure of the FE software where the solution is calculated for all the nodes, while the external analysis calculates the energy density based only on the mode shapes at the excitation point. In what follows, the numerical procedure is described and some tests performed to verify its precision.

2.3.2 Model development and solutions

A geometrical model was created with the same dimensions as the plate used in the experimental analysis. The ANSYS® element SHELL63 was adopted, which is a four node element with six degrees of freedom at each node and both bending and membrane capabilities. Only bending motion was considered in the analysis. The mesh discretization was defined in order to represent the mode shapes with sufficient accuracy. The common rule of 6 elements per half wavelength was adopted. The wavelength was determined considering pure bending motion of an isotropic plate given by [25] as

$$\lambda_B = \sqrt[4]{\frac{\pi^2 h^2 E_{ym}}{f_{\max}^2 \rho\left(1-\upsilon^2\right)}}, \tag{2.7}$$

where h is the plate thickness, E_{ym} is the Young's modulus, ρ is the material density and υ is the Poisson's coefficient.

The ANSYS® element MASS21 was used to represent the point masses. The

MASS21 is a point element having up to six degrees of freedom: translations in the nodal x, y, and z directions and rotations about the nodal x, y, and z axes. Only one node is sufficient to define the mass element and nodes previously created in the meshing process of the plate in quad elements were used. The positions of the mass elements were generated externally using MATLAB® and imported to ANSYS®. The plate mesh with an example of the mass positions is given in Figure 2.20.

The plate was modelled with free-free boundary conditions and it was not necessary to define a load case since only a modal analysis was carried on with ANSYS®. The block Lanczos method was used for the extraction of eigenvalues and eigenvectors in view of its faster convergence. The LIS file used as the input for the analysis using ANSYS® is given in Appendix A.3.

The natural frequencies and the mode shapes at the excitation point were saved in a TXT file and imported to MATLAB® to perform post processing. The procedure was repeated for an ensemble size of 500 members. The MATLAB® file used in the analysis can be seen in Appendix A.4.

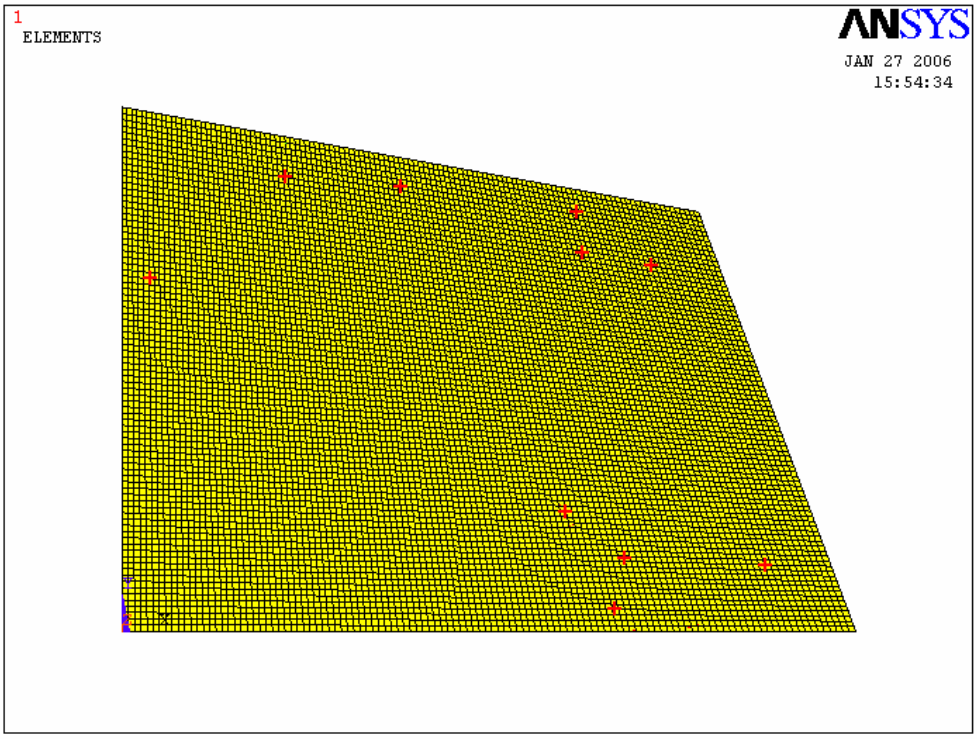

Figure 2.20 – Example of mesh used in the numerical approach. Mass elements in red.

2.3.3 Energy density

The response of a dynamic system may be expressed in the form of a modal summation [5]. Considering a system with proportional damping, the transfer function X at frequency ω for a point force applied at x_0 and the response obtain at point x can be given by

$$X(\omega, \mathbf{x}_0, \mathbf{x}) = \sum_{n=1}^{N} \frac{\phi_n(\mathbf{x}_0)\phi_n(\mathbf{x})}{\omega_n^2 - \omega^2 + i\eta\omega\omega_n}, \tag{2.8}$$

where ω_n is the natural frequency of the nth mode, ϕ_n is the nth mode shape and η is the loss factor. A constant loss factor is assumed, although a loss factor value for each mode can also be considered. The assumption may be justified in view of the experimental results for the loss factor shown in Figure 2.18 and Figure 2.19. The orthogonality relationship for mass-normalized mode shapes is defined as

$$\int_A \rho'(\mathbf{x})\phi_n(\mathbf{x}_0)\phi_p(\mathbf{x})\mathrm{d}\mathbf{x} = \begin{cases} 0 & n \neq p \\ 1 & n = p \end{cases}, \tag{2.9}$$

with $\rho'(\mathbf{x})$ being the mass distribution function and is given in mass per unit area (in the case of a plate). The time-averaged kinetic density T of a system under harmonic excitation at frequency ω applied with amplitude F at x_0 is given by

$$T(\omega, \mathbf{x}_0) = \frac{E(\omega, \mathbf{x}_0)}{2A} = \frac{F^2\omega^2}{4A}\int_A \rho'(\mathbf{x})\left|H(\omega, \mathbf{x}_0, \mathbf{x})\right|^2 d\mathrm{x}. \tag{2.10}$$

The transfer function given by Equation (2.8) may be substituted into Equation (2.10) giving a result of the form

$$T(\omega, \mathbf{x}_0) = \frac{F^2\omega^2}{4A}\sum_n\sum_p \frac{\phi_n(\mathbf{x}_0)\phi_p(\mathbf{x}_0)\int_A \rho'(\mathbf{x})\phi_n(\mathbf{x}_0)\phi_p(\mathbf{x})\mathrm{d}\mathbf{x}}{\left(\omega_n^2 - \omega^2 + i\eta\omega\omega_n\right)\left(\omega_p^2 - \omega^2 + i\eta\omega\omega_p\right)}. \tag{2.11}$$

The resulting double summation in Equation (2.11) may be reduced to a single summation taking into account the orthogonal relation between mode shapes given in Equation (2.9), or

$$T(\omega, \mathbf{x}_0) = \frac{F^2 \omega^2}{4A} \sum_n \frac{\phi_n{}^2(\mathbf{x}_0)}{\left(\omega_n^2 - \omega^2\right)^2 + \left(\eta \omega \omega_n\right)^2}. \tag{2.12}$$

Equation (2.12) allows the calculation of the kinetic energy density of a system under point loading once the natural frequencies and mode shapes at the excitation point are known. The results given by Equation (2.12) are verified in Appendix A.5.1 by comparing with the energy density obtained through the space averaged square velocity

The modal summation presented in Equation (2.12) is an infinite sum and it becomes necessary to truncate the process at a specific point. The number of modes in the frequency range of interested will vary for each member of the ensemble, but would include around 170 modes. Therefore, a good accuracy of the mode summation was achieved considering 250 modes. A convergence test of the energy density curve for the number of modes considered is verified in Appendix A.5.2.

Using the natural frequencies and mode shapes calculated with the FE models it is possible to obtain the energy density for an ensemble of structures and determine the energy density statistics. Figure 2.21 gives the mean energy density for an ensemble of 500 members and the energy density for some members of the ensemble.

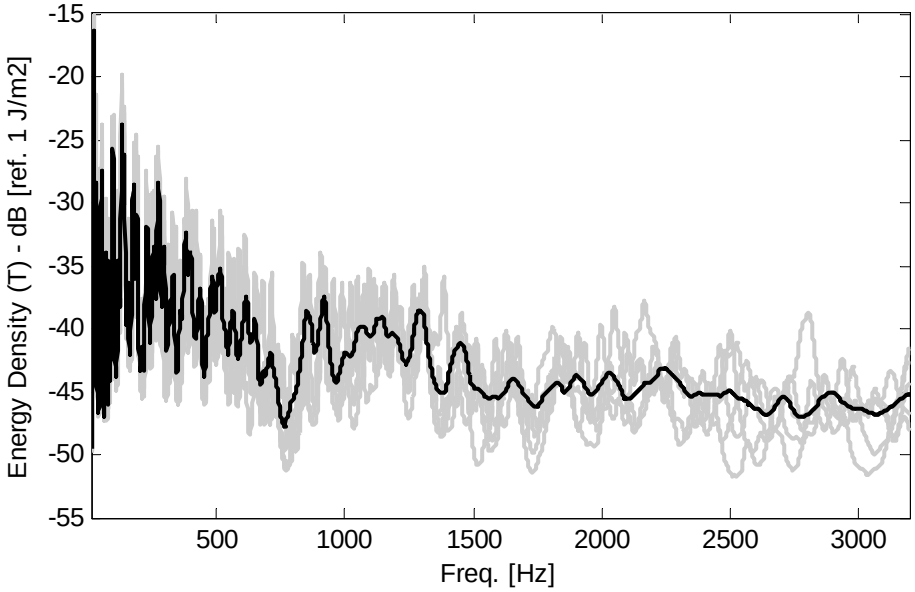

Figure 2.21 – Numerical energy density. ——— ensemble mean, ——— typical ensemble members.

Band-averaged results were also calculated for each member of the ensemble using the same procedure adopted for the experimental results and are given in Figure 2.22. It can be noted that there is a similar dispersion of the narrow-band and band-averaged results for the experimental (Figure 2.8 and Figure 2.10) and the numerical results.

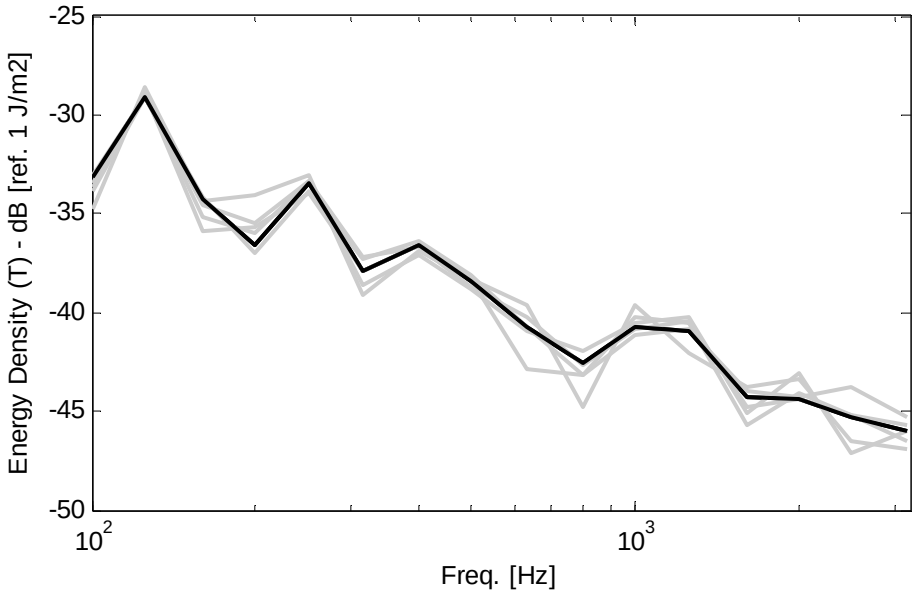

Figure 2.22 – Numerical band-averaged energy density. ——— ensemble mean, ——— typical ensemble members.

The convergence issue was also investigated for the numerical results. In view of the ensemble size, the conclusions may be presented with more confidence. The energy density mean is given in Figure 2.23 for three different ensemble sizes, with one of the curves being calculated for the same ensemble size used in the experimental procedure. Little difference can be observed between the curves, which suggests that the ensemble size used in experimental analysis was sufficient to obtain the convergence of the mean energy density. This behaviour is also observed in Figure 2.24, with only small oscillations being observed for an ensemble size larger than 200 members.

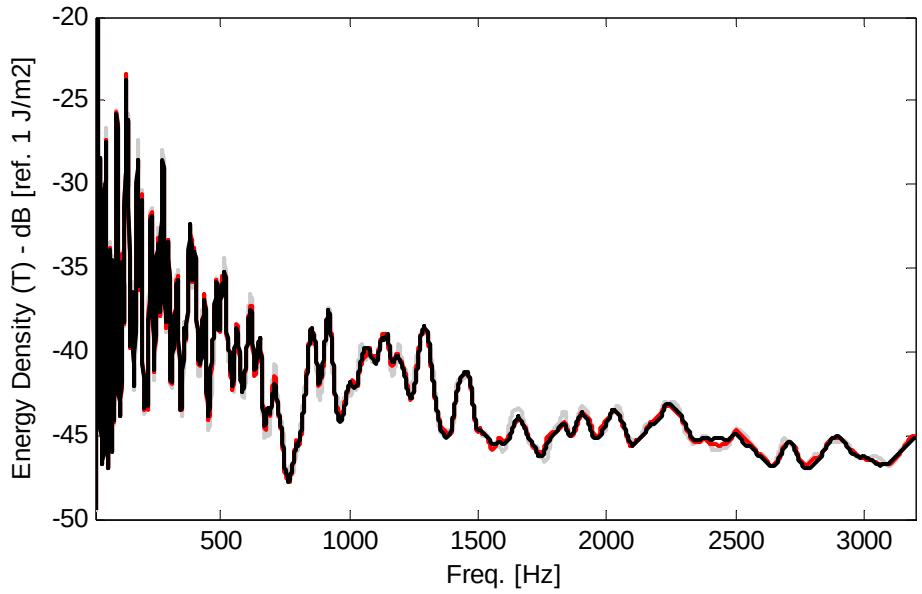

Figure 2.23 – Numerical mean energy density – Spectra convergence of the mean.
10 member ensemble, 20 member ensemble, 35 member ensemble.

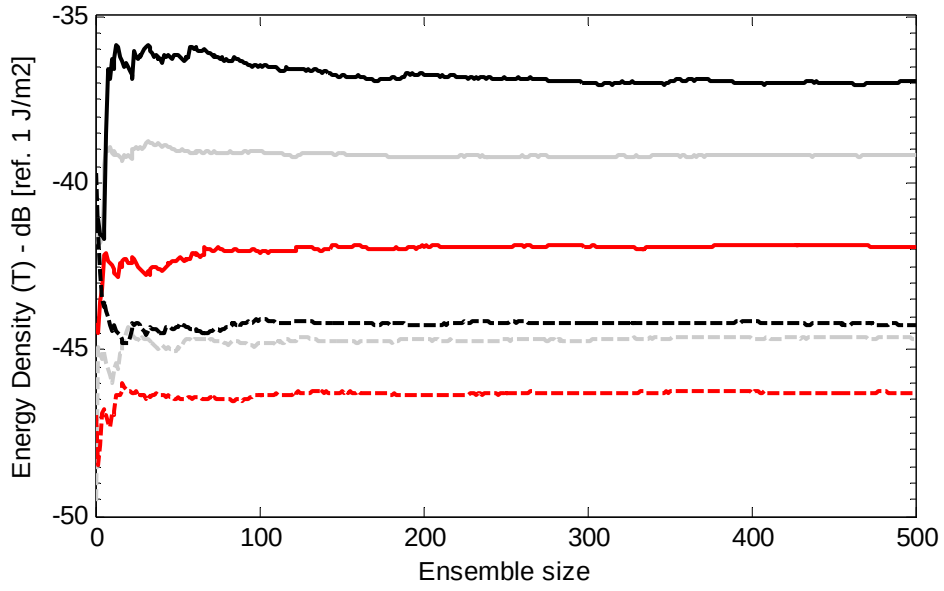

Figure 2.24 – Numerical mean energy density – Discrete frequency convergence of the mean.
100 Hz, 500 Hz, 1000 Hz, 1500 Hz, 2000 Hz,
3000 Hz.

The convergence of the mean band-averaged energy density is also verified in Figure 2.25 and Figure 2.26. Again, a faster convergence than the narrow-band results can be observed for the band-averaged curves. The ensemble size used in the experimental approach seems to be sufficient for the convergence of the mean band-averaged energy density.

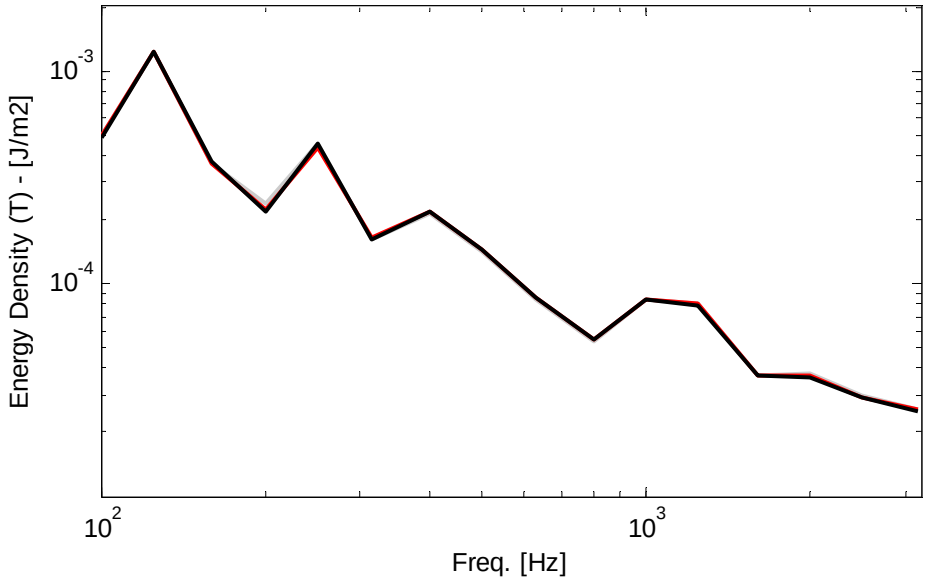

Figure 2.25 – Numerical mean band-averaged energy density – Spectra convergence of the mean. 35 member ensemble, 100 member ensemble, 500 member ensemble.

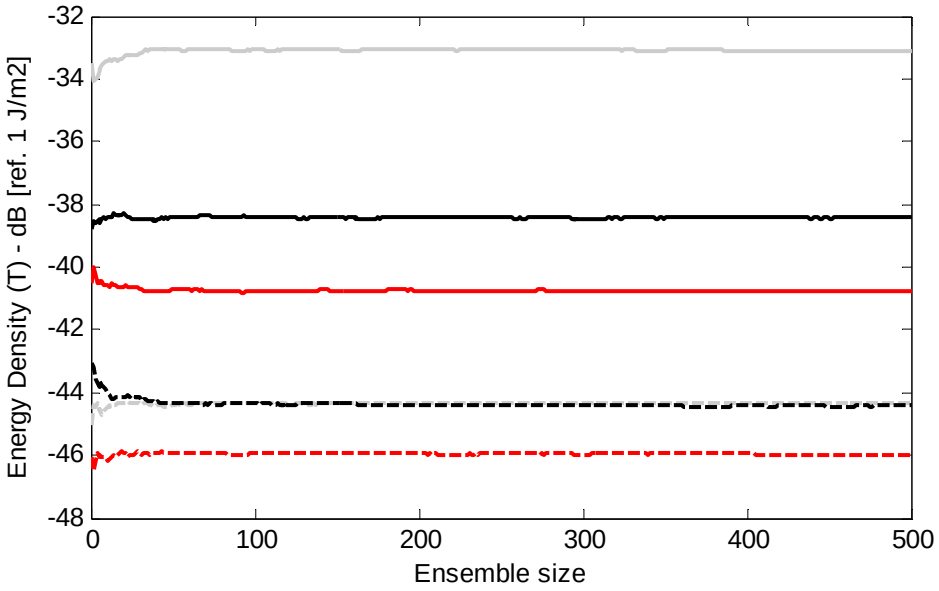

Figure 2.26 – Numerical mean band-averaged energy density – Frequency-band convergence of the mean. 100 Hz, 500 Hz, 1000 Hz, 1600 Hz, 2000 Hz, 3150 Hz.

The ensemble size adopted in the numerical analysis allows a better view of the variance convergence. It can be noted from Figure 2.27 and Figure 2.28 that an ensemble size of around 300 members may be enough for the variance convergence. However, the use of a smaller ensemble may still provide a reasonable estimate of the variance trend but with much more oscillation in the curve as seen in Figure 2.27.

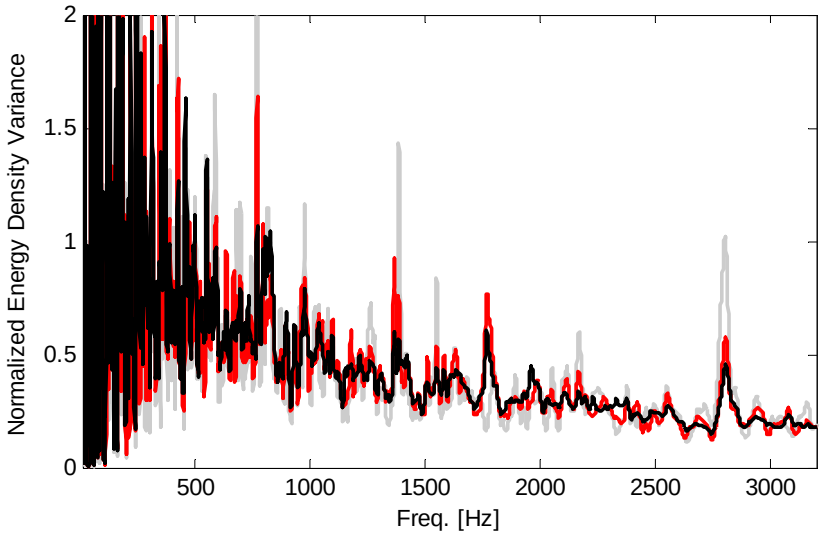

Figure 2.27 – Numerical normalized energy density variance – Spectra convergence of the normalized variance. 35 member ensemble, 100 member ensemble, 500 member ensemble.

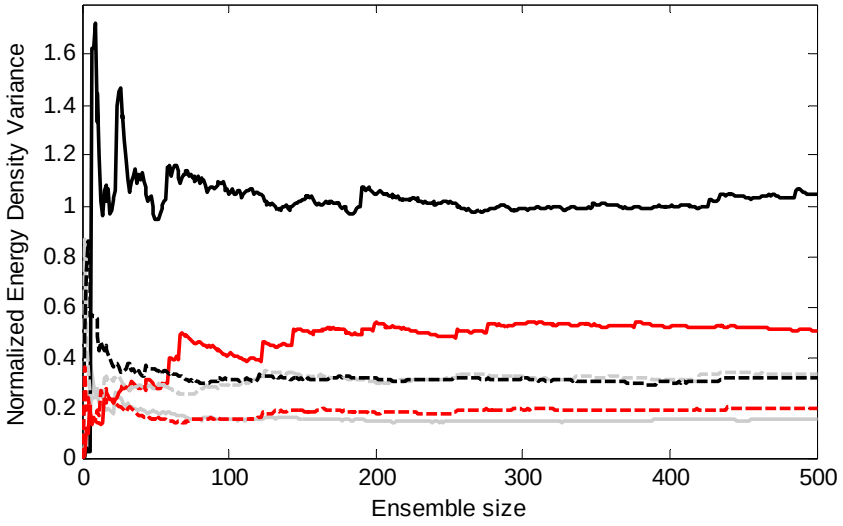

Figure 2.28 – Numerical normalized energy density variance – Discrete frequency convergence of the normalized variance. 100 Hz, 500 Hz, 1000 Hz, 1500 Hz, 2000 Hz, 3000 Hz.

The convergent behaviour of the results is also investigated for band-averaged results in Figure 2.29 and Figure 2.30. It is interesting to observe that the convergence of the band-averaged results does not seem to be faster than that of the narrow-band results. In fact, the curves of the variance versus the ensemble size still display some oscillation even for ensemble sizes larger than 400 members. This may be due to the considerably small values of the variance observed for the band-averaged energy density. Therefore, the results may become more sensitive to extreme data.

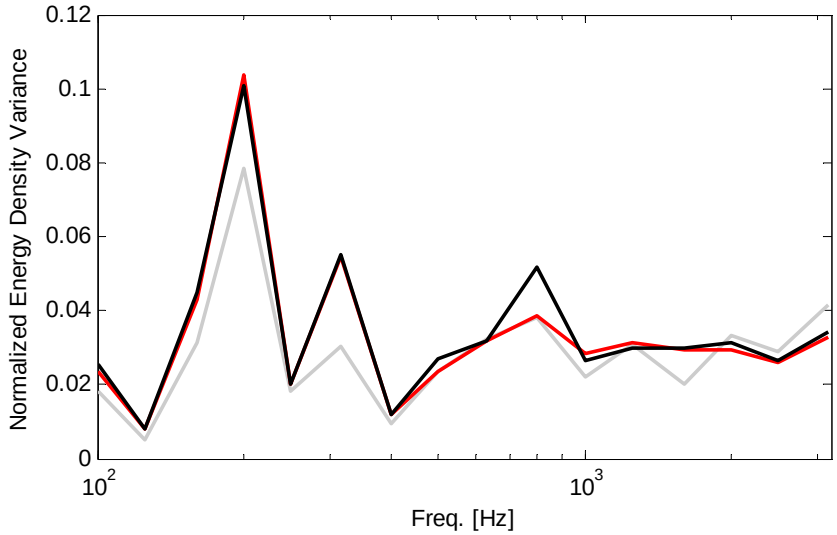

Figure 2.29 – Numerical normalized variance of the band-averaged energy density – Spectra convergence of the normalized variance. 35 member ensemble, 100 member ensemble, 500 member ensemble.

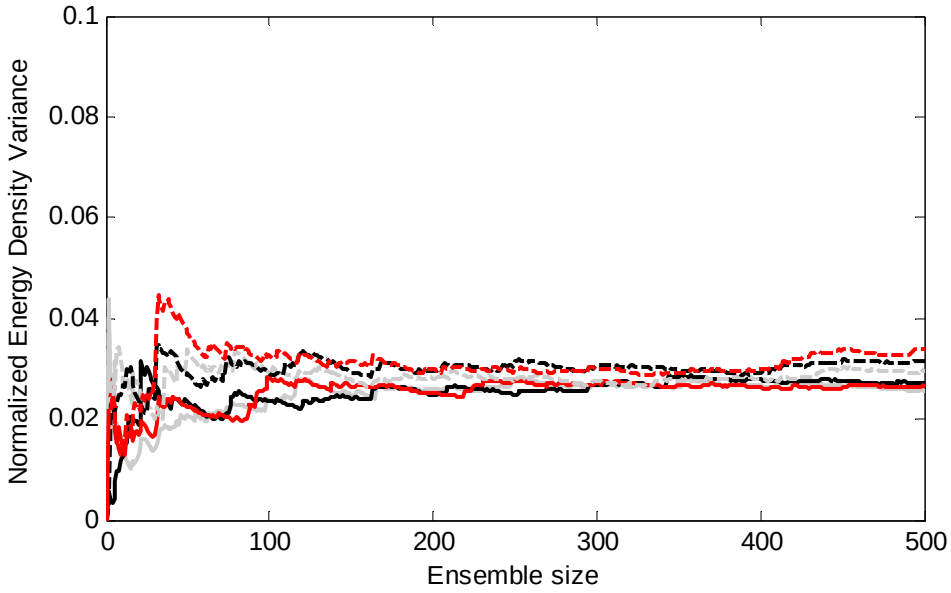

Figure 2.30 – Numerical normalized variance of the band-averaged energy density – Frequency-band convergence of the normalized variance. 100 Hz, 500 Hz, 1000 Hz, 1600 Hz, 2000 Hz, 3150 Hz.

2.4 SEA RESULTS

In order to verify the numerical and experimental procedures, the results were also compared with SEA results for the mean energy density of a plate under point force loading. Considering a unit point force and substituting Equation (2.5) into Equation (2.4) yields

$$E = \frac{\langle \mathrm{Re}(Y(\omega)) \rangle}{2\omega\eta}. \tag{2.13}$$

The relation between the space averaged conductance (real part of the mobility) and the modal density is given by Lyon and DeJong [25] for a system with a uniformly distributed mass as

$$\langle \mathrm{Re}(Y(\omega)) \rangle = \frac{\pi v(\omega)}{2M}. \tag{2.14}$$

An expression for the energy density can then be obtained by substituting Equation (2.14) into Equation (2.13) and dividing by the area, giving

$$T(\omega) = \frac{\pi v(\omega)}{8\omega\eta MA}. \tag{2.15}$$

The modal density is also given by Lyon and DeJong [25] for the flexural modes of an isotropic plate as

$$v(\omega) = \frac{A}{4\pi\kappa c_L'}, \tag{2.16}$$

where c_L' is the longitudinal wave speed in a plate and is given by

$$c_L' = \sqrt{\frac{E_{ym}}{\rho(1-\upsilon^2)}}, \tag{2.17}$$

and κ is the bending radius of gyration or

$$\kappa = \frac{h}{2\sqrt{3}}. \tag{2.18}$$

It is also mentioned by Lyon and DeJong [25] that Equation (2.15) may be obtained considering the conductance of an infinite plate. This derivation is given by Cremer *et al.* in [38] where Equation (2.14) is obtained by assuming the Sommerfield radiation condition, i.e., the displacement at large distances from the excitation point must behave like a decaying wave.

2.5 COMPARING RESULTS

The experimental and numerical mean energy densities are shown in Figure 2.31. The experimental curve considers the mean for an ensemble of 35 members, while an ensemble of 500 members was adopted for the numerical results. Superimposed on the curves is the standard SEA result for the mean energy density. A very good agreement can be observed between the three curves. As expected, the SEA results provide only the trend of the energy density while the numerical and experimental data display an oscillatory behaviour. A smoother curve would be obtained through the numerical and experimental approaches if averages over the space for the excitation point were considered. This would be more in line with the SEA prediction.

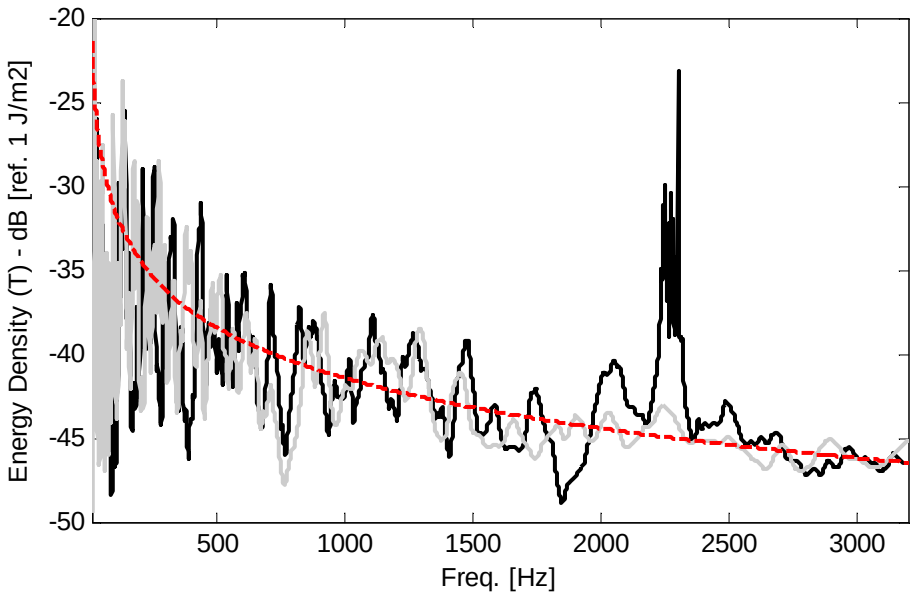

Figure 2.31 – Mean energy density – Narrow-bands. ——— experimental results (35 member ensemble), ——— numerical results (500 member ensemble), - - - - - SEA prediction.

The differences between the numerical and experimental results for the energy density may be due to some assumptions in the FE modelling. It is expected that the bare plate used in the experimental analysis has some small uncertainties in its geometrical and material properties which would result in some discrepancies since the bare plate is modelled deterministically. Another source of error may be the representation of the lead cylinders as point masses in the numerical analysis, ignoring its dimensions.

Similar results were obtained for the band-averaged energy density and are shown in Figure 2.32. Both curves display the same trend and agree well with the SEA predictions. The larger discrepancies between the numerical and experimental data for both narrow-band and band-averaged results can be observed at the frequency bands around the stringer natural frequency at 2250 Hz.

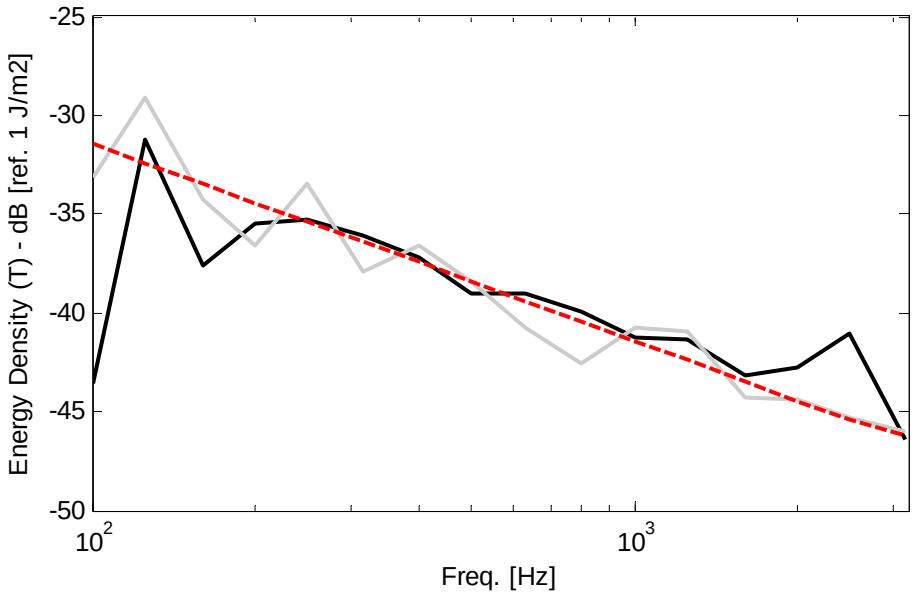

Figure 2.32 – Mean band-averaged energy density – 1/3 octave band. ——— experimental results (35 member ensemble), ——— numerical results (500 member ensemble), - - - - - SEA prediction.

The energy density relative variance results are compared in Figure 2.33 for narrow-band and in Figure 2.34 for band-averaged data. Again, a good agreement can be observed. As a result of its reduced ensemble size, the experimental curves display a more oscillatory behaviour and this was expected in view of the convergence analysis previously performed.

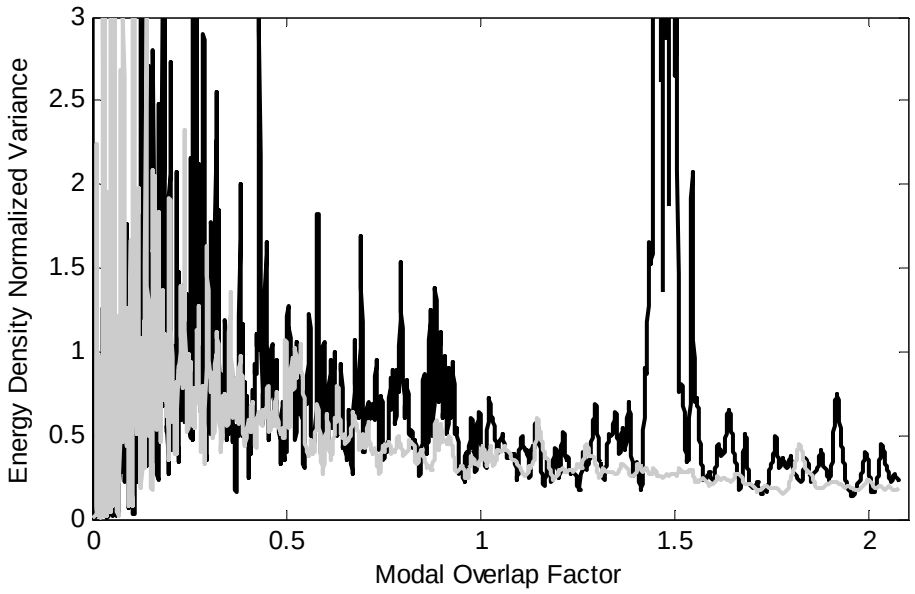

Figure 2.33 – Energy density normalized variance – Narrow-band. ——— experimental results (35 member ensemble), ——— numerical results (500 member ensemble).

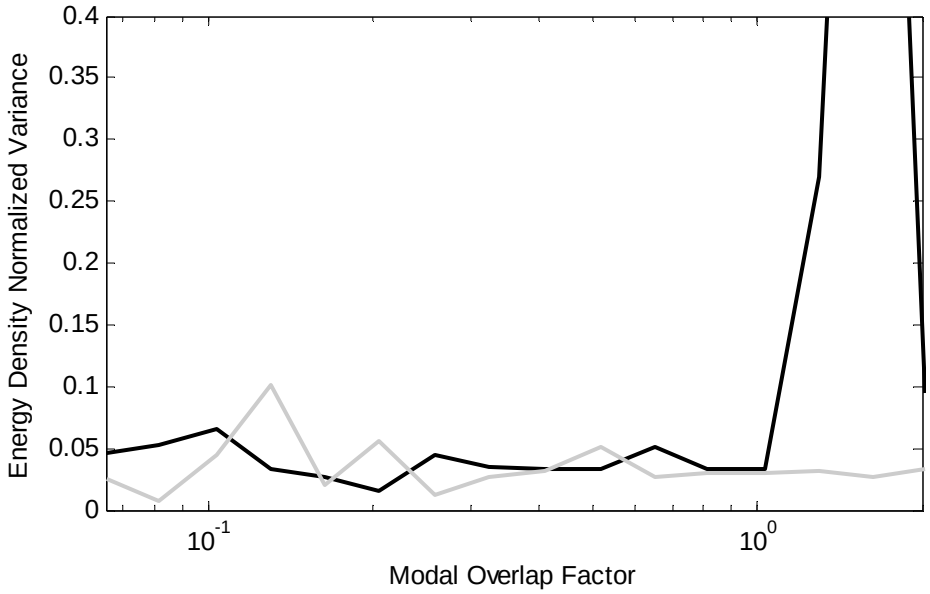

Figure 2.34 – Normalized variance of the band-averaged energy density – 1/3 octave band. ——— experimental results (35 member ensemble), ——— numerical results (500 member ensemble).

Curves for the 95% confidence limits were calculated considering a log-normal distribution of the energy density and are compared in Figure 2.35 and Figure 2.36. It can be noted that, even with the reduced ensemble size of the experimental analysis, very similar results were obtained.

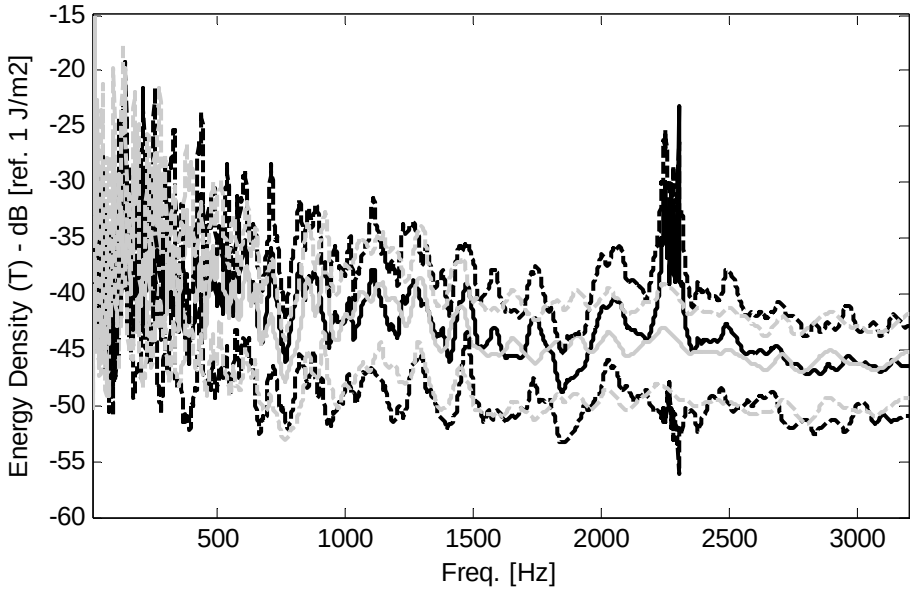

Figure 2.35 – Mean energy density and confidence limits. ——— experimental mean (35 member ensemble), - - - - - experimental 95% confidence limit, ——— numerical mean (500 member ensemble), - - - - - numerical 95% confidence limit.

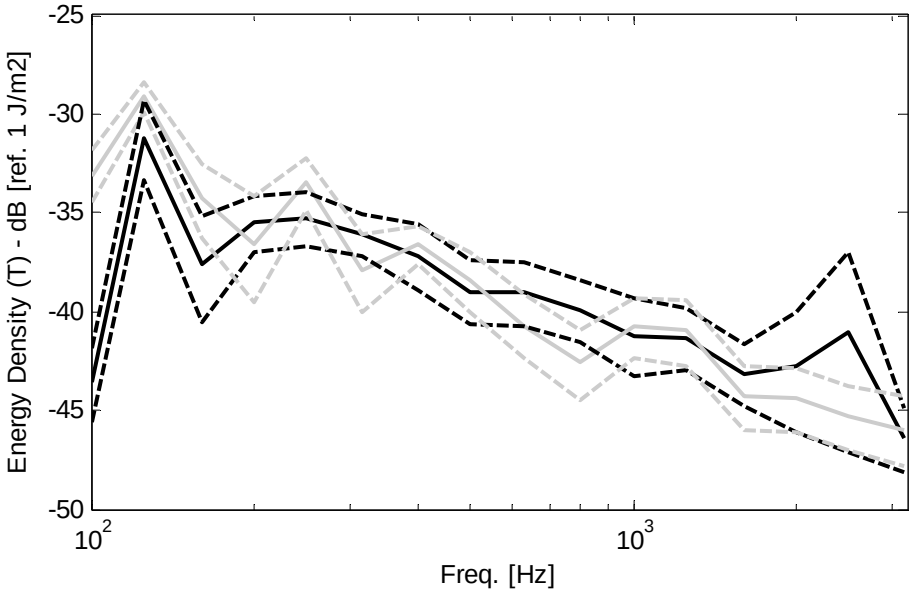

Figure 2.36 – Mean band-averaged energy density and confidence limits. ——— experimental mean (35 member ensemble), - - - - - experimental 95% confidence limit, ——— numerical mean (500 member ensemble), - - - - - numerical 95% confidence limit.

2.6 SUMMARY AND DISCUSSIONS

A validation procedure of the numerical method that will be later adopted in this thesis has been given and discussed. The validation was performed by comparing the numerical results with experimental data obtained for an ensemble of structures formed by a plate loaded with masses in random positions. This type of structure was chosen because it allows the easy generation of an ensemble of real structures and then the experimental evaluation of the dynamic characteristics of each member of the ensemble. The validation was mainly interested in the verification of the energy density mean and variance in view of the application that will be made of the numerical method in the following Chapters.

The experimental approach was based on the measurement of transfer functions between an excitation point and 26 points in the plate. The measured FRFs were then used to calculate the energy density associated with a unitary force. In view of the time required to generate, to assembly and to evaluate each structure, the experimental ensemble was limited to 35 members. The convergence of the energy density mean and variance was also verified. It was concluded that the ensemble size was sufficient for the convergence of the mean but this was not the case for the variance results.

The numerical procedure included the determination of the natural frequencies and mode shapes at the excitation point by means of the FE method. The commercial software ANSYS® was used to generated the mesh and to solve the model. The software MATLAB® was used to generate the mass positions, calculate the energy density by means of a modal summation and calculate the statistics of the energy density. An ensemble size of 500 members was considered which allows the investigation of the convergence behaviour of the energy density mean and variance. It was observed that a small ensemble may be sufficient when the statistics are restricted to the mean, but a larger ensemble may be necessary if accurate results are required for the variance. However, it was noted that even with a small ensemble the variance tendency can be obtained. The results for the mean energy density were also compared with the standard SEA results with a good level of agreement.

The numerical and experimental results for the energy density variance were compared and a close agreement was also observed. Although the numerical approach is based on idealizations of the dynamic system, the results demonstrated the capacity of the numerical approach adopted for the prediction of the energy density statistics of real systems. It is expected that the numerical approach will be also capable of predicting the statistics of the eigenvalues and eigenvectors, although these were not compared directly. The validation procedure was also useful to verify all the aspects concerning the numerical approach.

CHAPTER 3

RANDOM MATRIX THEORY

3.1 INTRODUCTION

The Random Matrix Theory (RMT) was initially developed in the late 50's and early 60's to study the statistics of the spectra of complex nuclei. Recently, it was conjectured that the RMT predictions would be applicable to all chaotic systems, including random dynamic systems. Considering a large matrix whose elements are random variables, the main aim of RMT is to determine the statistics of the eigenvalues and eigenvectors. Of particular interest to dynamic analysis is a special type of random matrix known as the Gaussian Orthogonal Ensemble (GOE). It has been observed by many authors that the statistics of the eigenvalues of a dynamic system with a high degree of uncertainty follow the GOE statistics. It was based on the assumption of GOE statistics that a theory for the prediction of the energy density variance was developed.

In what follows some concepts from RMT that are important for the present study are reviewed and discussed, together with some numerical results with the aim of verifying the agreement between the statistics of the eigenvalues of elastic systems and the RMT models. The mathematical details concerning RMT and the derivation of its results are beyond the scope of this work and will not be discussed in detail; more information is available in [10,94,96].

3.2 GAUSSIAN ENSEMBLES

A brief introduction to RMT was presented in Chapter 1 and it was seen that the initial aim of the field was to obtain a statistical description of the energy levels associated with complex nuclei. Deterministic models based on quantum mechanics are available and the energy levels can be described by the eigenvalues of a Hermitian matrix operator called Hamiltonian. However, the ensembles of Hamiltonians obtained directly from nuclear data are quite complex and analytical solutions for their statistics do not appear to be available. However, idealized ensembles of Hamiltonians have been defined following basic requirements in order to make them mathematically tractable and ensure that their statistics would be applicable to the nuclear-table ensembles [94]. The three best known ensembles of

random matrices are: the Gaussian Orthogonal Ensemble (GOE), the Gaussian Unitary Ensemble (GUE) and the Gaussian Symplectic Ensemble (GSE). All the ensembles are invariant under time reversal and orthogonal transformations [10].

The GOE is the most important ensemble for practical application. Many results suggest that not only the energy level fluctuations of nuclei but also the eigenvalues of dynamic systems follow its behaviour. The ensemble is formed by random symmetric matrices, with the entries having zero mean and being uncorrelated Gaussian random variables, with the diagonals having twice the variance of the off-diagonal elements. This structure has little relation with the matrices arising from the mathematical model of any dynamical system, but even so the statistics of their eigenvalues are surprisingly similar [97]. More details about the statistics of GOE are presented in the following sections.

The GUE corresponds to the GOE for Hermitian matrices which are statistically invariant under unitary transformation. The last ensemble is the GSE composed of quaternion-real self-dual matrices, being statistically invariant under a symplectic transformation. Following Langley in [97], the ‘universality’ principle states that large random matrices with the specified structures (random symmetric, random Hermitian or random quaternion-real self-dual matrices) would have eigenvalue statistics following one of the Gaussian ensembles. More information about GUE and GSE and their statistics can be found in [10].

3.3 EIGENVALUE STATISTICS

As seen in Chapter 1, the main aim of the RMT would be the derivation of the jpdf of the eigenvalues. The jpdf fully describes the statistics of the eigenvalues but it includes a large amount of information which is not always necessary. In fact, most studies on RMT were actually interested in lower order statistics which are more easily obtained and analysed. The first studies in RMT where interested in the pdf of the spacing between successive energy levels (also called Nearest Neighbour Spacing Distribution – NNSD). Wigner in 1957 [100] was the first to propose that the pdf of the energy level spacings would have a specific distribution, in this case the Rayleigh distribution (also called the Wigner distribution in the physics literature). Wigner’s statement is now commonly known as the “Wigner Surmise” and has been supported by many experimental results.

A simple numerical example is sufficient to show the applicability of the Wigner Surmise and its characteristics. An ensemble of matrices with size 50x50 was generated numerically. The elements of the matrices were randomly chosen assuming a normal distribution and zero mean with the diagonal terms having variance equal to 2 and the off-

diagonal terms having a variance of 1. The eigenvalue problem was then solved and the spacing between eigenvalues calculated for each matrix of the ensemble. The pdf was obtained for the 25^{th} spacing. Figure 3.1 shows the exponential and Gaussian pdfs together with the Rayleigh pdf and the numerical results for the ensemble of matrices described. A perfect agreement between the numerical results and the Rayleigh distribution can be observed, which shows that the results are in agreement with the Wigner surmise. The fact that the results conform well to the Wigner surmise is not surprising since the statistical structure adopted for the ensemble of matrices is the same as the GOE structure. A phenomenon usually referred to in the physics literature as the "level repulsion" [87,94,95] and associated with the Wigner Surmise can also be noted in Figure 3.1. The phenomenon is characterized by a tendency of the eigenvalues to repel each other, avoiding clustering and, consequently, small spacings have a low probability of occurrence. The Rayleigh distribution is also characterized by a low probability of large spacings occurring.

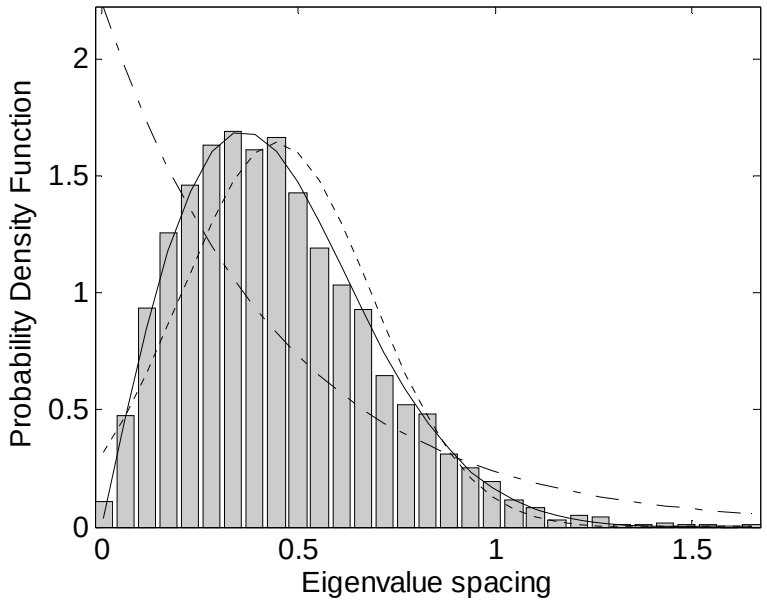

Figure 3.1 – Probability density function (pdf): – - – exponential pdf, ------ Gaussian pdf, —— Rayleigh pdf, ▭ numerical results for a matrix with GOE structure (size 50x50, 5000 member ensemble).

The pdf of the spacings is an important statistical feature, however, of much more practical interested are the so-called "correlation functions" of the eigenvalues. In fact, most applications of the RMT predictions are performed through the use of the correlation functions. The correlation functions are defined by Mehta [10] as the probability density of finding an eigenvalue in each of the small non-overlapping regions of length $d\lambda$ centred in the points of the eigenvalue space $\lambda_1, \lambda_2, \ldots, \lambda_k$ and, in the case of the *k*th correlation function is

given by

$$R_k(\lambda_1,\lambda_2,\ldots,\lambda_k)=\frac{N!}{(N-k)!}\int\int\ldots\int p(\lambda_1,\lambda_2,\ldots,\lambda_N)\mathrm{d}\lambda_{k+1}\mathrm{d}\lambda_{k+2}\ldots\mathrm{d}\lambda_N\,, \qquad (3.1)$$

where N is the size of the system and $p(\lambda_1,\lambda_2,\ldots,\lambda_N)$ is the jpdf of the eigenvalues. As can be observed, the calculation of the kth correlation function requires an N - k fold integration, which is a quite complex task given the nature of the integrand. However, in the case of the Gaussian ensembles mentioned before, the integration can be performed using methods like the supersymmetry method [10,96]. An important case occurs for $k = 2$ and the function is known as the "two-point correlation function" $R_2(\lambda_1, \lambda_2)$. The two-point correlation function can be interpreted as the probability density that at least two eigenvalues are found in two distinct small regions $d\lambda$ around λ_1 and λ_2, regardless of the occurrence of eigenvalues outside these regions. Without loss of generality, one can write

$$R_2(\lambda_1,\lambda_2)=R_2(\lambda_1-\lambda_2)=R_2(\Delta\lambda)=1-Y_2(\Delta\lambda), \qquad (3.2)$$

where it is anticipated that R_2 is dependent only on the difference between the two eigenvalues. Also shown is the relation between R_2 and the function Y_2, known as the "two-level cluster function". The two-level cluster function is given by Stockmann [96] for the GOE case as

$$Y_2(\Delta\lambda)=\left(\frac{\sin\pi\Delta\lambda}{\pi\Delta\lambda}\right)^2+\left[\frac{\pi}{2}\mathrm{sgn}(\Delta\lambda)-Si(\pi\Delta\lambda)\right]\left[\frac{\cos\pi\Delta\lambda}{\pi\Delta\lambda}-\frac{\sin\pi\Delta\lambda}{(\pi\Delta\lambda)^2}\right], \qquad (3.3)$$

where $sgn(\Delta\lambda)$ is the signum function

$$\mathrm{sgn}(\Delta\lambda)=\begin{cases}1 & \Delta\lambda>0\\ 0 & \Delta\lambda=0\\ -1 & \Delta\lambda<0\end{cases}, \qquad (3.4)$$

and $Si(x)$ is the integral sine function given by

$$Si(x) = \int_0^x \frac{\sin t}{t} \mathrm{d}t \,. \tag{3.5}$$

The reason for the function Y_2 being cited here is that its Fourier transform is used by Langley and Brown [91] in their derivation of the energy density relative variance. The function Y_2 is the link between the variance theory and the RMT. Figure 3.2 shows the two-point correlation function R_2 for the GOE model and the Poisson model. The low levels of R_2 for low $\Delta\lambda$ mean that, as an eigenvalue occurred in $\Delta\lambda$ = 0, there is a low probability of finding another eigenvalue close to that initially considered. In the Poisson model, as there is no correlation between the eigenvalues (eigenvalues are independent), the probability of finding another eigenvalue at $\Delta\lambda$ of a given eigenvalue is constant and equal to one.

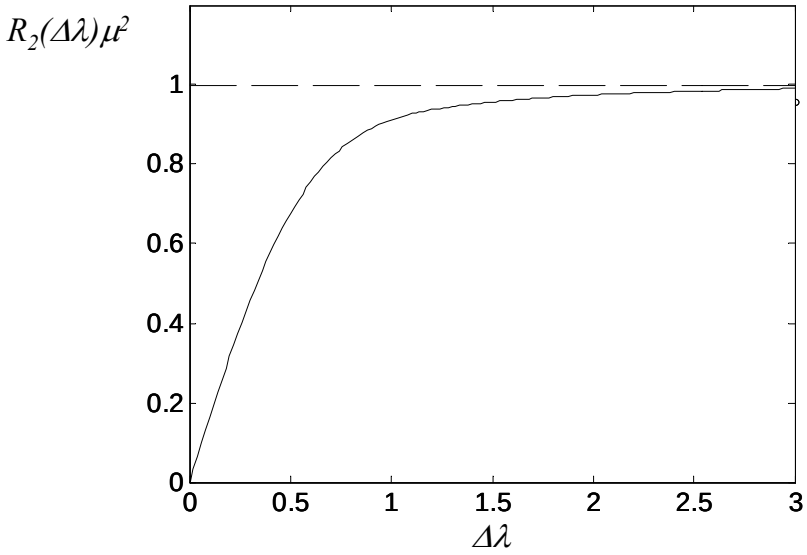

Figure 3.2 – Two-point correlation function: — — Poisson model, ——— GOE model.

There has been much work on verifying the agreement between the statistics of a sequence of numbers and the statistics of one of the Gaussian ensembles [87,91,96,101]. The question is of great importance since to apply the theoretical statistics with confidence one should check experimentally the validity of the assumptions. Different approaches have been used depending on the available data and the statistics that one is interested in applying. For example, in [87], Weaver was interested in verifying the occurrence for dynamic systems of the two phenomena predicted by the RMT: the “level repulsion” and the “spectral rigidity”. In his study, Weaver considered the pdf of spacings and two other statistics known as the number variance and the Δ_3 function to verify the applicability of the GOE statistics.

In this thesis, the main interest is in the use of the Y_2 function for the statistics of

the eigenvalues of dynamic systems. One possibility would be to compare the theoretical two-level correlation function R_2 with experimental or numerical data. Unfortunately, numerical tests showed that the size of the ensemble necessary for the convergence of experimental two-level correlation function is considerably large. Figure 3.3 shows the results for R_2 for different sizes of the ensemble considering the same matrix described in the previous numerical example (Figure 3.1). The results for R_2 were calculated as the mean of 5 eigenvalues ($23 \leq \lambda \leq 27$) to speed up the convergence. Even so, it is possible to observe that an ensemble of 5,000 members still has an oscillation around the theoretical results. The convergence of R_2 would be between an ensemble size of 5,000 and 100,000 members.

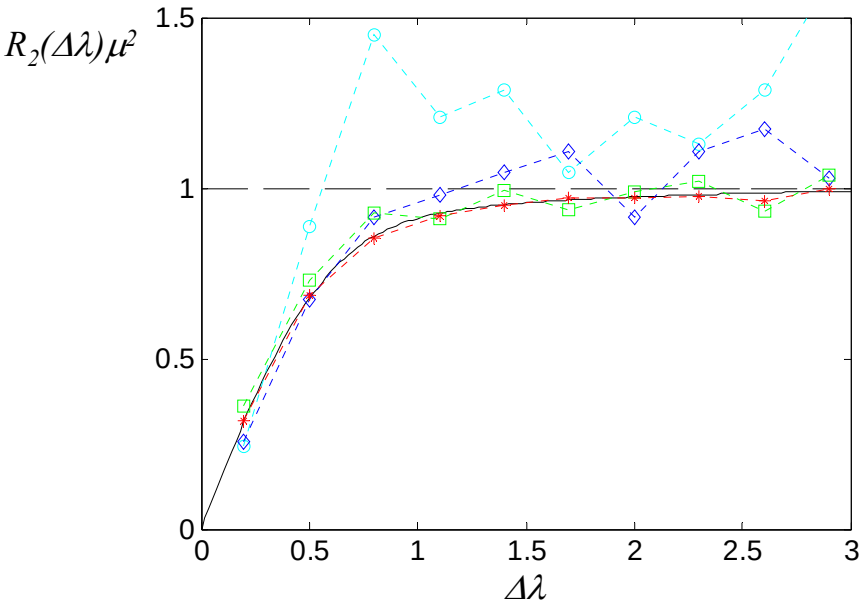

Figure 3.3 – Convergence of the R_2 function: —— GOE model, — — Poisson model, ---○--- 100 member ensemble, ---◇--- 500 member ensemble, ---□--- 5000 member ensemble, ---✳--- 100000 member ensemble.

The convergence issue made the use of R_2 for the present study impractical. However, Y_2 (and consequently R_2) are directly related with the concept of spectral rigidity. Therefore, use will be made of the same statistics used by Weaver to check the "spectral rigidity": the number variance Σ^2 and the Δ_3 function. These two statistics were first introduced by Dyson and Mehta [125] and were chosen here as they are directly related with the Y_2 function and have a much faster convergence. There are many other statistics used in the literature to verify the agreement with GOE results. A review of these statistics can be found in [10,94]. The two statistics adopted here are considered the most popular ones [10].

The number variance refers to the variance in the number of eigenvalues lying in a

range of length $\Delta\lambda$ centred on a given λ or

$$\Sigma^2(\Delta\lambda) = \left\langle \left(n(\lambda, \Delta\lambda) - \frac{\Delta\lambda}{\mu} \right)^2 \right\rangle, \tag{3.6}$$

where μ is the mean spacing between successive natural frequencies. The relation between the number variance and the two-level cluster function Y_2 is given by

$$\Sigma^2(\Delta\lambda) = \Delta\lambda - \mu^2 \int_0^{\Delta\lambda} (\Delta\lambda - r\mu) Y_2(r\mu) \mathrm{d}r \,. \tag{3.7}$$

Once more, the example previously described is used to verify the number variance convergence. Figure 3.4 gives the number variance for different ensemble sizes. It can be observed that the convergence is much faster than that obtained for the R_2 function, even though the calculation considered only one eigenvalue while the R_2 considered the mean for five eigenvalues. An ensemble size around 500 members would be enough to obtain results with an acceptable oscillation.

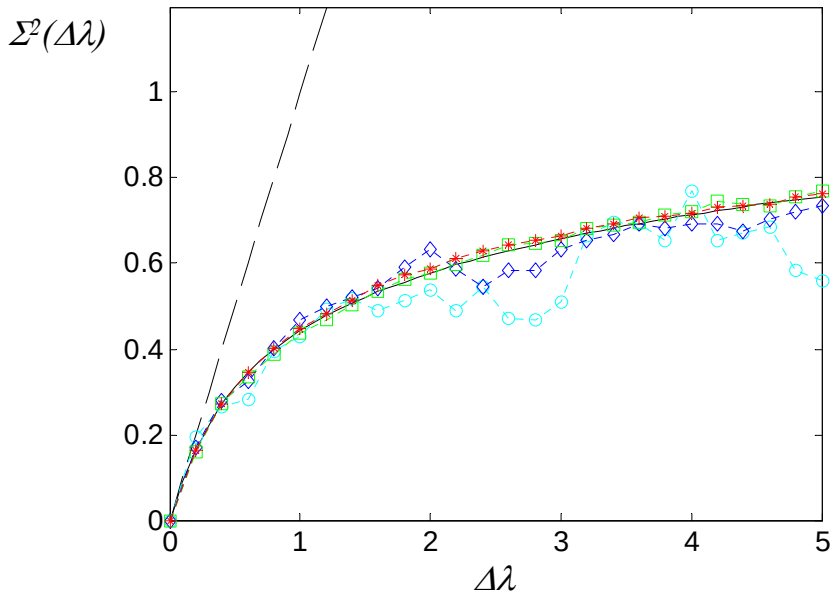

Figure 3.4 – Convergence of the number variance. —— GOE model, — — Poisson model, ---○--- 100 member ensemble, ---◇--- 500 member ensemble, ---□--- 5000 member ensemble, ---✱--- 100000 member ensemble.

In the physics literature, it was customary to present the experimental results for a sequence of numbers as a staircase function $n(\lambda)$. Drawing a line with the same slope as the staircase, it was possible to calculate the average spacing of the numbers. Figure 3.5 gives an example of a staircase function, in this case associated with one of the matrices of the previous example ensemble. The Δ_3 statistic was introduced as a way of verifying if the overall irregularity of the sequence considered would follow the statistical model predicted by RMT. Therefore, the Δ_3 function is defined as the mean-square deviation of the staircase function away from its best straight line fit for a given range $\Delta\lambda$, or

$$\Delta_3(\Delta\lambda) = \left\langle \min_{a,b} \int_{\lambda-\Delta\lambda/2}^{\lambda+\Delta\lambda/2} [n(\lambda) - a - b\lambda]^2 \, \mathrm{d}\lambda \right\rangle, \tag{3.8}$$

where *a* and *b* are the minimum coefficient associated with the best straight line fit.

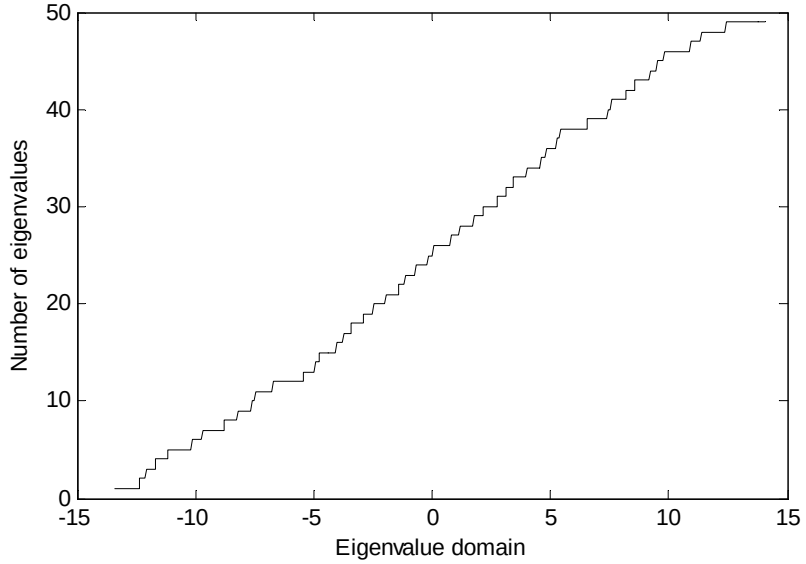

Figure 3.5 – Example of staircase function.

The Δ_3 function may also be related to the two-level cluster function Y_2 by

$$\Delta_3(\Delta\lambda) = \frac{\Delta\lambda}{15} - \frac{\mu^2}{15\Delta\lambda^4} \int_0^{\Delta\lambda} (\Delta\lambda - r\mu)^3 \left[2\Delta\lambda^2 - 9\Delta\lambda r\mu - 3(r\mu)^2\right] Y_2(r\mu)\mathrm{d}r \,. \tag{3.9}$$

In some references, the equations for the relation between number variance and the two-level cluster function or between the latter and the Δ_3 functions may vary from Equations (3.7) and (3.9), as some authors adopt the assumption of a unitary mean spacing between

eigenvalues. The convergence behaviour of the Δ_3 function is shown in Figure 3.6. In view of the much faster convergence, only the curves for ensemble sizes of 100 and 500 members are shown. An ensemble of 100 members was enough for the Δ_3 function to converge and a nearly perfect match can be observed between numerical and theoretical results.

Also shown in Figure 3.4 and Figure 3.6 are curves associated with the Poisson model, once a popular model for the statistics of the eigenvalues of a dynamic system. Both functions are given by Weaver [87] for a system with Poisson statistics as

$$\Sigma^2{}_{Poisson}(\Delta\lambda) = \Delta\lambda\,, \tag{3.10}$$

$$\Delta_{3\,Poisson}(\Delta\lambda) = \frac{\Delta\lambda}{15}\,, \tag{3.11}$$

A low value of the number variance Σ^2 and the Δ_3 function suggests a high degree of correlation between eigenvalues, in other words, a high spectral rigidity. The numerical procedures used to calculate the Σ^2 and Δ_3 statistics can be quite tricky and were implemented using MATLAB®. The file with the MATLAB® code is given in Appendix B.1. As a consequence of their faster convergence and popularity with other authors, the Σ^2 and Δ_3 will be used in this study to verify the agreement of the eigenvalue statistics of dynamics systems with GOE predictions.

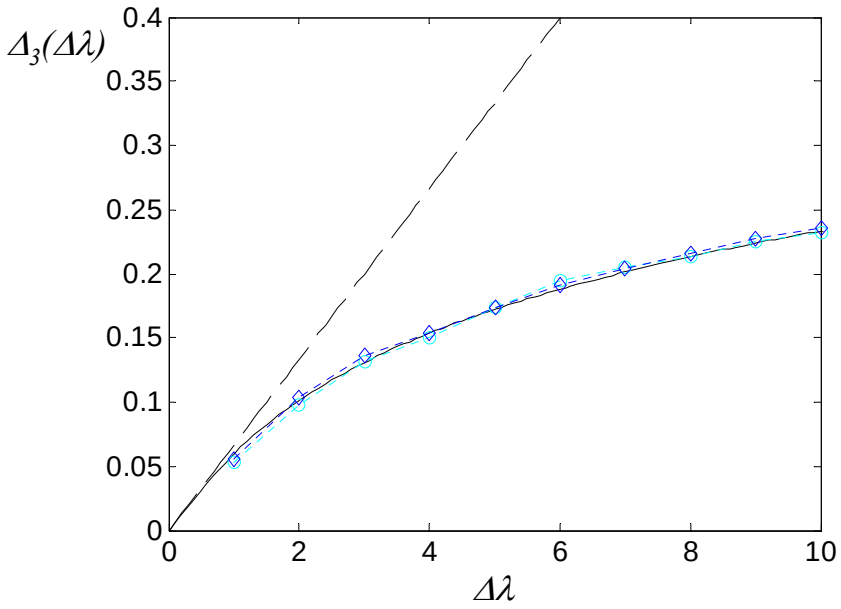

Figure 3.6 – Convergence of the Δ_3 function: —— GOE model, — — Poisson model, ----○---- 100 member ensemble, ----◇---- 500 member ensemble.

3.4 UNIVERSALITY CONCEPT AND APPLICATIONS OF RMT TO DYNAMIC SYSTEMS

The agreement between the numerical pdf and Rayleigh's distribution observed in Figure 3.1 is not surprising as the ensemble considered is one of the Gaussian ensembles. However, many experimental results suggest that the GOE prediction would be applicable to systems represented by random matrices that do not follow the GOE structure. This phenomenon is related with the previously mentioned concept of universality.

The concept was first introduced by Bohigas *et al.* in [95] where tools from the RMT were used to compare the level fluctuations of the quantum Sinai's billiard (a billiard shape used in the study of quantum mechanics) with the GOE predictions. Really good agreement was observed and led Bohigas *et al.* to conjecture that provided the system is sufficiently chaotic the GOE eigenvalue statistics would be applicable.

Langley in [97] investigated the conditions required for a random matrix to display universal statistics associated with one of the Gaussian ensembles. Langley adopted a different approach to derive local eigenvalue statistics from the conditional jpdf of the eigenvalues based on the trapezoidal integration rule and thus avoiding the use of the supersymmetry method or consideration based on the quaternion determinants. A condition for the occurrence of universal statistics was derived and it was shown that it corresponds to a sufficient degree of randomization of the eigenvectors.

The universality concept and its wide applicability may be observed through another numerical example. Let's consider a random matrix where each term can assume only values of -1 and 1. The statistical structure of this matrix is totally different from the GOE structure. The entries are not Gaussian variables. In fact, their pdfs are formed by two delta functions at -1 and 1. There is also no distinction between diagonal and off-diagonal terms. It would be hard to expect that any relation between the statistics of the eigenvalues of this matrix and GOE would exist. Again, a matrix of dimensions 50x50 was considered and the eigenvalues were calculated and the pdfs of the spacings between eigenvalues obtained. Figure 3.7 compares the numerical results for the 25^{th} spacing with the Exponential, Gaussian and Rayleigh distributions. Surprisingly, the results conform considerably well with the Rayleigh distribution. A question arises that if the GOE results are applicable to a random matrix like the one considered in Figure 3.7, why would they not be applicable to a random dynamic system.

After Bohigas *et al.* [95] presented their conjecture that RMT prediction would be applicable to any sufficiently chaotic system, many authors developed studies to verify this assumption in different fields. Weaver [87] was the first to verify its applicability to

elastodynamic systems and to have his results published outside the physics literature. Weaver carried out his studies through the experimental analysis of aluminium blocks. Cuts were drilled in the sides of the blocks to break the symmetries. The natural frequencies of three rectangular blocks with different degrees of symmetry were then measured using equipment designed for the investigation of ultrasound at acoustic emission frequencies of hundreds of kilohertz. The equipment allowed the measurement of hundreds of natural frequencies and the identification of their position with a good resolution. The data was analyzed in order to normalize the spacing between natural frequencies. The procedure was necessary since the GOE theory assumes a constant spacing, while a 3D structure like the blocks would have an increasing modal density (a decreasing spacing) with frequency. The pdf, Σ^2 and Δ_3 were calculated considering a frequency average and compared with the GOE predictions. It was observed that the blocks with all symmetries broken displayed GOE statistics, while the block that had one of its symmetries left showed results similar to the predictions for a system with two overlapping GOE groups. In [88] Weaver, applied the GOE model (by considering the Y_2 function for the natural frequencies) to the prediction of reverberation room spectral fluctuations, extending a previous derivation develop by Davy [84,86].

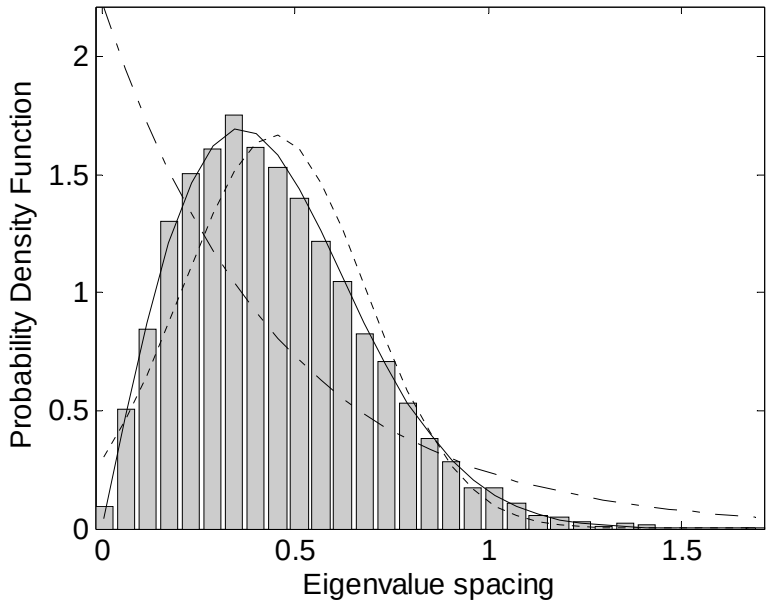

Figure 3.7 – Probability density function (pdf): – - – Exponential pdf, ------ Gaussian pdf, —— Rayleigh pdf, ▭ numerical results for a matrix with {-1,1} entries (size 50x50, ensemble of 5000 members).

Ellegaard *et al.* developed a similar study in [102]. Aluminium blocks were again used, but Elleggard *et al.* showed that it would be possible to obtain not only GOE statistics but also statistics similar to the Poisson model. This was achieved when carrying out the same

measurements for a perfect cubic block with no cuts. The transition between the Poisson model and the GOE model was observed by machining octants of a sphere from one of the corners of the original block. The work was extended in [103], where Ellegaard *et al.* used quartz blocks and considered a greater number of cases with different radii of the octant extracted from the original block. The results were compared with GOE results for a single spectrum and for a superposition of spectra, whose results are also predicted in the RMT.

Numerical verification of the agreement between the statistics of natural frequencies of dynamic systems and GOE predictions were performed by Burkhardt and Weaver [105] for membranes with irregular shapes. They were especially interested in the effect of damping in the prediction. Burkhardt and Weaver considered a mix of spectra and ensemble average by calculating the statistics from a combination of the natural frequencies of 10 realizations. It is found that the natural frequencies of a damped dynamic system are consistent with the predictions of the GOE provided damping is moderate. As dissipation levels rise, results indicated that the agreement between GOE predictions and observed statistics weakens.

Bertelsen *et al.* [101] also investigated the pdf, the number variance Σ^2 and the Δ_3 function of the eigenvalues for plates through experiments. The results showed a good agreement with the superposition of two independent GOE spectra, since the data obtained included both flexural and longitudinal waves. By introducing cuts in the surface of the plate, Bertelsen *et al.* obtained the coupling of the two wave types and the resulting statistics for the natural frequencies conformed well to a single GOE spectrum.

In [106], Ellegaard *et al.* presented an overview of the use of elastodynamic systems as an analogue case to quantum systems for the study of RMT and its applications. Ellegaard *et al.* give an introduction to wave theory in solids and review some results from other authors showing the agreement between experimental results and RMT predictions. Some results are presented for plates with different shapes and degrees of symmetry and similar conclusions to those of Bertelsen *et al.* [101] are obtained. However, Ellegaard *et al.* extend the analysis comparing eigenvector amplitude distribution with the Porter-Thomas distribution predicted by the RMT, obtaining good agreement. The distribution of peak amplitudes (related with damping) is also investigated. The damping level is varied by changing the air pressure to which the structure is exposed. This method also allowed the separation between flexural and in-plane modes, as only the former ones have their damping affected. Therefore, it was possible to obtain the NNSD for only the flexural modes, which matched the results for a single GOE spectrum.

The application of GOE statistics to dynamic systems is verified numerically by

Langley and Brown in [91]. At first, a rectangular plate was considered and the pdf of the spacing between natural frequencies (spectrum average) conformed to the Poisson model. The plate was then loaded with masses randomly distributed. The masses were responsible for breaking the symmetry of the system and then coupling the modes, which resulted in a spacing pdf close to a Rayleigh distribution. Langley and Brown also verified the correlation between the natural frequencies. In the case of the plate with random masses, a good agreement with the GOE prediction was observed. More recently, McWillian *et al.* [107] investigated the pdf of spacings for the natural frequencies of rings with random mass imperfections. Although the authors do not mention RMT and its predictions, the NNSD is compared with the Rayleigh distribution with a good agreement.

As seen in some of the above mentioned studies, the RMT also allows the prediction of statistics of the loss factor for a chaotic system. The issue is beyond the scope of this study and it is not further discussed here. However, the application of RMT for the statistical modelling of the damping of random dynamic systems has been the subject of recently published papers [104,108].

3.5 SYMMETRIES AND ERGODICITY

An important issue regarding the application of the RMT for dynamic systems is related to the presence of symmetries in the system. Many authors have observed, when studying the statistics of the eigenvalues of dynamic systems, that the occurrence of symmetries results in a deviation of the experimental data from the GOE predictions [87,101,103,106]. It was argued that the symmetries allow the existence of two or more independent sets of eigenvalues with GOE characteristics. In many cases, the statistics obtained experimentally were compared with the RMT prediction for two overlapping GOE groups and a good level of agreement was observed. The statistics for the case of two superimposed independent GOE spectra of equal mean spacing are given in [87] as

$$\Sigma^2_{comp}(\Delta\lambda) = 2\Sigma^2_{GOE}(\Delta\lambda/2), \tag{3.12}$$

$$\Delta_{3,comp}(\Delta\lambda) = 2\Delta_{3,GOE}(\Delta\lambda/2), \tag{3.13}$$

$$p_{comp}(x) = \frac{1}{2}\left\{E_1(x/2)p_{GOE}(x/2) + \left[1 - E_2(x/2)\right]^2\right\}, \tag{3.14}$$

where Σ^2_{GOE} and $\Delta_{3,GOE}$ are statistics for a single GOE group, p_{GOE} is the Rayleigh distribution and the two integral functions are given by,

$$E_1(y) = \int_y^\infty [1 - E_2(z)]\mathrm{d}z \text{ and } E_2(y) = \int_0^y p_{GOE}(z)\mathrm{d}z \,. \tag{3.15}$$

The independence attributed to the two GOE overlapping groups in Equations (3.12), (3.13) and (3.14) may not be complete and a level of coupling may exist between the two groups. Therefore, an intermediate result between the two overlapping GOE spectra and a single GOE spectrum may be observed and this issue was also investigated by some authors [101,103,106]. In [103], the study was developed using quartz blocks and the level of symmetry was controlled by the size of the sphere octant machined from the block. Increasing the radius of the sphere octant, there was an increase in the coupling between the modes and it was possible to observe a transition between the two behaviours. Similar studies were performed in [101,106] considering the case of plates. It is the current understanding that a system with no symmetries would display GOE statistics, allowing one symmetry in the system would result in the statistics of two overlapping GOE groups and allowing an increasing number of symmetries would tend towards Poisson statistics.

It is likely that many engineering structures like plates or cavities will have a certain level of symmetry, at least nominally. However, it is expected that the uncertainties from the manufacturing process will be responsible for breaking the existing symmetries at a certain level. In view of what was discussed in Chapter 1, it is also expected that the level to which the symmetries are reduced will depend on the frequency. Therefore, it may be that a region in the eigenvalue domain displays GOE statistics while another displays Poisson statistics. This kind of behaviour is investigated in section 3.6.

Although not always mentioned in the studies related to RMT, it is usually assumed that the statistics of the system have ergodicity behaviour. The ergodicity assumption ensures that there exists equivalence between the theoretically calculated ensemble statistics and the physically more relevant spectral statistics. The importance of this concept comes from the fact that most of the experimental results are obtained based on spectral averages instead of ensemble averages. It is impractical to repeat measurements for a statistical representative ensemble of cases, while the spectral statistics are directly available from a single measurement. However, the ensemble statistics are the main interest in the forgoing discussion and are the statistics used in the variance theory.

The validity of the ergodicity assumption has been verified for the case of Gaussian

ensembles. Pandey in [109] gives a detailed description of the problem and presents proof for the validity of the assumption of local ergodicity for several statistics in the case of Gaussian ensembles. The term "local" here should be interpreted as that the assumption is valid for a limited region of the spectrum. In the same study, it is also shown that the statistical properties of the Gaussian ensembles can be considered as stationary, which is an important conclusion for the variance theory. Brody *et al.* [94] also discussed the concept of ergodicity, highlighting the definition of "locally generated". Weaver [87] also mentions the concept, but does not present any further explanation for considering the ergodicity assumption as valid. In fact, most of the studies mentioned above do not discuss the validity of the ergodicity assumption for random dynamic systems and the GOE statistics are believed to be applicable for ensemble averages. A verification of the ergodicity assumption for the case of random dynamic systems has not been performed before and a discussion about the concept based on numerical results is presented in the next section.

3.6 NUMERICAL ANALYSIS OF RANDOM STRUCTURES

3.6.1 Overview

Although the application of RMT to random dynamic system has been the subject of many publications, some questions still remain. The main issues are regarding the presence of symmetries and the ergodicity assumption. In what follows, the numerical procedure presented in Chapter 2 is used to generate and solve the eigenproblem for ensembles of structures. In Chapter 2, the randomization approach used aimed to reproduce the experimental ensemble which consisted of plates with randomly positioned masses. In the following analysis, spectral and ensemble averages are considered and different randomization approaches are investigated. The pdf of the eigenvalue spacings and the statistics given in section 3.3 (number variance Σ^2 and Δ_3 function) are used to verify the agreement of the eigenvalue statistics with the RMT predictions for the GOE case.

3.6.2 Spectral average

An initial analysis was carried out considering the spectral average to calculate the eigenvalue statistics. Structures with different shapes were analysed with the shapes being defined in order to obtain a transition between a symmetric system formed by a rectangular plate to a plate with an irregular shape. Figure 3.8 gives the shapes and dimension of the two extreme cases considered, with the rectangular plate being defined as Case A1 and the

irregular shape plate being named Case A4. The dimensions of the intermediate cases can be accessed in Table 3.1

Since the interest is in spectral average, there is no need to generate an ensemble of structures. Therefore, the eigenvalue problem was solved only once for each case with its nominal dimensions and 350 modes were extracted and used in the calculation of the eigenvalue statistics. The procedure presented in section 3.3 and described in detail in Appendix B.1 needed to be modified in order to allow the calculation of spectral averages. In this case, the fixed point used to calculate the above mentioned statistics when considering ensemble average was varied across the frequency (or the eigenvalue domain) to obtain spectral averages.

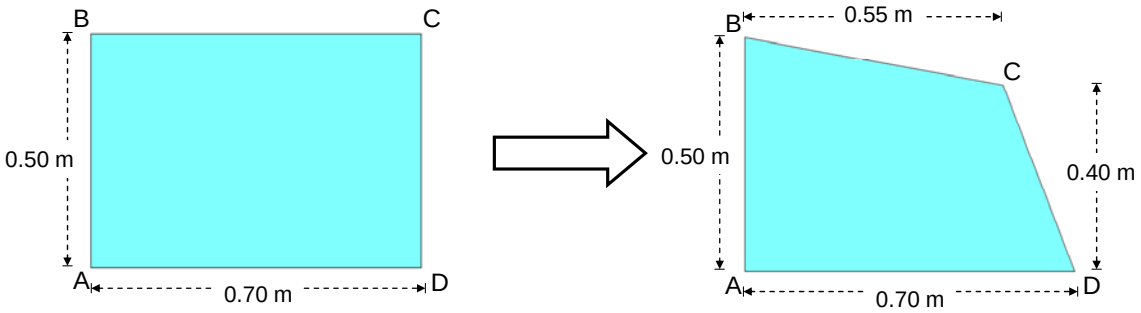

Figure 3.8 – Shifting from a rectangular plate to an irregular plate.

Table 3.1 – Plate dimensions – Cases A1 to A4.

Cases	x_C [m]	y_C [m]
A1	0.700	0.500
A2	0.650	0.466
A3	0.600	0.433
A4	0.550	0.400

The pdf of the eigenvalue spacings, the number variance Σ^2 and the Δ_3 function can be observed in Figure 3.9 for Cases A1 to A4. The results conform very well with the theory predictions for the extreme cases. As a function of its symmetries, the rectangular plate (Case A1) displayed Poisson statistics, with an Exponential distribution for the spacing pdf and the number variance Σ^2 and the Δ_3 function following the predictions given by Equations (3.10) and (3.11). As the level of symmetries is reduced, the statistics of the system change from a Poisson model to GOE statistics. A very good agreement between the eigenvalue statistics and the GOE model can be observed for Case A4, the one with the most irregular shape. The question now is if the systems would display the same statistics in an ensemble average and this is investigated in the next section.

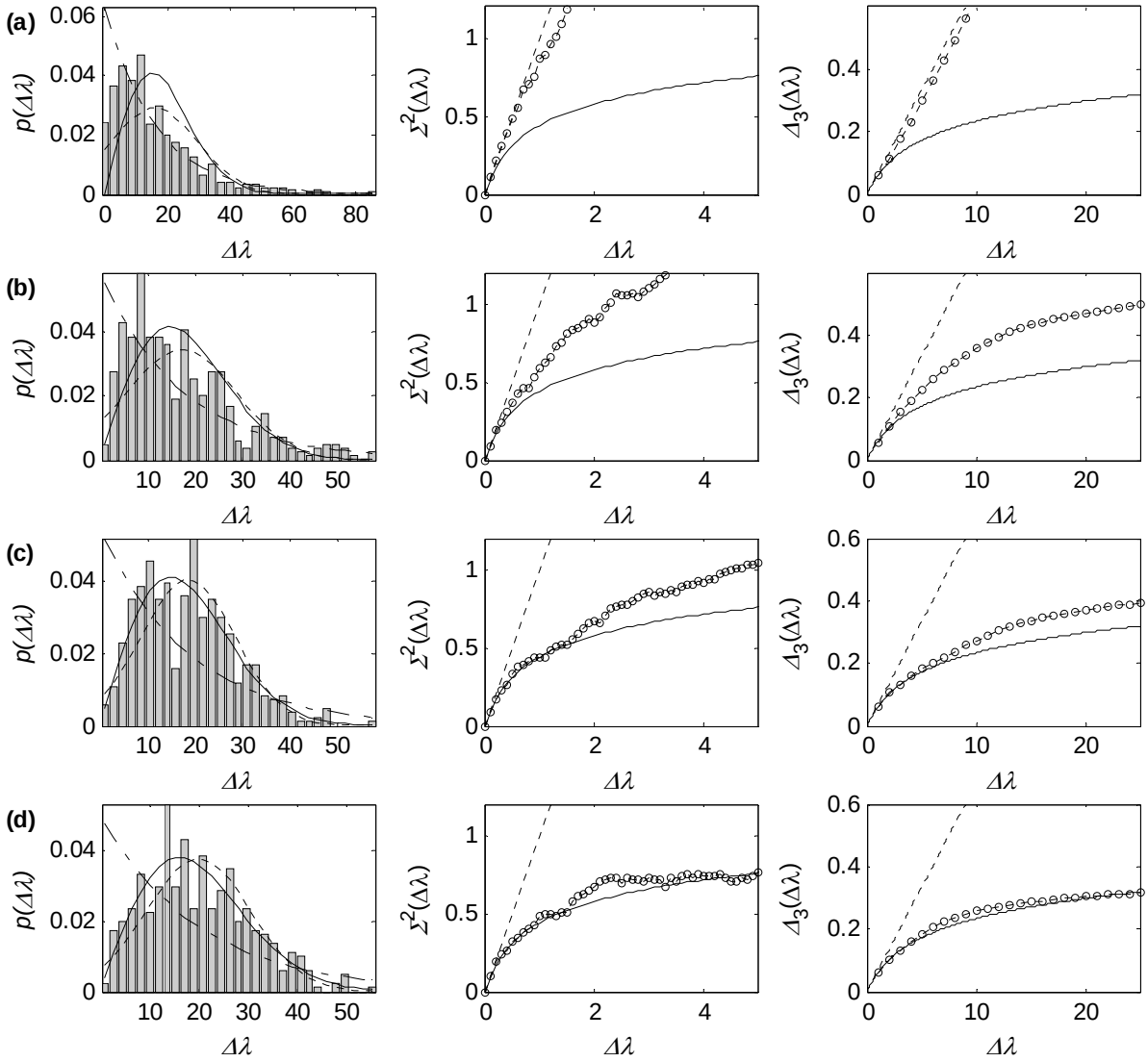

Figure 3.9 – Eigenvalue statistics (frequency average) – Breaking the symmetries. a) Case A1, b) Case A2, c) Case A3 and d) Case A4. Pdf plots: ------ Normal distribution, – - – Exponential distribution, —— Rayleigh distribution. Number variance and Δ_3 plots: —— GOE statistics, ------ Poisson statistics, -◇- numerical data.

3.6.3 Ensemble average – Breaking the symmetries

In order to study the issues regarding the application of RMT predictions for random dynamic systems, different randomization approaches (or probabilistic models) were used to generate ensembles of structures and investigate the eigenvalue statistics in an ensemble average.

The first situation investigated considered two nominally equal systems but with different randomization approaches. The probabilistic models adopted for the first two cases are given in Table 3.2 . In order to differentiate from the cases analysed in the previous section where spectral average was considered, the following cases are named as B1 to B7.

The nominal and possible shapes for cases B1 and B2 are presented in Figure 3.10 and Figure 3.11.

Table 3.2 – Ensemble average – Randomization approaches for Case B1 and B2.

Cases	**Nominal Dimensions**	**Variables**	**Statistics**
B1	Case A1	x_C and x_D	Gaussian variable, μ = 0.7 m, σ = 0.07 m (10%).
		x_B and x_C	Gaussian variable, μ = 0.5 m, σ = 0.05 m (10%).
B2	Case A1	x_C	Gaussian variable, μ = 0.7 m, σ = 0.07 m (10%).
		x_C	Gaussian variable, μ = 0.5 m, σ = 0.05 m (10%).

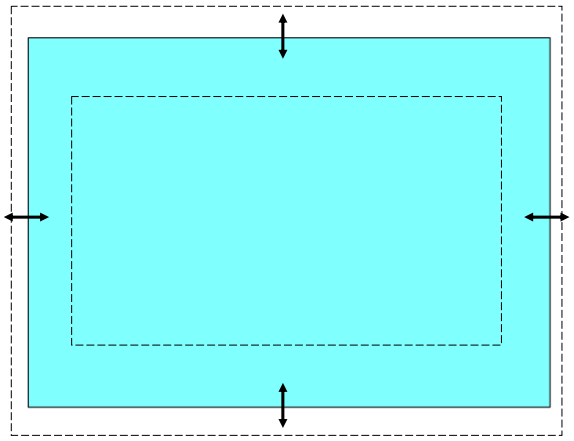

Figure 3.10 – Nominal (solid line) and possible shapes for ensemble considered in Case B1.

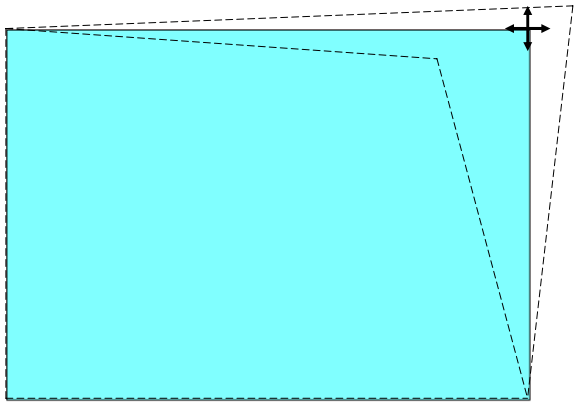

Figure 3.11 – Nominal (solid line) and possible shapes for ensemble considered in Case B2.

In Case B1, the randomization approach considers the length and width of the plate as being random variables. This probabilistic model is similar to the one used in some previous studies in SEA [71,73] and it is characterized by all the members of the ensemble being rectangular. On the other hand, the probabilistic model in Case B2 considered the

coordinates of one of the corners of the plate as being random. Therefore, irregular shapes like the ones considered in section 3.6.2 are likely to occur. The nominal dimensions are the same for both cases.

The eigenvalue statistics of Case B1 are given in Figure 3.12 for three modes or spacings: the 20th, the 70th and the 200th modes or spacings. A very good agreement between the numerical data and the Poisson model can be noted for the 70th and the 200th modes. The results for the 20th mode, although conforming reasonably to Poisson statistics for the number variance Σ^2 and the Δ_3 function, display a pdf different from the exponential pdf predicted by the Poisson model. This is due to a reduced effect of the introduced uncertainties over the first modes. Therefore, the level of mixing of the eigenvalues is reduced and an Exponential pdf is not achieved. In fact, although not shown here, it is possible to demonstrate numerically that the superposition of several independent Gaussian variables led to an Exponential pdf of the spacing between variables.

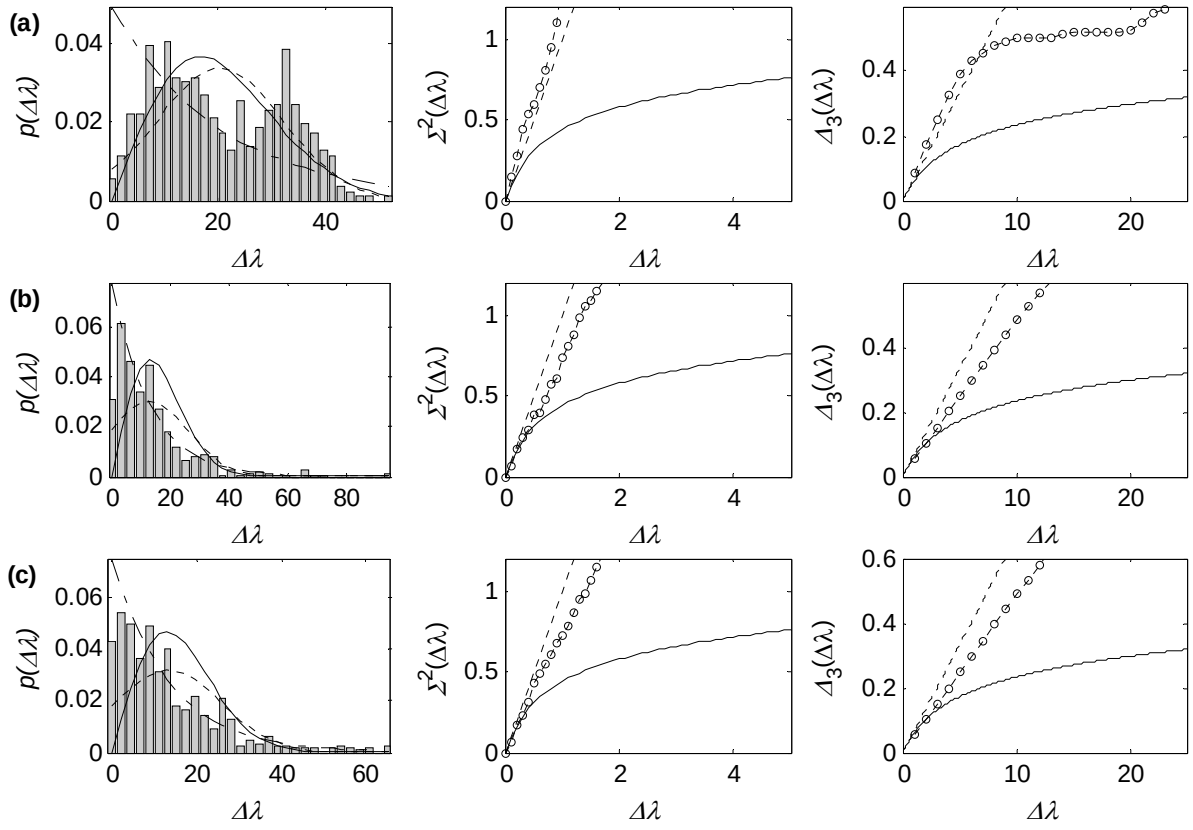

Figure 3.12 – Eigenvalue statistics (ensemble average) – Case B1. a) Mode 20, b) Mode 70 and c) Mode 200. Pdf plots: ------ Normal distribution, – - – Exponential distribution, —— Rayleigh distribution. Number variance and Δ_3 plots: —— GOE statistics, ------ Poisson statistics, -⊙- numerical data.

Figure 3.13 shows the eigenvalue statistics for Case B2. Although nominally equal, Cases B1 and B2 display completely different eigenvalue statistics. In Case B2, the adoption of a randomization approach where the symmetries are broken caused the eigenvalue statistics to shift towards the GOE predictions. It seems that the level to which the symmetries are broken is not sufficient to ensure a better agreement with the GOE model. The same behaviour observed for the pdf of the 20th spacing in Figure 3.12 is observed here, which suggests that both probabilistic models have a low level of randomization for the first modes. The results show that the occurrence of ergodicity between the spectral and ensemble average is dependent on the randomization approach adopted. The ergodicity assumption would be valid for Case B1 but it would not hold for Case B2.

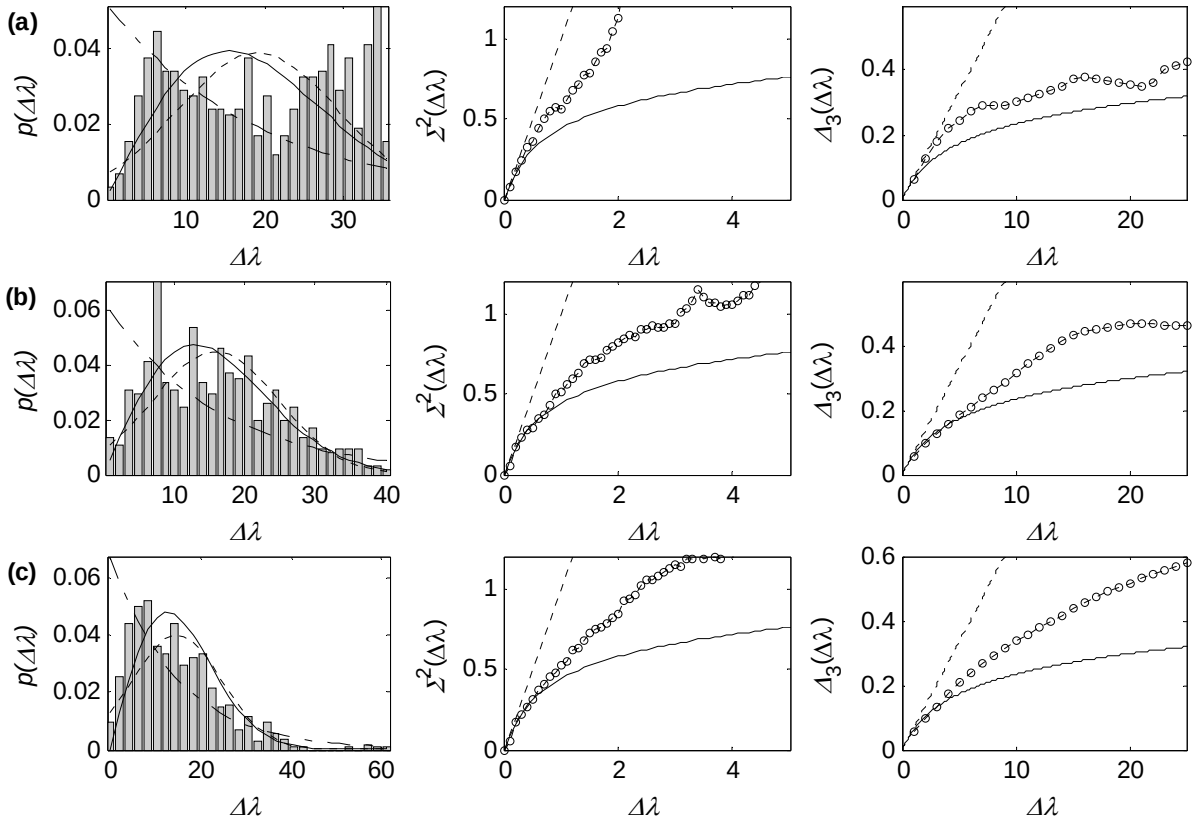

Figure 3.13 – Eigenvalue statistics (ensemble average) – Case B2. a) Mode 20, b) Mode 70 and c) Mode 200. Pdf plots: ------ Normal distribution, – - – Exponential distribution —— Rayleigh distribution. Number variance and Δ_3 plots: —— GOE statistics, ------ Poisson statistics, -⊙- numerical data.

It was shown in Chapter 1 that the statistical overlap factor is a parameter that has been previously used to quantify the level of randomness of a system and verify the occurrence of GOE statistics. The parameter is given by Equation (1.10) and it was also mentioned that the parameter fails to predict GOE statistics in certain situations. In the

literature, it is possible to find two distinct definitions for the statistical overlap factor: one considering the local mean spacing between eigenvalues and the other considering the global mean spacing. By local mean spacing one should understand the ensemble mean value of the spacing between two eigenvalues while the global mean spacing represents the mean spacing over both the ensemble and spectral domains. Figure 3.14(a) presents the global and local mean spacings together with the standard deviation of the eigenvalues. Both curves are used to calculate the statistical overlap factor. Figure 3.14(b) gives the statistical overlap factors considering both global and local mean spacing. It can be noted that a value greater than unity can be observed in both cases which, based on some publications, would suggest GOE statistics. However, it was seen from Figure 3.12 and Figure 3.13 that this is not the case.

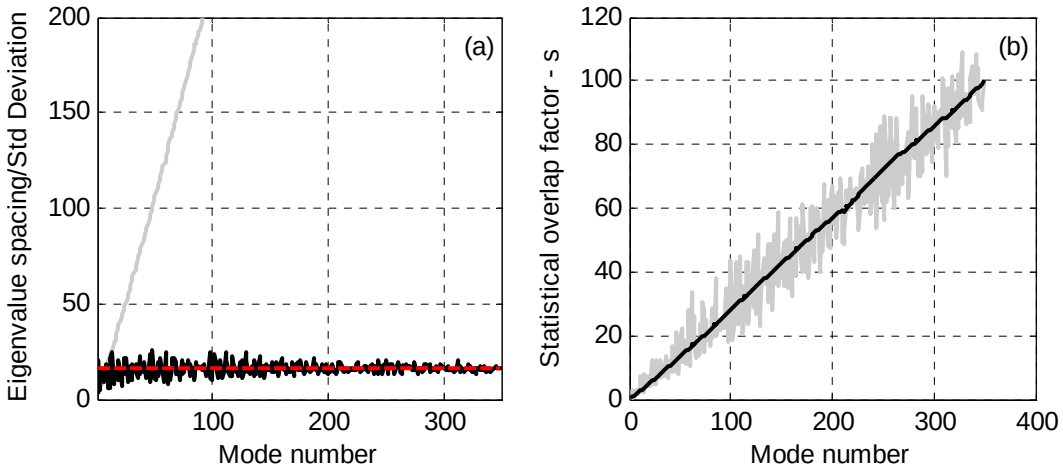

Figure 3.14 – Statistical overlap factor – Case B1. Plot (a): ----- global eigenvalue spacing, ——— local eigenvalue spacing, ——— eigenvalue standard deviation. Plot (b): Statistical overlap factor. ——— global mean spacing, ——— local mean spacing.

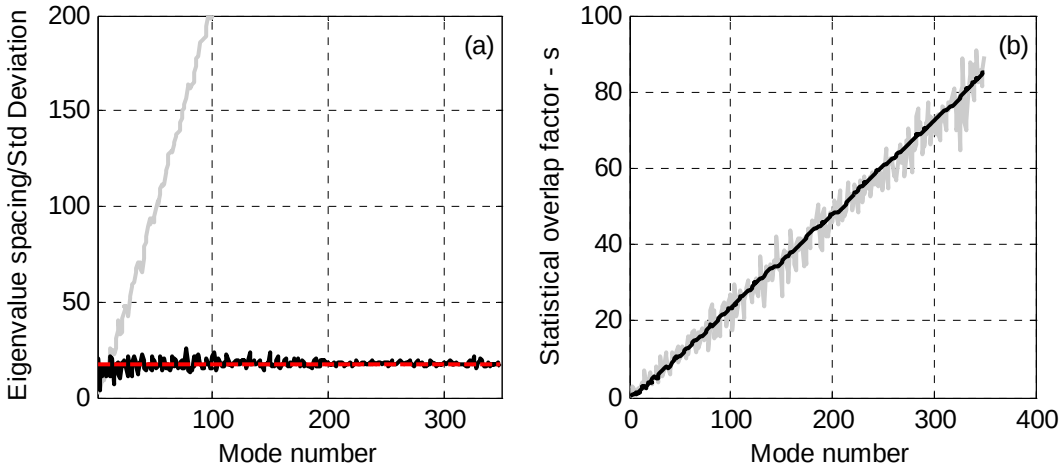

Figure 3.15 – Statistical overlap factor – Case B2. Plot (a): ----- global eigenvalue spacing, ——— local eigenvalue spacing, ——— eigenvalue standard deviation. Plot (b): Statistical overlap factor. ——— global mean spacing, ——— local mean spacing.

3.6.4 Ensemble average – Level of randomness

The next situation investigated was interested in the effects of the level of randomness in the statistics. Therefore, two cases were considered with the same random variables and the only difference being the standard deviation associated with the variables for each case. The probabilistic models considered in both cases can be accessed in Table 3.3 The nominal dimensions adopted are the same as in Case A4, which is known to display GOE statistics in a spectral average. Figure 3.16 allows the visualization of the nominal shape and of two possible outcomes.

Table 3.3 – Ensemble average – randomization approaches for Case B3 and B4.

Cases	Nominal Dimensions	Variables	Statistics
B3	Case A4	x_D	Gaussian variable, μ = 0.7 m, σ = 0.07 m (10%).
		y_B	Gaussian variable, μ = 0.5 m, σ = 0.05 m (10%).
		x_C	Gaussian variable, μ = 0.55 m, σ = 0.055 m (10%).
		y_C	Gaussian variable, μ = 0.4 m, σ = 0.04 m (10%).
B4	Case A4	x_D	Gaussian variable, μ = 0.7 m, σ = 0.014 m (2%).
		y_B	Gaussian variable, μ = 0.5 m, σ = 0.01 m (2%).
		x_C	Gaussian variable, μ = 0.55 m, σ = 0.011 m (2%).
		y_C	Gaussian variable, μ = 0.4 m, σ = 0.008 m (2%).

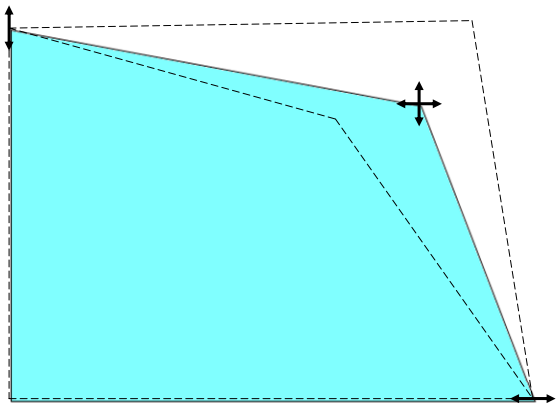

Figure 3.16 – Nominal (solid line) and possible shapes for the ensembles considered in Cases B3 and B4.

The eigenvalue statistics for Case B3 (10% standard deviation) can be observed in Figure 3.17. A very good agreement with the GOE model can be noted even for the 20th mode. On the other hand, Figure 3.18 gives the eigenvalue statistics for Case B4 (2% standard deviation). It can be observed that the pdfs display behaviours closer to the Gaussian distribution, while lower values and a more oscillatory behaviour were found for the other statistics. Lower values of the number variance Σ^2 and the Δ_3 function are usually associated with a high degree of spectral rigidity and this is in agreement with the results for a system with a low level of uncertainty. In other words, a system with low uncertainty has a spectrum with reduced variability.

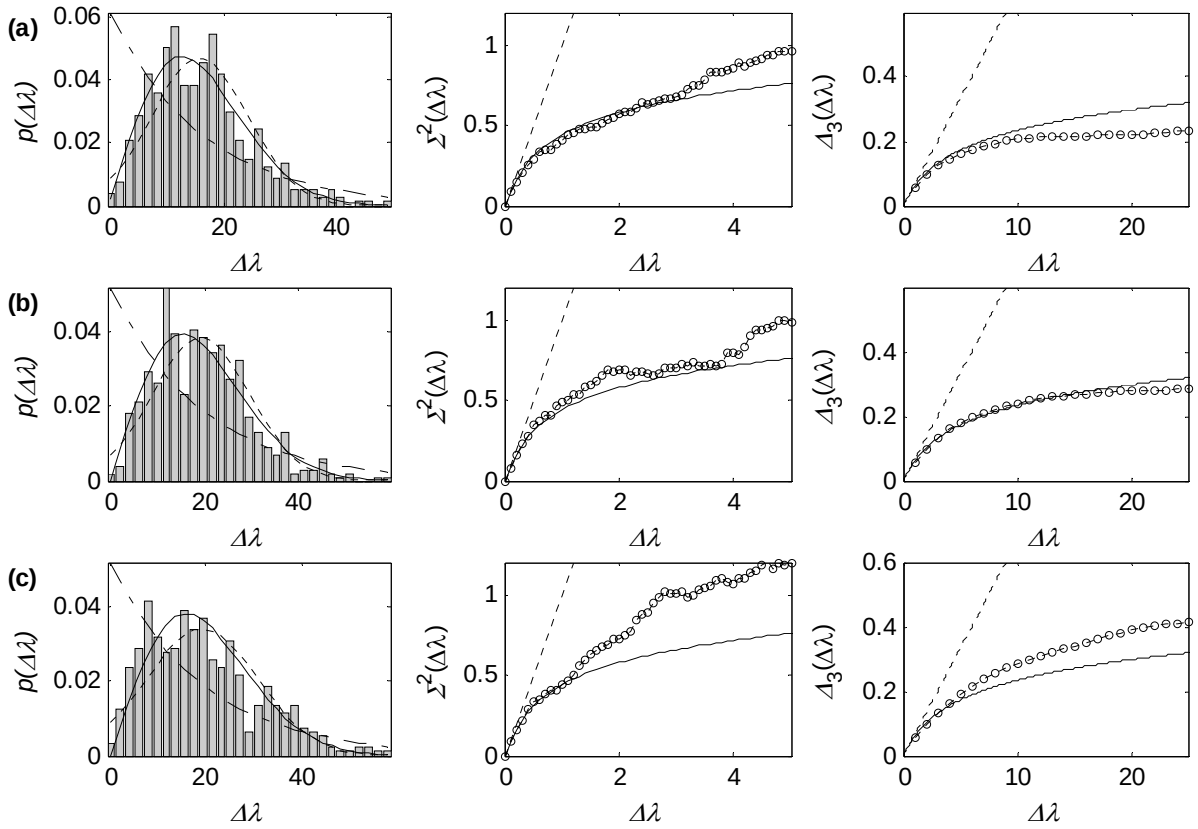

Figure 3.17 – Eigenvalue statistics (ensemble average) – Case B3. a) Mode 20, b) Mode 70 and c) Mode 200. Pdf plots: ------ Normal distribution, – - – Exponential distribution, —— Rayleigh distribution. Number variance and Δ_3 plots: —— GOE statistics, ------ Poisson statistics, -◇- numerical data.

A little surprising are the results of the number variance Σ^2 and the Δ_3 function associated with the 200th mode in Figure 3.17. Although the results for the modes with lower orders agree with the GOE predictions, the results for the 200th mode seem to deviate from the GOE model. This behaviour is probably due to a combination of effects over the eigenvalue statistics. On one side, a low level of randomness leads to a reduced value of the statistics. On

another side, the Poisson model displays values for the number variance Σ^2 and the Δ_3 function higher than the GOE prediction. Therefore, in the case of a probabilistic model where the symmetries are not completely broken and the level of randomness is continuously increased from a very low level, there will be a point where the results will display values similar to the GOE prediction, although the GOE model is not applicable. In this case, the statistics adopted here are not appropriate to verify the occurrence of GOE statistics.

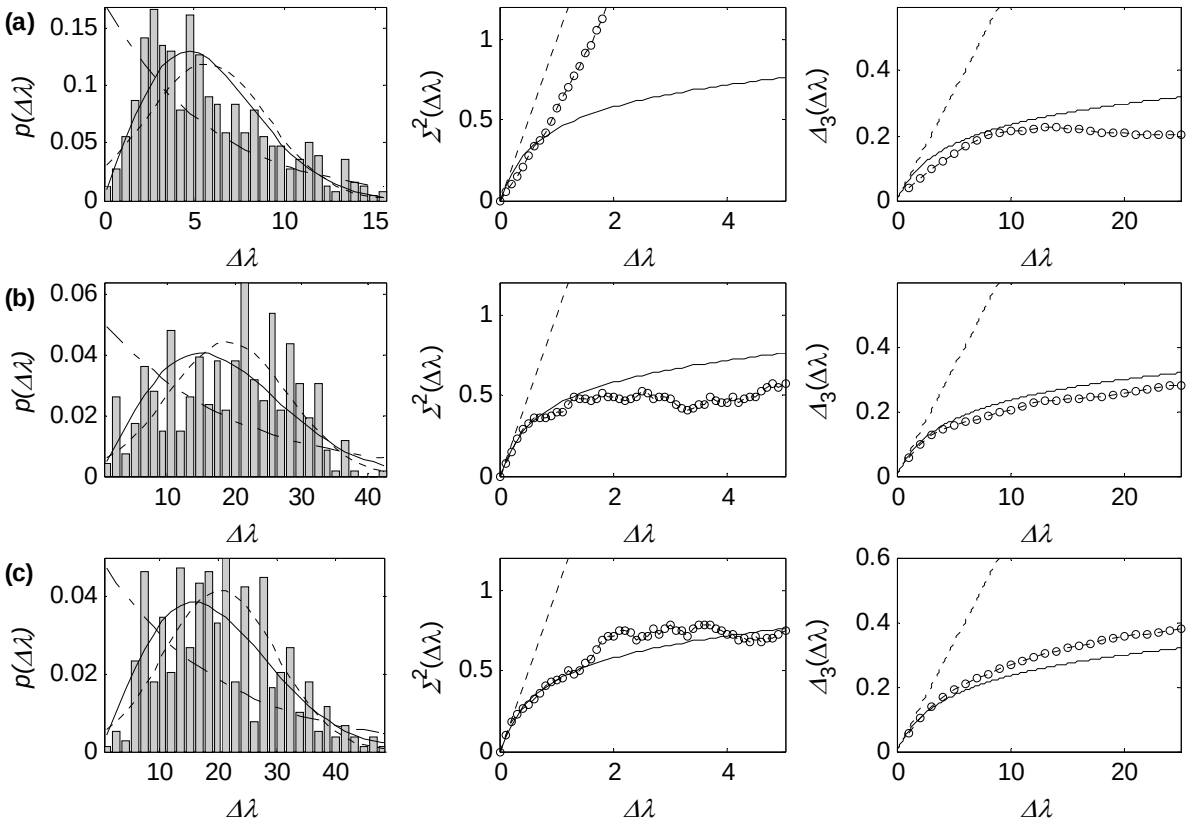

Figure 3.18 – Eigenvalue statistics (ensemble average) – Case B4. a) Mode 20, b) Mode 70 and c) Mode 200. Pdf plots: ------ Normal distribution, – - – Exponential distribution, —— Rayleigh distribution. Number variance and Δ_3 plots: —— GOE statistics, ------ Poisson statistics, -◇- numerical data.

The results for the statistical overlap factor for Cases B3 and B4 can be observed in Figure 3.19 and Figure 3.20. As expected, the values of the statistical overlap factor for Case B4 are lower than the values for Case B3. However, the results are still above the unity value for most of the frequency range.

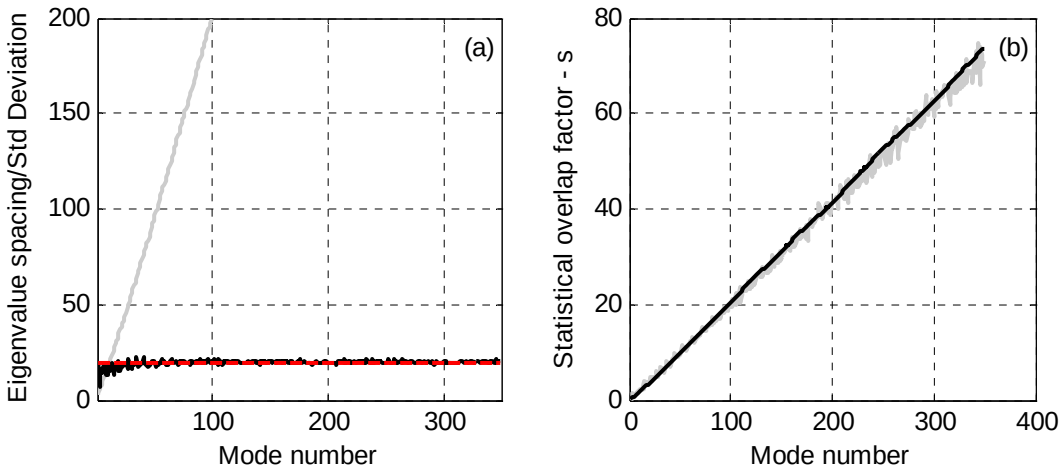

Figure 3.19 – Statistical overlap factor – Case B3. Plot (a): ----- global eigenvalue spacing, ——— local eigenvalue spacing, ——— eigenvalue standard deviation. Plot (b): Statistical overlap factor. ——— global mean spacing, ——— local mean spacing.

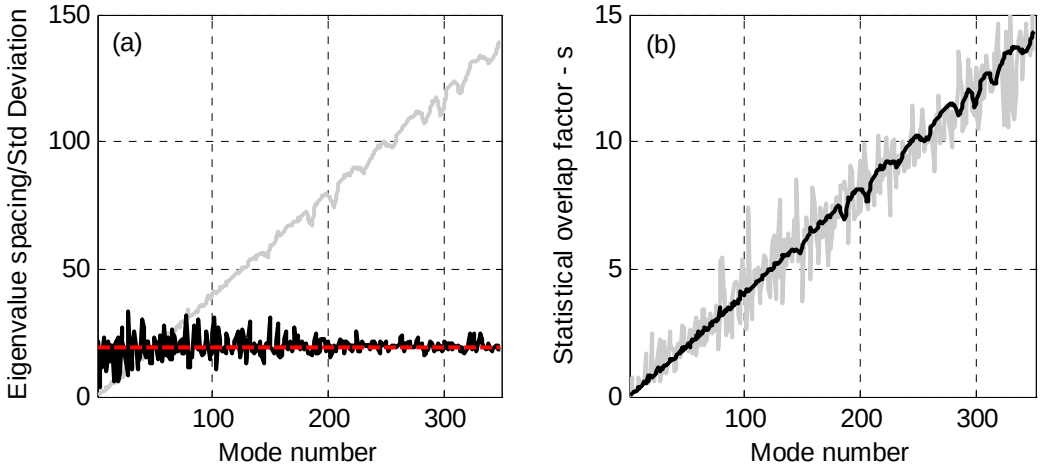

Figure 3.20 – Statistical overlap factor – Case B4. Plot (a): ----- global eigenvalue spacing, ——— local eigenvalue spacing, ——— eigenvalue standard deviation. Plot (b): Statistical overlap factor. ——— global mean spacing, ——— local mean spacing.

3.6.5 Ensemble average – Real systems and random masses

The probabilistic models considered in the previous situations allowed the investigation of some specific features of the eigenvalue statistics. However, they are considerably unreal and it is not expected that a real system would display these types of uncertainties. In the same way, the behaviour of the eigenvalue statistics observed for these cases are unlikely to be displayed by real systems. Therefore, another case was investigated where an attempt was made to adopt a probabilistic model more similar to that of a real structure and, as a consequence, obtain a behaviour for the eigenvalue statistics closer to that expected for real structures. This probabilistic model is described in Table 3.4 and named Case B5. In Case B5, the sides of a nominally rectangular plate are treated as discrete Gaussian random processes. An autocorrelation is attributed to the points of each side of the plate in order to prevent shapes with pronounced peaks or valleys since these shapes would be unlikely to occur in real structures. The plate shapes of some realizations are shown in Figure 3.21.

Table 3.4 – Ensemble average – randomization approach for Case B5.

Cases	**Nominal Dimensions**	**Variables**	**Statistics**
B5	Case A1	Side $\overline{AB}$, y fixed, x as a random process.	Gaussian random process, μ = 0.0 m, σ = 0.014 m (2 % of the nominal length), autocorrelation $R(y_i, y_j) = \exp(-\beta\|j-i\|)$
		Side $\overline{BC}$, x fixed, y as a random process.	Gaussian random process, μ = 0.5 m, σ = 0.01 m (2 % of the nominal width), autocorrelation $R(x_i, x_j) = \exp(-\beta\|j-i\|)$
		Side $\overline{CD}$, y fixed, x as a random process.	Gaussian random process, μ = 0.7 m, σ = 0.014 m (2 % of the nominal length), autocorrelation $R(y_i, y_j) = \exp(-\beta\|j-i\|)$
		Side $\overline{DA}$, x fixed, y as a random process.	Gaussian random process, μ = 0.0 m, σ = 0.01 m (2 % of the nominal width), autocorrelation $R(x_i, x_j) = \exp(-\beta\|j-i\|)$

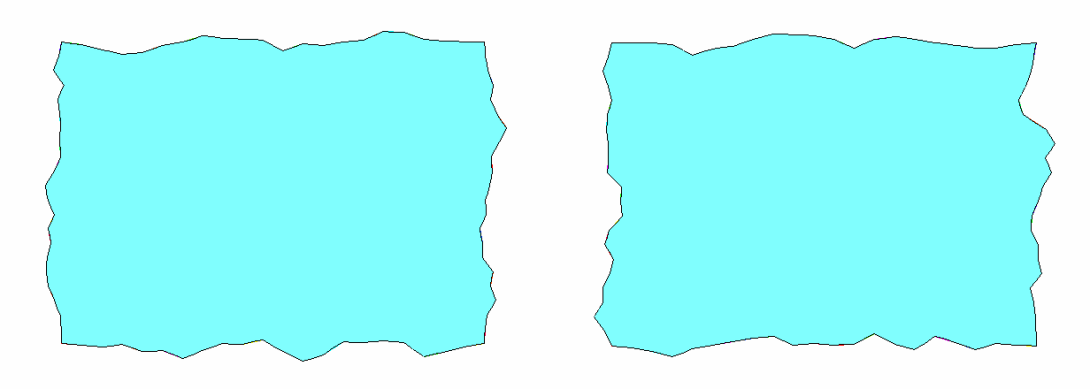

Figure 3.21 – Irregular plate with the sides as random processes – 2 realizations.

Of course, this probabilistic model is considerably limited. Real structures would have uncertainties associated with a greater number of variables, like the density, Elasticity modulus, thickness, etc as random variables or as spatial random processes. However, the main similarity between the adopted probabilistic model and that of real structures is an increasing effect over the eigenvalues as the frequency increases.

The eigenvalue statistics for Case B5 are shown in Figure 3.22. In order to allow a better analysis of the uncertainty effects of the eigenvalues with increasing frequency, Figure 3.22 gives the results for four modes. As expected, the eigenvalues display an increasing agreement with the GOE model as higher order modes are considered. It is interesting to observe the transition of the spacing pdf from a Gaussian distribution to a Rayleigh distribution. The same behaviour is observed for the number variance Σ^2 and the Δ_3 function, but in this case from Poisson statistics to GOE statistics. This is in agreement with that which has been previously discussed in this study since it can be noted in Figure 3.21 that the symmetries for the first modes were not significantly affected by the probabilistic model adopted. An oscillation can also be observed in the number variance Σ^2 and the Δ_3 function for the 20^{th} mode and this is due to the low level of randomness caused by the probabilistic model.

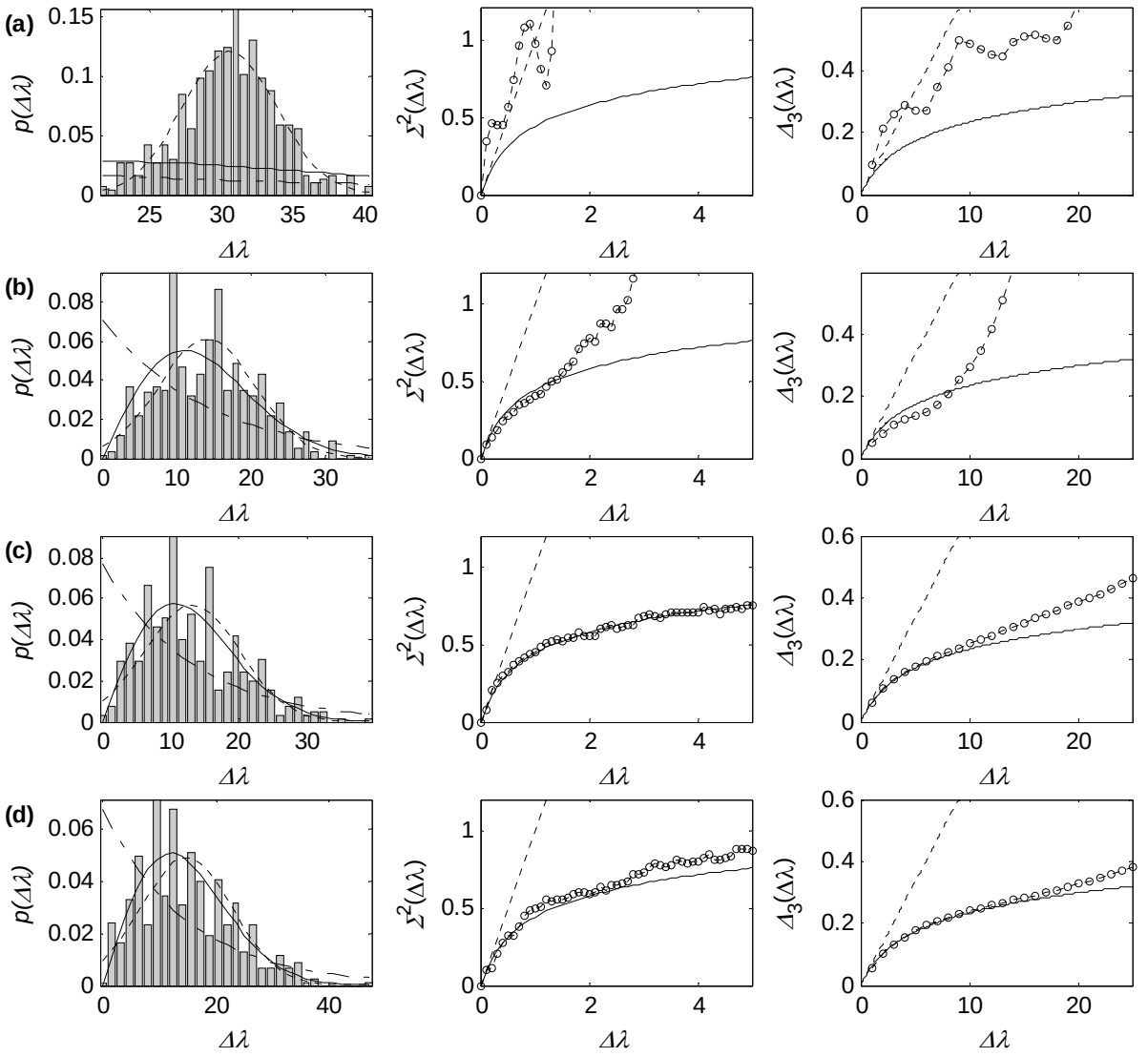

Figure 3.22 – Eigenvalue statistics (ensemble average) – Case B5. a) Mode 20, b) Mode 70, c) Mode 200 and d) mode 300. Pdf plots: ------ Normal distribution, – - – Exponential distribution, —— Rayleigh distribution. Number variance and Δ_3 plots: —— GOE statistics, ------ Poisson statistics, -⋄- numerical data.

Figure 3.23 gives the statistical overlap factor for Case B5. It can be noted that the values are considerably lower than those displayed by the cases previous investigated but they are still over the unity for a mode order greater than 50.

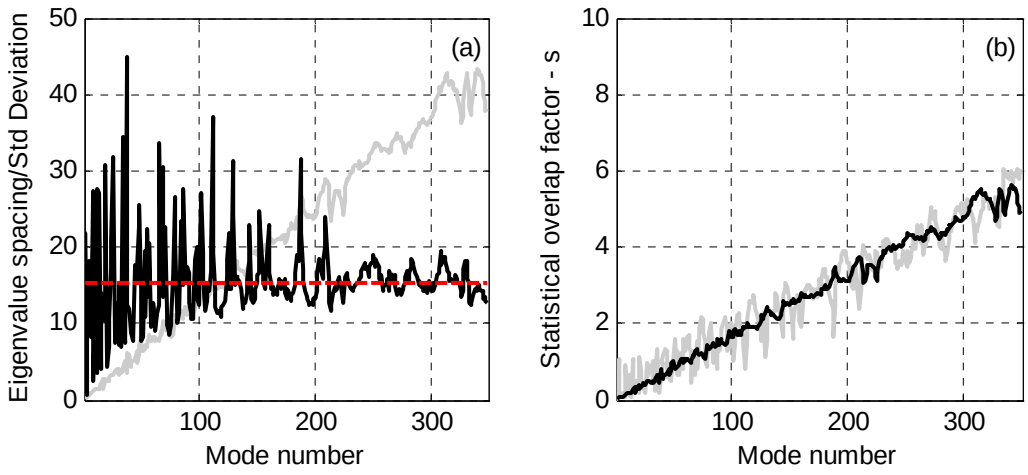

Figure 3.23 – Statistical overlap factor – Case B5. Plot (a): ------ global eigenvalue spacing, ——— local eigenvalue spacing, ——— eigenvalue standard deviation. Plot (b): Statistical overlap factor. ——— global mean spacing, ——— local mean spacing.

Although it is not expected that real systems would have uncertainties similar to those adopted for the experimental analysis carried out in Chapter 2, it would be interesting to verify the type of eigenvalue statistics that a plate with random masses would display. Therefore, Case B6 considered the same uncertainties adopted in Chapter 2, while Case B7 consider the same probabilistic model but with higher uncertainties. The probabilistic models are given in Table 3.5

Table 3.5 – Ensemble average – randomization approach for Case B6 and B7.

Cases	**Nominal Dimensions**	**Variables**	**Statistics**
B6	Case A4	Point mass positions	10 masses with 0.7% of the bare plate mass each Spatial uniform distribution of the mass positions
B7	Case A4	Point mass positions	10 masses with 1.5% of the bare plate mass each Spatial uniform distribution of the mass positions

The eigenvalue statistics for Cases B6 and B7 are shown in Figure 3.26 and Figure 3.24, respectively. The results are also given for four modes or spacings. As a function of its lower level of randomness, Case B6 displays a Gaussian distribution for the 20^{th} spacing while Case B7 shows a pdf of the 20^{th} spacing already conforming to the Rayleigh distribution. This suggests that the higher level of randomness is responsible for reducing the frequency of the transition region from a deterministic behaviour to a chaotic behaviour. Similar results are observed for the other modes with a very good agreement with the GOE

predictions. The main difference in the results is an oscillatory behaviour in some of the Case B6 results which, as discussed before, is believe to be due to its reduced level of randomness.

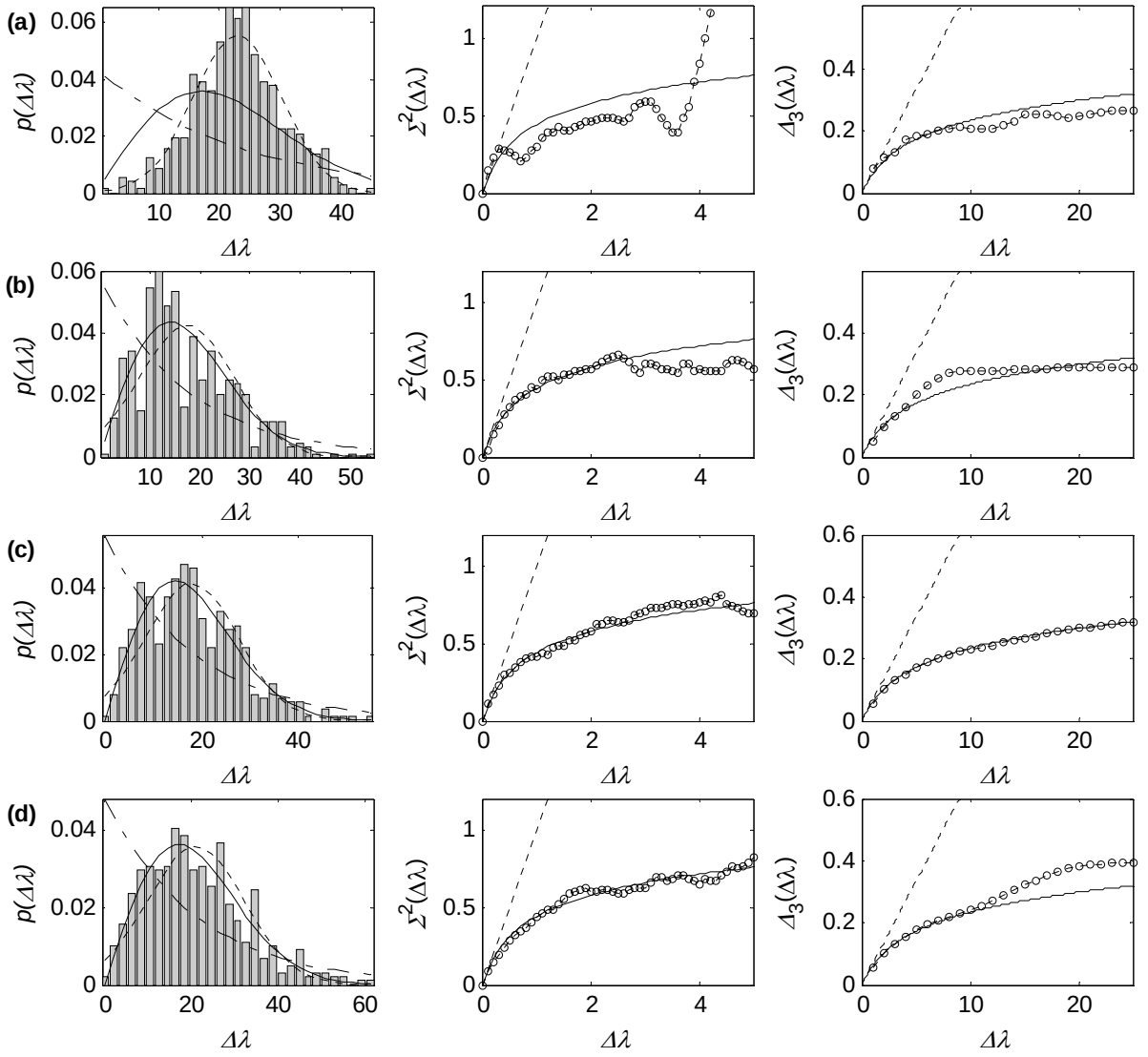

Figure 3.24 – Eigenvalue statistics (ensemble average) – Case B6. a) Mode 30, b) Mode 80, c) Mode 170 and d) Mode 210. Pdf plots: ------ Normal distribution, – - – Exponential distribution, —— Rayleigh distribution. Number variance and Δ_3 plots: —— GOE statistics, ------ Poisson statistics, -◇- numerical data.

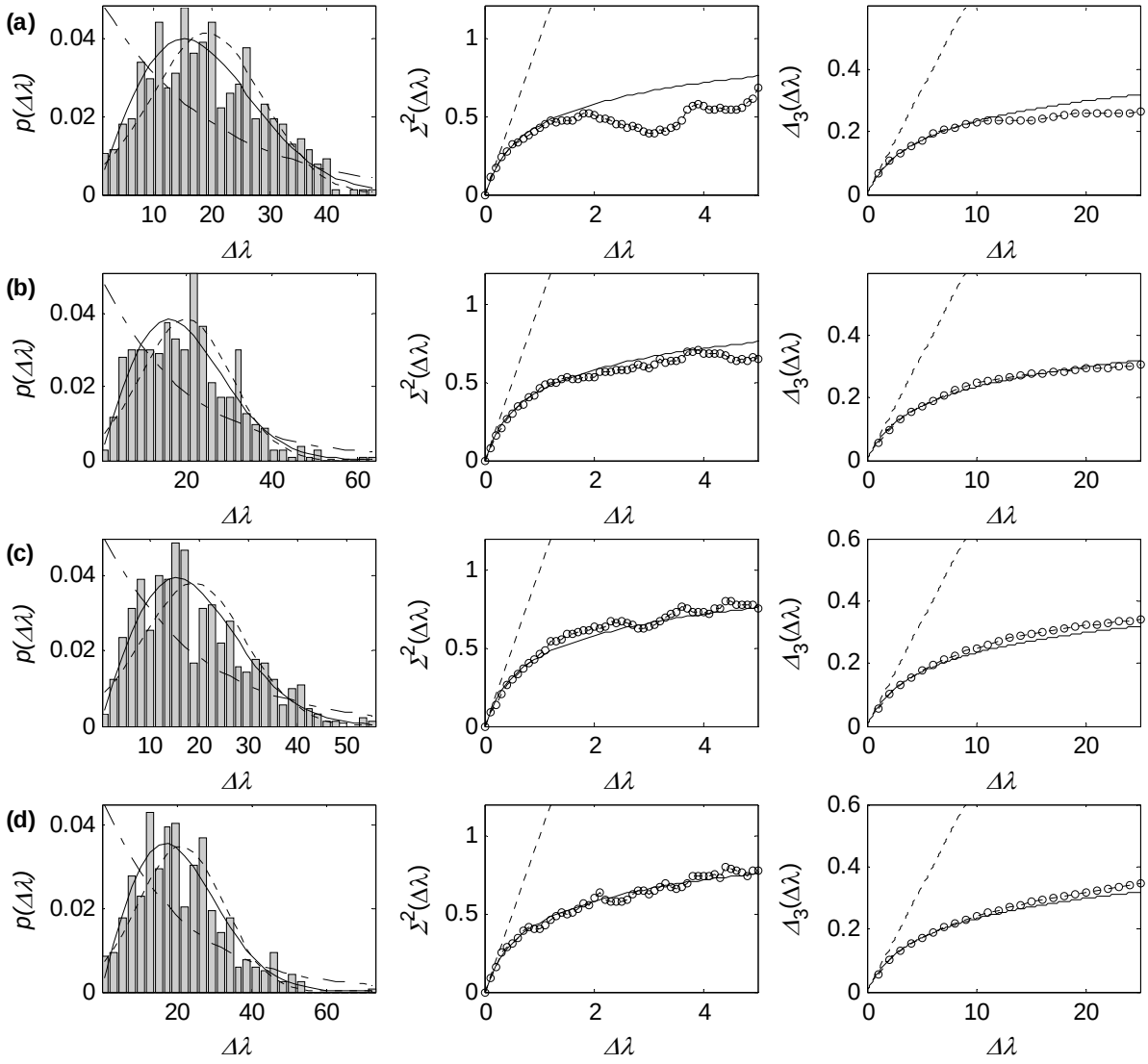

Figure 3.25 – Eigenvalue statistics (ensemble average) – Case B7. a) Mode 30, b) Mode 80, c) Mode 170 and d) Mode 210. Pdf plots: ------ Normal distribution, – - – Exponential distribution, —— Rayleigh distribution. Number variance and Δ_3 plots: —— GOE statistics, ------ Poisson statistics, -◇- numerical data.

The statistical overlap factor is shown for Case B6 in Figure 3.27 and for Case B7 in Figure 3.25. As expected, the values for the statistical overlap factor for Case B7 are higher than for Case B6 and are due to the higher level of randomness of Case B7. It is interesting to observe that Cases B6 and B7 display a completely different behaviour for the statistical overlap factor when compared with the previous cases investigated. This can be explained by the different probabilistic models adopted. For the latter two cases, the plate shape and size where kept fixed while the other cases considered geometrical properties as the random variables. Randomizing a geometrical property results in a considerable shift of the natural frequencies and, as a consequence, a higher standard deviation of the natural frequencies. This can be observed in the figures associated with the statistical overlap factor where the standard

deviation of the eigenvalues is shown. Therefore, a higher statistical overlap factor was observed. However, it has been seen that higher values of the statistical overlap factor are not sufficient to ensure GOE statistics.

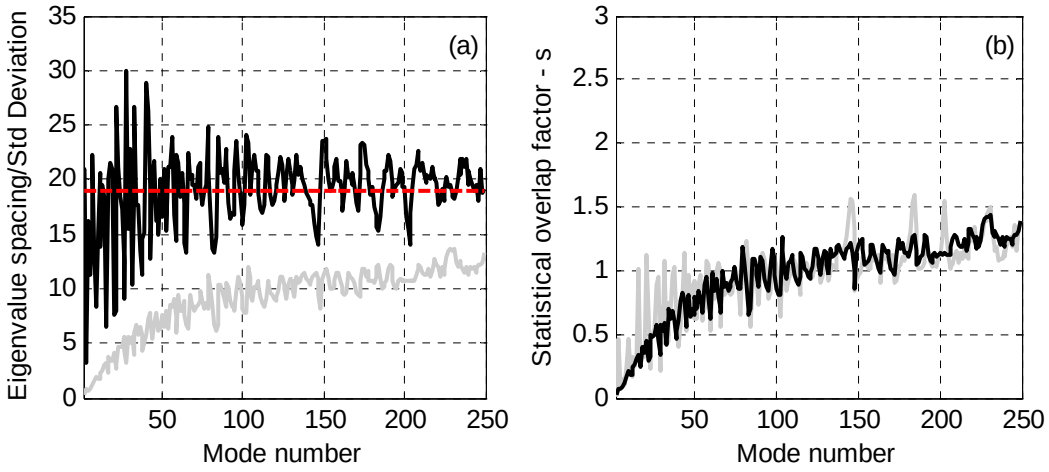

Figure 3.26 – Statistical overlap factor – Case B6. Plot (a): ----- global eigenvalue spacing, ——— local eigenvalue spacing, ——— eigenvalue standard deviation. Plot (b): Statistical overlap factor. ——— global mean spacing, ——— local mean spacing.

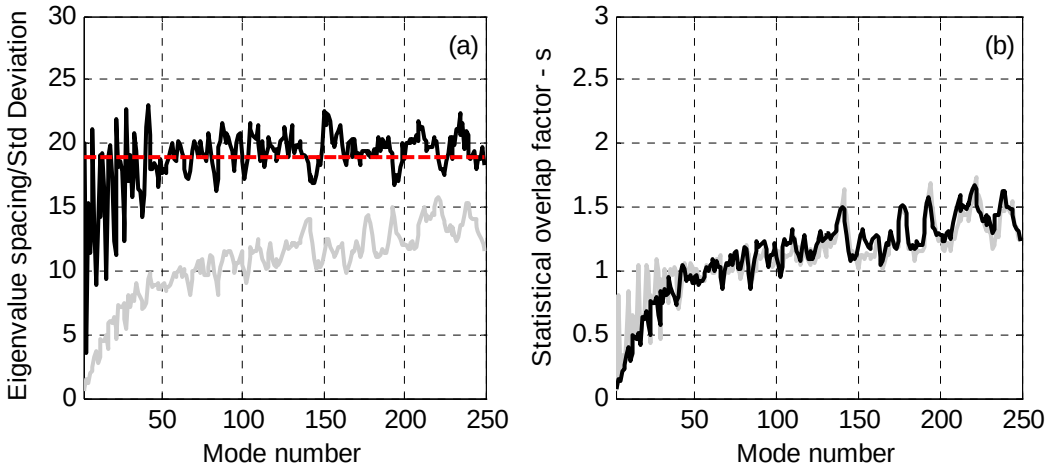

Figure 3.27 – Statistical overlap factor – Case B7. Plot (a): ----- global eigenvalue spacing, ——— local eigenvalue spacing, ——— eigenvalue standard deviation. Plot (b): Statistical overlap factor. ——— global mean spacing, ——— local mean spacing.

3.7 SUMMARY AND DISCUSSION

A detailed review about the use of Random Matrix Theory (RMT) to predict the statistics of random dynamic systems has been presented. It was shown that the RMT was initially developed in the field of nuclear physics and its results are now being applied in many other areas. This wider range of application is due to the concept of universality which conjectures that the RMT predictions are applicable to any sufficiently chaotic random system. Special attention was given to the studies related with the application of the RMT to dynamic systems and it has been seen that the eigenvalue statistics of random dynamic systems conform to the predictions of RMT for a special type of ensemble of random matrices named Gaussian Orthogonal Ensemble (GOE). It was shown that the RMT predictions usually involve the derivation of correlation functions for the eigenvalues of one of the Gaussian ensembles. However, when verifying the agreement between the RMT predictions and experimental results, other statistics are usually preferred to the correlation functions. The two most popular statistics for such applications are the number variance Σ^2 and the Δ_3 function. In view of their faster convergence and being directly related to the two-level cluster function, these statistics were adopted to study the agreement between the eigenvalue statistics of random dynamic systems and the GOE model. The literature review also showed that some question about the application of the GOE model to random dynamic systems still remain concerning the presence of symmetries and the ergodicity concept.

In order to try to answer these questions, a series of numerical cases were studied and the spectral and ensemble averages calculated. A first analysis considered only spectral statistics and a transition between Poisson statistics to GOE statistics was observed when a rectangular plate had its symmetries broken. Ensembles of structures were generated considering different probabilistic models and the eigenvalue statistics were determined for each case. It was seen that two nominally identical structures may have completely different ensemble statistics and, therefore, the validity of the ergodicity assumption is dependent on the probabilistic model adopted. However, if GOE statistics are observed in an ensemble average, it is expected that the ergodicity assumption would hold “locally” and “in general”. By “locally” one should understand that the assumption will be valid for a region in the spectral domain and by “in general” that it would be valid for most of the members of the ensemble.

It was observed that a low level of randomness usually results in a Gaussian distribution for the spacing pdf and in an oscillatory behaviour for the number variance Σ^2 and the Δ_3 function. These observations suggest that, in real systems, the lower modes will display

a Gaussian pdf and, as the frequency increases, a transition to a GOE model or Poisson model will occur, depending on the level of symmetry of the system. The transition from an almost-deterministic behaviour (Gaussian pdf and oscillatory statistics) to GOE statistics was observed for Case B5, where a more realistic probabilistic model was adopted and, therefore, this is the kind of behaviour that would be expected for real structures. In fact, the uncertainties associated with manufactured structures are expected to be much more complex than those attributed to Case B5. Structural non-uniformities, inhomogeneities, or discontinuity of material or geometrical properties are likely to occur and would add more randomness to the system as well as breaking its symmetries. Therefore, it is expected that the GOE model would be more the rule than the exception for real system statistics.

The transition region from Gaussian to GOE statistics observed in Case B5 would not necessarily be the same in all cases since manufactured structures display different levels of uncertainties. For example, it is unlikely that a plate produced for a satellite would have the same level of uncertainty as a plate produced for a ship. The quality control requirements are completely different in these cases. Therefore, in view of the higher level of uncertainty associated with the plate produced for a ship, it would be expected that the transition from a Gaussian behaviour to a GOE model would occur earlier in the frequency domain than for the satellite plate. If a precise prediction of the response variance is required, one should know the location of the transition region in the frequency domain and the effects of discrepancies between the actual eigenvalue statistics and the GOE model over the variance predictions. This is discussed in the next Chapter.

The statistical overlap factor was also calculated for the cases considered and it was noted that values higher than one were obtained even for systems which did not display GOE statistics. Therefore, the parameter is not recommended to verify the applicability of the GOE model and there is a need of a new parameter.

CHAPTER 4

VARIANCE THEORY FOR RANDOM DYNAMIC SYSTEMS

4.1 INTRODUCTION

The literature review given in Chapter 1 has shown the great interest among the vibro-acoustic community in extending the SEA capacity for the prediction of the response variance. It has been also seen that a new theory was recently presented by Langley, Brown and Cotoni [91-93] with the aim of predicting the variance of SEA results. This theory is based on the assumption that the system transfer functions may be treated as a random point process [70] with the natural frequencies having a specific statistical behaviour. Different statistical models have been adopted in the literature for the natural frequencies and it has been shown that the GOE model provides a good description of the natural frequency statistics. In fact, it was seen in Chapter 3 that the GOE model is likely to describe the statistics of most real cases, with the main question concerning the determination of the transition region between almost-deterministic to GOE statistics.

In what follows, the derivation of the equations for the energy density variance of a random dynamic system under point load is reviewed based on the study by Langley and Brown in [91]. The Poisson and GOE models are considered for the statistics of the natural frequencies and equations for the variance are obtained for each model. The numerical approach described in Chapter 2 is used to calculate the mean and variance of the energy density for some of the cases given in Chapter 3. The numerical results are compared with the derived theoretical formulations and it is possible to observe the effects of the different statistics of the natural frequencies (as seen in Chapter 3) on the mean and variance. It is noted that both formulations are sensitive to the parameter named here as the mode shape statistics factor K. The behaviour of K with different randomization approaches and its spatial distribution are also investigated.

4.2 ENERGY DENSITY VARIANCE

4.2.1 Random dynamic system

The derivation may proceed from the analysis given in section 2.3.3. Equation (2.12) gives the energy density of a general dynamic system considering proportional damping. Assuming a unitary punctual force, Equation (2.12) can be rewritten as

$$T(\omega) = \sum_n \frac{\omega^2 a_n}{\left(\omega_n^2 - \omega^2\right)^2 + \left(\eta\omega\omega_n\right)^2}, \tag{4.1}$$

where a_n is given by

$$a_n = \frac{\phi_n{}^2(\mathbf{x}_0)}{4R}. \tag{4.2}$$

In the case of different excitations, Equation (4.2) would be modified. However, only point force excitation will be considered in this study. The constant *R* is the span of the system and for a plate it is equal to the area. In order to allow the application of Point Process concepts, Equation (4.1) can be expressed as

$$T(\omega) = \sum_n a_n g(\omega_n - \omega), \tag{4.3}$$

with the function *g* being given by

$$g(\omega_n - \omega) = \frac{\omega^2}{4\omega^2(\omega_n - \omega)^2 + \left(\eta\omega^2\right)^2}, \tag{4.4}$$

and the following approximation was assumed given that each mode bandwidth is small in comparison to the natural frequency

$$\left(\omega_n^2 - \omega^2\right)^2 + \left(\eta\omega\omega_n\right)^2 \approx 4\omega^2(\omega_n - \omega)^2 + \left(\eta\omega^2\right)^2. \tag{4.5}$$

The approximation adopted in Equation (4.5) has no significant effect on the energy density calculation and this can be observed in Appendix C.1.

The aim here is at the derivation of an equation for the energy density variance and it is possible to observe through Equations (4.1) and (4.2) that the energy density statistics will be determined by the statistical behaviour of the natural frequencies and mode shapes. It was seen in Chapter 1 that different statistical models have been adopted in the literature for the eigenvalues and eigenvectors, including the Poisson model and the GOE statistics. Chapter 3 has shown that for a random structure arising from a manufacture process it is likely that the GOE model would be an appropriate statistical model given that the system is sufficiently random and has a low level of symmetry. In what follows, the derivation of the energy density variance is given for the Poisson and GOE model based on [91]. More details on the derivation can be obtained in [39,91].

4.2.2 Poisson statistics

The Poisson model for the statistics of the natural frequencies was first adopted by Lyon in [83] and was used to derive the statistics of the energy of a system under point loading. The Poisson model assumes that the natural frequency spacings are independent and display an exponential pdf. Lyon's option for the Poisson model was more motivated by its mathematical tractability than its physical significance, although systems with symmetries may display these statistics.

In the case where natural frequencies form a Poisson point process [70], Campbell's Theorem can be applied and the mean and variance of the energy density are given by

$$\mu_T = \mathrm{E}[T] = 2\mathrm{E}[a_n]\int_0^\infty vg(\Omega)\mathrm{d}\Omega, \tag{4.6}$$

$$\sigma_T{}^2 = \mathrm{Var}[T] = 2\mathrm{E}[a_n{}^2]\int_0^\infty vg^2(\Omega)\mathrm{d}\Omega. \tag{4.7}$$

Equations (4.6) and (4.7) also assume that the coefficients a_n are identically distributed and statistically independent from the natural frequencies. Evaluating the integrals gives

$$\mu_T = \frac{E[a_n]\pi v}{2\eta\omega}, \tag{4.8}$$

$$\sigma_T{}^2 = \frac{E[a_n{}^2]\pi v}{4\eta^3\omega^3}. \tag{4.9}$$

The energy density relative variance is then given by

$$r_T{}^2 = \frac{\sigma_T{}^2}{\mu_T{}^2} = \frac{\alpha}{\pi m}, \tag{4.10}$$

where α is called the spatial factor and given by

$$\alpha = \frac{\mathrm{E}[a_n{}^2]}{\mathrm{E}[a_n]^2}. \tag{4.11}$$

In the case of a point force load, Equation (4.2) can be substituted in (4.11) to obtain

$$\alpha = K = \frac{\mathrm{E}[\phi_n{}^4]}{\mathrm{E}[\phi_n{}^2]^2}, \tag{4.12}$$

where the constant K is associated with the statistics of each mode and is named in this study as the “mode shape statistics factor”.

4.2.3 GOE statistics

The derivation of the statistics of a random process formed by random pulses with the spacings being statistically independent and having an arbitrary distribution is given by Stratonovich in [110]. Langley and Brown [91] extended this derivation for the case where the natural frequency statistics conform to the GOE model. Equation (4.3) can be rewritten as

$$T(\omega) = \int_{-\infty}^{\infty} g(\omega' - \omega)\xi(\omega')\mathrm{d}\omega', \tag{4.13}$$

where $\xi(\omega)$ is a random function given by

$$\xi(\omega) = \sum_{j=1}^{\infty} a_n \delta(\omega - \omega_j), \tag{4.14}$$

and $\delta(x)$ is the Dirac delta function. Assuming that $\xi(\omega)$ forms a stationary random process, it follows that

$$S_T(\theta) = |F(\theta)|^2 S_\xi(\theta), \tag{4.15}$$

with $S_T(\theta)$ and $S_\xi(\theta)$ being, respectively, the spectral density of the energy density and the random function $\xi(\omega)$, while the function $F(\theta)$ is the Fourier transform of the function $g(\Omega)$, or

$$F(\theta) = \int_{-\infty}^{\infty} g(\omega' - \omega) \exp(-i\theta\omega') \mathrm{d}\omega' . \tag{4.16}$$

It follows from Equation (4.15) that in the case of the function $S_\xi(\theta)$ being adjusted to give zero mean, the energy density variance can be given by

$$\sigma_T{}^2 = 2\int_0^{\infty} |F(\theta)|^2 S_\xi(\theta) \mathrm{d}\theta . \tag{4.17}$$

The function $F(\theta)$ can be obtained by evaluating the integral in Equation (4.16) which gives

$$F(\theta) = \frac{\pi}{2\eta\omega} \exp\left(\frac{-\eta\omega|\theta|}{2} - i\theta\omega \right). \tag{4.18}$$

The spectral density of the function $\xi(\omega)$ is a little more complicate to obtain for the case of GOE statistics. Langley and Brown [91] employ an expression for $S_\xi(\theta)$ given by Lin [83] where

$$S_{\xi}(\theta)=\frac{1}{2\pi}\left\{\mathrm{E}\left[a_n{}^2\right]g_1+\mathrm{E}\left[a_n\right]^2 G_2(\theta)\right\}, \tag{4.19}$$

where g_1 is the first cumulant of the random process and $G_2(\theta)$ is the Fourier transform of the second cumulant or

$$G_2(\theta)=\int_{-\infty}^{\infty} g_2(\omega)\exp(-i\theta\omega)\mathrm{d}\omega\,. \tag{4.20}$$

The first cumulant of $\xi(\omega)$ is actually the rate at which the natural frequencies occur, in other words, the modal density *v*. The second cumulant is determined by higher order statistics, but it was observed by Weaver [88] that its definition is very similar to the definition of the two-level cluster function Y_2 given in section 3.3, so that

$$g_2(\omega)=-vY_2(v\omega). \tag{4.21}$$

The Fourier transform of the two-level cluster function is then given by Mehta [10] as

$$b(\theta)=\int_{-\infty}^{\infty} Y_2(r)\exp(-2\pi ir\theta)\mathrm{d}r=\begin{cases}1-2|\theta|+|\theta|\ln(1+2|\theta|), & |\theta|\le 1\\ -1+|\theta|\ln\left(\dfrac{2|\theta|+1}{2|\theta|-1}\right), & |\theta|\ge 1\end{cases}, \tag{4.22}$$

which results in

$$G_2(\theta)=-vb\left(\frac{\theta}{2\pi v}\right). \tag{4.23}$$

Equations (4.18), (4.19) and (4.23) can be substituted in Equation (4.17) leading to

$$r_T{}^2=\frac{1}{\pi v}\int_0^{\infty}\left[\alpha-b\left(\frac{\theta}{2\pi v}\right)\right]\exp(-\eta\omega\theta)\mathrm{d}\theta\,. \tag{4.24}$$

The evaluation of the integral is given by Brown in [39] and yields

$$r_T{}^2 = \frac{1}{\pi m}\left\{\alpha - 1 + \frac{1}{2\pi m}\left[1 - \exp(-2\pi m)\right] + E_1(\pi m)\left[\cosh(\pi m) - \frac{1}{\pi m}\sinh(\pi m)\right]\right\}, \tag{4.25}$$

where $E_1(x)$ is the exponential integral given by

$$E_1(x) = \int_x^\infty \frac{\exp(-t)}{t}\,\mathrm{d}t\,. \tag{4.26}$$

The exponential integral can be evaluated numerically, but for large arguments an approximation can be given by

$$r_T{}^2 \approx \frac{\alpha - 1}{\pi m} + \frac{1}{(\pi m)^2}, \tag{4.27}$$

and it is expected to give accurate results for $m > 0.6$.

4.2.4 Spatial factor

It can be noted from Equation (4.10) and Equation (4.25) that both formulations are directly related to the spatial factor α and, as a consequence, to the constant *K*. The concept of a mode shape statistics factor *K* was first introduced by Lyon [83] and is given by

$$K = \frac{\mathrm{E}\left[\phi_n{}^4(\mathbf{x}_f)\right]}{\mathrm{E}\left[\phi_n{}^2(\mathbf{x}_f)\right]^2}, \tag{4.28}$$

where $\phi_n(\mathbf{x}_f)$ is the amplitude of the *n*th mode shape at the excitation point given by the vector $\mathbf{x}_f$. The definition of the average E[ ] may vary for different authors. In [83], Lyon considered a spatial average and, assuming sinusoidal mode shapes, found a value of $K = 2.25$ for 2D systems. However, the average considered in the variance formulation described above is strictly over an ensemble of structures and this is the definition adopted by Langley and Brown in [91]. Langley and Brown assumed that the eigenvector element possesses a Gaussian distribution as predicted by the GOE model, which gives a value of $K = 3$. However, the numerical simulations displayed a strong tendency for *K* to be less than 3, although the pdf

of eigenvector elements appears to be near-Gaussian.

Lobkis *et al.* also discussed in [90] what would be the correct value of K. It was argued that it would be peculiar if the GOE predictions for the natural frequency statistics agreed so well with experimental and numerical studies, while the modal amplitudes did not. Lobkis *et al.* suggested that the low values of K may be a result of the coupling caused by the dissipation in the dynamic equations, which may be interpreted as the occurrence of complex modes. However, Langley and Brown's simulations did not considered complex modes and also found low values of K. Both Langley and Brown and Lobkis *et al.* consider that the subject still required further investigation.

An interesting discussion about the eigenvector statistics in RMT is also given by Brody *et al.* in [94]. Brody *et al.* showed that for the GOE case the eigenvector components are asymptotic Gaussian with increasing size of the system. Therefore, the assumption of a Gaussian distribution for the eigenvectors, and consequently that $K = 3$, would only be valid when there is a considerable number of eigenvectors interacting.

A discussion about mode shape statistics is given in what follows based on some numerical results.

4.3 NUMERICAL RESULTS

4.3.1 Energy density mean

The numerical procedure proposed in Chapter 2 allows the calculation of the energy density for an ensemble of structures and the determination of the energy density statistics. The different ensemble definitions adopted in Chapter 3 when studying the statistics of the eigenvalues where also considered here and the energy density was calculated for each member of the ensembles for a point force at the position $x = 0.11$ and $y = 0.135$. In what follows, the results for the mean energy density are compared with the SEA standard results obtained through Equation (2.15) for Cases B1, B5, B6 and B7, defined in Chapter 3, for different damping levels. These cases were chosen since they represent the extreme results regarding the statistics of the eigenvalues, including both Poisson and GOE statistics. Although not shown in what follows, the results for the other cases display an intermediate behaviour between the results showed below.

The energy density for four members of the ensemble and the mean for the whole ensemble are given in Figure 4.1 for Case B1, together with the standard SEA prediction. A very good agreement can be observed between the mean energy density and the SEA results

for all damping levels. It can be noted that the increase in the damping level is responsible for a considerable reduction in the variation of the energy density results within the ensemble. It may also be observed that the dispersion of the energy density curve also reduces with increasing frequency.

Table 4.1 – Ensemble descriptions.

Cases	**Nominal Dimensions**	**Descriptions**
B1	Case A1	Rectangular plates with random length and width
B5	Case A1	Plates with the sides as random processes
B6	Case A4	Randomly positioned masses (7% of the bare plate)
B7	Case A4	Randomly positioned masses (15% of the bare plate)

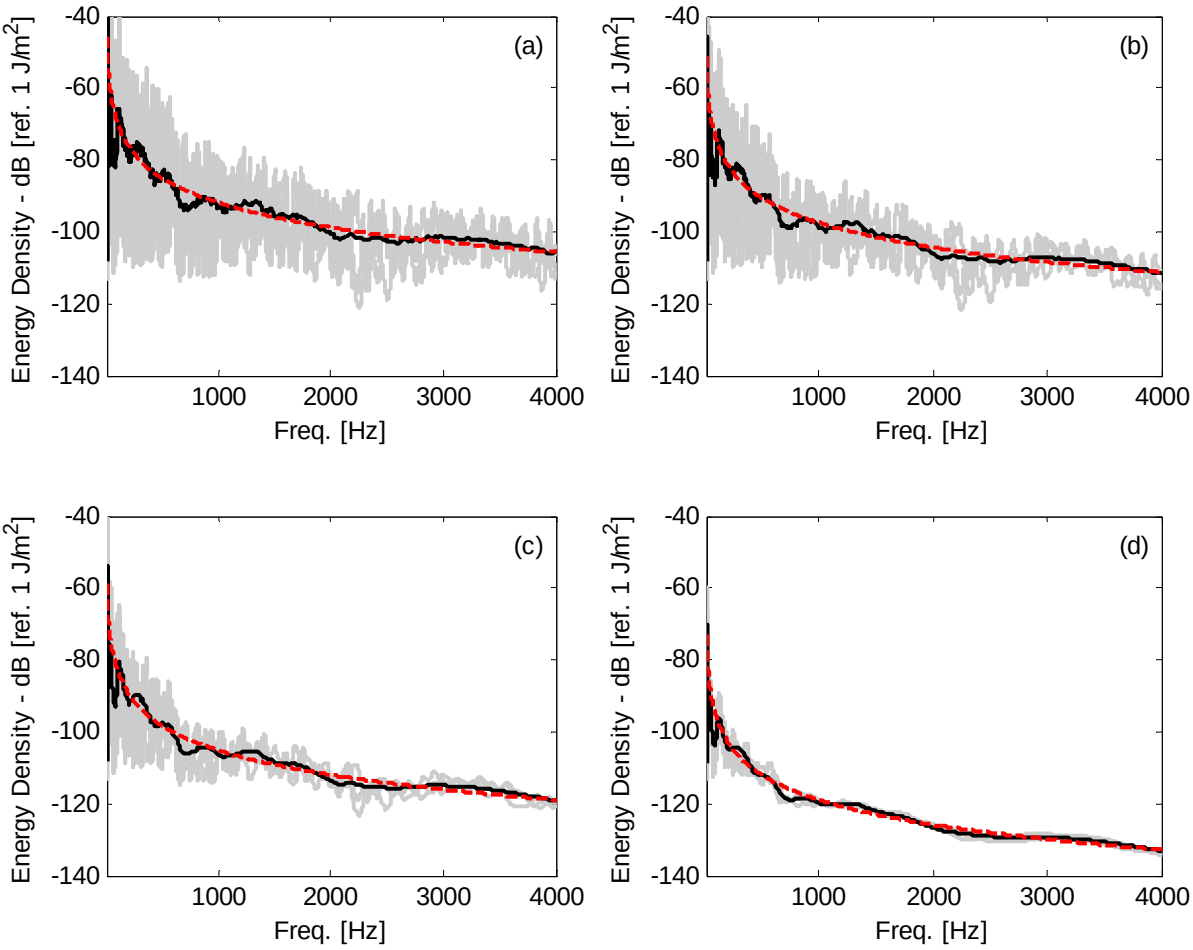

Figure 4.1 – Energy density – Case B1. a) $\eta = 0.008$, b) $\eta = 0.014$, c) $\eta = 0.03$ and d) $\eta = 0.12$. realizations, mean, standard SEA.

The energy density numerical results for Case B5 are shown in Figure 4.2 with the SEA predictions and a very similar behaviour to that observed for Case B1 can be noted.

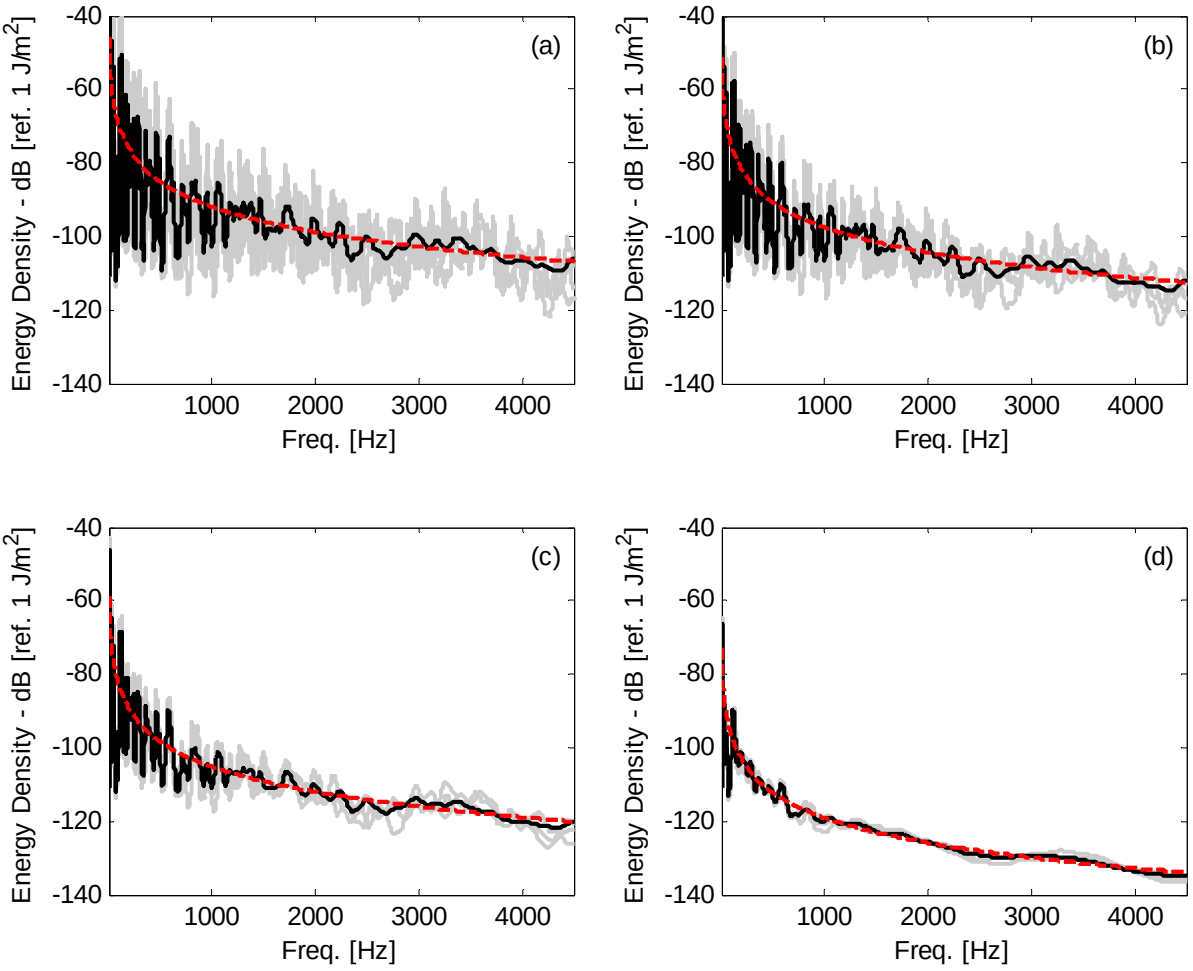

Figure 4.2 – Energy density – Case B5. a) $\eta = 0.008$, b) $\eta = 0.014$, c) $\eta = 0.03$ and d) $\eta = 0.12$. realizations, mean, standard SEA.

Figure 4.3 and Figure 4.4 show the results for the energy density for Cases B6 and B7. Again, Cases B6 and B7 display similar results to those observed for Cases B1 and B5.

It can be noted that the ensemble definition has little effect on the mean and a very good agreement between the mean and SEA predictions can be noted for all the analyzed cases and different loss factors. Although all the curves display a similar behaviour, some curves show a higher oscillation around the SEA prediction, especially for low damping levels and at low frequencies. These oscillations are due to the fact that low order modes are less sensitive to some of the randomization approaches used. This is especially important for low levels of damping where the peaks are more pronounced. In Case B1, it seems that the ensemble definition has a similar effect over the whole frequency range, while the randomization approach adopted in Case B5 caused a reduced variability at the low order

modes. In Case B5, the modal behaviour (pronounced peaks) for the curves at low frequency is quite clear. A similar consideration can be used for Cases B6 and B7. Both cases have the same randomization approach based on random masses but the ensemble adopted in Case B7 considered a higher level of randomness. As a consequence, the mean energy curve obtained for Case B7 displays a much smoother behaviour.

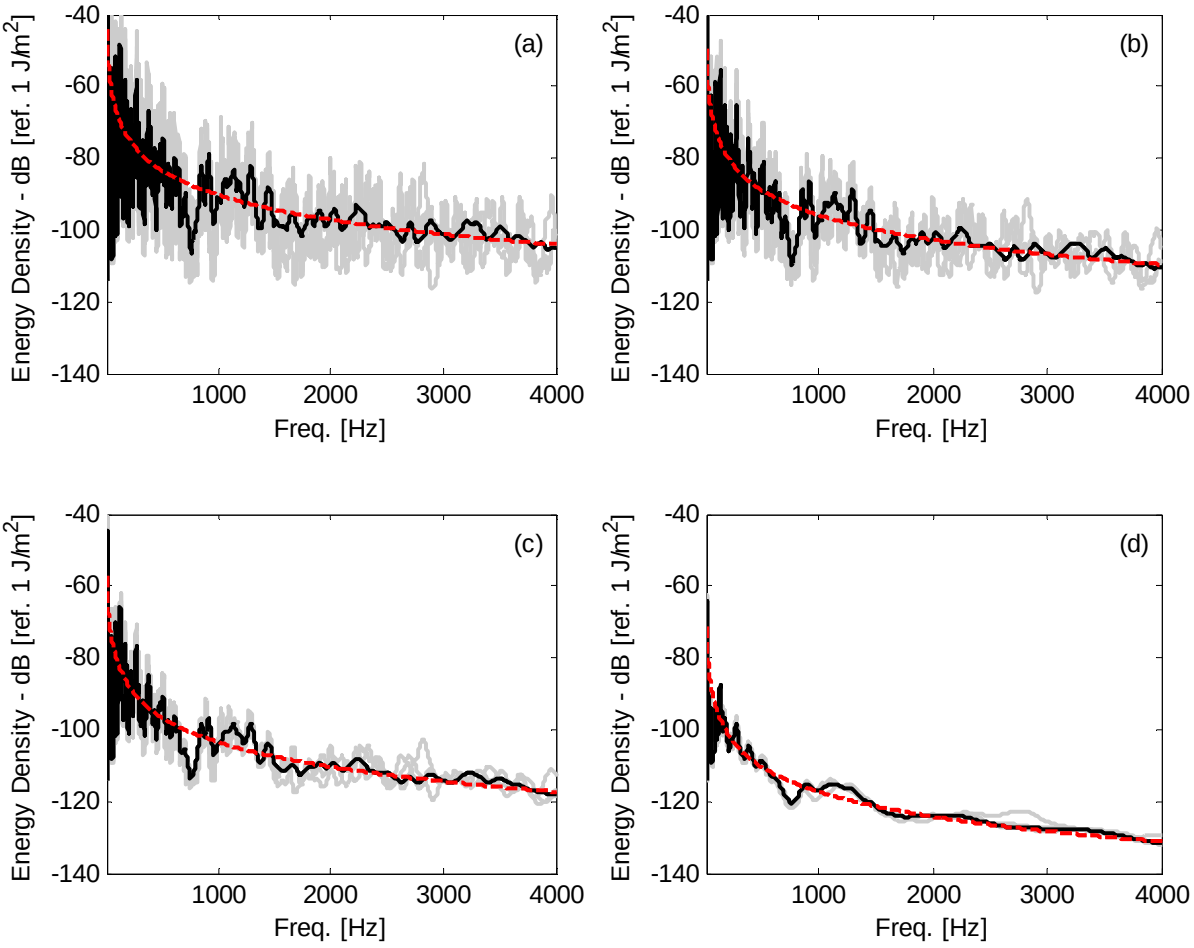

Figure 4.3 – Energy density – Case B6. a) $\eta = 0.008$, b) $\eta = 0.014$, c) $\eta = 0.03$ and d) $\eta = 0.12$. realizations, mean, standard SEA.

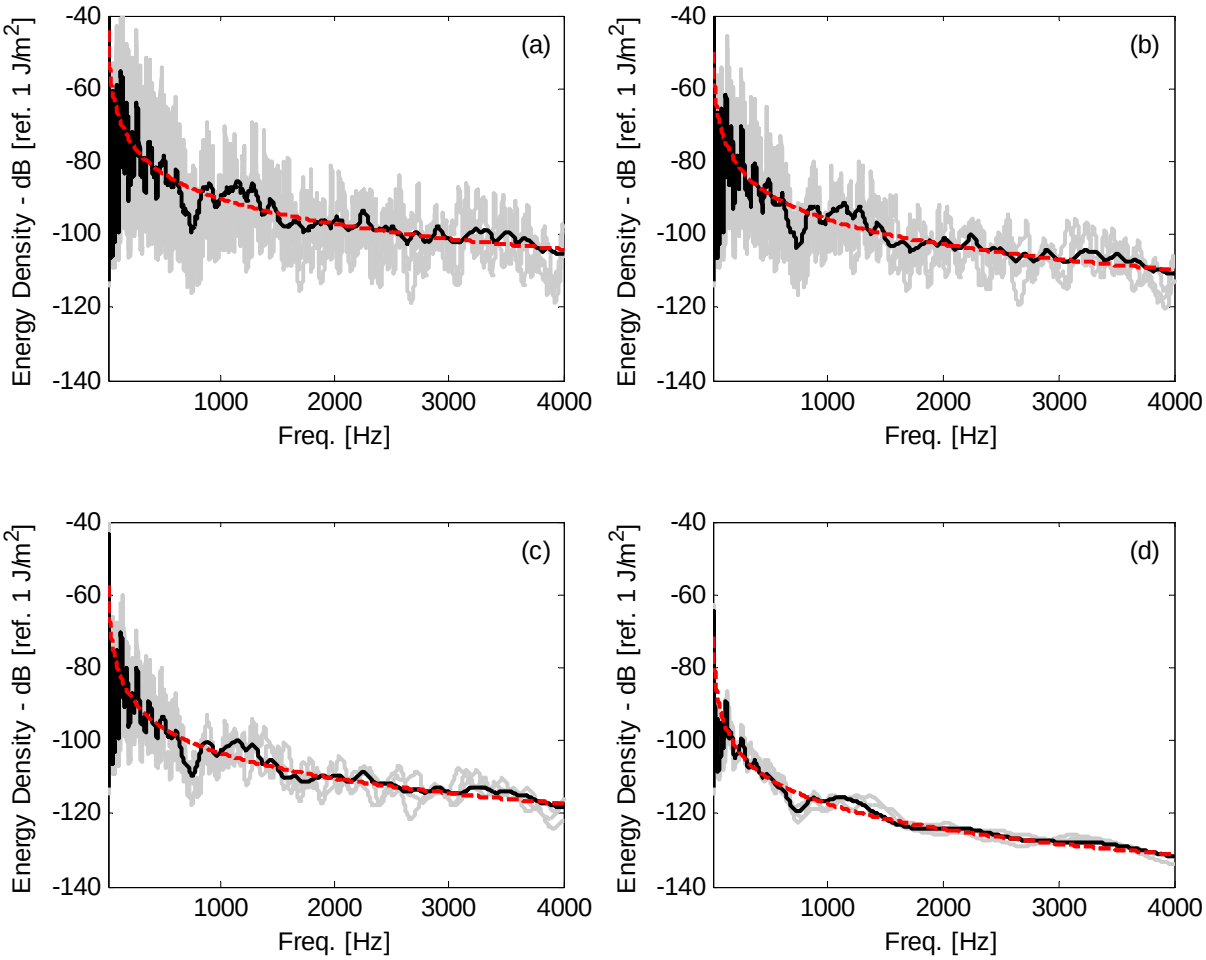

Figure 4.4 – Energy density – Case B7. a) η = 0.008, b) η = 0.014, c) η = 0.03 and d) η = 0.12. realizations, mean, standard SEA.

4.3.2 Energy density variance

Following the calculation of the mean energy density, the normalized variance was also obtained for Cases B1, B5, B6 and B7. Figure 4.5 gives the results for the energy density normalized variance for Case B1 considering different levels of damping. The results are compared with the predictions considering three statistical models for the eigenvalues and eigenvectors: (i) Poisson model with K = 3, (ii) GOE model with K = 3 and (iii) GOE models with K = 2.5. The latter was included in view of the discussion presented in section 4.2.4. The results for the energy density variance are plotted against the modal overlap factor, since this parameter is the main variable in the variance equations. It should be noted that plates display a direct relation between the modal overlap factor and the frequency since the modal density is constant (Equations (1.1) and (2.16)).

The ensemble of structures generated for Case B1 considered only rectangular plates and it was seen in Chapter 3 that this definition produces natural frequency statistics

following the Poisson model. Therefore, it would be expected that the energy density variance would agree with Equation (4.10) which considered Poisson statistics for the eigenvalues but this does not seem to be the case. The theoretical curve seems to predict the overall trend of the variance at lower levels of damping. However, with increasing damping, the numerical results tend to display an oscillatory behaviour and the theoretical curves over predict the results.

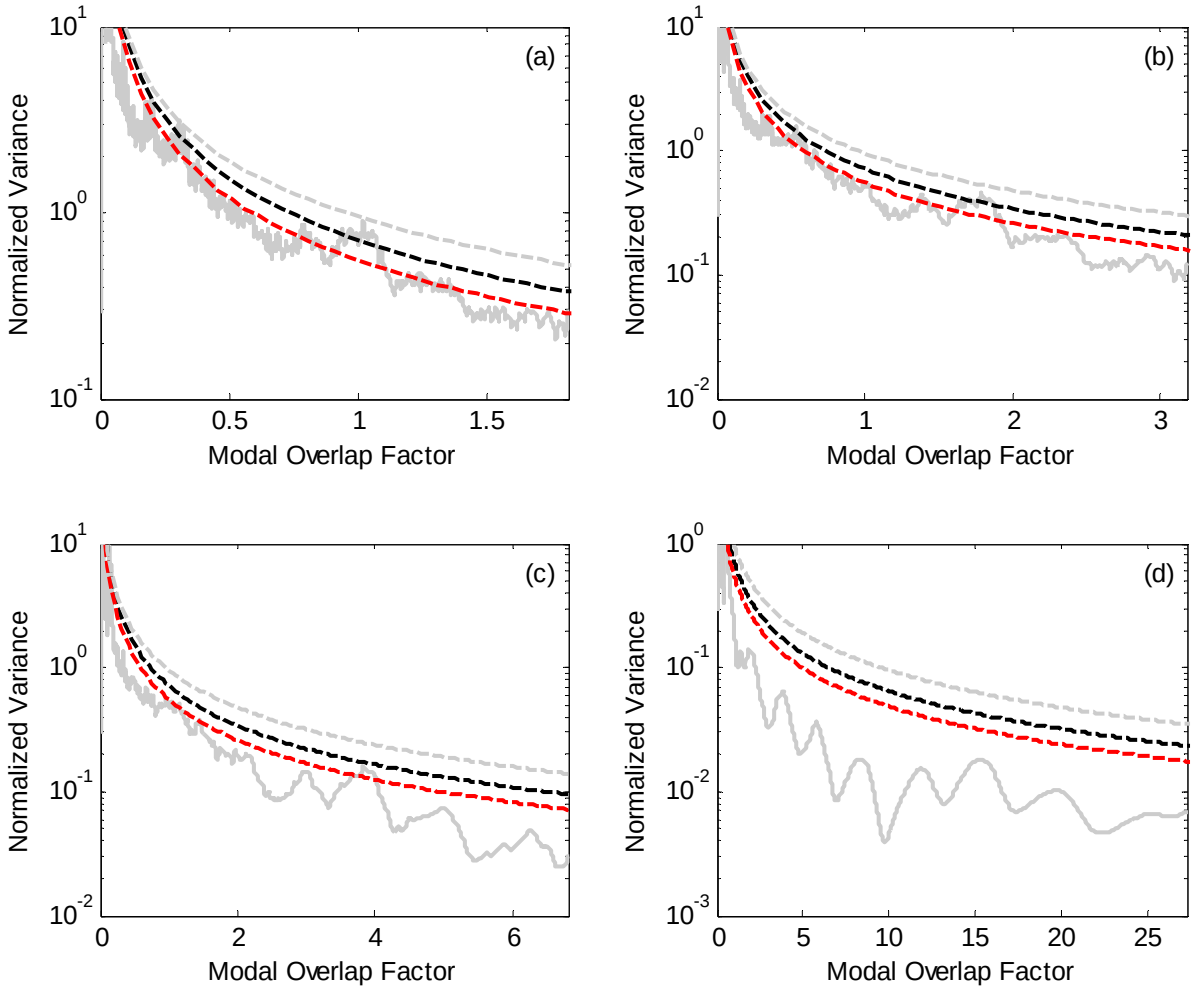

Figure 4.5 – Energy density normalized variance – Case B1. a) $\eta = 0.008$, b) $\eta = 0.014$, c) $\eta = 0.03$ and d) $\eta = 0.12$. numerical result, GOE theory $K = 3$, GOE theory $K = 2.5$, Poisson model $K = 3$.

The increase in damping also results in the consideration of a larger modal overlap factor range in the analysis and this can be noted by the abscissa of the plots in Figure 4.5. A higher value of the modal overlap factor may be interpreted as a greater number of modes contributing to the response. In a situation where a large number of modes are involved the degree of correlation between modes becomes more important. The Poisson model assumes that the natural frequencies are independent and the results for the number variance and Δ_3

function obtained for Case B1 suggest that the assumption would be valid. However, a more detailed analysis of the ensemble may provide a different explanation for the discrepancy between numerical and theoretical curves. In a rectangular plate, the flexural modes are decoupled in x and y directions (assuming the plate is in an x-y plane) and their natural frequencies are directly dependent on the plate dimensions. In fact, the modes in each group are directly related to each other by means of the dimension and therefore should display a high correlation. The statistics considered before did not show this correlation since their calculation considered both groups together. This type of behaviour would explain the results observed for the energy density variance obtained for Case B1.

The energy density normalized variance obtained for Case B5 is shown in Figure 4.6. The prediction considering the GOE model and $K = 2.5$ displays a good agreement for the low damping cases. Once more, as the damping level increases the theoretical curves over predict the numerical results. However, an interesting behaviour may be observed in Figure 4.6. Increasing the damping level, the numerical results deviate from the prediction unequally along the modal overlap range considered. In fact, the results seem to deviate more at low and mid frequencies. This is due to the behaviour observed in Chapter 3 for the eigenvalue statistics of Case B5 where an increasing agreement with the GOE statistics was noted as the frequency increases. At low damping level, the discrepancy between the eigenvalue statistics and the GOE model does not seem to be so important since only a few modes contribute to the response. As the level of damping increases, the modal overlap increases and a higher number of modes contribute to the response and the correlations between eigenvalues become more and more important.

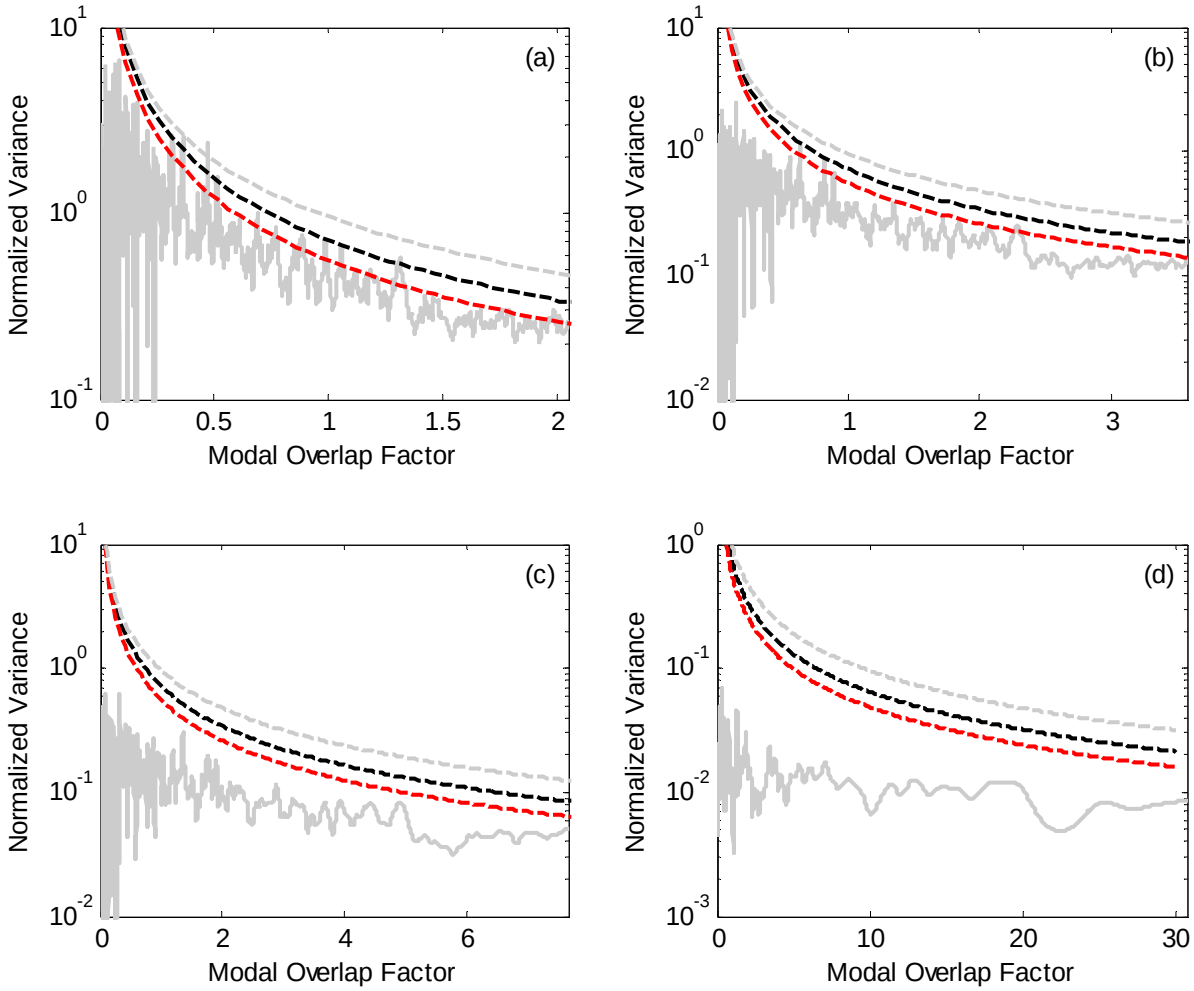

Figure 4.6 – Energy density normalized variance – Case B5. a) $\eta = 0.008$, b) $\eta = 0.014$, c) $\eta = 0.03$ and d) $\eta = 0.12$. numerical result, GOE theory $K = 3$, GOE theory $K = 2.5$, Poisson model $K = 3$.

The results for the energy density variance for Case B6 are given in Figure 4.7. A very similar behaviour to that obtained for Case B5 can be observed for Case B6. Again, the results display a good agreement for the cases with low damping. Increasing the damping, results in an over prediction by the theoretical curves of the numerical results. It is interesting to observe that the discrepancy between numerical and theoretical curves also occurs first in lower frequencies and this is in agreement with the eigenvalue statistics observed for Case B6.

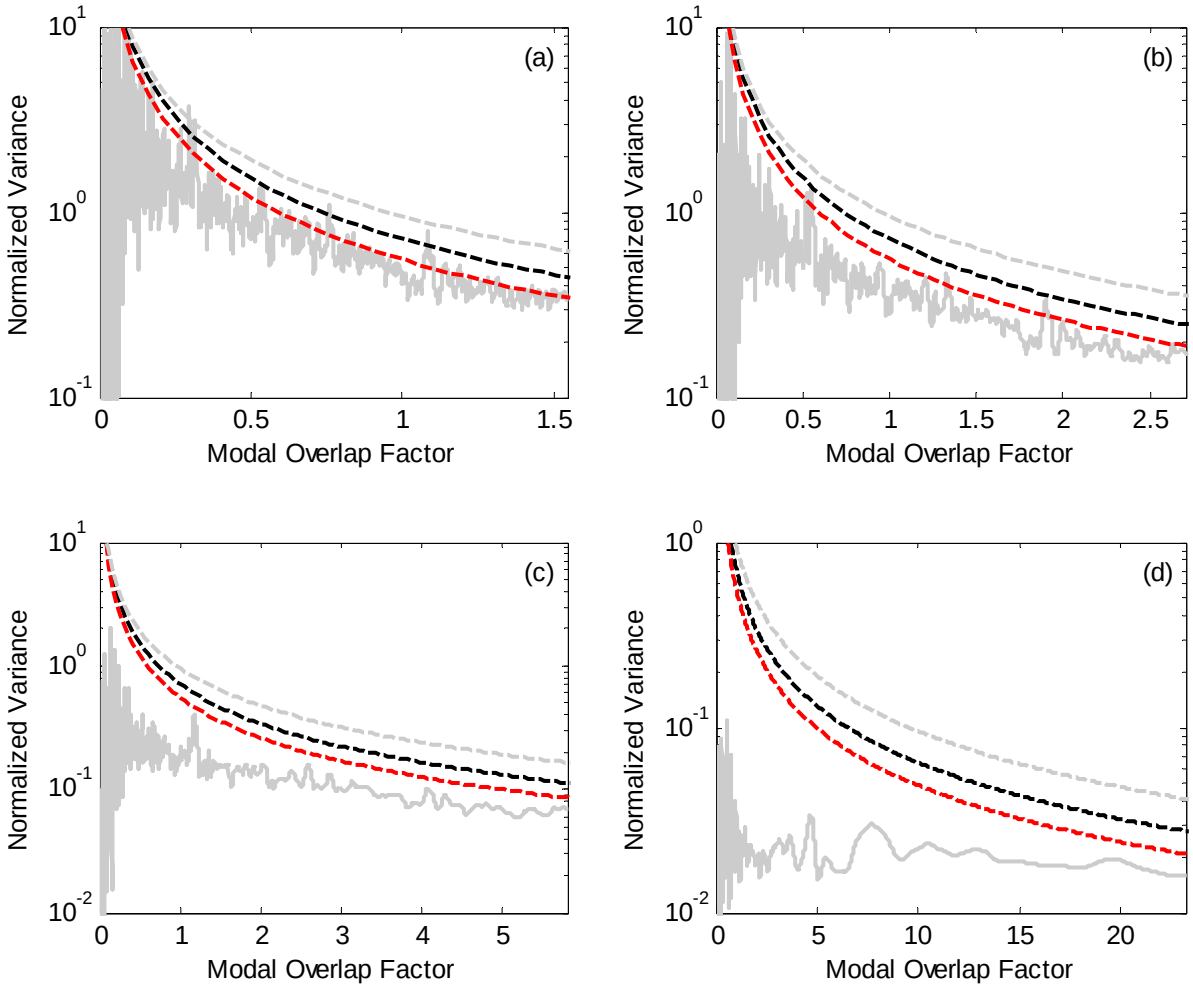

Figure 4.7 – Energy density normalized variance – Case B6. a) η = 0.008, b) η = 0.014, c) η = 0.03 and d) η = 0.12. ——— numerical result, - - - - - GOE theory K = 3, - - - - - GOE theory K = 2.5, - - - - - Poisson model K = 3.

Figure 4.8 shows the results obtained for the energy density normalized variance for Case B7. A very good agreement can be observed between the theoretical curve considering the GOE model and K = 2.5. This agreement would be expected in view of the eigenvalue statistics obtained for Case B7 in Chapter 3. However, it is interesting to observe that the agreement occurs with the curve which considered K = 2.5 instead of K = 3 which was the value predicted by RMT. A discussion about the mode shape statistics factor is given in the next section.

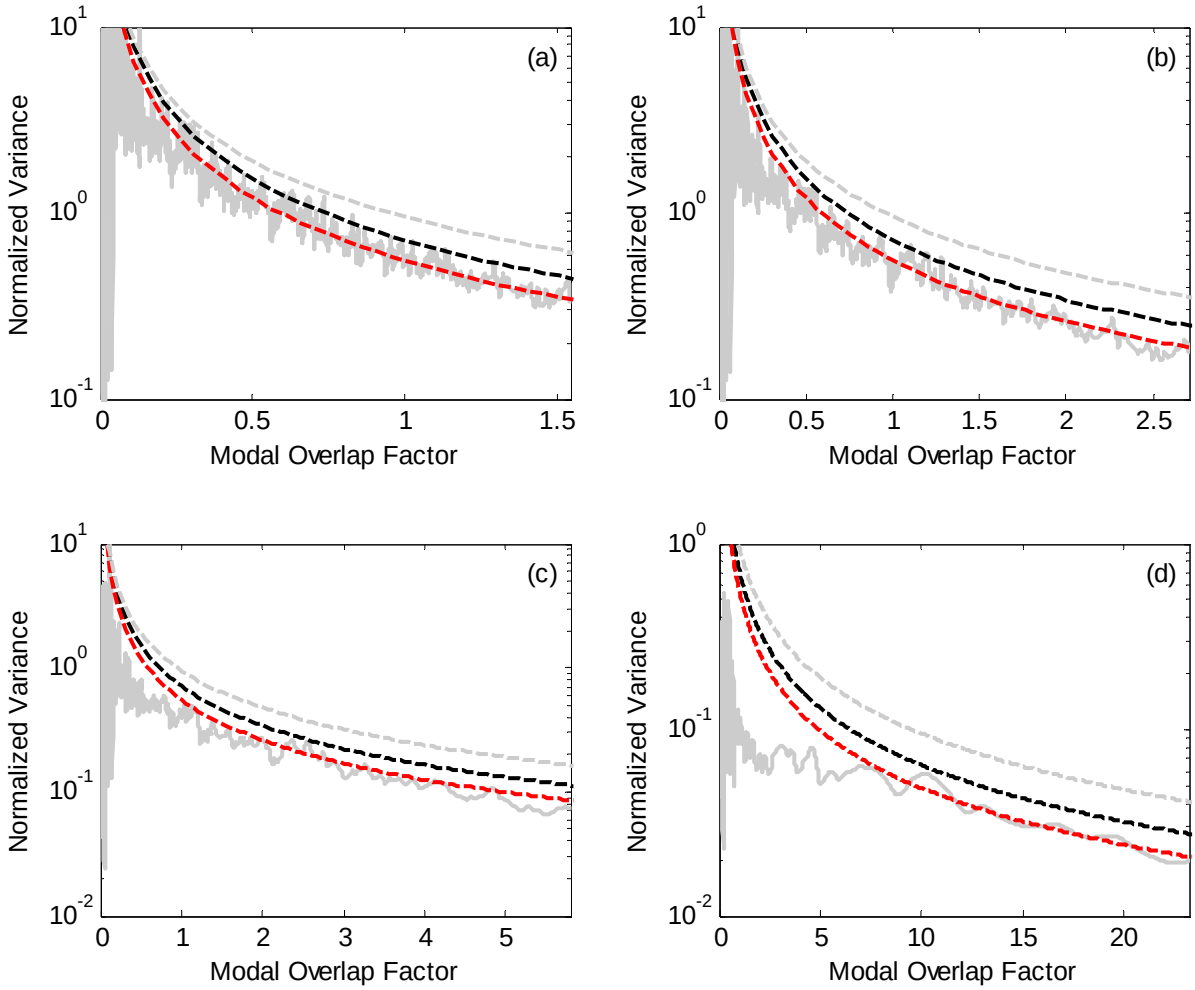

Figure 4.8 – Energy density normalized variance – Case B7. a) $\eta = 0.008$, b) $\eta = 0.014$, c) $\eta = 0.03$ and d) $\eta = 0.12$. ——— numerical result, - - - - - GOE theory $K = 3$, - - - - - GOE theory $K = 2.5$, - - - - - Poisson model $K = 3$.

4.3.3 Mode shape statistics factor

It has been seen in the previous section that the theoretical results considering the GOE model and $K = 3$ seems to over predict the numerical results while a very good agreement was observed when considering $K = 2.5$ and the system was sufficiently random (Case B7). Therefore, some analyses were carried out in order to verify the behaviour of the mode shape statistics factor K with increasing mode order and its spatial distribution.

In order to obtain K for other points of the plate, the mode shape amplitudes for a grid of 441 points around the excitation point were calculated. This grid covers a square of 0.10 x 0.10 m around the excitation point with a discretization of 0.005 m (the same discretization as the mesh). The mode shape statistics factor K was then calculated for each point of the grid using Equation (4.28). The investigation of K was restricted to the above described grid as a function of the computational memory required to store the mode shape

amplitudes for a larger number of points for each mode and each member of the ensemble. In what follows, the results for *K* are shown for Cases B6 and B7. The results obtained for Cases B1 and B5 may be observed in Appendix C.1.2.

Figure 4.9 gives *K* for two points of the grid considering the ensemble defined in Case B6. The mode shape statistics factor for the excitation point is shown in Figure 4.9 (a). The numerical results are lower than the value of 3 predicted by the GOE model. Figure 4.9 (b) shows the values of *K* at another position of the grid and give an idea of the variability of the results with location. The behaviour observed for the excitation point is similar to that obtained for the other points with increasing values as the mode order increases.

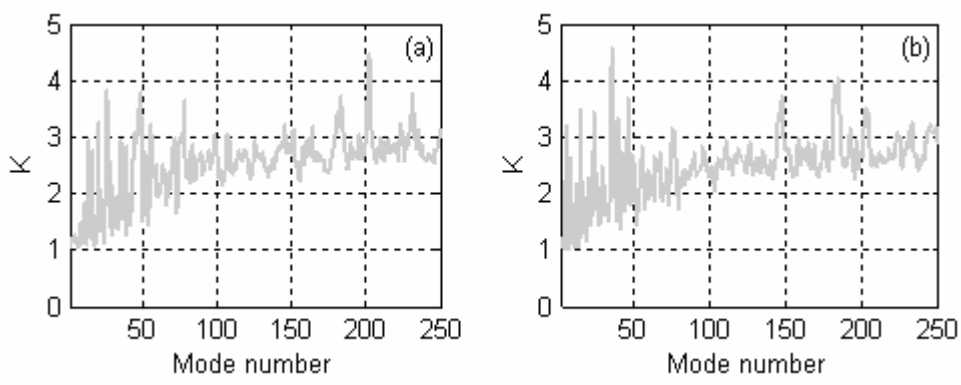

Figure 4.9 – Mode shape statistics factor *K* – Case B6. a) force position (x = 0.11, y = 0.135) b) another position. ——— numerical results.

The spatial distribution of *K* is shown in Figure 4.10 for four modes: the 10th mode, the 80th mode, the 100th mode and 200th mode. It can be observed that *K* varies considerably for different positions and values of 2.5 to 3.5 may be obtained for the same mode at different locations. As would be expected, higher modes display a more random distribution of the mode shape statistics factor.

Figure 4.11 gives the results of the mode shape statistics for Case B7. The results for *K* are slightly higher than those displayed by Case B6 and are closer to the theoretical value of 3. The results for the spatial distribution of *K* are shown in Figure 4.12 and seem to be more random than the distributions obtained for Case B6. Even the results for the 10th mode displayed a highly complex distribution. The numerical results obtained for the mode shape statistics factor are very similar to those given by Langley and Brown in 91.

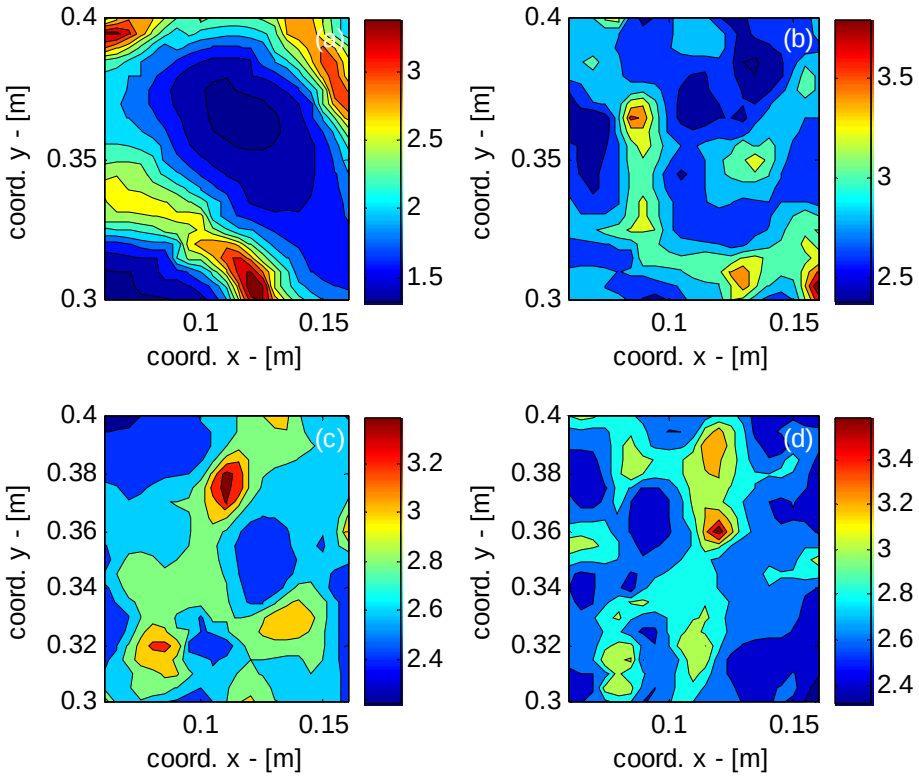

Figure 4.10 – Mode shape statistics factor *K* – Case B6. a) mode 10, b) mode 80, c) mode 200, d) mode 300.

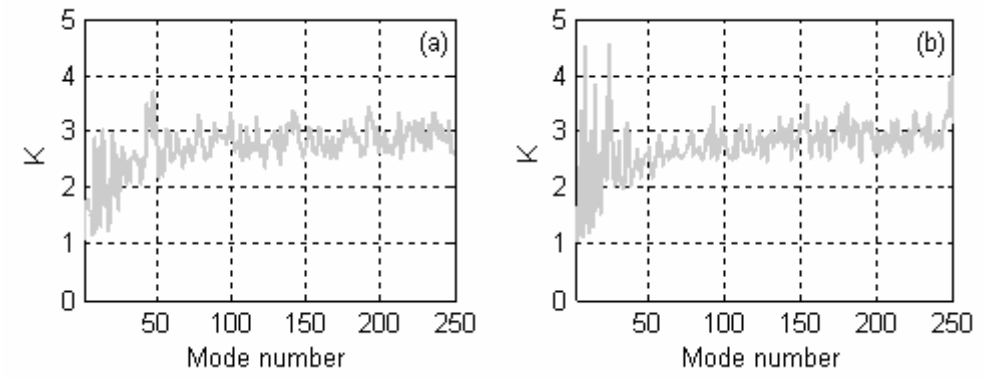

Figure 4.11 – Mode shape statistics factor *K* – Case B7. a) force position (x = 0.11, y = 0.135) b)another position. ——— numerical results.

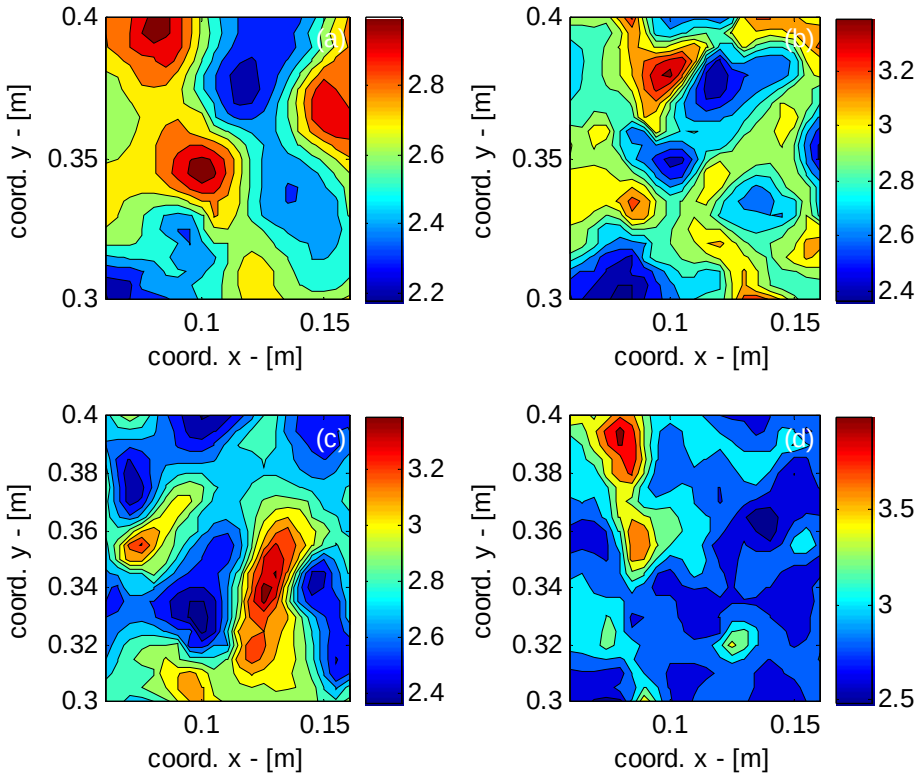

Figure 4.12 – Mode shape statistics factor K – Case B7. a) mode 10, b) mode 80, c) mode 200, d) mode 300.

The behaviour observed for K for Cases B6 and B7 does not seem to explain the differences between the numerical results for the energy density variance and the predictions considering the GOE model. It was observed in section 4.3.2 that the numerical results agree with the predictions considering a value of $K = 2.5$. However, the mode shape statistics factor obtained numerically is higher than this value and much closer to the theoretical value of 3. Therefore, another factor may be affecting the theoretical predictions.

In [94], Brody *et al.* also investigated the correlation between eigenvector components. It was shown that different components of the same eigenvectors or the same component of different eigenvectors cannot be independent for systems with limited sizes. In fact, it was demonstrated that the components are asymptotic statistically independent. Brody *et al.* stated that, for large systems, the correlations would be considerably weak and, in general, could be ignored. However, it was also mentioned that there were some cases were the correlations should be taken into account. In the derivation of the variance theory, this correlation is not considered and the same components of different eigenvectors are considered to be independent. This correlation may be the reason for the discrepancies observed between the mode shape statistics factor adopted in the theory in order for the result to agree and that obtained numerically. In order to verify this point, a different average procedure is proposed and discussed in the next section.

4.3.4 Random excitation point

In the previous sections, some results for the energy density statistics were presented considering an average over the ensemble for a fixed excitation point. In this averaging procedure, only one component of the eigenvector is considered for each mode. It was also observed that there was a lack of agreement between the value of the mode shape statistics factor K obtained numerically and that adopted in the theory in order to match the numerical data. The study by Brody *et al.* [94] suggests that this discrepancy may be due to a correlation between the eigenvector components. In order to verify this assumption, a different averaging process was applied which consisted of calculating the energy density for each member of the ensemble for a random point in the structure. With this new approach, it is expected that the correlation between the eigenvector components will be reduced and the results for the variance predictions considering $K = 3$ will display a better agreement with the numerical results.

The energy density variance calculated considering a random point of excitation for Case B7 is given in Figure 4.13. A significant improvement can be observed in the agreement between the numerical results and the theory for $K = 3$. The same behaviour is observed for all levels of damping. Figure 4.14 gives the mode shape statistics factor calculated considering the new averaging process. It can be noted that although the results are higher than those observed in Figure 4.11 (a) for the standard averaging process, the difference itself cannot explain the discrepancies between the numerical results. The results obtained are a strong indication of a correlation between mode shape amplitudes and its effects on the energy density variance.

Similar results were obtained for Case B6 and they are shown in Figure 4.15 and Figure 4.16.

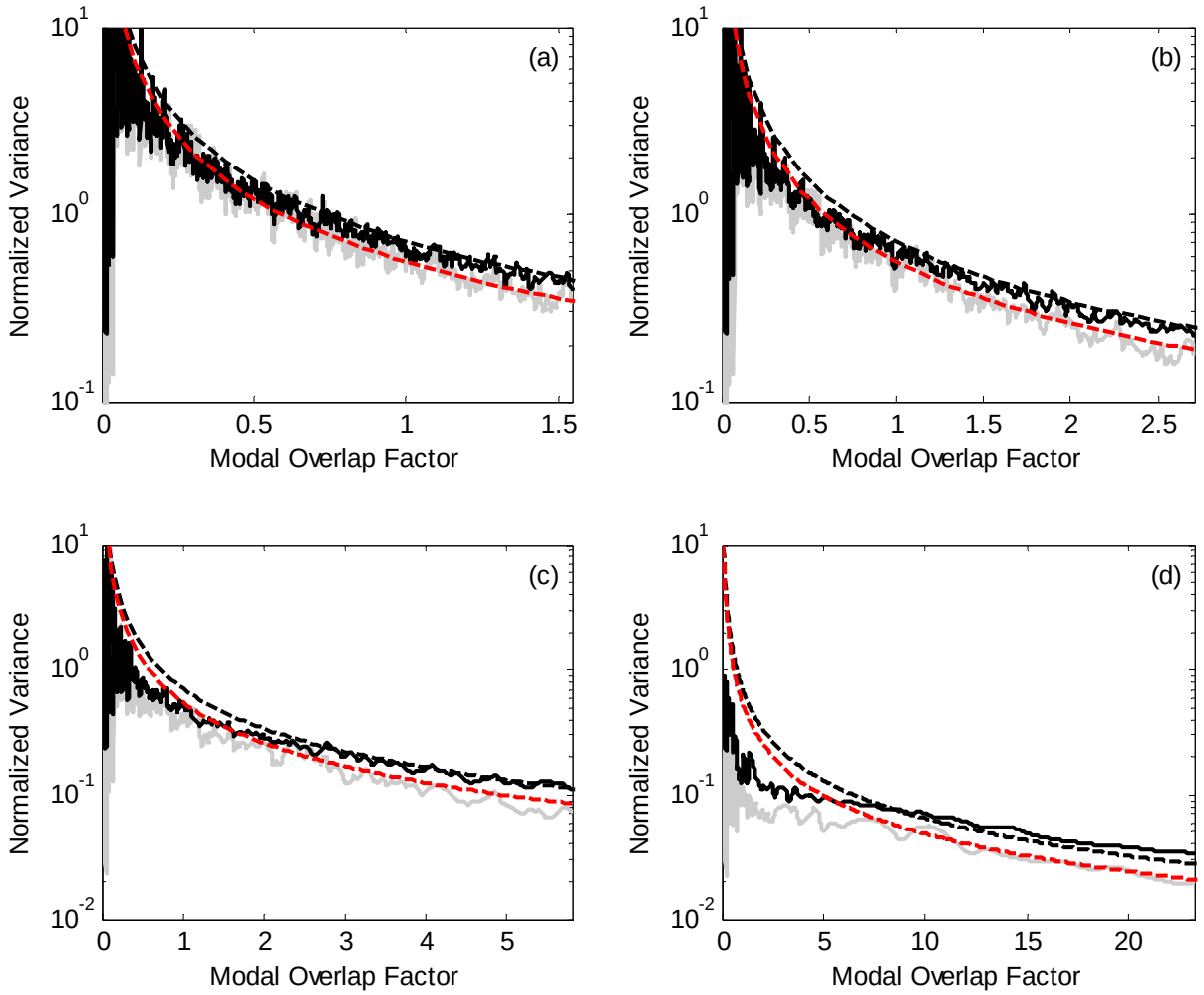

Figure 4.13 – Energy density normalized variance – Case B7. a) η = 0.008, b) η = 0.014, c) η = 0.03 and d) η = 0.12. ——— numerical result (fixed point), ——— numerical result (random point),- - - - - GOE theory K = 3, - - - - - GOE theory K = 2.5.

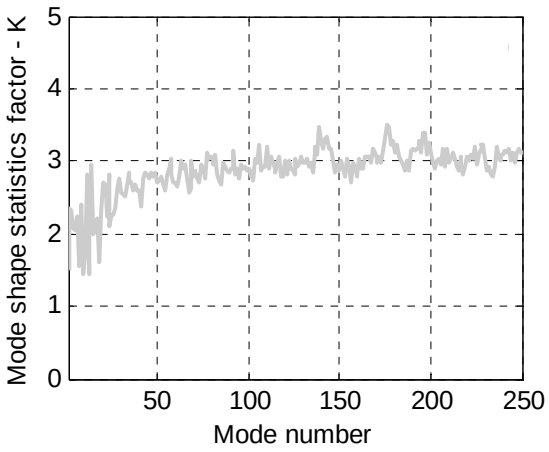

Figure 4.14 – Mode shape statistics factor K, random position – Case B7. ——— numerical results.

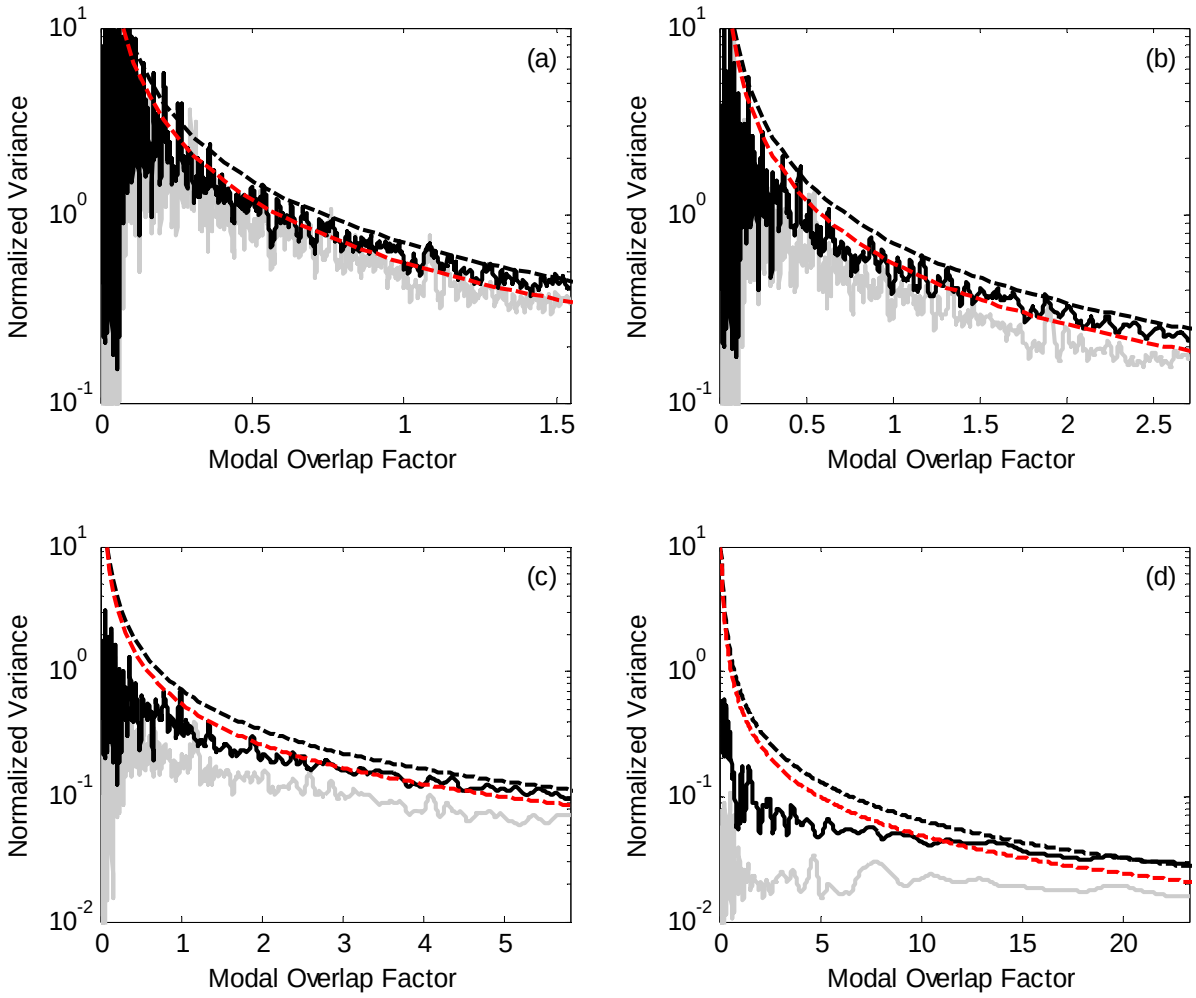

Figure 4.15 – Energy density normalized variance – Case B6. a) $\eta = 0.008$, b) $\eta = 0.014$, c) $\eta = 0.03$ and d) $\eta = 0.12$. ——— numerical result (fixed point), ——— numerical result (random point), - - - - - GOE theory $K = 3$, - - - - - GOE theory $K = 2.5$.

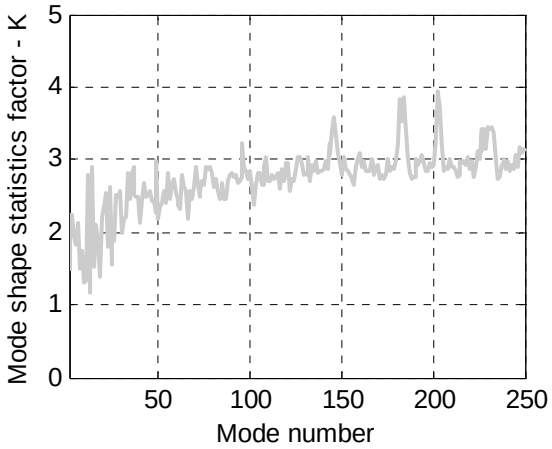

Figure 4.16 – Mode shape statistics factor K, random position – Case B6. ——— numerical results.

4.4 SUMMARY AND DISCUSSIONS

The theory for the prediction of the energy density variance of random systems recently presented by Langley and Brown has been reviewed. The theory assumes that energy density forms a Poisson point process and that the eigenvalue statistics conform to the GOE model predicted by RMT. The formulation for the variance considering a Poisson model for the natural frequencies has also been derived again. Numerical results for the energy density mean and variance were obtained through the approach given in Chapter 2 and considering the ensemble defined in Chapter 3 and compared with the theoretical curves.

It was observed that different probabilistic models have little effect over the energy density mean and a very good agreement with the standard SEA results was obtained for all the ensembles. However, a distinct behaviour was observed for the variance results. The energy density variance was shown to be very sensitive to the eigenvalue statistics observed in Chapter 3. It was noted that the theoretical curves over predict the numerical results for the case of Poisson statistics (Case B1) and for those cases or regions in the frequency domain with a low level of randomness (and therefore near Gaussian eigenvalues). A good agreement with the formulation considering the GOE model was observed when a value of 2.5 for the mode shape statistics factor K was considered, provided the system is sufficiently random.

It was argued that the agreement with the theory for $K = 2.5$ would be due to the mode shape amplitudes not being Gaussian as predicted by RMT. However, a numerical investigation has shown that mode shape amplitudes are near-Gaussian and values around 2.8 and 2.9 were observed for the mode shape statistics factor. These results suggested that another phenomenon may be affecting the variance predictions. It was then argued that the correlation between the same component of different eigenvectors may the responsible for the discrepancy observed since the theory assumes independence of the mode shape amplitudes. A different averaging process was used to calculate the variance where a random position of the excitation point was considered. Correlations between mode shape amplitudes are likely to be reduced in this averaging process since different components of different eigenvectors are considered in the calculation. The new results for the energy density variance displayed a better agreement with the predictions considering the GOE model and $K = 3$, which suggests that the correlations between mode shape amplitudes play an important role and are the responsible for the discrepancies observed.

Although the new variance theory displayed some discrepancies with the numerical results, it is an important improvement on the previous formulation that considers a Poisson model. It is expected that a good agreement will be obtained for sufficiently random cases or,

in the case of a real system, for a sufficiently high frequency. In fact, as the level of randomness is increased, the agreement should be considerably improved since the correlations between mode shape statistics would be reduced and the eigenvalue statistics would agree even better with the GOE model. Therefore, for real systems, the concern is with the definition of the limits between an almost-deterministic behaviour and the GOE behaviour.

The analyses carried out until this point were based in numerical results obtained using the approach described in Chapter 2. However, in order to proceed with the investigation into the limits for the application of the GOE model, there is a requirement for a much faster method. With the computational power available, more than 48 hours was needed to solve the eigenproblem and calculate the energy density for all the members of only one of the ensembles considered. Therefore, an artificial approach is proposed in the next Chapter where the stiffness matrix of a general dynamic system is considered as random and the only source of uncertainty.

CHAPTER 5

RANDOM DYNAMIC SYSTEMS

5.1 INTRODUCTION

In order to study the statistics of random dynamic systems and the applicability of the GOE model it is necessary to generate ensembles of dynamic systems, obtain their eigenvalues and then calculate their statistics. If done experimentally, it would be necessary to construct such ensembles of structures with controlled statistics of their physical properties and perform a modal analysis of each structure, which would be extremely expensive and impractical. Choosing a numerical approach, where the system is modelled using one of the deterministic methods (FE Method, Boundary Elements Method, etc), would require a great computational power to solve the eigenproblem for each member of the ensemble covering the frequency range of interest (with a statistically representative number of modes) and the number of cases required. The method adopted should also be capable of applying different probabilistic models and allow the calculation of the energy density statistics. In view of the limitations of other methods and the established objectives, an artificial approach is proposed here to study the statistics of the energy density of a random dynamic system. In this new approach, the stiffness matrix of a general dynamic system is assumed as being random and the only source of uncertainty. The new approach should allow the calculation of the eigenvalues for the ensemble in a reasonable time and the modification of the input statistics of the ensemble in a practical way. This Chapter presents the derivation of the energy density for a system with a random stiffness matrix. Different randomization approaches are investigated. The aim is to obtain the same behaviour for the eigenvalue statistics and the energy density variance observed in Chapter 3 and Chapter 4 for random plates, which would validate the method as a tool to study the statistics of random dynamic systems. Another approach was also investigated in order to link the statistics of a random matrix with the energy density variance predictions. The approach did not display good results but it is briefly described in Appendix D.1.

5.2 RESPONSE OF A RANDOM SYSTEM

The equations of motion of a general linear dynamic system may be written in the form [5]

$$\mathbf{M}\ddot{\mathbf{x}} + \overline{\mathbf{K}}\mathbf{x} = \mathbf{f}\,, \tag{5.1}$$

where $\overline{\mathbf{K}} = \mathbf{K}(1 + i\eta)$ assumes proportional damping, **K** is the stiffness matrix, **M** is the mass matrix, **f** is a vector containing the external forces and **x** is a vector with the displacements in generalized coordinates. The eigenvalue problem can be defined as

$$\mathbf{KU} = \mathbf{\Lambda MU}\,,\ \mathbf{U}^T\mathbf{MU} = \mathbf{I}\,,\ \mathbf{U}^T\mathbf{KU} = \mathbf{\Lambda}\,, \tag{5.2}$$

with $\mathbf{U} = \begin{bmatrix}\mathbf{u}_1 & \mathbf{u}_2 & \dots & \mathbf{u}_N\end{bmatrix}$ being a matrix whose columns are the eigenvectors $\mathbf{u}_j$ and $\mathbf{\Lambda} = diag\begin{pmatrix}\omega_1^2 & \omega_2^2 & \dots & \omega_N^2\end{pmatrix}$ a diagonal matrix with the natural frequencies ω_j. A coordinate transformation from the generalized coordinate system to the modal or natural coordinate system can be performed considering

$$\mathbf{x} = \mathbf{Uq}\,, \tag{5.3}$$

with **q** being a vector with the displacements in natural coordinates. Substituting Equation (5.3) into Equation (5.1) yields

$$\ddot{\mathbf{q}} + \overline{\mathbf{\Lambda}}\mathbf{q} = \mathbf{U}^T\mathbf{f}\,, \tag{5.4}$$

where $\overline{\mathbf{\Lambda}} = \mathbf{\Lambda}(1 + i\eta)$.

Consider that the system is now a member of an ensemble of systems, each one with its matrices **U** and **Λ**. Instead of adopting the natural coordinates of each system, let's write the equations of motion of all the members of the ensemble based on the natural coordinates of the original or nominal system. In this case, one can write

$$\ddot{\mathbf{q}} + \overline{\mathbf{A}}\mathbf{q} = \mathbf{U}^T\mathbf{f}\,, \tag{5.5}$$

where $\overline{\mathbf{A}} = \mathbf{A}(1 + i\eta)$, with **A** being a random symmetric matrix. **A** would become diagonal

only in the case of the original system. It would not make sense to recalculate the eigenvalues for Equation (5.4), since the eigenvalues are already the diagonal of $\mathbf{\Lambda}$. However, in Equation (5.5), $\mathbf{A}$ is not diagonal anymore and allows the definition of a new eigenvalue problem,

$$A\mathbf{U}_R = \mathbf{\Lambda}_R \mathbf{M}\mathbf{U}_R\,, \tag{5.6}$$

where $\mathbf{U}_R = \begin{bmatrix}\mathbf{u}_1^R & \mathbf{u}_2^R & \dots & \mathbf{u}_N^R\end{bmatrix}$ is a matrix with the new eigenvectors and $\mathbf{\Lambda}_R = diag\begin{pmatrix}\omega_1^{R\,2} & \omega_2^{R\,2} & \dots & \omega_N^{R\,2}\end{pmatrix}$ is a diagonal matrix with the new eigenvalues. The superscript R indicates the eigenvalues and eigenvectors of the random system (a system randomly chosen from the ensemble). A new coordinate transformation can also be proposed,

$$\mathbf{q} = \mathbf{U}_R \mathbf{q}_R\,, \tag{5.7}$$

with $\mathbf{q_R}$ being a vector with the displacements in "natural random coordinates". The above procedure can be repeated and the equations of motion become

$$\ddot{\mathbf{q}}_R + \overline{\mathbf{\Lambda}}_R \mathbf{q}_R = \mathbf{U}_R^T \mathbf{U}^T \mathbf{f}\,, \tag{5.8}$$

where $\overline{\mathbf{\Lambda}}_R = \mathbf{\Lambda}_R(1+i\eta)$. Equation (5.8) can be solved to obtained $\mathbf{q_R}$,

$$\mathbf{q}_R = \left[-\omega^2\mathbf{I} + \overline{\mathbf{\Lambda}}_R\right]^{-1}\mathbf{U}_R^T\mathbf{g}\,, \tag{5.9}$$

where it is assumed that the mass matrix is equal to the identity matrix, and the vector $\mathbf{g}$ is given by,

$$\mathbf{g} = \mathbf{U}^T\mathbf{f}\,. \tag{5.10}$$

Equation (5.9) can be rewritten in natural coordinates,

$$\mathbf{q} = \mathbf{U}_R\left[-\omega^2\mathbf{I} + \overline{\mathbf{\Lambda}}_R\right]^{-1}\mathbf{U}_R^T\mathbf{g}\,, \tag{5.11}$$

or in generalized coordinates,

$$\mathbf{x} = \mathbf{U}\mathbf{U}_R\left[-\omega^2\mathbf{I} + \overline{\mathbf{\Lambda}}_R\right]^{-1}\mathbf{U}_R^T\mathbf{g}. \tag{5.12}$$

The aim of this analysis is to find the energy density associated with a random stiffness matrix **A**. The kinetic energy V of a general dynamic system can be given by

$$V = \frac{1}{2}\dot{\mathbf{x}}^{T*}\mathbf{M}\dot{\mathbf{x}}. \tag{5.13}$$

Considering Equation (5.13) and that the system span is given by its dimension, it follows that the kinetic energy density can be written as

$$T(\omega) = \frac{\omega^2}{2N}\mathbf{x}^{T*}\mathbf{x}. \tag{5.14}$$

Substituting Equation (5.12) in Equation (5.14), would give

$$T(\omega) = \frac{\omega^2}{2N}\left[\mathbf{g}^T\mathbf{U}_R\mathbf{B}^{-1*}\mathbf{B}^{-1}\mathbf{U}_R^T\mathbf{g}\right], \tag{5.15}$$

where $\mathbf{B} = \left[-\omega^2\mathbf{I} + \overline{\mathbf{\Lambda}}_R\right]$. Equation (5.15) can also be expressed as a modal summation,

$$T(\omega) = \frac{\omega^2}{2N}\sum_n \frac{|r_n|^2}{\left(\omega_n^2 - \omega^2\right)^2 + \left(\eta\omega\omega_n\right)^2}, \tag{5.16}$$

where $\mathbf{r} = \mathbf{U}_R^T\mathbf{g}$. The reason for rewriting Equation (5.15) in the form of Equation (5.16) is that the latter is more similar to Equation (4.1), which facilitates the identification of the coefficient a_n and the spatial factor α. Both parameters will be used in Equation (4.25) for the prediction of the energy density variance of the artificial random system. Here α is given by,

$$\alpha = \frac{E\left[r_n^4\right]}{E\left[r_n^2\right]^2}. \tag{5.17}$$

Equation (5.16) yields the kinetic energy density for each member of the ensemble and it is only necessary to define the matrix **A** associated with each member. Thus, based on

an ensemble of **A** matrices with controlled statistical inputs, it is possible to calculate the statistics of the energy density. This feature allows the study of the influence of the statistical inputs on the natural frequency and mode shape statistics and, consequently, on the energy density statistics, as initially required. The procedure is considerably fast and allows the solution of an ensemble with a statistically representative size. Ways of defining matrix **A** are discussed in the next section.

5.3 RANDOM STIFFNESS MATRIX

Let's consider matrix **A** as being defined as

$$\mathbf{A} = \mathbf{A_0} + R\mathbf{A_{ran}}, \tag{5.18}$$

where $\mathbf{A_0}$ is a diagonal matrix and $\mathbf{A_{ran}}$ is a random symmetric matrix . Matrix $\mathbf{A_0}$ can be interpreted as the stiffness matrix in modal coordinates of the original dynamic system considered in the previous section. The system randomness (the deviation of each member from the original system) is introduced through matrix $\mathbf{A_{ran}}$ and can be controlled by the constant *R*. The statistics of the entries of $\mathbf{A_{ran}}$ will determine the statistics of the eigenvalues of **A**, and thus those of the energy density.

The entries of $\mathbf{A_{ran}}$ were divided into three groups to allow the randomization of the system in particular ways. The diagonal terms were included in Group A, while the off-diagonal terms were divided into Groups B and C. If the matrix is divided into quadrants, the off-diagonal terms in quadrants 1 and 4 will be included in Group B, while the off-diagonal terms at other quadrants will constitute group C. The groups can also be defined as,

$$\begin{aligned}
&\text{Group A} \Rightarrow a_{jk}, \quad j = k, \qquad j = 1\ldots N, \qquad k = 1\ldots N, \\
&\text{Group B} \Rightarrow \begin{cases} b_{jk}, & j \neq k, \qquad j = 1\ldots N/2, \qquad k = 1\ldots N/2 \\ b_{jk}, & j \neq k, \qquad j = N/2+1\ldots N, \qquad k = N/2+1\ldots N \end{cases}, \\
&\text{Group C} \Rightarrow \begin{cases} c_{jk}, & j \neq k, \qquad j = 1\ldots N/2, \qquad k = N/2+1\ldots N \\ c_{jk}, & j \neq k, \qquad j = N/2+1\ldots N, \qquad k = 1\ldots N/2 \end{cases}.
\end{aligned} \tag{5.19}$$

Equation (5.20) gives a better understanding of the division of $\mathbf{A_{ran}}$ into groups, using the example of an 8x8 matrix.

$$\begin{bmatrix} a_{jk} & b_{jk} & b_{jk} & b_{jk} & c_{jk} & c_{jk} & c_{jk} & c_{jk} \\ b_{jk} & a_{jk} & b_{jk} & b_{jk} & c_{jk} & c_{jk} & c_{jk} & c_{jk} \\ b_{jk} & b_{jk} & a_{jk} & b_{jk} & c_{jk} & c_{jk} & c_{jk} & c_{jk} \\ b_{jk} & b_{jk} & b_{jk} & a_{jk} & c_{jk} & c_{jk} & c_{jk} & c_{jk} \\ c_{jk} & c_{jk} & c_{jk} & c_{jk} & a_{jk} & b_{jk} & b_{jk} & b_{jk} \\ c_{jk} & c_{jk} & c_{jk} & c_{jk} & b_{jk} & a_{jk} & b_{jk} & b_{jk} \\ c_{jk} & c_{jk} & c_{jk} & c_{jk} & b_{jk} & b_{jk} & a_{jk} & b_{jk} \\ c_{jk} & c_{jk} & c_{jk} & c_{jk} & b_{jk} & b_{jk} & b_{jk} & a_{jk} \end{bmatrix}. \tag{5.20}$$

Each entry of $\mathbf{A}_{\mathbf{ran}}$ was considered as a Gaussian random variable with zero mean and with the variance being dependent on the group (σ_a^2 for group A, σ_b^2 for group B and σ_c^2 for group C). This randomization approach of the matrix $\mathbf{A}_{\mathbf{ran}}$ results in an almost constant randomization level for the eigenvalues. This situation is rarely found for a real dynamic system, since the uncertainties from the manufacture process are likely to have more effect on higher order modes. The randomization level is not exactly constant over the eigenvalues as a result of the limited size of the problem considered. The first and last eigenvalues will always interact with a reduced number of eigenvalues compared to the eigenvalues in the middle of the eigenvalue range. The results presented below will be usually related to the eigenvalues and eigenvalue spacings located in the middle of the eigenvalue range.

The diagonal elements of matrix $\mathbf{A}_{\mathbf{0}}$ are associated with the natural frequencies of the nominal system. In Chapter 3, the numerical analyses were carried out with plates as dynamic systems. This type of structure is characterized by a constant modal density for the flexural modes as can be noted from Equation (2.16), where the modal density is independent of the frequency. Therefore, in order to allow a better comparison with the results previous obtained, the diagonal elements of the matrix $\mathbf{A}_{\mathbf{0}}$ were defined as $\left(101^2 \quad 102^2 \quad \ldots \quad (100+N)^2\right)$. This definition provides an almost constant modal density and avoids negative eigenvalues. The modal density not being exactly constant and the effects over the calculation of the statistics parameters (Number variance and Δ_3) were discussed by Weaver in [87]. The causes of a non-constant modal density were named “secularities”. Weaver developed his studies with aluminium blocks, which are known to have a non-constant modal density and a method was required to remove the “secularities”. However, in the present study, the effect of the non-constant modal density can be neglected and it will be seen that the statistics are not affected by this assumption. The non-constant spacing between natural frequencies was taken into account in the randomization process in order to have a

constant randomization level over the whole eigenvalue range.

An example of the MATLAB® code used to generate an ensemble of matrices is presented in Appendix D.2.

5.4 NATURAL FREQUENCY STATISTICS

5.4.1 GOE statistics

An initial numerical simulation was performed with the aim of obtaining GOE statistics. A system with size N = 200 and an ensemble of 500 members was considered. A question arises regarding how high the variance of the $\mathbf{A}_{\mathbf{ran}}$ entries must be defined in order to achieve GOE statistics. The parameter called statistical overlap factor s_i proposed by Manohar and Keane in [76] and defined by Equation (1.10) has been previously used to verify the randomization level of a random system. A slightly different definition of the statistical overlap factor can also be found in the literature, where the global mean spacing rather than the local mean spacing is considered [98]. Langley and Brown [91] suggested that a statistical overlap factor greater than unity would be a good indication of GOE statistics. However, it has been seen in Chapter 3 that a statistical overlap factor greater than one may be obtained for systems with symmetries depending on the randomization approach adopted. In this first analysis, the matrix $\mathbf{A}_{\mathbf{ran}}$ was defined following the GOE definition given by Mehta [10]. Mehta states that in the GOE ensemble the off-diagonal elements have the same variance, while the diagonal elements have twice that variance. Therefore, the statistics of $\mathbf{A}_{\mathbf{ran}}$ entries were given by σ_a^2=2 and $\sigma_b^2 = \sigma_c^2$=1. The value of R was set as 2. The diagonal elements of $\mathbf{A}_{\mathbf{ran}}$ will have a direct influence over the eigenvalues of $\mathbf{A}$ and thus $R\sigma_a^2$ can be viewed as the variance of the eigenvalues. In fact, $R\sigma_a^2$ is the minimum variance associate with the eigenvalues, since the off-diagonal elements of $\mathbf{A}_{\mathbf{ran}}$ will also contribute to the eigenvalue dispersion. The value of σ_a^2 and R should ensure a statistical overlap factor greater than unity and, as the system does not possess symmetries, should provide the required GOE statistics.

The ensemble of matrices was generated and the eigenproblem solved for each member of the ensemble. Figure 5.1 gives the local ($\mathrm{E}\left[\lambda_{n-1}{}^2 - \lambda_n{}^2\right]$) and global ($\mathrm{E}\left[\mathrm{E}\left[\lambda_{n-1}{}^2 - \lambda_n{}^2\right]\right]_n$) mean spacing between eigenvalues, the eigenvalues standard deviation and the global and local statistical overlap factor.

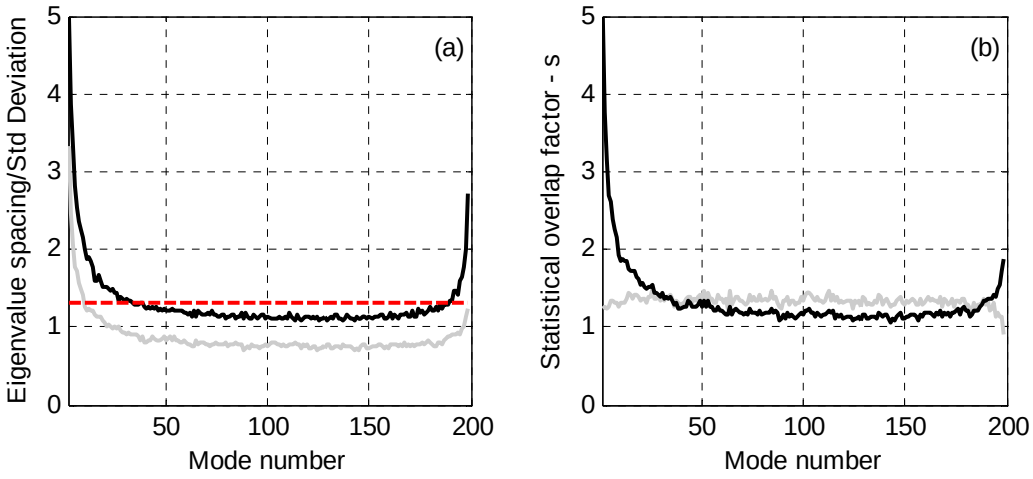

Figure 5.1 – Plot (a): global eigenvalue spacing, local eigenvalue spacing, eigenvalue standard deviation. Plot (b): Statistical overlap factor. global mean spacing, local mean spacing.

As predicted, the statistical overlap factor is higher than one and should be sufficient to provide GOE statistics. It can be noted that large values for the spacing and the standard deviation are obtained for the eigenvalues at the limits of the eigenvalue range, which also gives large values for the statistical overlap factor when considering the global mean spacing. This behaviour is due to a reduced number of eigenvalues interacting in this region and to the repulsion caused by the eigenvalues located more towards the centre of the eigenvalue range. This repulsion is compensated when the eigenvalue is located in the centre of the spectrum, since there are eigenvalues at both sides. This effect is not usually observed in a real system such as those studied in Chapter 3, since the randomization level of the first modes is small and there is no interaction between the first modes.

It should be noted that, except for the first and last eigenvalues, the statistical overlap factor is almost constant across the eigenvalue range which differs from the statistical overlap factor observed for real systems in Chapter 3. This is due to the artificial randomization approach adopted. The application of a variable randomization level for the eigenvalues (in order to have an increasing level of randomness as the numerical results) would be possible but would increase the complexity of the problem and make it difficult to analyze the results. In what follows, the analysis of the results will be carried out for a single eigenvalue or spacing between eigenvalues at the centre of the eigenvalue range since the neighbour eigenvalues would display similar results. The approach can be interpreted as the analysis of a set of eigenvalues of a real system that possesses a similar randomness level and would be associated with a region of the statistical overlap factor curve.

The statistics of the eigenvalues for this first analysis were then calculated and are given in Figure 5.2. Numerical results for the pdf of the spacing between successive natural frequencies can be observed in Figure 5.2(a), together with the exponential pdf, the Gaussian pdf and the Rayleigh pdf. The numerical results conform well to the GOE prediction (Rayleigh distribution). Figure 5.2(b) and Figure 5.2(c) show the number variance Σ^2 and Δ_3, respectively, calculated using Equation (3.6) and Equation (3.8). Again, a good correlation can be observed between the numerical data and the GOE statistical model. Also shown in the plots are curves associated with the Poisson model. A low value of Σ^2 and Δ_3 suggests a high degree of correlation between eigenvalues and is usually associated with a low level of randomization. The results are given for the 100th spacing or 100th eigenvalue for Figure 5.2(a), Figure 5.2(b) and Figure 5.2(c).

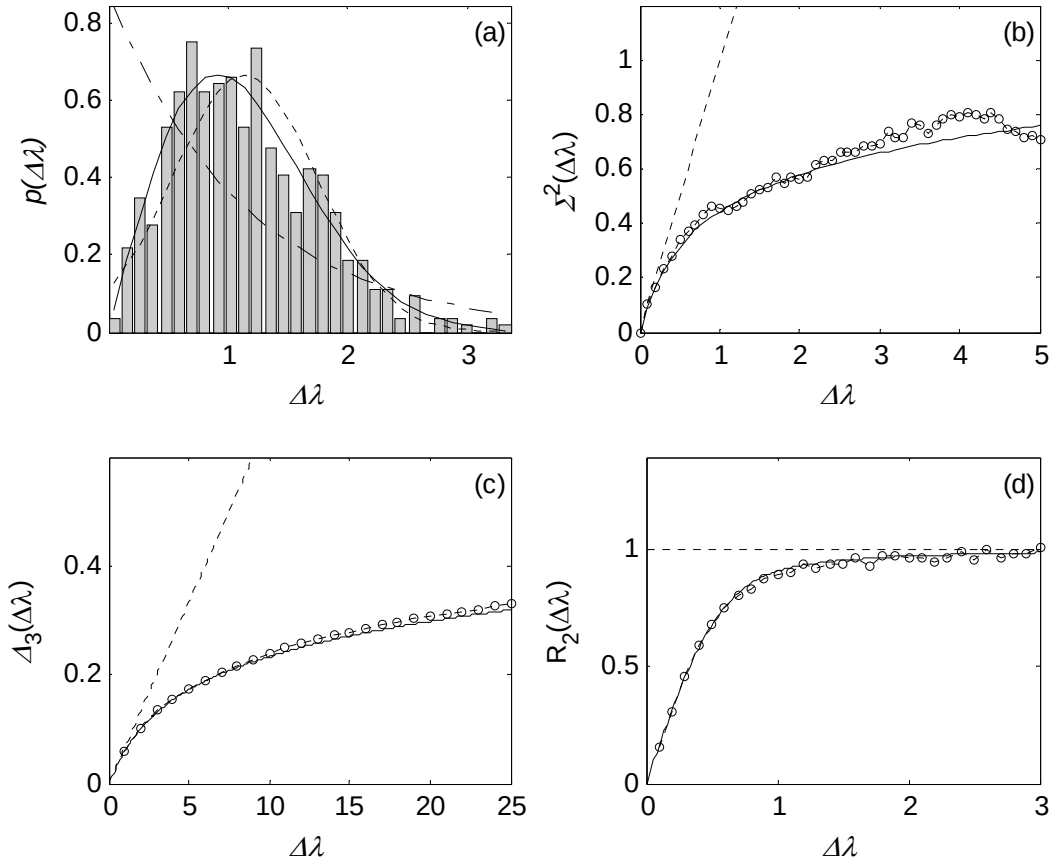

Figure 5.2 – Statistics of the eigenvalues of a random matrix. Plot (a): ------ Normal distribution, – - – Exponential distribution, —— Rayleigh distribution. Plots (b), (c) and (d): —— GOE statistics, ------ Poisson statistics, -◇- numerical data.

Figure 5.2(d) shows results obtained for the R_2 function considering a system with a reduced size of $N = 50$ and a much larger ensemble with 70.000 members, in order to allow the convergence of the results. In fact, the convergence was only achieved by also averaging R_2 for the eigenvalues in the range $\lambda_{23} \leq \lambda_j \leq \lambda_{27}$. As a consequence of its much more costly convergence, the function R_2 will not be used in the following analysis and only the pdf, Σ^2 and Δ_3 will be further employed.

There follows an analysis of how the statistics of the eigenvalues and the energy density behave for three different situations in view of what has been previously observed for real systems in Chapter 3. First, there is the case where the ensemble shifts from an almost deterministic behaviour to a condition of high level randomness. This situation can be associated with two distinct scenarios for real systems: the increasing of the randomization level used to define the ensemble or an increase in the frequency range considered. An example of an increase in the randomness level can be observed for Case B6 and Case B7 analysed in Chapter 3, where the size of the random masses were increased. The other scenario occurs when the level of randomness is kept fixed but higher modes are considered. The higher modes being more sensitive to the system uncertainties also result in an increase in the eigenvalue dispersion. An example of this scenario can be observed in Figure 3.22, where the higher modes display a better agreement with the GOE model.

The next situation is related to the occurrence of Poisson statistics. The Poisson model has been previously used for the statistics of the eigenvalues [83,84] and it has been seen in Chapter 3 that real systems may display this type of statistical model. This can be observed when comparing Cases B1 and B5 analysed in Chapter 3. Both systems are nominally equal but are randomized in different ways: one leading to Poisson and the other to GOE statistics. Thus, the second situation studied is associated with the gradual transition from GOE statistics to Poisson statistics.

Finally, the last situation deals with systems with different levels of symmetry and the effect on the statistics of the eigenvalues. It has been argued that the presence of symmetries allows the existence of two or more independent sequences of eigenvalues, each one displaying GOE statistics [101,103,106]. This issue was discussed in Chapter 3 and equations for the statistics of the eigenvalues for two overlapping GOE groups were given. It was not possible to obtain the statistics for two overlapping GOE groups in Chapter 3 since it would be necessary to include in-plane modes in the analysis. However, a similar analysis was performed by Bertelsen *et al.* in [101] and Ellegaard *et al.* in [106] and this type of statistics were obtained for a plate. Therefore, an attempt is made to generate a random system composed of two overlapping groups of eigenvalues, both with GOE characteristics. The

coupling between the sub-systems is then increased and its effects on the eigenvalue statistics verified.

5.4.2 Varying the overall level of randomness

A study was carried out reducing continuously the level of randomness of the system through the constant *R*, but keeping the same values for σ_a^2, σ_b^2 and σ_c^2 (and consequently the GOE relation). The results shown in Figure 5.2 are associated with Case C1, while Figure 5.3 gives the results for another three cases: Case C2, with $R = 1$; Case C3, with $R = 0.5$ and Case C4, with $R = 0.2$. Once more, the results are given for the 100th spacing or 100th eigenvalue.

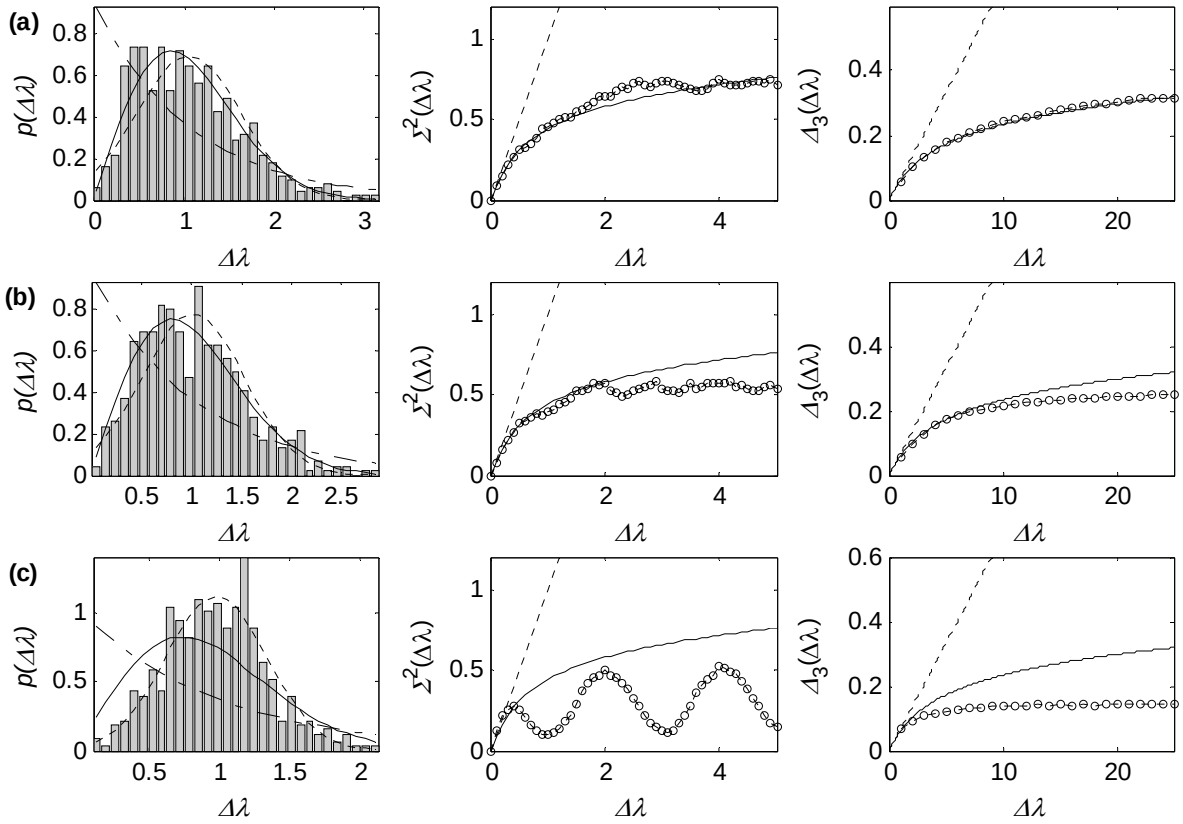

Figure 5.3 – Statistics of the eigenvalues of a random matrix – varying the overall level of randomness. Pdf plots: ------ Normal distribution, – - – Exponential distribution, —— Rayleigh distribution. Number variance and Δ_3 plots: —— GOE statistics, ------ Poisson statistics, -◇- numerical data.

As expected, the reduction in the randomization level represents a deviation from the GOE model. As the level of randomness is reduced, the pdf of the spacing between eigenvalues shifts from a Rayleigh distribution to a Gaussian distribution, as there is no more mixing between the eigenvalues. For an engineering structure, a similar behaviour to Case C1 would be expected for high frequencies, where the response is highly affected by uncertainties from the manufacturing process. On the other hand, similar statistics to those for Case C4 would be expected for low frequencies. Σ^2 and Δ_3 also deviate increasingly from the GOE model as the randomness goes down. It is interesting to observe, that there is a reduction in both statistics, which can be interpreted as an increase in the level of spectral rigidity. In other words, an ensemble of structures with a low level of randomness would have very similar spectra.

It is important to note the similarity between the transitions of the eigenvalue statistics with the behaviour observed for real structures in Chapter 3. This similarity is a very good indication that the approach proposed for the randomization of an artificial dynamic system possesses the basic characteristics that would allow its use to study the statistics of real systems.

5.4.3 Inducing Poisson statistics

The Poisson model predicts an exponential distribution for the spacing between natural frequencies and considers the natural frequencies as statistically independent. On analyzing the structure of $\mathbf{A}_{\mathbf{ran}}$, it is clear that an off-diagonal entry would imply a correlation between two natural frequencies. Therefore, to obtain Poisson statistics, a study was developed where the variance of the off-diagonal elements (Groups B and C of $\mathbf{A}_{\mathbf{ran}}$ elements) was continuously reduced. The constant R and σ_a^2 were kept fixed, both with a value of 2. Three ensembles were then generated: Case C5, with $\sigma_b^2 = \sigma_c^2 = 0.2$, Case C6, with $\sigma_b^2 = \sigma_c^2 = 0.05$ and Case C7, with $\sigma_b^2 = \sigma_c^2 = 0$.

Figure 5.4 shows the statistics for these cases. The transition from a GOE to a Poisson model is quite clear and the results agree very well with the statistical models for the extreme cases. Again, the randomization approach proposed seems to display the same trend observed for systems composed of random plates studied in Chapter 3.

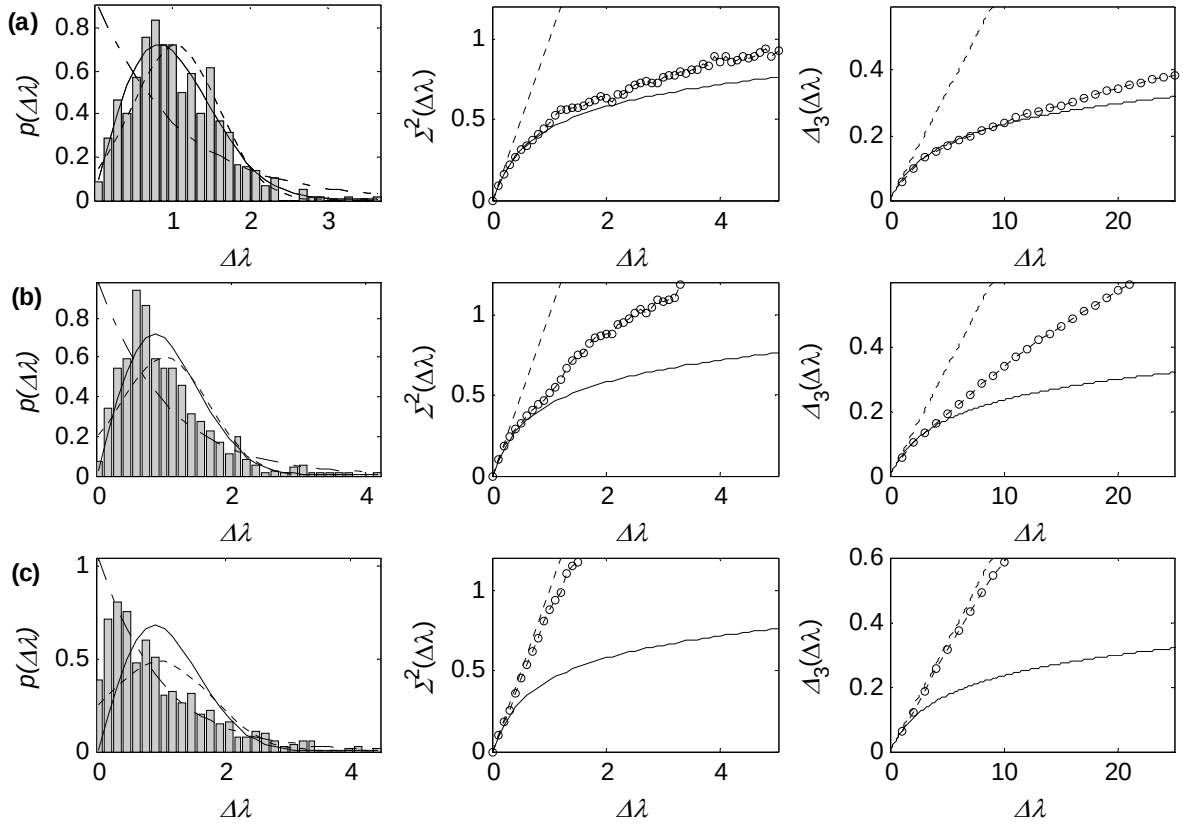

Figure 5.4 – Statistics of the eigenvalues of a random matrix – inducing Poisson statistics. Pdf plots: ------ Normal distribution, – - – Exponential distribution, —— Rayleigh distribution. Number variance and Δ_3 plots: —— GOE statistics, ------ Poisson statistics, -·-·- numerical data.

5.4.4 Inducing symmetries

Let's consider now the case of systems with symmetries. Many previous studies have suggested that these systems do not display GOE statistics. This phenomenon was well investigated in [103] by Ellegard *et al.* for the case of quartz blocks and in [101] by Bertelsen *et al.*. for plates. The current understanding is that the symmetries allow two or more groups of eigenvalues that overlap to be independent of each other, resulting in eigenvalue statistics between the GOE and Poisson model [106]. Equations for the eigenvalue statistics can be obtained if the number of overlapping groups and the modal density of each one are known. Equations (3.12), (3.13) and (3.14) give the eigenvalue statistics for the case of two overlapping groups with the same modal density.

In order to simulate a system with symmetries using the previously proposed artificial approach, it becomes necessary to modify the deterministic matrix $\mathbf{A_0}$. Therefore, the diagonal elements of $\mathbf{A_0}$ are defined as

$$\mathbf{A}_0 = \begin{cases} a_{jk}^0, & j = k \\ 0 & j \neq k \end{cases}, \; a_{jj}^0 = \begin{cases} (100 + j)^2, & j = 1, \ldots, N/2 \\ [100 + (j - N/2)]^2 & j = N/2 + 1, \ldots, N \end{cases}. \tag{5.21}$$

With this new definition, $\mathbf{A_0}$ now includes two groups of overlapping eigenvalues. Each group comprises 100 eigenvalues and a statistical coupling between the two groups may be introduced through the off-diagonal elements of $\mathbf{A_{ran}}$ represented by Group C. It is expected that making the variance of Group C elements zero would allow the two overlapping groups to become statistically independent of each other. Again, a transition between a situation of strong coupling to one with no coupling was investigated by the analysis of three different cases: Case C8, with σ_c^2 = 0.1; Case C9, with σ_c^2 = 0.01 and Case C10, with σ_c^2 = 0. The other inputs were kept as $R = \sigma_a^2 = 2$ and $\sigma_b^2 = 1$ for all cases.

The eigenvalue statistics obtained for Cases C8 to C10 are shown in Figure 5.5. Also superposed on the plots are the curves for the statistics of two overlapping GOE groups with the same modal density as given by Equations (3.12), (3.13) and (3.14). A small value of the variance of Group C elements seems to be enough to provide a reasonable coupling between the two groups, leading to GOE statistics as shown by the good agreement between numerical and GOE predictions (single GOE sequence) for Case C8. This is an indication that a small perturbation in real systems may be sufficient to produce eigenvalue statistics following the GOE model even in the presence of symmetries. The numerical data obtained for Case C10, where the coupling is reduced to zero, conforms well to the RMT predictions for two overlapping GOE sequences. It may be noted that the level of repulsion observed in a GOE system is reduced and small spacings between eigenvalues become more likely when two overlapping groups are present.

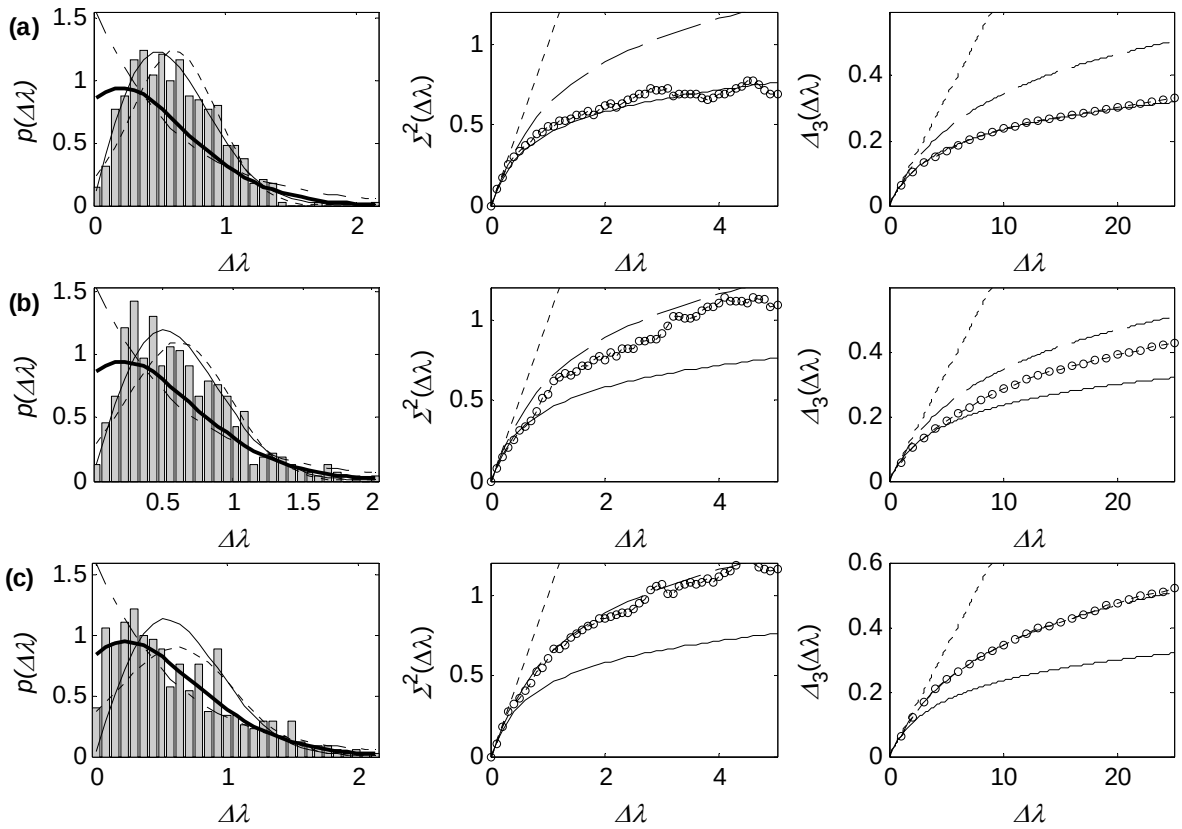

Figure 5.5 – Statistics of the eigenvalues of a random matrix – inducing symmetries in the system. Pdf plots: ------ Normal distribution, – - – Exponential distribution, —— Rayleigh distribution, —— two GOE groups (Equation (3.12)). Number variance and Δ_3 plots: —— GOE statistics, ------ Poisson statistics, – – – two GOE groups, -·-·- numerical data.

In order to allow a better overview of the studied cases, a summary of the input parameters is presented in Table 5.1 .

Table 5.1 – Summary of the considered cases.

Cases	**Deterministic system $\mathbf{A_0}$**	R	σ_a^2	σ_b^2	σ_c^2
C1	One sequence	2.00	2.00	1.00	1.00
C2	One sequence	1.00	2.00	1.00	1.00
C3	One sequence	0.50	2.00	1.00	1.00
C4	One sequence	0.20	2.00	1.00	1.00
C5	One sequence	2.00	2.00	0.20	0.20
C6	One sequence	2.00	2.00	0.05	0.05
C7	One sequence	2.00	2.00	0.00	0.00
C8	Two overlapping sequences	2.00	2.00	1.00	0.10
C9	Two overlapping sequences	2.00	2.00	1.00	0.01
C10	Two overlapping sequences	2.00	2.00	1.00	0.00

The proposed randomization approaches seem to represent well the transition between GOE statistics and the other situations (almost deterministic, Poisson statistics and systems with symmetries). The results are also in agreement with the numerical data obtained for plates in Chapter 3 and provide confidence for using the approach for the study of GOE statistics. A new question now arises: how close to GOE statistics must a system be to allow the application of the GOE model? For example, on analyzing the statistics obtained for Case C5 (Figure 5.4), the pdf agrees quite well with the GOE prediction. The statistics Σ^2 and Δ_3 exhibit a good fit at low values of $\Delta\lambda$, but the results diverge for higher values of $\Delta\lambda$. Is this agreement sufficient to allow the application of the GOE statistics? Clearly, this will depend on the particular application of the statistical model. If someone is only interested in applying the pdf of the spacing between eigenvalues, the answer to this question may be "yes". But if the interest is in the application of higher order statistics, answering this question may not be straightforward. It then becomes necessary to define a particular application of the statistical model. Therefore, the foregoing discussion is centred on the application of GOE statistics in the determination of the energy density variance of a dynamic system as proposed by Langley and Brown in [91]. Equation (5.16) is used to calculate the energy density of each member of ensembles generated as previous described. The effects of a non perfect match of the statistics with the GOE model on the energy density variance are then verified. The results are also compared with the variance theory proposed by Langley and Brown [91].

5.5 ENERGY DENSITY STATISTICS

Numerical results were calculated using Equation (5.16) for systems with size $N = 200$ and an ensemble of 500 members. Equation (5.16) requires the definition of the vector **g** associated with the excitation applied. The vector **g** is given by Equation (5.10) and can be viewed as the force vector **f** in modal coordinates (modes of the nominal structure). In order to allow a comparison with the Chapter 4 numerical results, it would be necessary to consider a point load in the analysis, which would mean a vector **f** with only one non-zero element. However, the present analysis is carried out wholly in modal coordinates, with the ensemble being defined only in terms of deviations from the original modes and thus the modes of the unperturbed structure are not known. In fact, the analysis was carried out in a general form and the modes could be associated with any type of structure. In a real system, a point force is likely to excite the modes in different levels depending on the mode shape at the excitation point and, as the original structure is not defined, the entries of vector **g** may assume any value. The definition of vector **g** does not affect considerably the analysis as can be seen in

Appendix D.3. Therefore, vector **g** was randomly generated and kept the same for all the analyses, simulating a punctual force in modal coordinates.

Figure 5.6 shows some results for the simulation considering $\mathbf{A}_{\mathbf{ran}}$ with GOE statistics (Case C1). Some realizations for the energy density are given with the mean in Figure 5.6 (a). The drop in the curve after 300 rad/s is caused by the limited size of the system. In a real dynamic system with infinite eigenvalues and a constant level of randomness applied to all the modes, a similar curve would be expected but without this drop. It is important to mention that, in the case of real random structures, the uncertainties from the manufacturing processes are not likely to result in a constant level of randomness for all the modes. This does not affect the validity of the current analysis as the results should be interpreted as being associated with a region of the frequency domain where the modes would be similarly randomized.

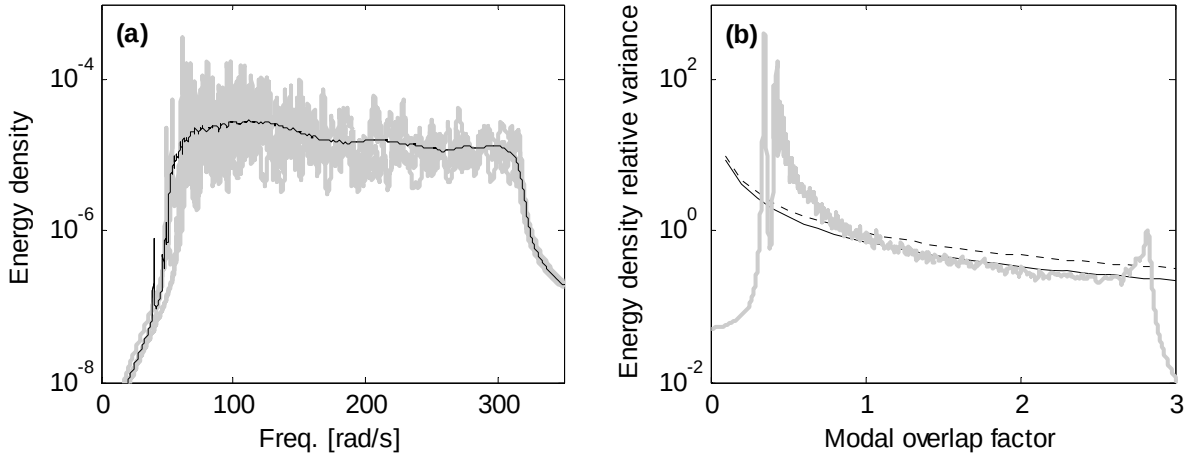

Figure 5.6 – Energy density statistics. Plot (a): —— ensemble mean, —— typical ensemble members. Plot (b): —— GOE statistics, - - - - - - Poisson statistics, —— numerical data.

Figure 5.6 (b) compares the relative variance of the energy density calculated numerically with the results obtained using Equation (4.25). A curve considering the Poisson model is also presented (Equation (4.10)). The results in Figure 5.6 (b) show a good agreement between the numerical results and the model based on GOE statistics.

Although good, the agreement observed in Figure 5.6 (b) is not the same for the whole range, with the theoretical model being sometimes above or below the numerical results. This behaviour is caused by a non-constant mean modal density (ensemble average) as can be observed in Figure 5.7 (a), while a single value is used in the theory (dashed curve in Figure 5.7 (a)). The difference between the value adopted in the theory and the numerical modal density is very similar to the discrepancy between the numerical and theoretical relative variance.

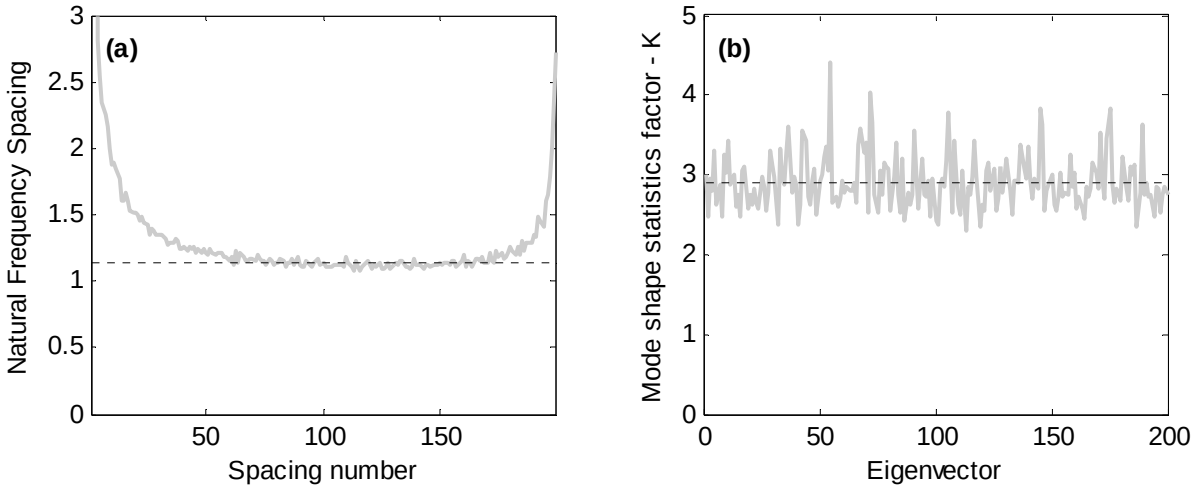

Figure 5.7 – Natural frequency spacings and mode shape statistics factor – Case C1. Plot (a): ——— numerical results, - - - - - - value used in the theoretical models (μ = 1.141). Plot (b): ——— numerical results, - - - - - - mean value (K = 2.911).

The spatial factor α has been considered as equal to K in view of the point load adopted. A Gaussian distribution is assumed for the eigenvectors, leading to a value of K = 3. Figure 5.7 (b) shows the curve obtained numerically for K and, although displaying some oscillation, the assumption of Gaussian eigenvector elements seems to be valid for the GOE case (Case C1). The values of K shown in Figure 5.7 (b) are the average of K across the elements of the eigenvectors.

Figure 5.8 gives the comparison between numerical data and the theoretical models for the situation where the randomness level is continuously reduced (Cases C1 to C4). As would be expected, the numerical values become much lower than the theory prediction when ensembles with less variability are considered. At a low level of randomness most of the assumptions made by Langley and Brown [91] are no longer valid (the system is no longer stationary and GOE statistics do not apply). A little surprising are the results observed for Case C2. Although the statistics shown in Figure 5.3 for Case C2 match the GOE statistics very well, a small discrepancy can already be observed in the results for the relative variance. This suggests that a small deviation from the GOE statistics may be sufficient to cause some errors in the variance prediction. It is important to note that the variance theory is always conservative.

Figure 5.9 presents the mean natural frequency spacings and the mode shape statistics factor for the case with the lowest randomness level (Case C4). It is interesting to observe that the mean spacings are reduced to the value defined for $\mathbf{A_0}$. The perturbation provided by $\mathbf{A_{ran}}$ is responsible for an increase in the modal density caused by the previously mentioned repulsion. The mode shape statistics factor is also considerably reduced and

displays a highly oscillatory behaviour since the assumption of a Gaussian distribution for the eigenvectors is no longer valid.

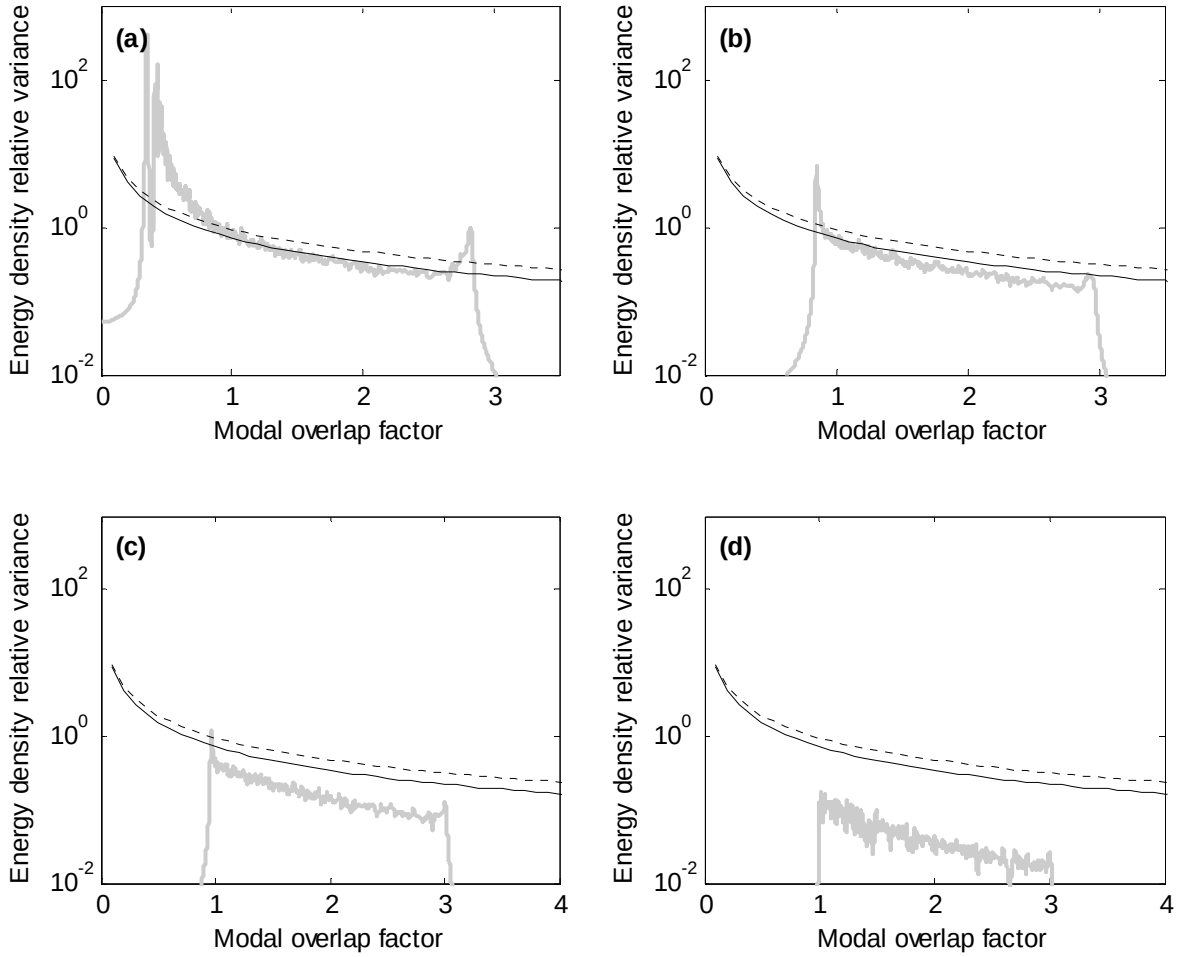

Figure 5.8 – Energy density relative variance for Cases C1 to C4. —— numerical results, ------ Poisson model, —— GOE model.

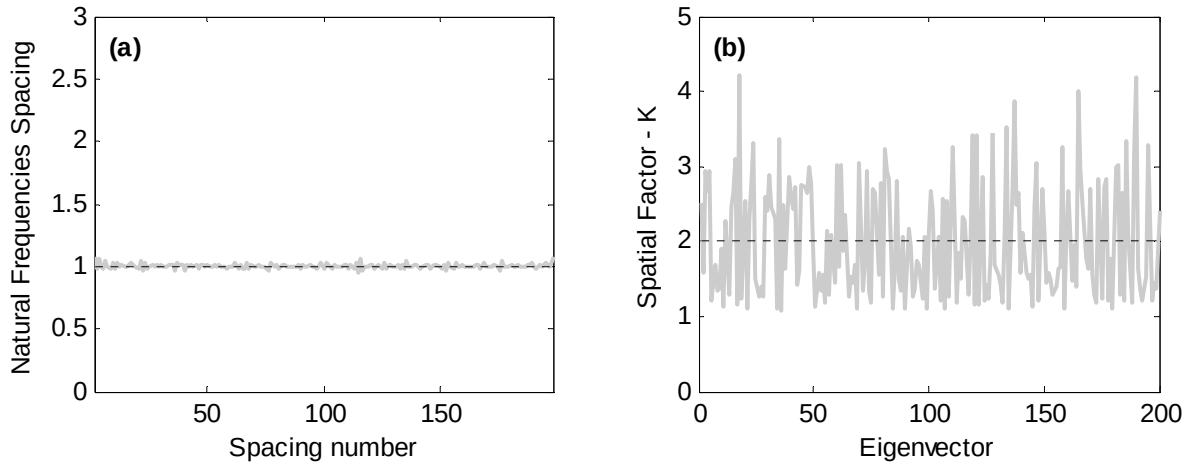

Figure 5.9 – Natural frequency spacings and spatial factor – Case C4. Plot (a): —— numerical results, ------ value used in the theoretical models (μ = 1.002). Plot (b): —— numerical results, ------ mean value (K = 2.019).

In Figure 5.10, the results for the cases where $\mathbf{A}_{\mathbf{ran}}$ is modified to obtain Poisson statistics can be observed. Once more, the variation in the ensemble towards a Poisson system causes a discrepancy between the theory and the numerical data. One would expect the results for Case C7 to agree with the theoretical model based on Poisson statistics. However, this is not the case. Although the eigenvalues are independent as seen in Figure 5.4 (the results for Σ^2 and Δ_3 match the Poisson curve that assumes independent eigenvalues), they are strongly coupled by the **g** vector when calculating the energy density (**g** does not change across the ensemble). This explains the erratic behaviour of the numerical results in Figure 5.10(d).

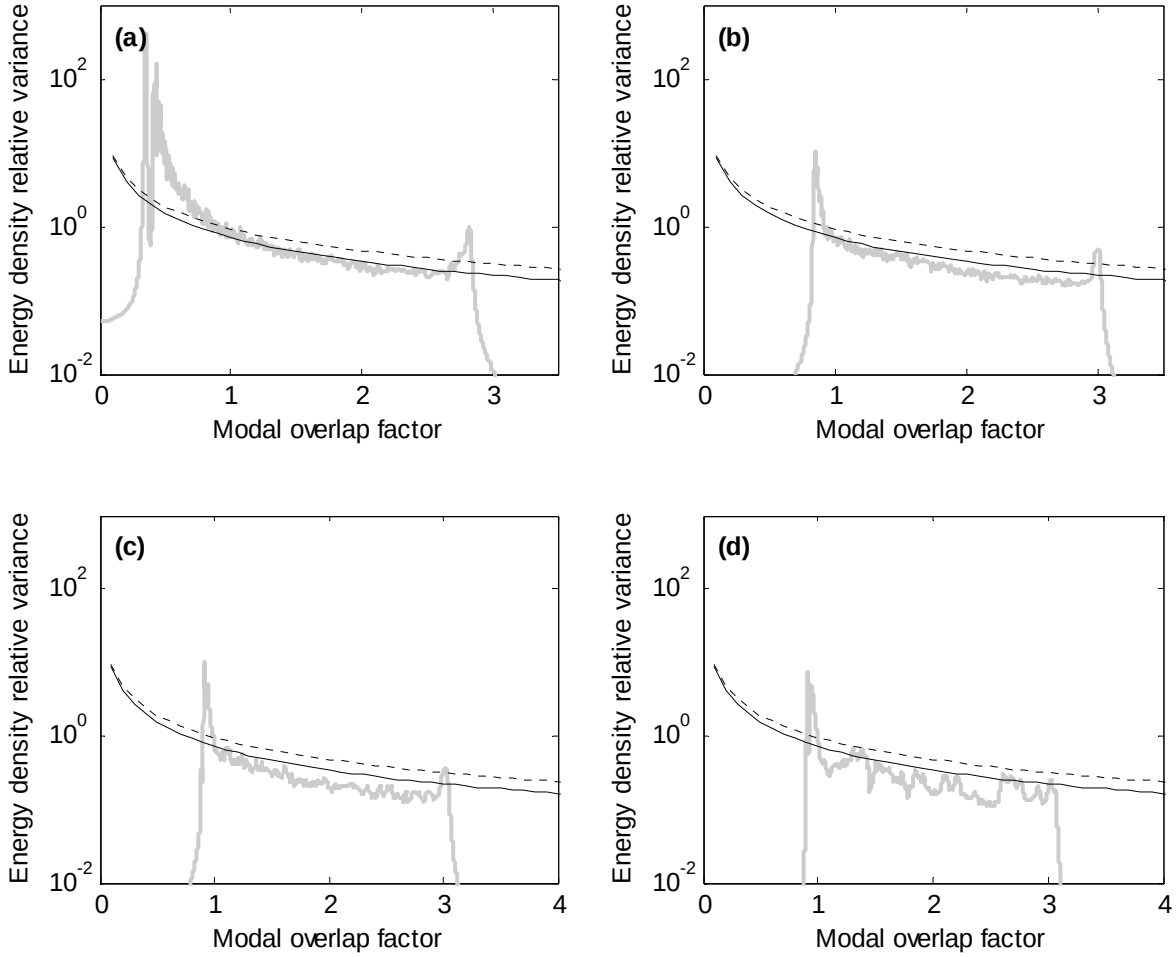

Figure 5.10 – Energy density relative variance for cases C1 and C5 to C7. —— numerical results, ------ Poisson model, —— GOE model.

The results observed in Figure 5.10(d) are very similar to those obtained in Chapter 4 for the ensemble of plates with Poisson statistics (Case B1). However, in Case B1, the oscillatory behaviour observed in the numerical variance was attributed to the fact that the eigenvalues were composed of two groups that are independent of each other but there is a

high correlation between the eigenvalues within each one. Cases C5 and C6 have intermediate behaviours between Case C1 and Case C7.

Since the repulsion is not present, the eigenvalues can move freely and do not interact with each other. Therefore, the modal density is not increased as observed for Case C1 and keeps the same value as the original system. As can be seen in Figure 5.11, the exceptions are the spacings located at the limits of the eigenvalue range where higher values are associated with the eigenvalue dispersion. The oscillatory behaviour of K is also linked to vector **g** and this is further discussed in Appendix D.3.

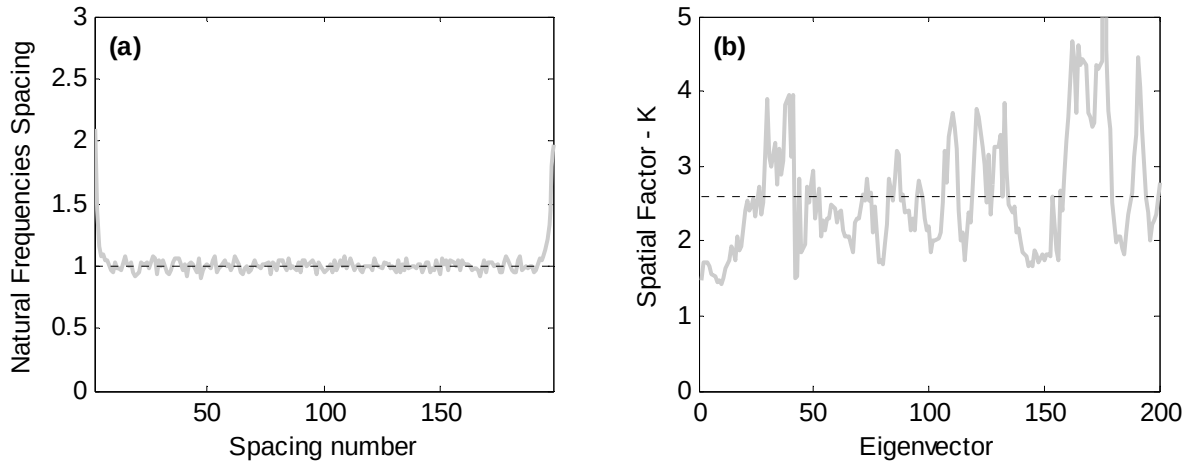

Figure 5.11 – Natural frequency spacings and spatial factor – Case C7. Plot (a): numerical results, ------ value used in the theoretical models (μ = 0.9997). Plot (b): numerical results, ------ mean value (K = 2.597).

Finally, Figure 5.12 shows the results for the cases associated with systems with different levels of symmetry. In Case C8, the two overlapping groups are coupled through the entries of $\mathbf{A}_{\mathbf{ran}}$ associated with Group C. This coupling causes a veering of the eigenvalues from each other and GOE statistics can still be observed (Figure 5.5). The results for the relative variance for Case C8 are consistent with the statistics in Figure 5.5, displaying a good agreement between numerical results and the theoretical prediction as also observed for Case C1. In a similar way, it would be expected that a poor agreement would be seen in Figure 5.12 (c) and (d), as these cases did not display GOE statistics. However, a surprising agreement can be observed for these cases. This agreement can be explained by an interesting coincidence. In Equation (4.25), the relative variance is inversely proportional to the modal overlap factor ($M = \omega\eta v$). One effect of having two overlapping groups of eigenvalues (Cases C8 to C10) is that the modal density is higher than the value for a single group, being twice this value for Case C10 (there are 200 eigenvalues in the same frequency region where there

were previously 100 eigenvalues). This can be noted comparing Figure 5.13 with the natural frequency spacings for Case C10 with the data obtained for Case C1 in Figure 5.7. According to Equation (4.25), a higher modal density implies a reduced relative variance. However, Mehta [10] in Chapter 16 shows that in the case of two overlapping groups, the total variance is the sum of each group variance which compensates the reduction caused by the higher modal density and may explain the agreement observed. Figure 5.13 also shows that the mode shape statistics factor K is not affected by the presence of symmetries in the system and is consistent with the good agreement observed for the variance.

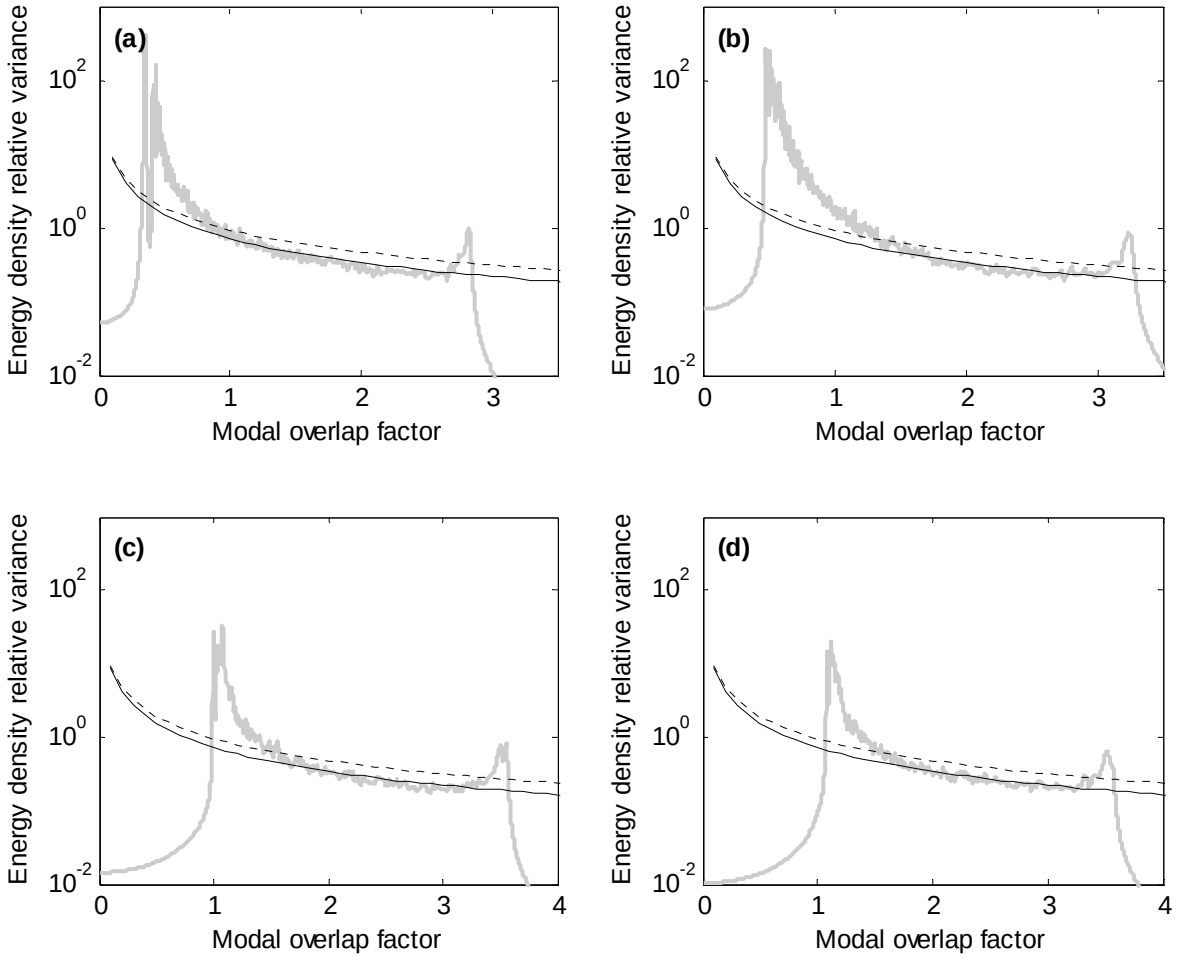

Figure 5.12 – Energy density relative variance for cases C1 and C8 to C10: —— numerical results, - - - - - - Poisson model, —— GOE model.

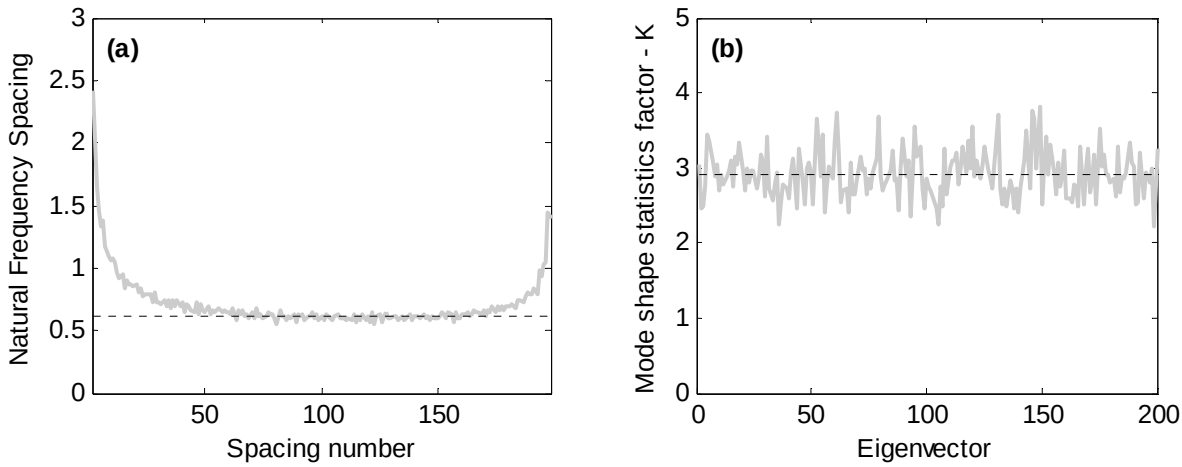

Figure 5.13 – Natural frequency spacings and spatial factor – Case C10. Plot (a): ——— numerical results, - - - - - - value used in the theoretical models ($\mu = 0.616$). Plot (b): ——— numerical results, - - - - - - mean value ($K = 2.92$).

5.6 DISCUSSION, SUMMARY AND CONCLUSIONS

A new approach has been proposed for the study of the statistics of random dynamic systems. Numerical results suggest that the main features regarding the statistics of dynamic systems as seen in Chapter 3 and 4 for plates may be reproduced using the new approach. The new approach is based on the analysis of a general dynamic system in modal coordinates where the system randomness is due only to the stiffness matrix. The fact that the random behaviour of the system is determined by the stiffness matrix has been shown not to limit the reproduction of the statistics of real systems. The new approach also displayed the characteristics required for a method as defined in the introduction of this Chapter: fast solution (allowing the analysis of statistically representative ensembles) and easy application of different probabilistic models.

Three randomization approaches were studied in view of what was observed for random plates in Chapter 3. The approaches included the transition between known statistical behaviours: GOE model to the statistics of systems with a low level of randomness, GOE to Poisson statistics and GOE statistics to the statistics of a system with symmetries. The eigenvalue statistics in the form of the pdf, number variance and Δ_3 were calculated for 10 cases including the situations described above. A very good agreement was observed between the numerical results and the theoretical models for the cases randomized in order to obtain GOE statistics (Case C1), Poisson statistics (Case C7) and the statistics of a system with two overlapping GOE groups (Case C10). It was also possible to observe through the numerical results the transitions between the statistical models.

The effects of different eigenvalue statistics on the energy density variance were also investigated. As expected, the reduction of the randomness level result in a low variance of the energy density and the theory over predicts the variance in these cases. The Poisson statistics caused an oscillation of the energy density variance and the behaviour is consistent with the observations considering random plates in Chapter 4. Surprising results were obtained for systems with symmetries. Although the eigenvalue statistics diverged from the GOE predictions for a single sequence (model adopted in the theory), the variance theory still displayed a good agreement with the numerical variance. The increase in the modal density caused by the presence of two overlapping groups allows the theory to compensate for the increase in the variance as predicted by the RMT. However, this behaviour may be specific to the case of two overlapping systems with equal modal density. The theory may not display the same agreement for systems with overlapping groups of different modal densities.

Although not investigated, it is believed that the increase in the number of overlapping groups would allow Poisson statistics. In fact, the case of Poisson statistics studied in Case C7 would be a limiting case with N independent groups formed of only one eigenvalue. The groups do not overlap originally, but end up mixing as a function of the randomness of the system.

Finally, from the results discussed so far, it was possible to establish a link between the eigenvalue statistics and the errors of the relative variance model derived by Langley and Brown. However, one question still remains: can a single parameter be used to quantify this agreement? The statistical overlap factor has been previous proposed as a way of quantifying the randomness level of a system, but it fails when the system is randomized in particular ways. An attempt to derive a parameter with the required characteristics is carried out in the next Chapter using the new method proposed in this Chapter.

CHAPTER 6

SINGLE PARAMETER FOR GOE STATISTICS

6.1 INTRODUCTION

In the previous Chapters, it was seen that the GOE model is applicable to random dynamic systems in many situations. It was observed that the statistics of random dynamic systems may also display other behaviours associated with a low level of randomness and with the presence of symmetries. Chapter 4 has shown that a variance theory for the response of dynamic systems based on the GOE model is available and very good predictions may be obtained, depending on the level of agreement with the GOE model. It was argued that real systems will always display GOE statistics above a certain frequency and this frequency would depend on the uncertainties associated with the manufacturing process for each structure. In fact, real systems should be characterized by a transition region between an almost-deterministic behaviour to GOE statistics and the main problem then becomes the determination of frequency with the lowest acceptable level of agreement with the GOE model.

The statistical overlap factor was proposed as a way of quantifying the level of randomness of a system through the measurement of the dispersion of the eigenvalues. However, it was seen in Chapters 3 and 5 that the presence of symmetries in different degrees corrupts the results obtained with the statistical overlap factor and leads to an incorrect evaluation of the system randomness. Therefore, there is a requirement for a new parameter that would allow the verification of the level of uncertainty of a system and thus define the limits for the applicability of the GOE model. Such a parameter would allow an estimation of the errors associated with the variance theory.

In this Chapter, a new parameter is proposed based on the mixing of the eigenvectors of a random dynamic system. Numerical results using the approach given in Chapter 5 are used to verify the applicability of the new parameter and the results are compared with those obtained with the statistical overlap factor. Finally, in order to simplify the calculation of the parameter and reduce the computational cost involved a perturbation analysis is performed. The perturbation analysis results are then compared with the full analysis results.

6.2 SINGULAR VALUE DECOMPOSITION OF EIGENVECTORS

Let $\mathbf{u}_j^k$ be the *j*th eigenvector of the *k*th realization of matrix **A**, when the eigenvectors are ordered in terms of increasing eigenvalue for each realization. As **A** is an *NxN* matrix defined as in Chapter 5, *j=1,2,...,N* and, for an ensemble of *Ne* members, *k=1,2,...,Ne*. Let matrix $\mathbf{D}_j$ be defined by

$$\mathbf{D}_j = \left(\mathbf{u}_j^1 \quad \mathbf{u}_j^2 \quad \ldots \quad \mathbf{u}_j^{Ne}\right). \tag{6.1}$$

In order to simplify the following derivation, $\mathbf{D}_j$ will be taken as **D**. It would be interesting to estimate the effective column rank of **D**, so as to identify the number of independent basis vectors that are active across the ensemble for that specific eigenvector. This can be investigated by performing a Singular Value Decomposition (SVD) [111], such that

$$\mathbf{D}_{NxNe} = \mathbf{W}_{NxN}\mathbf{S}_{NxN}\mathbf{V}_{NxNe}, \ \left(\mathbf{D}\mathbf{D}^T\right)\mathbf{W} = \mathbf{W}\mathbf{S}^2. \tag{6.2}$$

The basis vectors are displayed in the columns of **W** and their importance is given by the singular values contained in the diagonal matrix **S**. The effective rank is given by the number of significant singular values. It can be noted that

$$Tr(\mathbf{D}\mathbf{D}^T) = Tr(\mathbf{S}^2) = J \quad \Rightarrow \quad \sum_i S_i^2 = J, \tag{6.3}$$

where S_i is the *i*th singular value, which is assumed to be labelled in *descending* order, and $Tr(\ )$ is the trace of the matrix. An example of the singular values observed in the diagonal of **S** for a matrix **D** obtained considering Case C1 defined in Chapter 5 is given in Figure 6.1. If the number of important basis vectors in matrix **D** is large, the curve would become flatter. On the other hand, if only a few basis vectors are sufficient to represent the domain with a reasonable precision, the number of important singular values is reduced and the slope becomes more pronounced at the beginning of the curve.

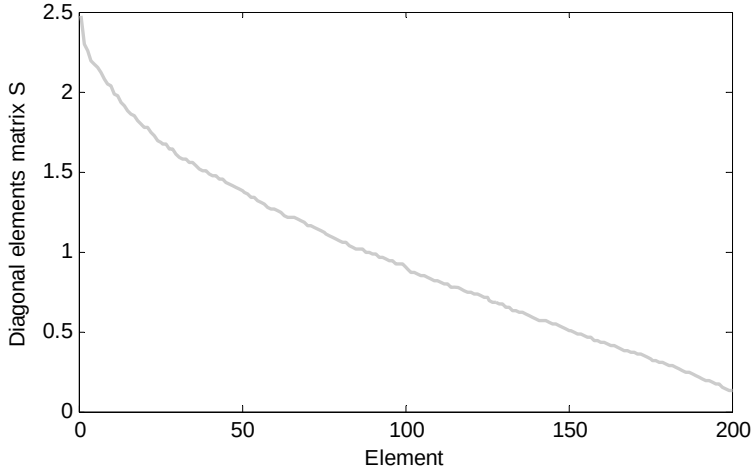

Figure 6.1 – Example of curve of the diagonal elements of S (Case C1).

Therefore, in view of Equation (6.3), a parameter P quantifying the number of important basis vectors can be defined such that

$$\sum_{i=1}^{P} S_i^2 = 0.9J\,, \tag{6.4}$$

where it is considered that a value of 90% of the trace would include all the important vectors. A flatter curve would display higher values of P, while a system with only a few important basis vectors would have a low value of P. With this definition, P can also be interpreted as a quantification of the mixing of eigenvalues. Whenever two eigenvalues cross each other (swap positions in the eigenvalue sequence), the associated eigenvector also changes its position and thus would be included in another matrix **D**. In view of these characteristics, P should display a similar behaviour to the statistical overlap factor. However, it has been noted that a parameter with these characteristics may not be capable of predicting GOE statistics in certain situations. Following the discussion presented by Langley in [97], it is assumed that the new parameter should be related to the mixing of eigenvectors. This can be investigated by projecting each realization of $\mathbf{u}_j$ in the basis vectors, or

$$\mathbf{R}_{NxNe} = \mathbf{W}_{NxN}^{T}\mathbf{D}_{NxNe} = \begin{pmatrix}\mathbf{r}_1 & \mathbf{r}_2 & \dots & \mathbf{r}_{Ne}\end{pmatrix}. \tag{6.5}$$

The vectors $\mathbf{r}_k$ contain the internal product of the kth eigenvector with the basis vectors obtained through the SVD. If only one value of $\mathbf{r}_k$ is high, it indicates that the eigenvector is almost aligned with that specific basis vector. In the situation where $\mathbf{r}_k$ has several values with significant amplitude, the eigenvector is composed of several basis

vectors. In an approach similar to that used to calculate P, it is possible to quantify the effective number of basis vectors that contribute to $\mathbf{r}_k$. After ordering the entries of each $\mathbf{r}_k$ in terms of *decreasing* modulus and noting that each $\mathbf{r}_k$ vector has a modulus of unity, Q_k can be defined as

$$\sum_{i=1}^{Q_k} r_{k,i}^2 = 0.9\,, \tag{6.6}$$

where it is considered again that Q_k elements of $\mathbf{r}_k$ are responsible for 90% of its modulus. Finally, we can take the mean value of Q_k as

$$Q = \frac{1}{M}\sum_k Q_k\ . \tag{6.7}$$

It is expected that Q would allow an estimation of the level of randomness of a system with more confidence that the statistical overlap factor since it should not be affected by the presence of symmetries as is the latter. Therefore, it may be used to verify the agreement with the GOE model.

It was seen in Chapter 5 that the presence of two overlapping groups does not affect the variance results and thus the theoretical predictions may be used with confidence. However, the identification of such symmetries in the system may be of interested. It is not expected that the parameters P and Q would be capable of predicting the occurrence of symmetries in the systems. In the case of two overlapping groups of eigenvalues, the value of P should stay the same as the two groups are still mixing. However, Q is expected to be half the value of that for a system with a single sequence (as the two groups of eigenvectors do not interact). However, although with reduced values, Q may still be over a certain value expected to be the limit for the occurrence of GOE statistics. This would occur in the case of the two sequences having GOE statistics. This problem may be overcome if the two parameters are used together to calculate a third parameter given by

$$Z = P/Q\,. \tag{6.8}$$

In the case of a system with symmetries, it is expected that the parameter Z will display values twice of those obtained for GOE systems. In what follows, some numerical analysis are carried out using the approach given in Chapter 5 and the proposed parameters P,

Q and *Z* are compared with the statistical overlap factor for the three transition situations previously investigated in Chapter 5.

6.3 NUMERICAL RESULTS

The procedure presented in section 6.2 for the calculation of the new parameters was implemented using MATLAB® and an example of the code is given in Appendix E.1. Numerical results were calculated for a system of size $N = 200$ and ensembles of different sizes were considered to verify the convergence of the parameters. The parameters were calculated considering the 100^{th} eigenvalue.

Results for the situation where the overall randomness is decreased are shown in Figure 6.2. The method given in Chapter 5 is much faster than the numerical simulations based on FE given in Chapter 2 which allows the consideration of many more ensembles and the evaluation of the transition with more precision. The cases considered in Chapter 5 are marked on the curves and allow an estimation of the eigenvalue statistics and the errors in the variance prediction from the results in Chapter 5. It is expected that the other values would be associated with intermediate behaviours of the eigenvalue statistics and the energy density variance.

Figure 6.2 gives three curves for each parameter considering different sizes of the ensemble: 250 members, 500 members and 1000 members. It can be noted that there is a little difference between the 500 member ensemble curve and the 1000 member ensemble. However, since this difference will not interfere in the analysis and in order to speed up the calculation the 500 member ensemble was considered for the other situations.

As expected, the parameters P and Q display a very similar behaviour, with decreasing values for a reduced constant *R*. This similar behaviour for these parameters is due to the fact that the cases considered do not display symmetries or Poisson statistics which are known to affect some of the parameter predictions. A different behaviour is observed for the statistical overlap factor and for the parameter *Z*, which both becoming almost constant above a certain level of randomness. While the statistical overlap factor converges for a value around 1.4, the parameter *Z* become stable around a value of 1.7.Some oscillation can be noted for *Z* at low levels of randomness, where a reduced number of eigenvalues may be interacting and a small change in the parameters *P* and *Q* may result in a large variation of *Z*. If one adopts Case C2 as the limit for the applicability of the variance theory, a value of *Q* greater than 20 should be sufficient to ensure GOE statistics.

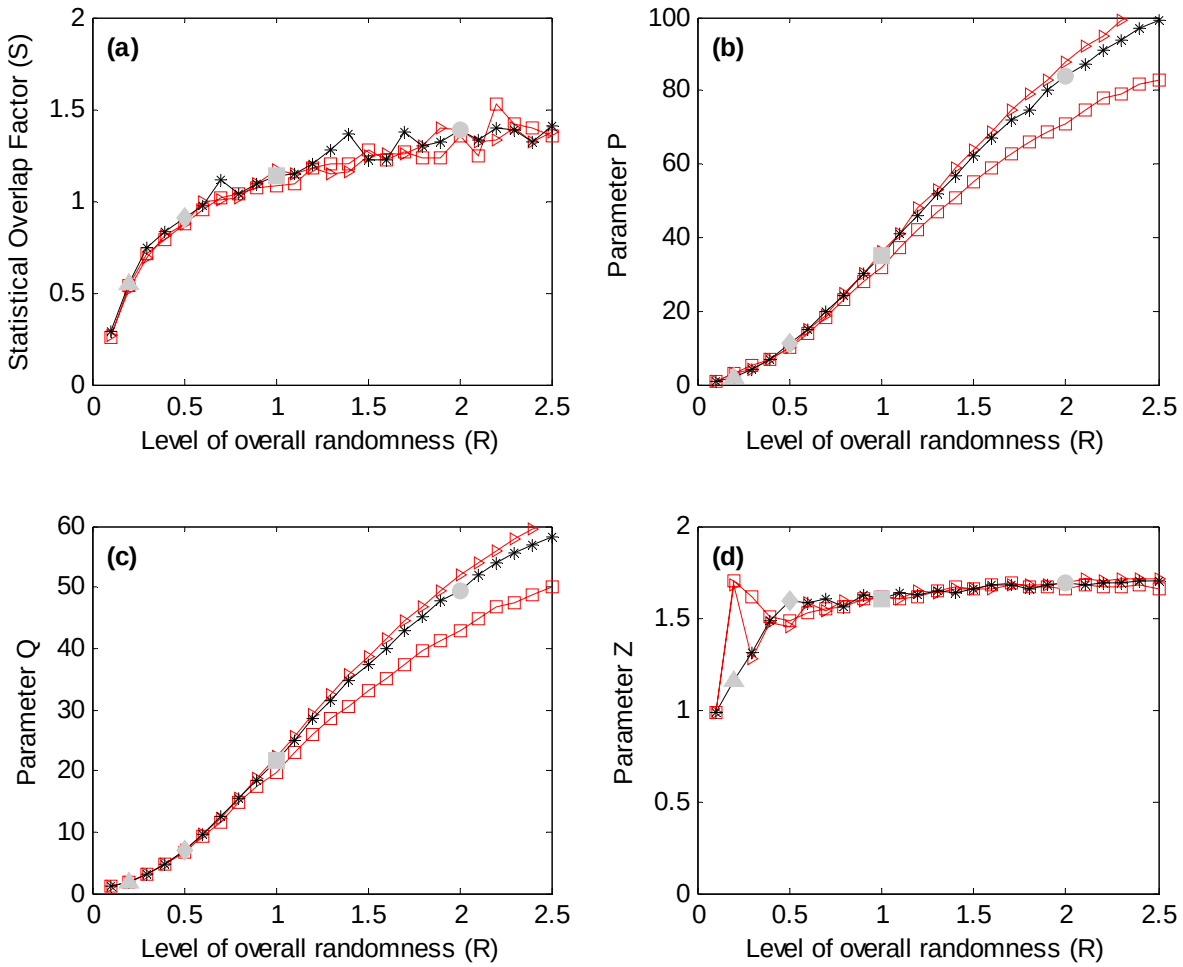

Figure 6.2 – Parameters – varying the overall level of randomness. —□— 250 member ensemble, —✳— 500 member ensemble, —▷— 1000 member ensemble. ● Case C1, ■ Case C2, ◆ Case C3, ▲ Case C4.

A very distinct behaviour for the parameters is observed for the situation where the system shifts from GOE to Poisson statistics as shown in Figure 6.3. The parameters were calculated considering two levels of the overall randomness: $R = 2$ and $R = 4$. The statistical overlap factor fails to predict that the system no longer displays GOE statistics, giving values higher than unity for the system with Poisson statistics. The parameter P, although showing a reduction with the decrease in the off-diagonal randomness, still get stable around a value of 10 for the curve considering $R = 2$. The initial reduction in P, even though the overall randomness is kept the same (and consequently the diagonal randomness), is a consequence of the fact that the off-diagonal randomness also contributes to the mixing of the eigenvalues. This behaviour is responsible for the parameter P not being appropriate for the proposed task of identifying the occurrence of GOE statistics. As can be observed in Figure 6.3(b) for $R = 4$, it is possible to increase the value of P by raising the overall randomness in a system with Poisson statistics. Although the system is not going to display GOE statistics, P would be higher than an established threshold.

On the other hand, the parameters Q displays a more appropriate behaviour, moving towards zero in the case of Poisson statistics. In fact, one characteristic of the Poisson model is that the mixing of eigenvectors does not occur. Figure 6.3(c) does not allow the verification of the convergence of the parameter Q to zero as a function of the adopted log axes, however, this can be observed in Figure 6.4 where both parameters P and Q are shown in linear axes.

A distinct behaviour can be noted for the parameter Z, which increases with the reduction of the off-diagonal randomness. In fact, a system with Poisson statistics can be interpreted as a system with N symmetric groups, each one totally independent of the others. This explains the high values observed for the parameter Z.

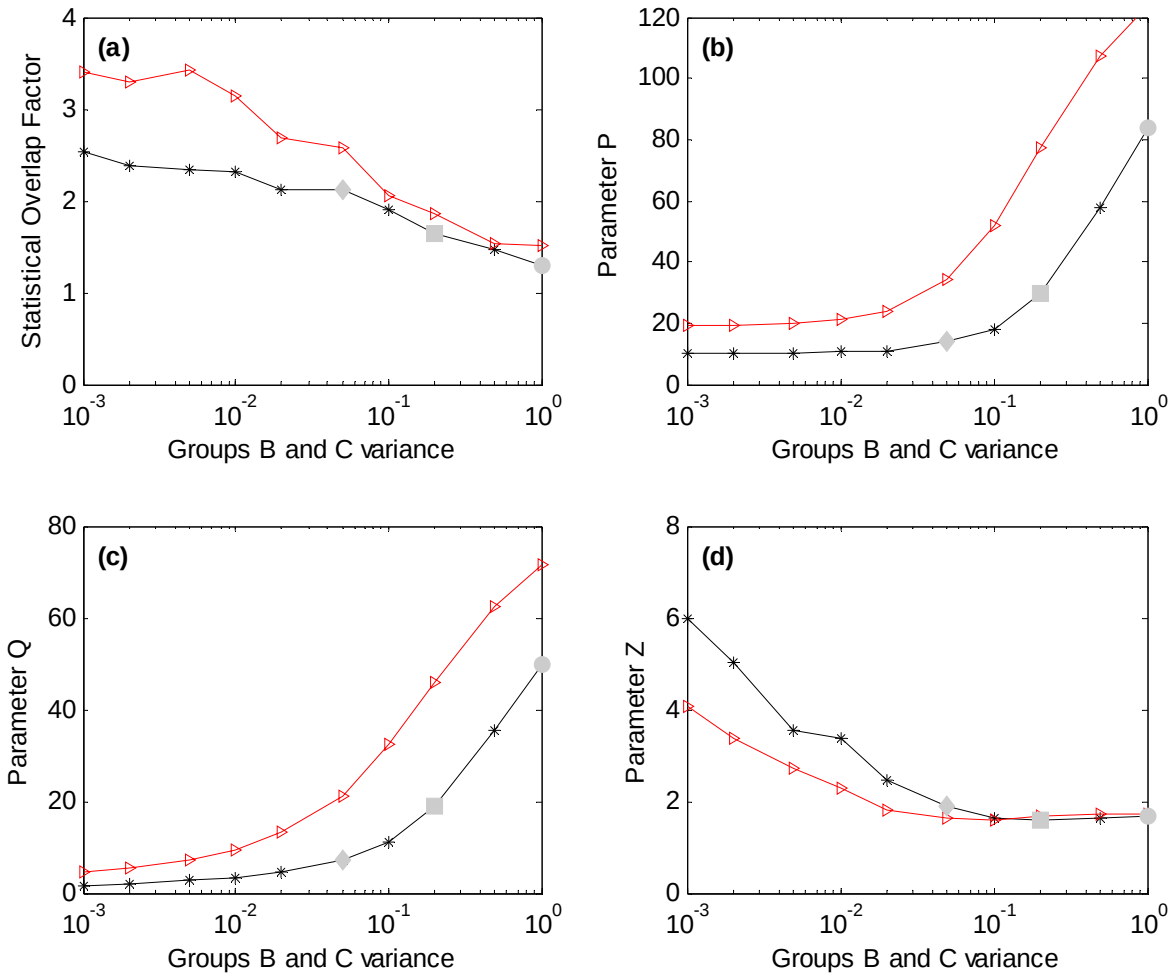

Figure 6.3 – Parameters – inducing Poisson statistics. —✱— $R = 2$, —▷— $R = 4$. ● Case C1, ■ Case C5, ♦ Case C6.

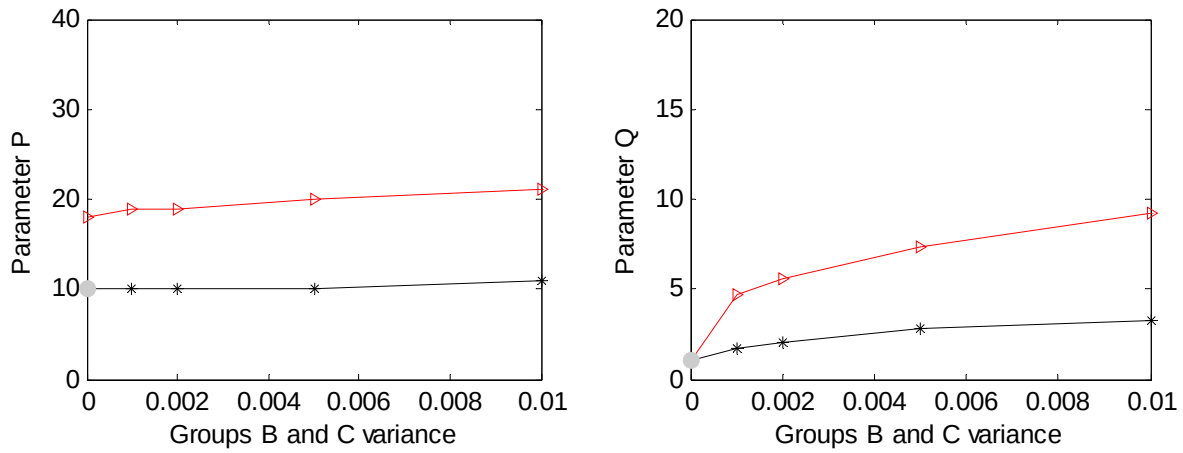

Figure 6.4 – Parameters – inducing Poisson statistics. —*—— *R* = 2, ——▷—— *R* = 4, ● Case C7.

The results for the situation where there is a transition from GOE statistics to a system with two overlapping GOE groups are shown in Figure 6.5. It can be observed that the parameters *P* and *Q*, although showing some reduction when the variance of Group C is reduced, still display values that would suggest the occurrence of the statistics of a single GOE group. As previously mentioned, the problem may not be of great significance in terms of the results of the variance theory, since the presence of two overlapping groups does not affect the errors. However, if the there is interest in identifying the occurrence of symmetric groups, the parameter *Z* may be used. It can be noted in Figure 6.5 that the parameter *Z* increases with the reduction of Group C variance and, in the case of two symmetric groups, should display a value of twice that observed for a single GOE group. Again, this is not possible to observe this through Figure 6.5 as a function of the adopted axes. Therefore, the parameters *Q* and *Z* are shown in Figure 6.6 in linear axes and it can be observed a value of around 3.4 for *Z*, exactly twice the value observed for a single GOE group in Figure 6.2.

Both parameters *Q* and *Z* would be a significant improvement on the statistical overlap factor to predict the occurrence of GOE statistics. While parameter *Q* can be used to ensure that the system is sufficiently random and the results of the variance theory are valid, the parameter *Z* may be used to verify the occurrence of symmetric groups. The values used as thresholds in both parameters *P* and *Q* to define the number of important singular values or basis functions may also be adjusted by each user to allow more precision in the predictions.

The main inconvenience of parameter *Q* is its computational cost. In order to obtain matrix **D** for each eigenvector it is necessary to solve the eigenproblem for each member of an ensemble of systems. Therefore, an attempt is made in the next section of obtaining a similar parameter directly from the statistics of the system input parameters.

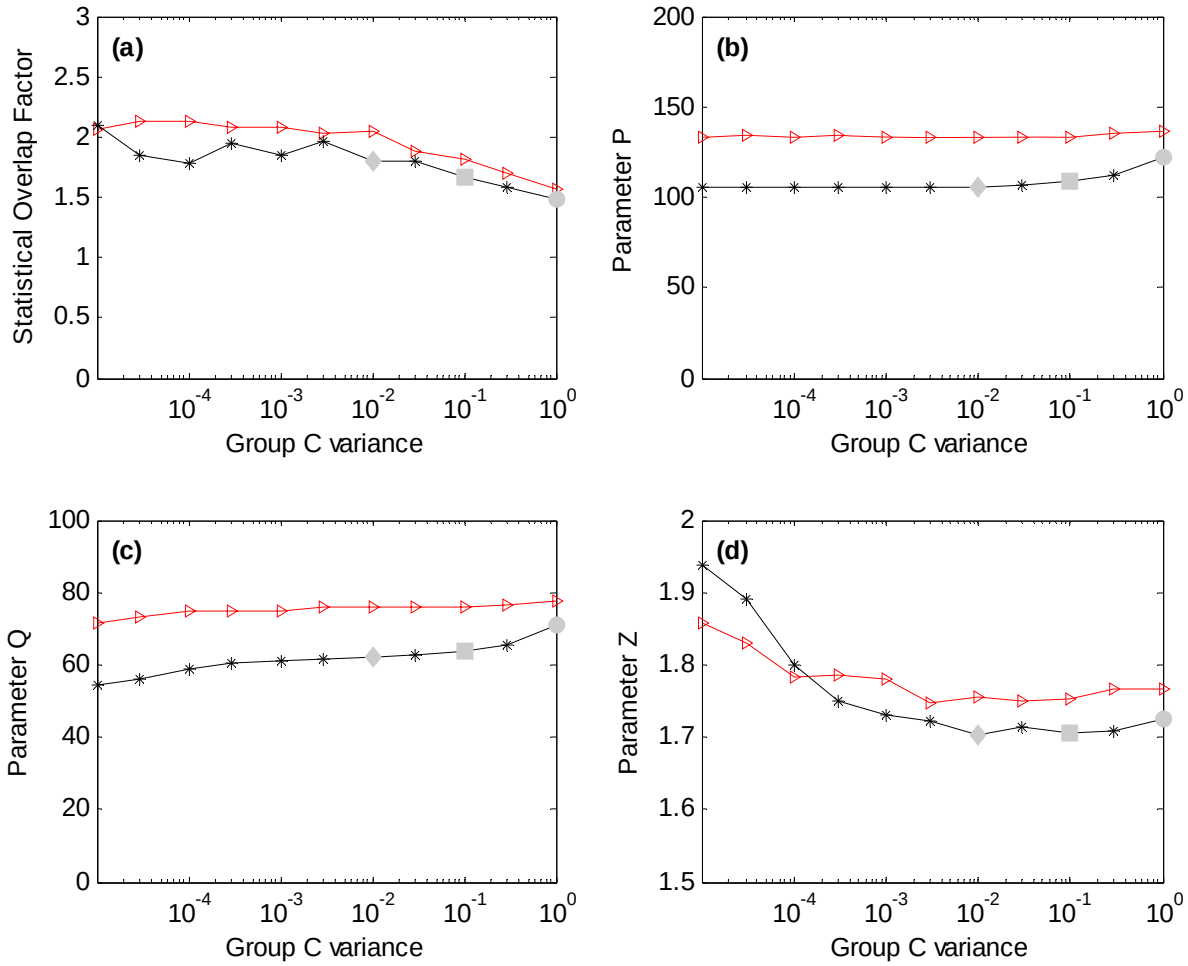

Figure 6.5 – Parameters – inducing symmetries in the system. ✱ $R = 2$, ▷ $R = 4$, ● Case C1 (with two groups), ■ Case C8, ♦ Case C9.

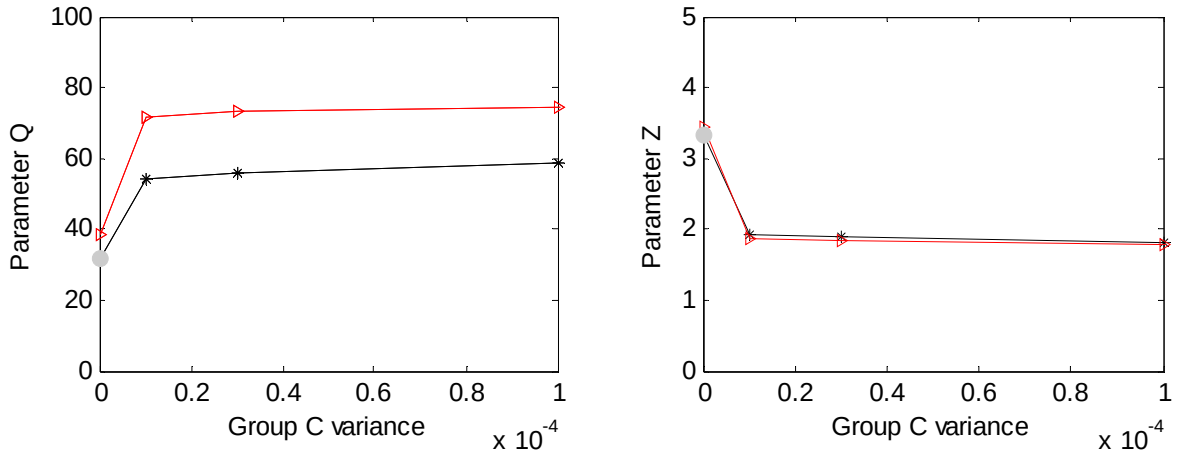

Figure 6.6 – Parameters – inducing Poisson statistics. ✱ $R = 2$, ▷ $R = 4$, ● Case C10.

6.4 PERTURBATION ANALYSIS

6.4.1 Perturbation analysis parameter

The parameters proposed in the previous section, despite representing an important improvement, require the generation of an ensemble of dynamic systems and the solution of the eigenproblem for each member of the ensemble in order to verify whether the GOE model is applicable. The computational cost of such a procedure may be prohibitive. In what follows, an approximate method is proposed based on a perturbation analysis.

Let's consider again the vector $\mathbf{u}_j^k$ as the *j*th eigenvector of the *k*th realization of random matrix **A** and the existence of a nominal matrix $\mathbf{A}^0$ with eigenvectors and eigenvalues $\mathbf{u}_j^0$ and λ_j^0, respectively. In order to create an ensemble, $\mathbf{A}^0$ undergoes small changes in its entries. For the *k*th realization, the small changes are given by the matrix $\mathbf{\Delta A}^k$. From a perturbation analysis, eigenvector $\mathbf{u}_j^k$ can be estimated neglecting higher-order terms in the Taylor series by

$$\mathbf{u}_j^k = \sum_{i=1}^{N} \beta_{j,i}^k \mathbf{u}_i^0 \,, \tag{6.9}$$

where

$$\beta_{j,i}^k = \begin{cases} 1, & i = j \\ \dfrac{\mathbf{u}_j^{0T} \mathbf{\Delta A}^k \mathbf{u}_i^0}{\lambda_i^0 - \lambda_j^0} & i \neq j \end{cases}. \tag{6.10}$$

Once more, the interest is in a parameter similar to *Q* and this would provide an estimation of the level of mixing between eigenvectors. The projection of $\mathbf{u}_j^k$ over the unperturbed eigenvectors would give such an estimation and is given by

$$\mathbf{v}_j^k = \mathbf{u}_j^{kT} \mathbf{U}^0. \tag{6.11}$$

Substituting Equations (6.9) and (6.10) into Equation (6.11) gives

$$\mathbf{v}_j^k = \left[\mathbf{u}_j^0 + \sum_{i=1}^{N} \frac{\mathbf{u}_j^{0T} \boldsymbol{\Delta}\mathbf{A}^k \mathbf{u}_i^0}{\lambda_i^0 - \lambda_j^0} \mathbf{u}_i^0 \right]^T \mathbf{U}^0 . \tag{6.12}$$

The components of the vector $\mathbf{v}_j^k$ can be given by

$$v_{j,i}^k = \begin{cases} 1 + \dfrac{\mathbf{u}_j^{0T} \boldsymbol{\Delta}\mathbf{A}^k \mathbf{u}_i^0}{\lambda_i^0 - \lambda_j^0}, & i = j \\ \dfrac{\mathbf{u}_j^{0T} \boldsymbol{\Delta}\mathbf{A}^k \mathbf{u}_i^0}{\lambda_i^0 - \lambda_j^0} & i \neq j \end{cases} . \tag{6.13}$$

However, it may be noted that the component of the vector $\mathbf{v}_j^k$ for $i = j$ displays an indetermination. This component will then be ignored and only the other ones will be considered. Restating that the analysis is carried out in modal coordinates, it can be shown that the components may be written as

$$v_{j,i}^k = \frac{\Delta A_{j,i}^{\ k}}{\lambda_i^0 - \lambda_j^0} \qquad i \neq j . \tag{6.14}$$

In view of the definition of matrix **A** given in Equation (5.18), Equation (6.14) may be expressed as

$$v_{j,i}^k = \frac{RA_{ran\,j,i}^{\ \ k}}{\lambda_i^0 - \lambda_j^0} \qquad i \neq j . \tag{6.15}$$

In the case of a Gaussian variable x, it may be shown that

$$\mathrm{E}\left[\mathrm{x}^2\right] = \mu^2 + \sigma^2 . \tag{6.16}$$

Therefore, as the entries of $\mathbf{A_{ran}}$ have zero mean, the mean-square value of each entry of vector $\mathbf{v}_j^k$ can be accessed through

$$\mathrm{E}[v_{i,j}^{k\ 2}] = \frac{R^2\sigma_{i,j}^2}{(\lambda_{j0} - \lambda_{i0})^2} \qquad i \neq j\,, \tag{6.17}$$

with $\sigma_{i,j}^2$ being the variance of $\mathbf{A_{ran}}$ entries.

Equation (6.17) is applicable to each eigenvector of the system and a vector $\mathbf{h}_j$ can then be taken as

$$\mathbf{h}_j = \left(E[v_{1,j}^{k\ 2}] \quad E[v_{2,j}^{k\ 2}] \quad \cdots \quad E[v_{N-1,j}^{k\ 2}]\right). \tag{6.18}$$

A new parameter H_j can be defined as the number of entries of $\mathbf{h}_j$ that are higher than a given threshold *Tr,* in a similar way to that used for *Q* and P, or

$$H_j = n\left(\mathbf{h}_j, Tr\right), \tag{6.19}$$

where $n\left(\mathbf{h}_j, Tr\right)$ gives the number of elements of $\mathbf{h}_j$ larger than *Tr*.

The significance of the new parameter is similar to that of *Q* defined in the previous section and the new parameter allows the approximate verification of the level of eigenvector mixing.

6.4.2 Numerical results

Once more, the three situations previously considered are used to check the applicability of the new parameter obtained through the perturbation analysis. Figure 6.7 shows the results for the situation where the level of randomness is continuously decreased. The parameter H_j is plotted for j = 100 and for different values of the threshold *Tr*, together with the parameter *Q*. A good agreement can be observed between *Q* and *H* with *Tr* = 0.01, with both curves displaying a similar slope. The good agreement would be expected for low levels of randomness, since the perturbation analysis assumes small changes in **A**. However, it would be expected that the high levels of randomness associated with GOE statistics would be likely to require considerable changes in the input parameters; but even so, the matching between the two parameters is still observed. It may be necessary to increase even more the

randomness of the system until there is a greater discrepancy between the two parameters.

Figure 6.8 and Figure 6.9 give the results for the parameter for the other two situations. The parameter H with Tr = 0.01 also conforms well to the parameter Q when Poisson statistics are induced and R is fixed at 2. In fact, this agreement suggests that the parameter H has the same characteristics as Q and it becomes an important improvement in view of its much lower computational cost.

In Figure 6.9, it can be observed that the perturbation analysis parameter displays a different behaviour to that observed for Q in the case of two overlapping systems. This difference is due to the reordering of the eigenvalues that occurs in the full analysis but does not take place in the perturbation analysis. This result is not so important since it is known that parameter Q is not capable of predicting the occurrence of two overlapping groups and this does not affect the variance of the response.

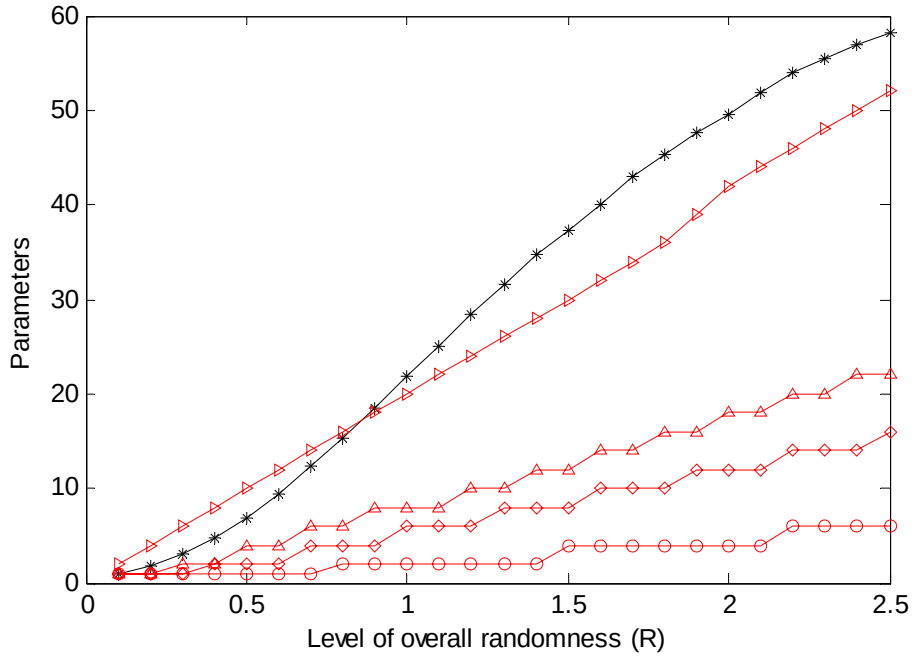

Figure 6.7 – Comparing the results for the parameter calculated through the perturbation analysis with the numerical approach – varying the level of randomness: —*— parameter Q, perturbation results: —○— Tr = 0.5, —◇— Tr = 0.1, —△— Tr = 0.05, —▷— Tr = 0.01.

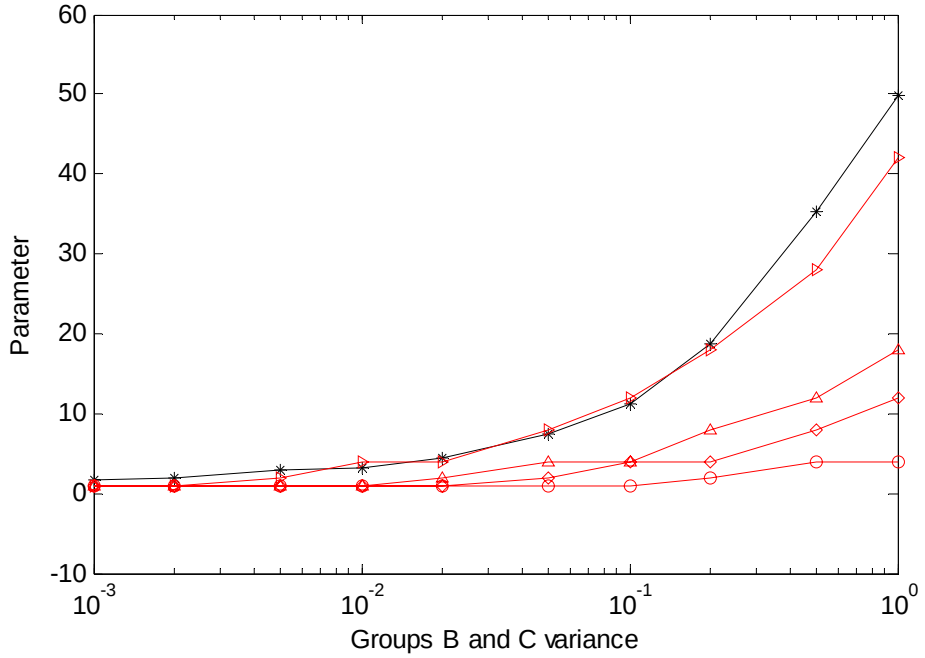

Figure 6.8 – Comparing the results for the parameter calculated through the perturbation analysis with the full numerical approach – inducing Poisson statistics: —*— parameter Q, perturbation results: —○— *Tr* = 0.5, —◇— *Tr* = 0.1, —△— *Tr* = 0.05, —▷— *Tr* = 0.01.

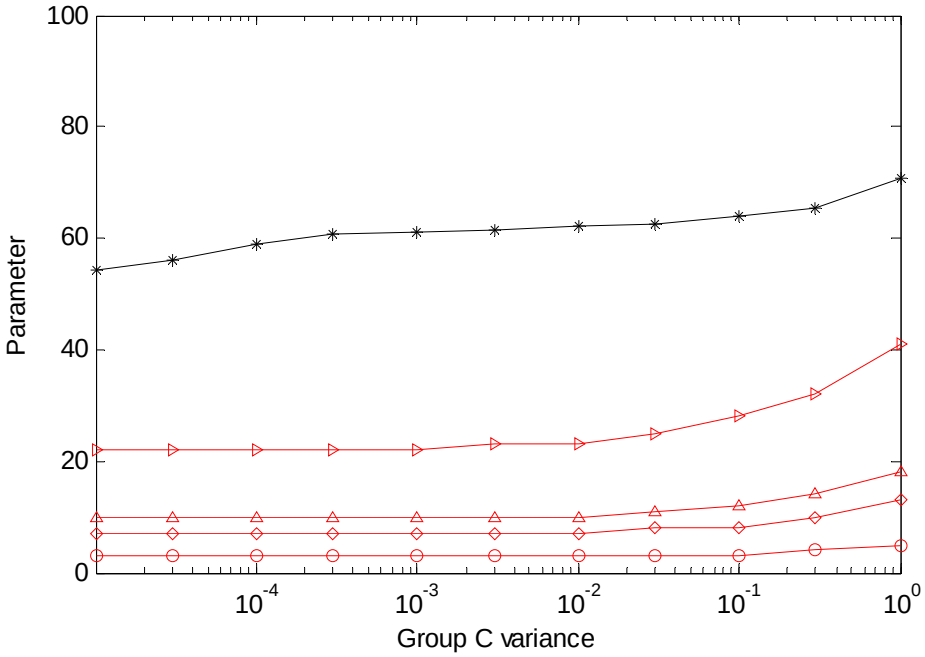

Figure 6.9 – Comparing the results for the parameter calculated through the perturbation analysis with the full numerical approach – inducing symmetries in the system: —*— parameter Q; perturbation results —○— *Tr* = 0.5, —◇— *Tr* = 0.1, —△— *Tr* = 0.05, —▷— *Tr* = 0.01.

6.5 RESULTS AND DISCUSSIONS

It was shown in the previous Chapters that there was a need for a single parameter to verify the occurrence of GOE statistics in a random dynamic system and therefore estimate the errors associated with the application of the variance theory. Three parameters (*P*, *Q* and *Z*) were then derived based on an SVD of the matrix composed of the realizations of an eigenvector. The applicability of the parameters was then investigated using the method proposed in Chapter 5. Once more, the transition situations (almost-deterministic to GOE, Poisson to GOE and two GOE groups to single GOE group) were used to evaluate the parameters. The parameter *Q* was shown to be a significant improvement over the previous parameter used, the statistical overlap factor, and to have the desired characteristics. It was also verified that the parameter *Z* seems to be capable of indicating the presence of two overlapping groups in the system. However, in view of the results for the energy density of a system with two overlapping groups, there is no need of identifying symmetries in the system and the use of the parameter *Q* alone would be sufficient to verify the applicability of the variance theory.

In order to reduce the computational costs, a perturbation analysis was performed and a fourth parameter was derived. The new parameter *H* displayed similar behaviour to *Q*, but it is expected to require a much reduced computational power since it can be calculated directly from the statistics of the input parameters. It is expected that *H* would be an important tool in the verification of the GOE model applicability and in the estimation of the error associated with the variance theory since the eigenvalue statistics may be evaluated prior to the generation of the ensemble and the solution of the eigenproblems.

Another application for a parameter like *H* may be in the methods usually adopted to model the variance problem at low frequency (or low level of uncertainty) like the stochastic FE methods. These methods required the adoption of a model for the statistics of the input parameters and much work has been done on the development of alternative descriptions of the input uncertainties that required less input data since this information is usually very limited (interval analysis, fuzzy variables, etc.). It is known that the amount of information required increases with increasing frequency since it becomes necessary to refine the statistical models. However, the occurrence of GOE statistics represents a limit for the discretization of the input parameter statistical data. Above this certain point, refining the statistical models would not change the statistics of the response. Therefore, the parameter *H* would also indicate the maximum required refinement of the input parameter statistics. Such

information may become useful with an increasing available computational power and a more common application of the low uncertainty methods.

CHAPTER 7

CONCLUSIONS AND FUTHER RESEARCH

7.1 CONCLUDING REMARKS

The success of an engineering design requires the consideration of the uncertainties arising from the manufacture processes in order to optimize the performance and reduce the risk of failure. When the performance is determined by vibro-acoustic characteristics, there is a need for modelling tools to predict the variability of the response. It was seen in the literature review that many studies were carried out with the objective of developing such tools. The characteristics of the response of random dynamic systems have lead to a division in the methods according to the level of uncertainty.

At a low level of uncertainty (usually also at low frequencies), the response statistics are determined by the statistics of the input parameters and deterministic methods, together with a probabilistic or possibilistic approach, are used to predict the statistics of the response. Examples of these methods are the stochastic FE methods, which includes the interval FE method and the fuzzy FE method. At a high level of uncertainty, it was seen that the increasing sensitivity of the modes to the uncertainties causes the response to be independent of the statistics of the input parameters and predictions from the Random Matrix Theory (RMT) may be used to estimate the statistics of the response. In fact, it has been shown that the eigenvalue statistics of random dynamic systems conform to the predictions of RMT for a special type of ensemble of random matrices named Gaussian Orthogonal Ensemble (GOE). A formulation for the energy density variance has been recently derived based on the GOE assumption and then extended to predict the variance of SEA results. However, many questions regarding the application of the GOE model were still unanswered and therefore were investigated in this thesis.

A numerical procedure based on the FE method was initially proposed for the study of the statistics of random dynamic systems and it was validated through the comparison of experimental results obtained for a plate loaded with masses in random positions. The numerical procedure included the determination of the natural frequencies and mode shapes at the excitation point by means of the FE method and the calculation of the energy density and its statistics by means of an external modal summation. Convergence issues were verified and results for the mean energy density were also compared with the standard SEA results,

displaying a good level of agreement.

A detailed review of the Random Matrix Theory (RMT) was carried out with the main interest being in its application to random dynamic systems and the procedures used to verify the agreement between a sequence of numbers and the GOE model. The number variance Σ^2 and the Δ_3 function were identified as the two most popular statistics for such applications and, in view of their faster convergence, were adopted. In order to investigate issues related to the presence of symmetries and the ergodicity concept, a series of numerical cases were studied and the spectral and ensemble averages calculated. Ensembles of plates were generated considering different probabilistic models and the eigenvalue statistics were determined for each case. It was seen that two nominally identical structures may have completely different ensemble statistics and, therefore, it was concluded that the validity of the ergodicity assumption is dependent on the probabilistic model adopted. However, if GOE statistics are observed in an ensemble average, it is expected that the ergodicity assumption would hold “locally” and “in general”. The numerical results suggest that, in real systems, the lower modes will display a Gaussian pdf and, as the frequency increases, a transition to a GOE model or Poisson model will occur, depending on the level of symmetry of the system. In fact, the uncertainties associated with manufactured structures are much more complex than the cases studied and, therefore, it is expected that most engineering structures will display GOE statistics above a certain point in the frequency domain. In order to have confidence in the variance prediction, it becomes necessary to define the limits for the application of the GOE model. It was shown that the statistical overlap factor fails to evaluate the level of randomness of a system in the presence of symmetries and there was a requirement for a new parameter.

The variance theory presented by Langley and Brown [91] was reviewed and the results compared with the numerical data obtained considering different ensemble definitions. It was observed that different probabilistic models have little effect over the energy density mean and a very good agreement with the standard SEA results was obtained for all the ensembles. However, a distinct behaviour was observed for the variance results. The energy density variance was shown to be very sensitive to the eigenvalue statistics and it was noted that the theory over predicts the numerical results for the case of Poisson statistics and for those cases or regions in the frequency domain with a low level of randomness. The theory displayed a good agreement with the numerical results when a value of 2.5 was considered for the mode shape statistics factor K, providing the system was sufficiently random. A numerical investigation has shown that mode shape amplitudes are near-Gaussian and values around 2.8 and 2.9 were observed for the cases where the GOE model also applies. However, the values

found for K did not explain the discrepancies between the theory and numerical data and it was argued that the correlation between the same component of different eigenvectors may the responsible for the discrepancy observed since the theory assumes independence of the mode shape amplitudes. A different averaging process was used and the results suggested that the correlations between mode shape amplitudes play an important role and are responsible for the discrepancies observed. Although the new variance theory displayed some discrepancies with the numerical results, it was concluded that a good agreement would be obtained for sufficiently random cases or, in the case of a real system, for a sufficiently high frequency. Therefore, for real systems, the main concern would be the definition of the limits between an almost-deterministic behaviour and the GOE behaviour.

In order to proceed with the study, a much faster artificial approach was proposed based on the analysis of a general dynamic system in modal coordinates where the system randomness is due only to the stiffness matrix. The fact that the random behaviour of the system is determined by the stiffness matrix has been shown to have no limitation over the reproduction of the statistics of real systems. Three randomization approaches were studied in view of what has been observed for random plates including the transition between known statistical behaviours: almost-deterministic to GOE, Poisson to GOE and single GOE group to two GOE groups. A very good agreement was observed between the numerical eigenvalue statistics and the theoretical models and the effects of different eigenvalue statistics over the energy density variance were also investigated. The energy density variance displayed the same behaviour observed for the numerical analysis carried out using the FE method, which validated the method as a tool for the study of random dynamic systems.

It was shown that there was a need for a parameter that would allow the estimation of the limits of the GOE model for random dynamic systems and, therefore, the prediction of errors associated with the application of the variance theory. An attempt to derive a parameter with this characteristic was carried out using the new method previously presented. Three parameters (P, Q and Z) were then derived based on an SVD of the matrix composed of the realizations of an eigenvector. Once more, the transition situations were used to evaluate the parameters. Q was shown to be an important improvement over the previous parameter used, the statistical overlap factor, and to have the desired characteristics. In order to reduce the computational costs, a perturbation analysis was performed and a fourth parameter was derived. The new parameter H displayed similar behaviour to Q, but it is expected to require a much reduced computational power.

Finally, it is believed that the objectives defined in Chapter 1 were mostly achieved and, in summary, the main contributions of this thesis are:

- A better understanding of RMT concepts and their application to the eigenvalue statistics of random dynamic systems, in particular, the ergodicity assumption and the effects of symmetries;
- The verification of the effects of different statistical models of the eigenvalues on the energy density variance;
- The derivation of a new method for the study of the statistics of random dynamic systems;
- The derivation of parameter Q to verify the level of agreement between the random dynamic system eigenvalues and the GOE model. The parameter should allow the estimation of the error associated with the variance theory;
- The derivation of parameter H with similar characteristics to Q by means of a perturbation analysis. H may be calculated directly from the statistics of the input parameters and represents a considerable reduction in the computational costs.

7.2 SUGGESTIONS FOR FURTHER RESEARCH

The parameter Q proposed in Chapter 6 seems to be an important improvement for the prediction of GOE statistics but it was verified only through the artificial approach based on a random stiffness matrix. Therefore, it would be interesting to verify its application to the analysis of FE models. In such a study, it would be important to note that the eigenvectors used in Equation (6.5) are assumed to be of the same size. This may not be the case when considering an ensemble of systems modelled using the FE method. In fact, in many of the ensembles considered in Chapter 3, the probabilistic models considered geometrical properties as random variables. As a consequence of a fixed mesh size, the total number of elements and nodes vary across the ensemble. In order to prevent this problem, it would be recommended that the method would deform the mesh. Of course, care should be taken to prevent the corruption of the mesh elements caused by inappropriate element shape.

It was seen in Chapter 4 that the correlation between mode shape amplitudes may be significant for the prediction of the energy density variance. The results obtained are only indirect and it would be interesting to investigate further the correlation between mode

shapes. It is expected that, as the frequency is increased, the effects of the correlations on the variance would be reduced. Even so, the consideration of the correlations in the variance theory may be an important improvement. However, the inclusion of the correlations seems to be a complex task in view of the mathematical tools available.

The analysis carried out in this thesis assumed the excitation only as point load force. However, many other excitation types are known to occur in real situations, like rain-on-the-roof excitation, incident wave, etc. It was seen in [91] that the variance theory is less sensitive to the eigenvalue statistics when a rain-on-the-roof excitation is considered. Therefore, it would be interesting to investigate the effects of different levels of agreement with the GOE model on the variance predictions when different loadings are considered. It is likely that the requirements for the agreement would be different. However, the point force load is expected to be the case with the highest level of requirement regarding the agreement with the GOE model. Such an analysis may be carried out using the artificial method proposed in Chapter 5.

To define the confidence limits of the response, the mean and the variance are not sufficient and it is also necessary to know the pdf of the response. Many results from the literature suggest that the lognormal pdf would be applicable to the energy density. It is also known that the pdf of the response is dependent on the excitation. It remains to be defined which would be the best pdf for each excitation. Again, use may be made of the approach given in Chapter 5.

Models for the distribution of the damping loss factor can be found in RMT. In [89] Burkhardt and Weaver investigated the application of this distribution to random dynamic systems and proposed a formulation for the variance considering such a distribution. The analysis described in this thesis has considered a constant loss factor. However, it is likely that many structures would have a non-constant loss factor and, in these cases, the Burkhardt and Weaver formulation may be a good alternative. Both approaches adopted in Chapter 2 and Chapter 5 may be used to investigate this problem.

It was suggested in the conclusions that the new parameter may provide an indication of the limits for the discretization of the statistical description of the system uncertainties. It would be interesting to verify this application.

Finally, the work described in this thesis has clarified some concepts regarding the statistics of random dynamic systems and has led to the derivation of the new parameter with promising application. However, much remains to be done in order to develop a robust approach for the analysis of engineering structures which takes into account their unavoidable uncertainties.

LIST OF REFERENCES

1. ANDERSON, M., Uncertainty quantification at Los Alamos National Laboratories. **Presentation at Workshop on Model Validation and Uncertainty Quantification at the 19th International Modal Analysis Conference**, Orlando, Florida, 2002.

2. MACE, B., WORDEN, K. and MANSON, G., Uncertainty in structural dynamics. **Journal of Sound and Vibration**, 288, 423-429, 2005.

3. KOMPELA, M.S. and BERNHARD, B.J., Measurements of the statistical variation of structural-acoustics characteristics of automotive vehicles, **Proceedings of the SAE noise and Vibration Conference**, Warrendale, USA, 1993.

4. CORNISH, R., A novel approach to optimizing and stabilizing interior noise quality in vehicles, **Proceedings of the Institute of Mechanical Engineers, Part D – Journal of Automobile Engineering**, 214 (D7), 685-692, 2000.

5. MEIROVITCH, L., **Fundamentals of Vibration**, McGraw-Hill, New York, USA, International Edition, 2001.

6. SHABANA, A. A., **Vibration of Discrete and Continuous Systems**. Spring-Verlag, USA, Second Edition, 1997.

7. FAHY, F. J., Statistical Energy Analysis: a critical overview. **Philosophical Transaction of Royal Society of London**, A346, 431-447, 1994.

8. LANGLEY, R.S., Mid and high-frequency vibration analysis of structures with uncertain properties. **Proceedings of the Eleventh International Congress on Sound and Vibration**, St. Petersburg, Russia, 2004.

9. ELISHAKOFF, I., Essay on uncertainties on elastic and viscoelastic structures: from A.M. Freudenthal's criticisms to modern convex modelling. **Computer and Structures**, 56(6), 871-895, 1995.

10. MEHTA, M. L., **Random Matrices**, Academic Press, New York, 1991.

11. IBRAHIM, R.A., Structural dynamics with parameter uncertainties. **Applied Mechanics Review**, 40(3), 309-328, 1987.

12. MANOHAR, C.S. and IBRAHIM, R.A., Progress in structural dynamics with stochastic parameter variation: 1987-1998. **Applied Mechanics Review**, 52(5), 177-197, 1999.

13. ADHIKARI, S., Rates of change of eigenvalues and eigenvectors in damped dynamic systems. **AIAA Journal**, 37(11), 1452-1458, 1999.

14. BINDER, K., **Monte Carlo methods in statistical physics**. Springer-Verlag, Berlin, Germany, 1979.

15. PETYT, M., **Introduction to Finite Element Analysis**. Cambridge University Press, England, 1990.

16. GHANEM, R.G. and SPANOS, P.D., **Stochastic finite elements: a spectral approach**. Springer, New York, 1991.

17. KLEIBER, M. and HIEN, T.D., **Stochastic finite element method**. Wiley, New York, 1993.

18. REN, Y.J. and ELISHAKOFF, I., New results in finite element method for stochastic structures. **Computers and Structures**, 67, 125-135, 1998.

19. BENAROYA, H. and REHAK, M., Finite element methods in probabilistic structural analysis: A selective review. **Applied Mechanics Review**, 41(5), 201-213, 1988.

20. MOENS, D., DE GERSEM, H., DESMET, W. and VANDEPITTE, D., An overview of novel non-probabilistic approaches for non-deterministic dynamic analysis. **Proceedings of NOVEN2005**, Saint-Raphael, France, 2005.

21. LANGLEY, R.S., SHORTER, P.J. and COTONI, V., Predicting the response statistics of uncertain structures using extended versions of SEA. **Proceedings of INTERNOISE 2005**, Rio de Janeiro, Brazil, 2005.

22. FOX, R.L. and KAPOOR, M.P., Rates of change of eigenvalues and eigenvectors. **AIAA Journal**, 6(12), 2426-2429, 1968.

23. COLLINS, J.D. and THOMSON, W.T., The eigenvalue problem for structural systems with statistical properties. **AIAA Journal**, 7(4), 642-648, 1969.

24. NELSON, R.B., Simplified calculation of eigenvector derivatives. **AIAA Journal**, 14(9), 1201-1205, 1976.

25. LYON, R. H. and DEJONG, R. G., **Theory and Application of Statistical Energy Analysis**. Butterworth-Heinemann, Boston – EUA, 1995.

26. BURROUGH, C. R., FISCHER, R. W. and KERN, F. R., An introduction to statistical energy analysis. **Journal of the Acoustical Society of America**, 101(4), 1779-1789, 1997.

27. WOODHOUSE, J., An introduction to statistical energy analysis of structural vibration. **Applied Acoustics**, 14, 455-469, 1981.

28. FAHY, F., Statistical Energy Analysis: A guide for potential users. **SEANET**, http://www.seanet.be/.

29. LYON, R. H. and MAIDANIK, G., Power flow between linearly couple oscillators. **Journal of the Acoustical Society of America**, 34, 623 – 639, 1962.

30. SMITH JR., P. W., Response and radiation of structural modes excited by sound. **Journal of the Acoustical society of America**, 34, 640 – 647, 1962.

31. MACE, B. R., On the statistical energy analysis hypotheses of coupling power proportionality and some implications of its failure. **Journal of Sound and Vibration**, 178(1), 95-112, 1994.

32. SCHARTON, T. D. and LYON, R. H., Power flow and energy sharing in random vibration. **Journal of the Acoustical Society of America**, 43(6), 1332-1343, 1968.

33. KEANE, A. J. and PRICE, W. G., Statistical energy analysis of strongly coupled systems. **Journal of Sound and Vibration**, 117, 363-386, 1987.

34. LANGLEY, R. S., A general derivation of the Statistical Energy Analysis equations for coupled dynamic systems. **Journal of Sound and Vibration**, 135(3), 499-508, 1989.

35. LANGLEY, R. S., A derivation of the coupling loss factor used in statistical energy analysis. **Journal of Sound and Vibration**, 141(2), 207-219, 1990.

36. MACE, B. R. e ROSEMBERG, J., The SEA of two coupled plates: An investigation into the effects of subsystems irregularities. **Journal of Sound and Vibration**, 212(3), 395-415, 1998.

37. LANGLEY, R. S., The modal density of anisotropic structural components. **Journal of the Acoustical Society of America**, 99(6), 3481-3487, 1996.

38. CREMER, L., HECKEL, M. e UNGAR, E. E., **Structure-Borne Sound**. Berlin: Spriger-Verlag; second edition, 1988.

39. BROWN, A.W.M., **The ensemble statistics of the response of structural components with uncertainty properties.** Ph.D. Thesis, University of Cambridge, UK, 2003.

40. LANGLEY, R. S. e HERON, K. H., Elastic wave transmission through plate/beam junctions. **Journal of Sound and Vibration**, 143(2), 241-253, 1990.

41. LANGLEY, R. S., Elastic wave transmission coefficients and coupling loss factor for structural junctions between curved panels. **Journal of Sound and Vibration**, 169(3), 297-317, 1994.

42. HERON, K. H., Predictive SEA using line wave impedances. **IUTAM Symposium on Statistical Energy Analysis**, Southampton, England, 1997.

43. HERON, K. H., The wave approach to predictive statistical energy analysis and equally spaced point connections with isolators. **NOISECON98**, Ypsilanti, EUA, 1998.

44. CORDIOLI, J.A., GERGES, S.N.Y., PEREIRA, A.K., CARMO, M.G. and GRANDI, C., Vibro-Acoustic Modelling of Aircrafts Using Statistical Energy Analysis, **SAE Technical Paper**, 2004-01-3337, 2004.

45. CORDIOLI, J.A., TRICHES JR, M. and GERGES, S.N.Y., Applications of the Statistical Energy Analysis to Vibro-Acoustic Modelling of Vehicles, **SAE Technical Paper**, 2004-01-3352, 2004.

46. CIMERMAN, B., BHARJ, T. e BORELLO, G., Overview of the experimental approach to Statistical energy Analysis. **Proceedings of the 1997 SAE Noise and Vibration Conference**, 97NV169, 1997.

47. HERMANS, L. e IADEVAIA, M., Guidelines on the use of the experimental SEA for modelling and understanding road noise in cars. **SAE Technical Paper**, 1999-01-1704, 1999.

48. DE LANGHE, K., High frequency vibrations: Contribution to experimental and computational SEA parameter identification techniques. **Ph.D. Thesis, Katholieke Universiteit Leuven**, Leuven, Belgium, 1996.

49. BIES, D. A. e HAMID, S., In situ determination of loss and coupling loss factors by the power injection method. **Journal of Sound and Vibration**, 70(2), 187-204, 1980.

50. DE LANGHE, K. e SAS, P., Statistical analysis of the power injection method. **Journal of the Acoustical Society of America**, 100(1), 294-303, 1996.

51. CLARKSON, B. L., The derivation of modal densities from point impedance. **Journal of Sound and Vibration**, 77(4), 583-584, 1981.

52. CLARKSON, B. L., Experimental determination of modal density. Elishakoff / Lyon (Eds.) **Random Vibration**, 59-85, 1986.

53. KESWICK, P. R. e NORTON, M. P., A comparison of modal density measurement techniques. **Applied Acoustics**, 20, 137-153, 1987.

54. RENJI, K., Experimental modal densities of honeycomb sandwich panels at high frequencies. **Journal of Sound and Vibration**, 237(1), 67-79, 2000.

55. BROWN, K. T. e NORTON, M. P., Some comments on the experimental determination of modal densities and loss factors for statistical energy analysis applications. **Journal of Sound and Vibration**, 102(4), 588-594, 1985.

56. RANKY, M. F. e CLARKSON, B. L., Frequency average loss factors of plates and shells. **Journal of Sound and Vibration**, 89(3), 309-323, 1983.

57. CRAIK, R. J. M. e STEEL, J. A., Statistical Energy Analysis of structure-borne sound transmission by Finite Element Methods. **Journal of Sound and Vibration**, 178(4), 553-561, 1994.

58. SHANKAR, K. e KEANE, A. J., Vibration energy flow analysis using a substructure approach: the application of receptance theory to FEA and SEA. **Journal of Sound and Vibration**, 201(4), 491-513, 1997.

59. YAN, H. H. e PARRETT, A., Calculation of Statistical Energy Analysis parameters using Finite Element Analysis. **INTERNOISE 2002**, Dearborn, USA, 2002.

60. MACE, B. R., Finite frequency band averaging effects in the statistical energy analysis of two continuous one-dimensional subsystems. **Journal of Sound and Vibration**, 189(4), 443-476, 1996.

61. KEANE, A. J., A note on modal summations and averaging methods as applied to statistical energy analysis (S.E.A.). **Journal of Sound and Vibration**, 164(1), 143-156, 1993.

62. SOIZE, C., A model and numerical method in the medium frequency range for vibroacoustic predictions using the theory of structural fuzzy. **Journal of Acoustical Society of America**, 94, 849-865, 1993.

63. SHORTER, P., **Combining Finite Elements and Statistical Energy Analysis**. Ph.D. Thesis, University of Auckland, 1998.

64. LANGLEY, R.S. and BREMNER, P.G., A hybrid method for the vibration analysis of complex structural-acoustic systems. **Journal of the Acoustical Society of America,** 105(3), 1657-1671, 1999.

65. SHORTER, P.J. and LANGLEY, R.S., Vibro-acoustic analysis of complex systems. **Journal of Sound and Vibration**, 288 (3), 669-699, 2005.

66. SHORTER, P.J. and LANGLEY, R.S., On the reciprocity relationship between direct field radiation and diffuse reverberant loading. **Journal of the Acoustical Society of America,** 117(1), 85-95, 2005.

67. LANGLEY, R.S., SHORTER, P.J. and COTONI, V., A hybrid FE-SEA method for the analysis of complex vibro-acoustic systems. **Proceedings of NOVEN2005**, Saint-Raphael, France, 2005

68. SHORTER, P.J., COTONI, V. and LANGLEY, R.S., Numerical and experimental validation of the hybrid FE-SEA method. **Proceeding of INTERNOISE2005**, Rio de Janeiro, Brazil, 2005.

69. LANGLEY, R.S., SHORTER, P.J. and COTONI, V., Predicting the response statistics of uncertain structures using extended versions of SEA. **Proceeding of INTERNOISE2005**, Rio de Janeiro, Brazil, 2005.

70. LIN, Y. K., **Probabilistic Theory of Structural Dynamics**. McGraw-Hill, USA, 1967.

71. DAVIES, H. G. and WAHAB, M. A., Ensemble Averages of Power Flow in Randomly Excited Coupled Beams. **Journal of Sound and Vibration** 77, 311-321, 1981.

72. DAVIES, H.G. and KHANDOKER, S.I., Random point excitation of random beams. **Journal of Sound and Vibration**, 84(4), 557-562, 1982.

73. FAHY, F. J. e MOHAMED, A. D., A Study of Uncertainty in Applications of SEA to Coupled Beam and Plate Systems, Part I: Computational Experiments. **Journal of Sound and Vibration,** 158(1), 45-67, 1992.

74. MANOHAR, C. S. e KEANE, A. J., Axial vibrations of a stochastic rod. **Journal of Sound and Vibration**, 165(2), 341-359, 1993.

75. KEANE, A. J. e MANOHAR, C. S., Energy flow variability in a pair of coupled stochastic rods. **Journal of Sound and Vibration**, 168(2), 253-284, 1993.

76. MANOHAR, C. S. e KEANE, A. J., Statistics of energy flows in spring-coupled one-dimensional subsystems. **Philosophical Transactions of the Royal Society of London, Series A,** 346, 525-542, 1994.

77. MANOHAR, C. S. e ADHIKARI, S., Statistics of vibration energy flow in randomly parametered trusses. **Journal of Sound and Vibration**, 217(1), 43-74, 1998.

78. MACE, B. R., The statistical energy analysis of two continuous one-dimensional subsystems. **Journal of Sound and Vibration**, 166(3), 429-461, 1993.

79. FINNVEDEN, S., Ensemble averaged vibration energy flows in a three-element structure. **Journal of Sound and Vibration**, 187(3), 495-529, 1995.

80. WESTER, E. C. N. e MACE, B. R., Statistical energy analysis of two edge-coupled rectangular plates: ensemble averages. **Journal of Sound and Vibration**, 193(4), 793-822, 1996.

81. SCHROEDER, M. R., Frequency-correlation functions of frequency response in rooms. **Journal of the Acoustical Society of America**, 34(12), 1819-1823, 1962.

82. RICE, S.O., in WAX, N., **Noise and Stochastic Processes**, Dover Publications, New York, 1951.

83. LYON, R. H., Statistical analysis of power injection and response in structures and rooms. **Journal of the Acoustical Society of America**, 45(3), 545-565, 1967.

84. DAVY, J.L., The relative variance of the transmission function of a reverberation room. **Journal of Sound and Vibration**, 77(4), 455-479, 1981.

85. DAVY, J.L., The ensemble variance of random noise in a reverberation room. **Journal of Sound and Vibration**, 107(3), 361-373, 1986.

86. DAVY, J.L., Improvements to formulae for the ensemble relative variance of random noise in a reverberation room. **Journal of Sound and Vibration**, 115(3), 145-161, 1987.

87. WEAVER, R. L., Spectral statistics in elastodynamics. **Journal of the Acoustical Society of America**, 85(3), 1005-1013, 1989.

88. WEAVER, R. L., On the ensemble variance of reverberation room transmission functions, the effect of spectral rigidity. **Journal of Sound and Vibration**, 130(3), 487-491, 1989.

89. BURKHARDT, J. and WEAVER, R.L., The effect of decay rate variability on statistical response predictions in acoustic systems. **Journal of Sound and Vibration**, 196(2), 147-164, 1996.

90. LOBKIS, O. I., WEAVER, R. L. and ROZHKOV, I., Power variances and decay curvature in a reverberant system. **Journal of Sound and Vibration**, 237(2), 281-302, 2000.

91. LANGLEY, R. S. and BROWN, A. W. M., The ensemble statistics of the energy of a random system subject to harmonic excitation. **Journal of Sound and Vibration**, 275(3), 823-846, 2004.

92. LANGLEY, R. S. and BROWN, A. W. M., The ensemble statistics of the band-averaged energy of a random system. **Journal of Sound and Vibration**, 275(3), 847-857, 2004.

93. LANGLEY, R. S. and COTONI, V., Response variance prediction in the statistical energy analysis of built-up systems. **Journal of the Acoustical Society of America,** 115(2), 706-718, 2004.

94. BRODY, T. A., FLORES, J., FRENCH, J. B., MELLO, P. A., PANDEY, A. and WRONG, S. S. M., Random-matrix physics: spectrum and strength fluctuations. **Reviews of Modern Physics**, 53(3), 385-480, 1981.

95. BOHIGAS, O., GIANNONI, M.J. and SCHIMIT, C., Characterization of chaotic quantum spectra and universality of level fluctuation laws. **Physical Review Letters**, 52(1), 1-4, 1984.

96. STÖCKMANN, H. J., **Quantum Chaos**, Cambridge University Press, 1999.

97. LANGLEY, R.S., Conditions for the occurrence of universal eigenvalue statistics in random matrix theory. Paper submitted for the **Philosophical Transactions of the Royal Society of London**, 2005.

98. KESSISSOGLOU, N.J. and LANGLEY, R.S., Application of the statistical overlap factor to predict GOE statistics. **Proceedings of NOVEN2005**, Saint-Raphael, France, 2005.

99. BALDANZINI, N. and PIERINI, M., An assessment of transducer mass loading effects on the parameters of an experimental statistical energy analysis (SEA) model. **Mechanical System and Signal Processing**, 16(5), 885-903, 2002.

100. WIGNER, E.P., Statistical properties of real symmetric matrices with many dimensions. **Proceedings of the Cambridge Philosophical Society**, (Toronto: University of Toronto Press), p. 174, 1957.

101. BERTELSEN, P., ELLEGAARD, C. e HUGUES, E., Distribution for eigenfrequencies for vibrating plates, **European Physical Journal B**, 15, 87-96, 2000.

102. ELLEGAARD, C., GUHR, T., LINDEMANN, K., LORENSEN, H.Q., NYGARD, J. and OXBORROW, M., Spectral statistics of acoustic resonances in aluminium blocks. **Physical Review Letters**, 75(8), 1546-1549, 1995.

103. ELLEGAARD, C., GUHR, T., LINDEMANN, K., NYGARD, J. and OXBORROW, M., Symmetry breaking and spectral statistics of acoustic resonances in quartz blocks. **Physical Review Letters**, 77(24), 4918-4921, 1996.

104. BURKHARDT, J. and WEAVER, R.L., Spectral statistics in damped systems. Part I: Modal decay rate statistics. **Journal of the Acoustical Society of America**, 100(1), 320-327, 1996.

105. BURKHARDT, J. and WEAVER, R.L., Spectral statistics in damped systems. Part II: Spectral density fluctuations. **Journal of the Acoustical Society of America**, 100(1), 327-334, 1996.

106. ELLEGAARD, C., SCHAAT, K. e BERTELSEN, P., Acoustic chaos. **Physica Scripta**, 90, 223-230, 2001.

107. MCWILLIAN, S., ONG, J. and FOX, C.H.J., On the statistics of natural frequency splitting for rings with random mass imperfections. **Journal of Sound and Vibration**, 279, 453-470, 2005.

108. LOBKIS, O. I., ROZHKOV, I., and WEAVER, R. L., Nonexponential dissipation in a lossy elastodynamic billiard: Comparison with Porter-Thomas and Random Matrix predictions. **Physical Review Letters** 91(19), 194101-1-4, 2003.

109. PANDEY, A., Statistical properties of many-particle spectra III: Ergodic .behaviour in random-matrix ensembles. **Annals of Physics**, 119, 170-191, 1979.

110. STRATONOVICH, R. L., **Topics in the Theory of Random Noise**. Gordon and Brach, Science Publishers, New York, 1963.

111. HORN, R.A. and JOHNSON, C.R., **Matrix Analysis**. Cambridge University Press, UK, 1985.

112. KREYSZIG, E. **Advanced engineering mathematics**. 8th Edition, John Wiley & Sons, Inc., USA, 1999.

113. ELISHAKOFF, I., **Probabilistic Methods in the Theory of Structures**. John Wiley & Sons, USA, 1983.

114. COTONI, V. and LANGLEY, R.S., Variance of the energy and energy density in the Statistical Energy Analysis of complex systems. **Proceedings of NOVEN2005**, Saint-Raphael, France, 2005.

115. LANGLEY, R. S. and COTONI, V., Variance prediction in SEA. **Tenth International Congress on Sound and Vibration**, Stockholm – Sweden, 2003.

116. SZECHENYI, E., Modal density and radiation efficiencies of unstiffened cylinders using statistical methods. **Journal of Sound and Vibration**, 19(1), 65-81, 1971.

117. BREMNER, P. G., Vibro-acoustics of ribbed structures – A compact modal formulation for SEA models. **NOISECON94**, 1994.

118. MCELMAN, M., Vibration of Stiffened shells. **NASA** TN D-3010, 1965.

119. FAHY, F. J. and RUIVO, H. M., Determination of Statistical Energy Analysis loss factors by means of an input power modulation technique. **Journal of Sound and Vibration**, 203(5), 763-779, 1997.

120. MANNING, J. E., Formulation of SEA parameters using mobility functions. **Philosophical Transactions of the Royal Society of London A**, 346, 477-488, 1994.

121. MANIK, D. N., A new method for determining coupling loss factors for SEA. **Journal of Sound and Vibration**, 211(3), 521-526, 1998.

122. LALOR, N., Practical considerations for the measurement of internal and coupling loss factors on the complex structures. **ISVR Technical Report No. 182**, 1990.

123. GÉLAT, P. and LALOR, N., The role and experimental determination of equivalent mass in complex SEA models. **Journal of Sound and Vibration**, 255(1), 97-110, 2002.

124. FORRESTER, P.J., SNAITH, N.C. and VERBAARSCHOT, J.J.M., Developments in random matrix theory. **Journal of Physics A: Mathematical and General**, 36, R1-R10.

125. DYSON, F.J. and MEHTA, M.L., Statistical theory of the energy levels of complex systems. IV, **Journal of Mathematical Physics**, 4(5), 701-712, 1963.

126. BURKHARDT, J. e WEAVER, R. L., The effect of decay rate variability on statistical response predictions in acoustic systems. **Journal of Sound and Vibration**, 196(2), 147-164, 1996.

127. MEIROVITCH, L., **Analytical Methods in Vibrations**. The Macmillan Company, London, 1967.

128. CHOL, S., PIERRE, C. e CASTANIER, M. P., Statistical energy methods for mid-frequency vibration transmission analysis. **SAE PAPER** 972010, 1103-1108, 1997.

129. WAX, N. (editor), **Selected papers on noise and stochastic process**. Dover publications, New York, 1954

130. ABROMOWITZ, M. e STEGUN, I. A., **Handbook of Mathematical Functions**. Dover Publication Inc., New York, USA, 1964.

APPENDIX A

ENERGY DENSITY STATISTICS USING THE FE METHOD

A.1 CALIBRATION PROCEDURE

The calibration procedure for the two small accelerometers and the acceleration transducer of the impedance head was to attach the transducer to the vibrating surface of the calibrator and inform the software about the frequency and level of the vibration generated by the calibrator. The software was responsible for identifying which channel was being calibrated and calculate a calibration constant. The calibration of the force transducer of the impedance head was a little more complex. After calibrating the acceleration transducer of the impedance head, a mass was attached to the top of the impedance head as shown in Figure A.1. Knowing the internal mass of the impedance head m_{ih} located in front of the force transducer, the added mass m_a and the acceleration level produced by the calibrator a_c, it was possible to calculate the force F_c imposed on the force transducer considering Newton's second law:

$$F_c = (m_a + m_{ih})a_c . \tag{A.1}$$

The calibration of the transducer force was then performed based on the calibration force calculated. Care was taken so that the mass positioned on the calibrator vibrating surface did not exceed the maximum mass allowed by the calibrator.

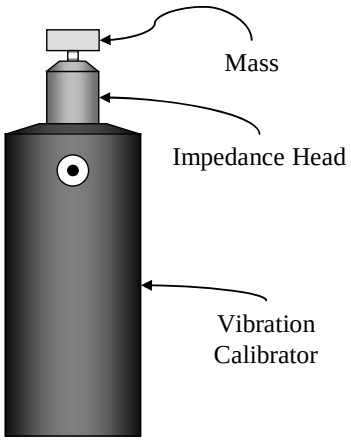

Figure A.1 – Calibration set-up.

A.2 MASS CORRECTION

The impedance head is a device specially designed for the measurement of point impedance. Therefore, the transducer mass positioned in front of the force transducer is minimized. However, a small mass is still added to the plate and, together with the mass of the bolt used to attach the impedance head to the plate, may cause measurement errors at high frequencies. In [99], a detailed discussion about the effects of transducer mass loading on measured FRF was given and some approaches were proposed for the correction of the errors. According to [99], the transducer mass effect is dependent on the difference between the structure impedance and the added mass impedance. The actual punctual inertance A_p may be obtained from the measured punctual inertance A_p^m by means of

$$A_p = \frac{A_p^m}{1 - m_T A_p^m}, \tag{A.2}$$

where m_T is the mass added to the plate by the presence of the transducer. The transfer inertances can be corrected using

$$A_t = \frac{A_t^m}{1 - m_T A_p^m}, \tag{A.3}$$

with A_t being the real transfer inertance and A_t^m the measured transfer inertance.

In the adopted assembly, the added mass at the force application point was the sum of the end plate of the impedance head (0.0048 kg) and the used screw (0.0008 kg). Figure A.2 and Figure A.3 compare the measured point and transfer inertances with the corrected curves. At low frequency, the effects are reduced, but become more significant with increasing frequency.

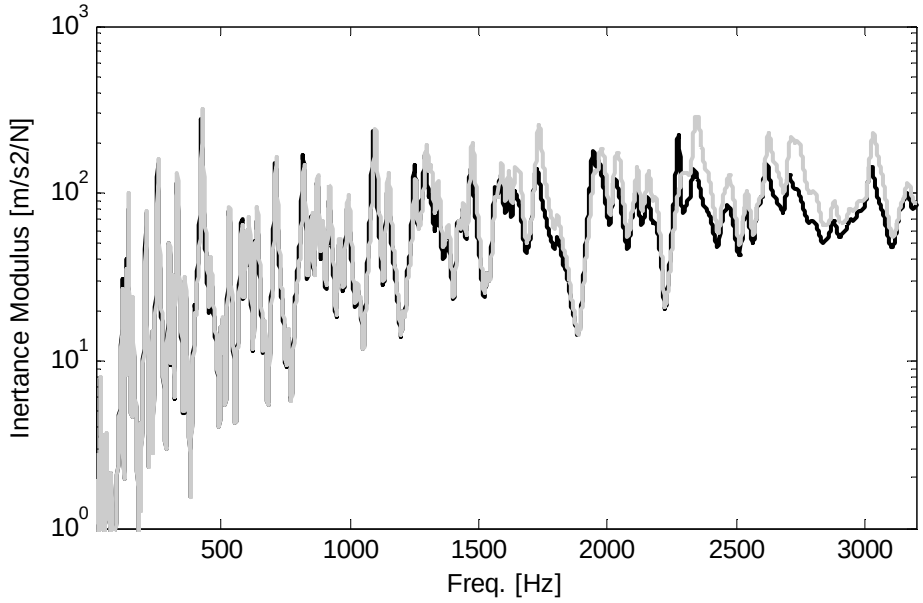

Figure A.2 – Driving point inertance. ▬ measured, ▬ mass corrected.

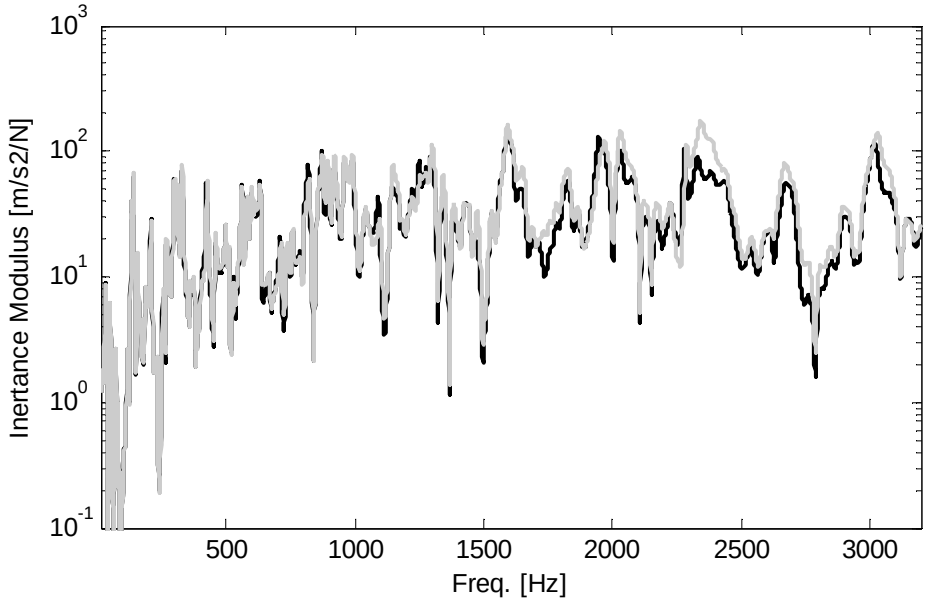

Figure A.3 – Transfer inertance. ▬ measured, ▬ mass corrected.

The mass of the accelerometers used was of 0.0007 kg and was neglected in view of its small effect and the complexity of its correction (it would be necessary to measure the point inertance at each point). This small effect can be observed in Figure A.4 and Figure A.5 where simulations were performed using an FE model with masses of the impedance head and accelerometers on the excitation and response points, respectively. It can be noted that the effects of the accelerometer mass are very small.

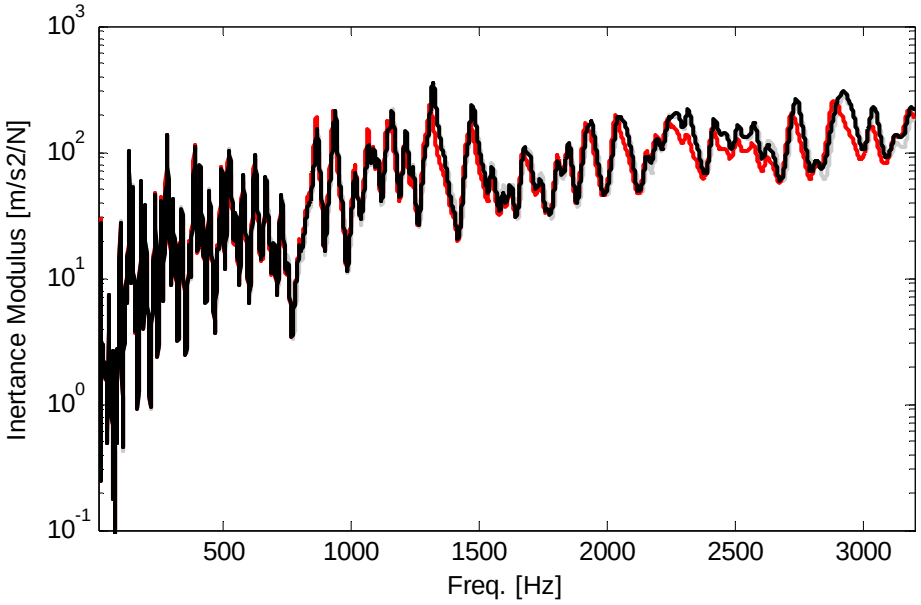

Figure A.4 – Numerical point inertances. ——— without masses, ——— with mass in the response point, ——— with mass in the response point and the force point.

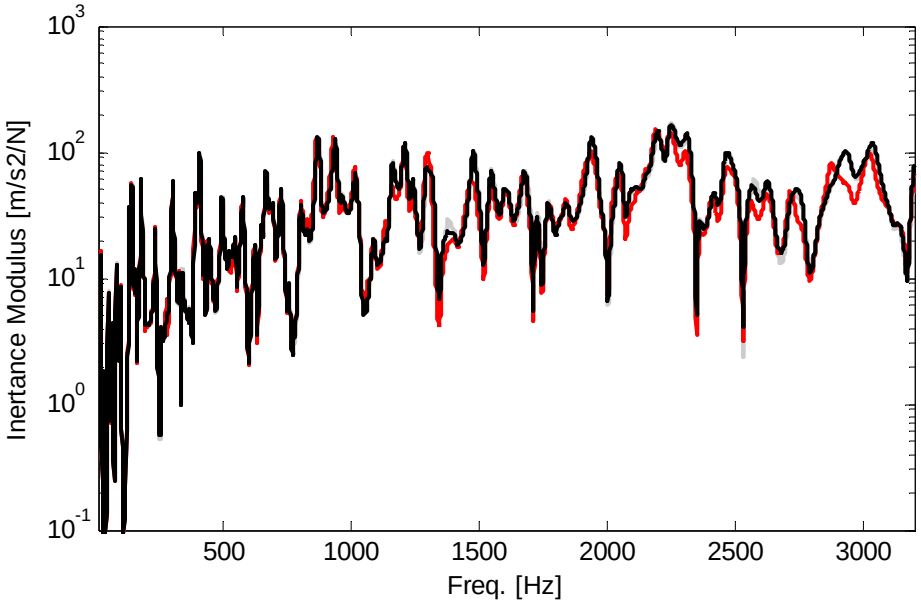

Figure A.5 – Numerical transfer inertances. ——— without masses, ——— with mass in the response point, ——— with mass in the response point and the force point.

A.3 EXAMPLE OF ANSYS® LIS FILE

An example of an ANSYS® LIS file is given below. This LIS file also reads other files generated by MATLAB® which contains some of the analysis parameters (mesh discretization, mass positions, etc.). Examples of the files are also given in what follows.

LIS file example:

```
!Reading input parameters
/INPUT,'param','txt'

/PREP7

!Element types and constants
ET,1,SHELL63
ET,2,MASS21
R,1,0.002, , , , , ,          !Thickness = 0,002 m
R,2,Pm,Pm,Pm, , , ,           !Mass [Kg]

!Material properties
MPTEMP,1,0
MPDATA,EX,1,,7.1e10           !Young modulus
MPDATA,PRXY,1,,0.33           !Poisson coef.
MPDATA,DENS,1,,2800           !Density

!Defining the geometry
K,1,0,0,0
K,2,0,0.5,0
K,3,0.7,0,0
K,4,0.55,0.4,0
A,1,3,4,2

!Creating the mesh
TYPE,1
MAT,1
REAL,1
ESIZE,Ms,0,                   !Mesh discretization
MSHAPE,0,2D                   !Element shape
MSHKEY,1                      !Free (0) or mapped (1) meshing
ASEL, , , ,      1            !Selecting the area to be meshed
CM,_Y,AREA                    !Create component
AMESH,_Y                      !Create mesh
CMDELE,_Y                     !Delete component

*GET,NodeM,NODE,1E10,NXTL     !Get the maximum node
Locf = NODE(0.11,0.35,0)      !Determine the node closest to the excitation point

!Creating the point mass elements
TYPE,2
MAT,1
REAL,2
Node1 = NINT(N1*NodeM)
E,Node1
Node2 = NINT(N2*NodeM)
E,Node2
Node3 = NINT(N3*NodeM)
E,Node3
Node4 = NINT(N4*NodeM)
E,Node4
Node5 = NINT(N5*NodeM)
E,Node5
Node6 = NINT(N6*NodeM)
E,Node6
Node7 = NINT(N7*NodeM)
E,Node7
Node8 = NINT(N8*NodeM)
E,Node8
Node9 = NINT(N9*NodeM)
```

```
E,Node9
Node10 = NINT(N10*NodeM)
E,Node10

!Solution
NumM=Nm+6                !Define the number of modes
/SOLU
ANTYPE,MODAL             !Define the solution method
MODOPT,LANB,NumM         !Define the modal method
SOLVE                    !Solve
FINISH

!Save eigenvalues and eigenvectors
/POST1
*DEL,EV
*DIM,EV,ARRAY,2,Nm       !Create variable to store results

*DO,C1,7,NumM,1
SET,1,C1
C2 = c1 - 6
*GET,EV(1,C2),ACTIVE,0,SET,FREQ
*VGET,EV(2,C2),NODE,Locf,U,Z,
*ENDDO

/INPUT,'Format_table','txt'      !Read external file with command to save the data

FINI
```

Input.txt file example:

```
Nm = 250
Ms = 0.006
Pm = 0.009152
N1 = 0.80136
N2 = 0.65459
N3 = 0.78375
N4 = 0.31317
N5 = 0.72006
N6 = 0.91027
N7 = 0.054186
N8 = 0.89124
N9 = 0.50335
N10 = 0.68581
```

Format.txt file exemple:

```
*MWRITE,EV,'resp','txt',,,
(250E14.4)
```

A.4 EXAMPLE OF MATLAB® CODE FOR FE ANALYSIS

An example of a MATLAB® file used to generate the files with the input parameters for the FE analysis and to control the number of loops to be performed is given below.

```
%%%%%%%%%%% Random analysis of a plate  %%%%%%%%%%
clear all;

%%%% Analysis Parameters
%Number of loops
Nl = 500;

%Number of modes
Nm = 250;

%Write file with the save command for ansys
T1=['*MWRITE,EV,"resp","txt",,,\n'];
T2=['(' int2str(Nm) 'E14.4)'];
fid = fopen('format_table.txt','w');
fprintf(fid,T1);
fprintf(fid,T2);
status = fclose(fid);

%Definition of variables
Nmass= 10;              %Number of masses (need to change LIS file)
Pm=0.009152;            %Mass of the point masses
Ms = 0.006;             %Mesh size

for j=1:Nl
   %Write file with parameters
   fid = fopen('param.txt','w');
   T1=['Nm = ' num2str(Nm) '\n'];
   fprintf(fid,T1);
   T2=['Ms = ' num2str(Ms) '\n'];
   fprintf(fid,T2);
   T3=['Pm = ' num2str(Pm) '\n'];
   fprintf(fid,T3);
   for k=1:Nmass
      mp(k)=unifrnd(0,1);
      T4=['N' int2str(k) ' = ' num2str(mp(k)) '\n'];
      fprintf(fid,T4);
   end
   status = fclose(fid);

   % Run the ansys analysis
   dos batch1

   resp=load('resp.txt');
   X(j,:)=resp(1,:);
   Xv(j,:)=resp(2,:);
   Mp(j,:)=mp;
end

save res_rmt_plate_masses X Xv Mp;
```

A.5 ENERGY DENSITY CALCULATION

A.5.1 Verifying Equation (2.12)

The energy density procedure given in Chapter 2 may be verified by comparing the results with a procedure following the experimental approach. In the experimental approach, the energy density of a system is calculated by averaging the velocity over the structure surface. The same approach may be applied numerically, in this case

$$T(\omega) = \frac{E(\omega)}{2A} = \frac{M\left\langle \overline{v^2} \right\rangle}{2A} = \frac{M\omega^2 \left\langle X^2 \right\rangle}{4A}, \tag{A.4}$$

where $\left\langle X^2 \right\rangle$ is the space average of the squared displacement amplitude obtained numerically.

Figure A.6 gives the energy density calculated with both approaches. Two curves for the approach based on a spatial average are given for different numbers of points. A very good agreement can be observed between the methods. In fact, increasing the number of points used in the spatial average method would lead to the results obtained with Equation (2.12).

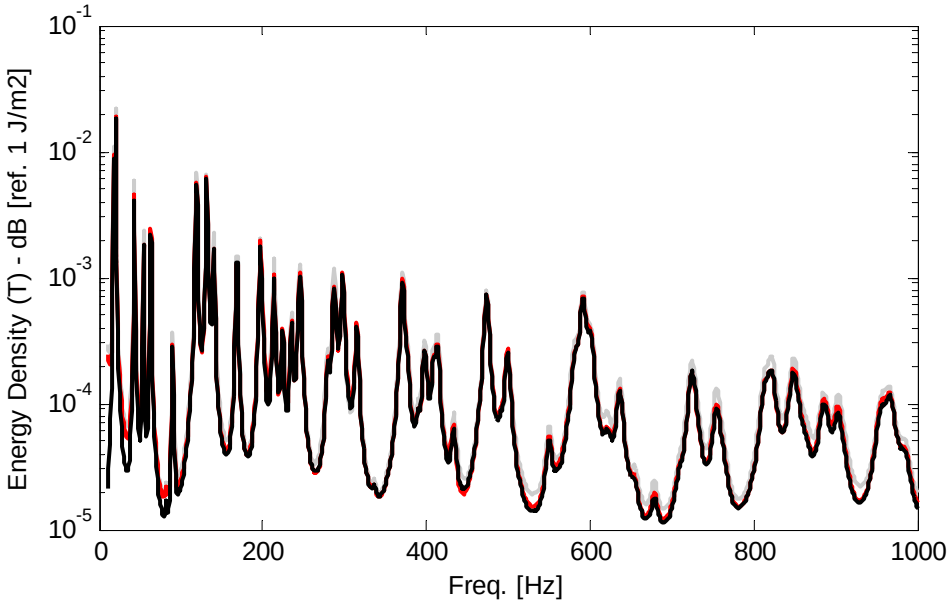

Figure A.6 – Comparing different methods for the energy density calculation. —— Equation (2.12), —— Equation (A.4) with 100 points, —— Equation (A.4) 500 points.

A.5.2 Truncation of the modal sum

The number of modes used in the modal sum given by Equation (2.12) must be a compromise between the accuracy of the results and the computational cost associated with extracting an increasing number of modes in the numerical analysis. The issue is especially important in view of the size of the ensemble required to obtain statistically significant results, allowing the convergence of the statistics.

Figure A.7 shows the energy density of one of the members of the ensemble considered in Chapter 2 for different numbers of modes. It can be noted that a number of 200 modes is sufficient to ensure the convergence of the results. The number of modes in the

frequency range considered may vary a little between members of the ensemble and, therefore, to ensure the accuracy of the results, a number of 250 modes were considered in the analysis.

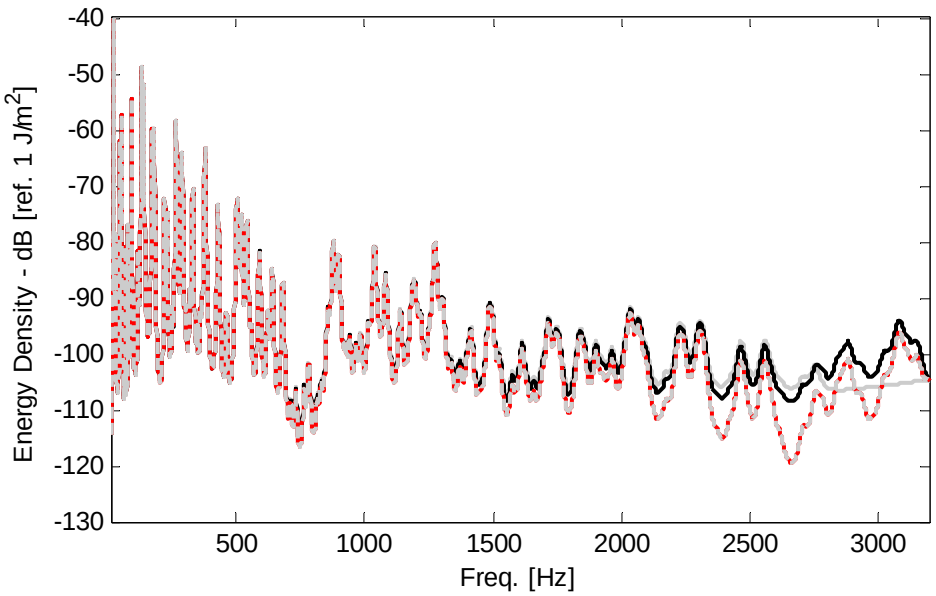

Figure A.7 – Verifying the modal truncation. —— 150 modes, —— 170 modes, —— 200 modes, - - - - - 250 modes.

APPENDIX B

RANDOM MATRIX THEORY

B.1 EXAMPLES OF MATLAB® CODE TO CALCULATE EIGENVALUE STATISTICS

```
%%      Calculation of the statistics - PDF - Number variance - Delta3
clear all;

Ne=500;          %Number of samples in the ensemble
N=200;           %Size of the matrix (NxN)

load res_rmt_egv_case03_2p.mat;    %Read file with the matrix X with the eigenvalues of the matrices

%Calculating the matrix with the spacings
for k=1:Ne
   for j=1:N-1
      Xdf(k,j)=X(k,j+1)-X(k,j);
   end
end

%Mean eigenvalues
Xm=mean(X);

%Defining the eigenvalue used to calculate the statistics
sp=100;

% %%%%%      PDF
[mu,sigma]=normfit(Xdf(:,sp(m)));
s=raylfit(Xdf(:,sp(m)));
x1=min(Xdf(:,sp(m)));
x2=max(Xdf(:,sp(m)));
x = x1:(x2-x1)/30:x2;
y = Xdf(:,sp(m));
[n,t]=hist(y,x);
n=n/(Ne*(x2-x1)/30);
%n and x may be used to plot the pdf of spacings

%%%%%%      Number Variance
Dnv=0.1;                  %Number variance discretization
Env=5;                    %Maximum value
Lnv=0:Dnv:Env;            %Number variance x axis values
Nnv=length(Lnv);

for k=1:Ne
   for r=1:Nnv
      count01=0;
      for n=1:N
         if X(k,n)>=(Xm(sp(m))-Lnv(r)*mu/2) & X(k,n)<(Xm(sp(m))+Lnv(r)*mu/2)
            count01=count01+1;
         end
      end
      Nv(k,r)=(Lnv(r) - count01)^2;
   end
end
MNv=mean(Nv);
```

```
%%%%%    Least Square Statistic - Delta 3

ds=0.1*mu;                %Discretization of the staircase function
Lz=25;                    %Maximum value
for k=1:Ne
   Ls=X(k,1):ds:X(k,N);
   Ns=length(Ls);
   for f=1:Ns
      for j=1:N
         if X(k,j)<=Ls(f)
            count01=j;
         else
            break;
         end
      end
      Ss(f)=count01;
   end
   count01=0;
   clear count02;
   for Lii=1:Lz
      for f=1:Ns
         if Ls(f)>=(Xm(sp(m))-Lii*mu/2) & Ls(f)<(Xm(sp(m))+Lii*mu/2)
            count01=count01+1;
            c_yy(count01)=Ss(f);
            c_xx(count01)=Ls(f);
         end
      end
      p=polyfit(c_xx,c_yy,1);
      for f=1:count01
         count02(f)=(c_yy(f)-(c_xx(f)*p(1)+p(2)))^2;
      end
      delta3(k,Lii)=mean(count02);
      count01=0;
      clear c_xx c_yy count02
   end
end
Mdelta3=mean(delta3);
```

APPENDIX C

CHAPTER 4: ENERGY DENSITY VARIANCE

C.1 VERIFYING THE APPROXIMATION IN EQUATION (4.5)

The approximation assumed in Equation (4.5) can be easily verified by comparing the energy density calculation through Equation (2.12) of a plate using both sides of the equation. The natural frequencies and mode shapes for a realization of the plate loaded with random masses was used and results can be observed in Figure C.1. It can be noted that the approximation has no significant effect on the energy density calculation.

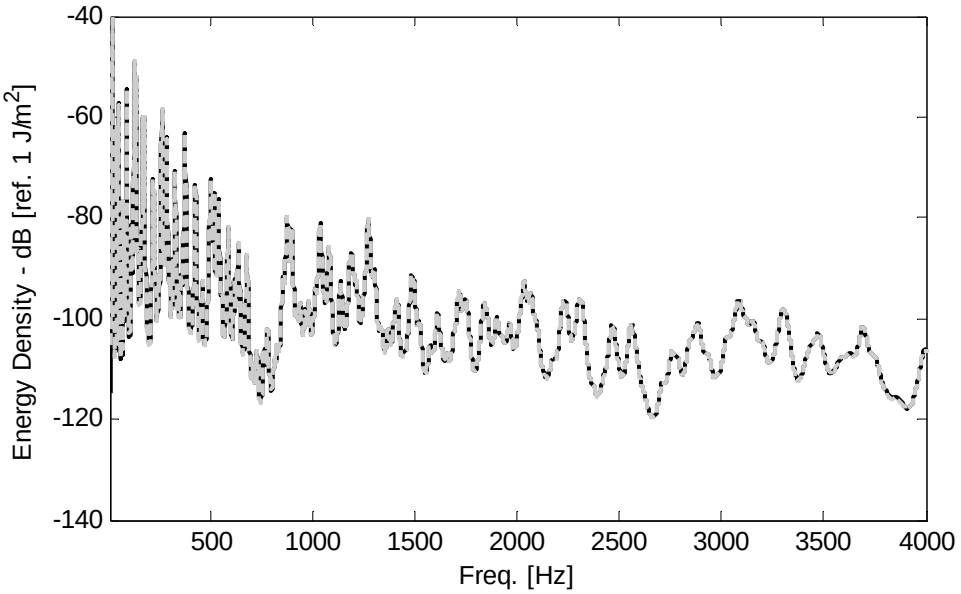

Figure C.1 – Evaluating the approximation in Equation (4.5). —— exact result, - - - - - approximation.

C.1.2 Mode shape statistics

The results for the mode shape statistics factor *K* are given in Figure C.2 and Figure C.3 for Case B1. Figure C.4 and Figure C.5 present the results for Case B5.

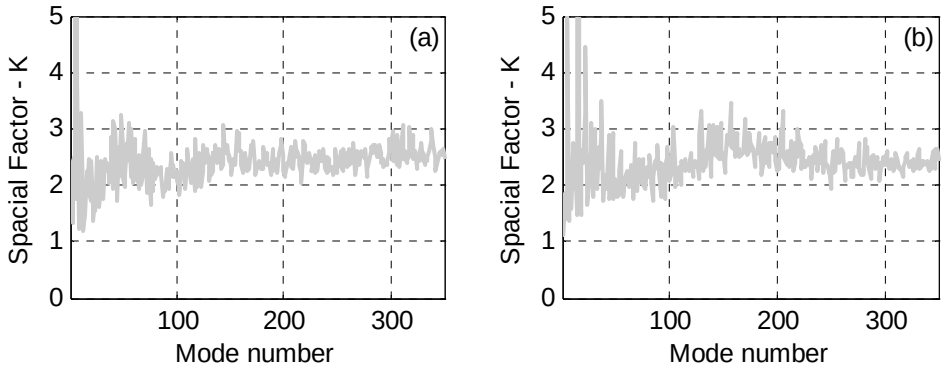

Figure C.2 – Mode shape statistics factor *K* – Case B1. a) force position (x = 0.11, y = 0.135) b) another position. ——— numerical results.

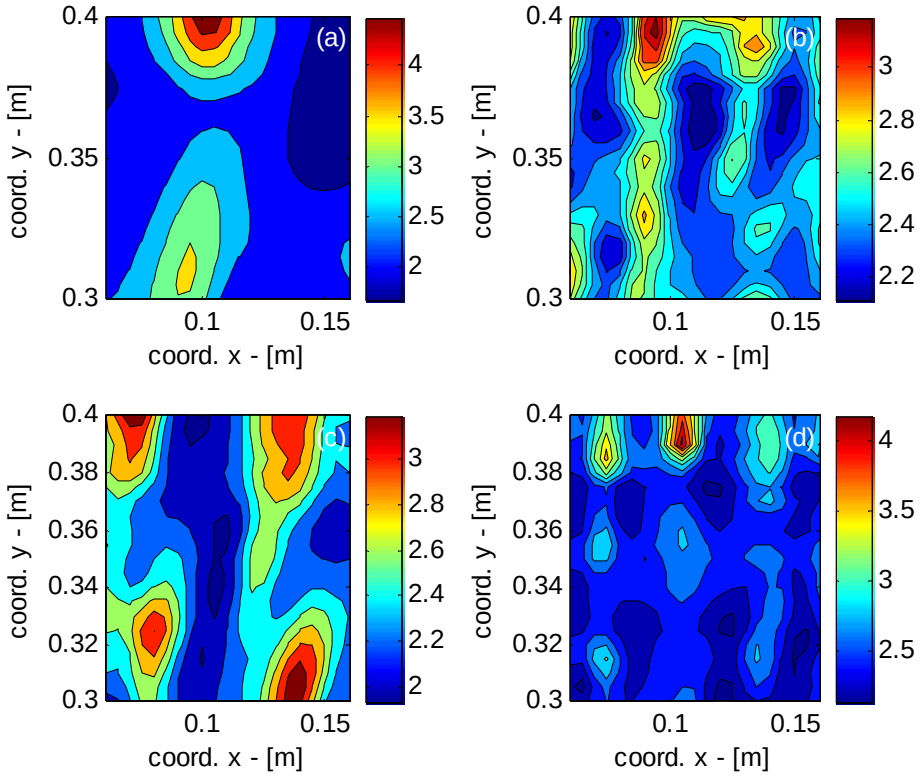

Figure C.3 – Mode shape statistics factor *K* – Case B1. a) mode 10, b) mode 80, c) mode 200, d) mode 300.

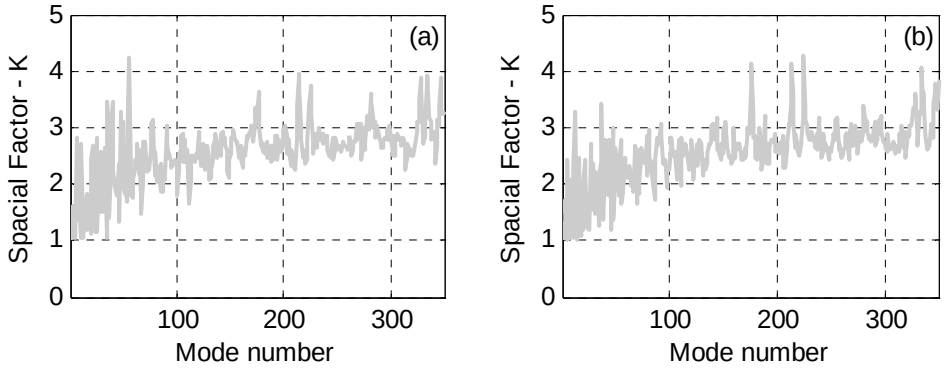

Figure C.4 – Mode shape statistics factor *K* – Case B5. a) force position (x = 0.11, y = 0.135) b) another position. ——— numerical results.

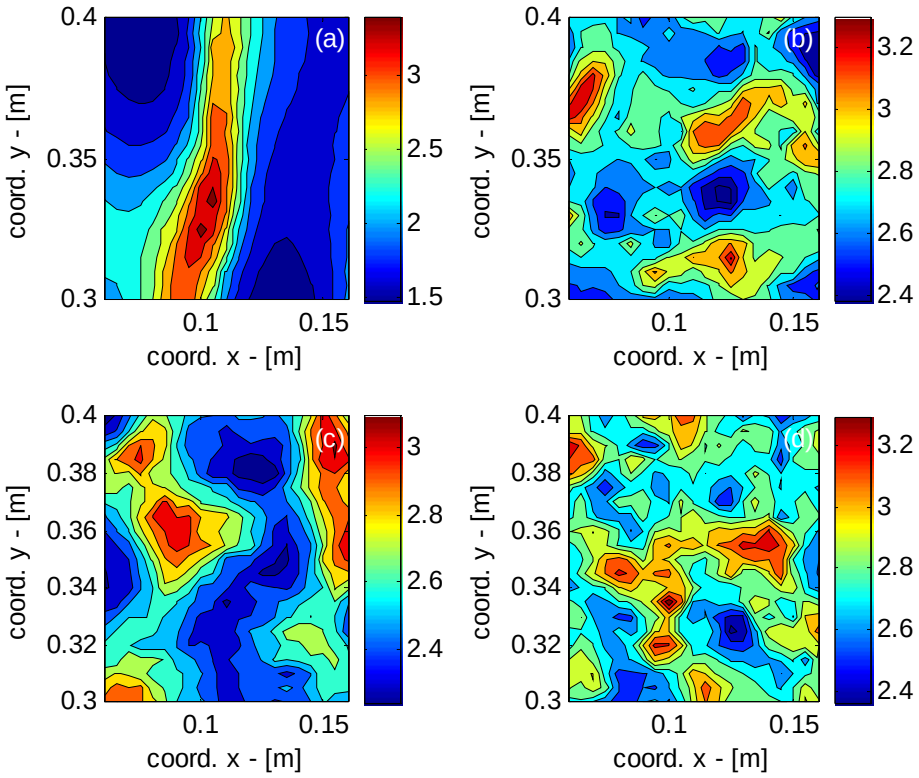

Figure C.5 – Mode shape statistics factor K – Case B5. a) mode 10, b) mode 80, c) mode 200, d) mode 300.

APPENDIX D

RANDOM DYNAMIC SYSTEMS

D.1 Alternative Approach to Link the Eigenvalue Statistics and Energy Density Variance Prediction

Prior to the development of the method given in Chapter 5, an attempt was made to directly link the eigenvalue statistics number variance Σ^2 and the Δ_3 function obtained for a general random matrix with the predictions of energy density variance. The aim was to verify the effects of different eigenvalue statistics on the variance predictions. The relations between the relative energy density variance and the Fourier transform of the two-level cluster function $b(\theta)$ is given by

$$r_T{}^2 = \frac{1}{\pi v}\int_0^{\infty}\left[\alpha - b\left(\frac{\theta}{2\pi v}\right)\right]\exp(-\eta\omega\theta)\mathrm{d}\theta\,. \tag{D.1}$$

One possibility would be to calculate directly Y_2 from a random matrix, perform a Fourier transform and then obtain the associated relative variance. However, as seen in Chapter 3, the convergence of Y_2 is very slow and requires the consideration of large ensembles, resulting in large computational costs. On the other hand, the number variance Σ^2 and the Δ_3 function have a much faster convergence and are directly related to Y_2 as given by Equation (3.7) and Equation (3.9). However, the relation is given by an integration of Y_2 that results in some loss of information, but in view of the smooth behaviour of Y_2, this loss may be negligible. An attempt was made to calculate Y_2 from the number variance Σ^2 and the Δ_3 function using an inverse integration trapezoidal rule. The results were shown to be quite sensitive to small perturbations in the number variance Σ^2 and the Δ_3 function. Some smoothing techniques (spline or a fitting curve process) were applied but the results were still very sensitive. An attempt was made to increase the number variance Σ^2 and the Δ_3 function discretization and, together with the smoothing methods, better results were obtained. In fact, it was possible to recover Y_2 from the number variance Σ^2 and the Δ_3 function for increasing discretization and increasing the ensemble size, but the computational costs were similar to those required to calculate Y_2 directly.

D.2 EXAMPLE OF MATLAB® CODE TO GENERATE AN ENSEMBLE OF MATRICES

```
%%%%%       Generation of the random matrix
clear all;

%%%%%       Variables -  Case C1
Ne=500;             %Number of samples in the ensemble
N=200;              %Size of the matrix (NxN)
det=1;              %Type of deterministic matrix. det=1 (one sequence), det=2 (two overlapping)
R=2;                %Level of randomness
a=2;                %Variance of de diagonal terms of Aran - Group A
b=1;                %Variance of the Off-diagonal terms of Aram - Group B
c=1;                %Variance of the Off-diagonal terms of Aram - Group C
x0=100;             %First natural frequency

%Generation of the deterministic part
if det==1
        for j=1:N
    A0(j,j)=(x0+j)^2;
        end
else
   for j=1:N/2
    A0(j,j)=(x0+j)^2;
        end
        for j=(N/2+1):N
    A0(j,j)=(x0+j-N/2)^2;
        end
end

%Frequency range
w=0.1:0.1:350;
eta1=0.01;

%Vector with the nominal spacing
j=(1:N)+x0;
j2=(2:N+1)+x0;
if det==1
   DF=(j2.^2-j.^2);
else
   DF(1:N/2)=(j2(1:N/2).^2-j(1:N/2).^2);
   DF(N/2+1:N)=(j2(1:N/2).^2-j(1:N/2).^2);
end

%Vector with the level of randomness as a function of the nominal spacing
RAN=R*DF;
g11=normrnd(0,1,N,1);
g1=g11./norm(g11);

%Generation of the random part and calculation of the eigenvalues
for z=1:Ne
   for j=1:N
      for k=1:N
         if j==k
            Aran(k,j)=RAN(j)*normrnd(0,a^0.5);
         else
            Aran(k,j)=RAN(j)*normrnd(0,b^0.5);
         end
         if k<=N/2 & j>=(N/2+1)
            Aran(k,j)=RAN(j)*normrnd(0,c^0.5);
         end
         if k>N/2 & j<(N/2+1)
            Aran(k,j)=RAN(j)*normrnd(0,c^0.5);
```

```
        end
        Aran(j,k)=Aran(k,j);
      end
   end

   A=A0+Aran;
   [V,D]=eig(A);
   I=eye(N);
   rn=V'*g1;
   wn=sqrt(diag(D));

   [WN,W]=meshgrid(wn,w);
   [RN,W]=meshgrid(rn,w);
   denom1=(WN.^2-W.^2).^2+(eta1*W.*WN).^2;
   ratio1=(RN.^2.*W.^2)./denom1;
   T(z,:)=sum(ratio1,2)/N;

   X(z,:)=wn;
   Xv(:,:,z)=V;
   z
end

T1=T;
X1=X;
Xv1=Xv;

save ener_var_case1 g1 T1 X1 Xv1;
```

D.3 DIFFERENT DEFINITIONS OF THE EXCITATION VECTOR

It was argued in Chapter 5 that the assumption of a random vector as the excitation vector **g** would not affect the variance results. In fact, vector **g** represents a punctual force in modal coordinates and thus may be given by any continuous function. To verify this assumption, a check was performed where different **g** vectors were considered. The investigation was performed for three different vectors: a random vector, a vector formed by a sine with low frequency and a vector formed by a sine with high frequency. The three vectors are given in Figure D.1.

Figure D.2, Figure D.3 and Figure D.4 give the energy density calculated for each vector. It can be observed that the analysis considering a sine with low frequency displays a different behaviour to the other two curves. This is due to the smoother behaviour of the **g** vector in this case which restricts the range of values for the mode shape amplitude that some modes may display. This is the case of the modes between 150 and 250 rad/s.

Figure D.5 compares the relative energy density variance for the three cases. It can be observed that the different **g** vectors do not affect the numerical results.

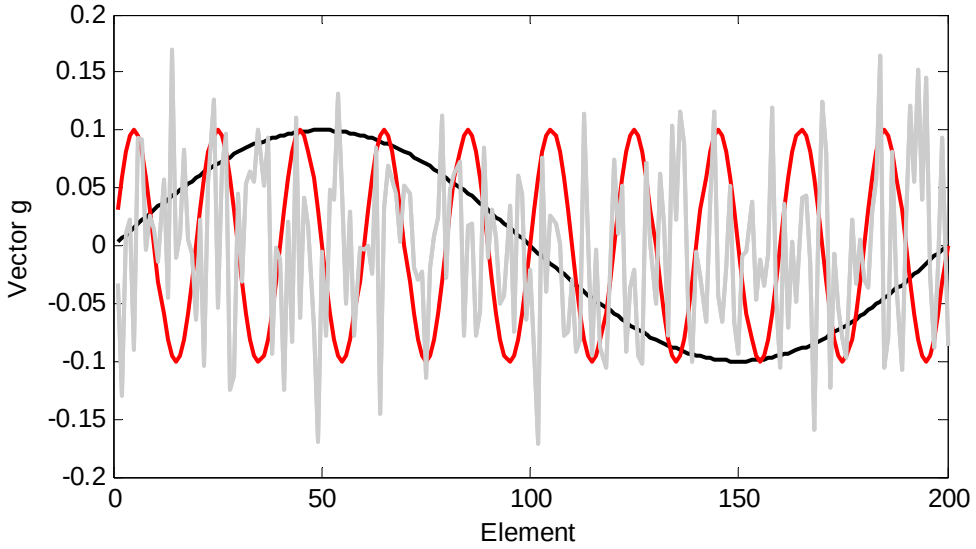

Figure D.1 – Different vectors **g** used.

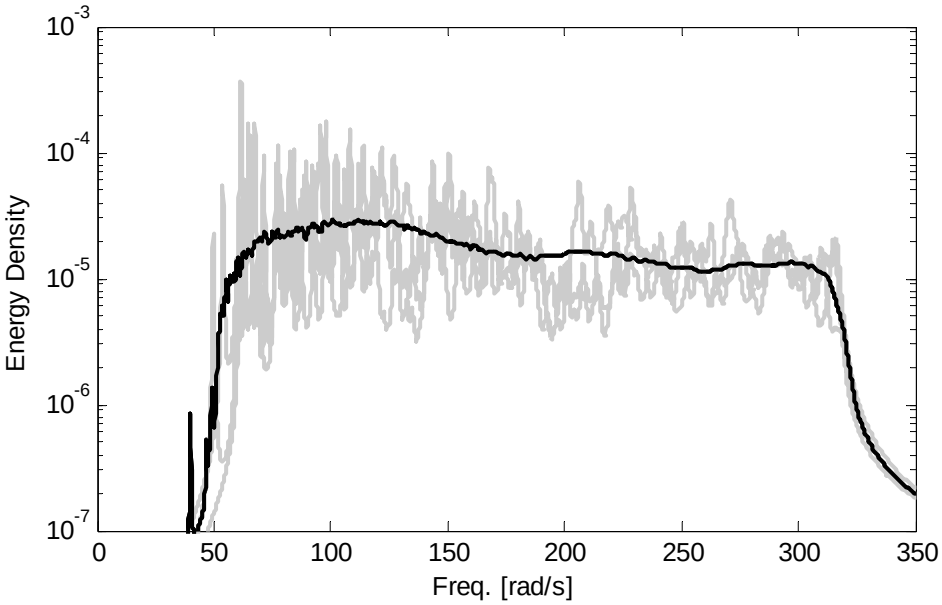

Figure D.2 – Energy density calculated considering a random vector **g**.

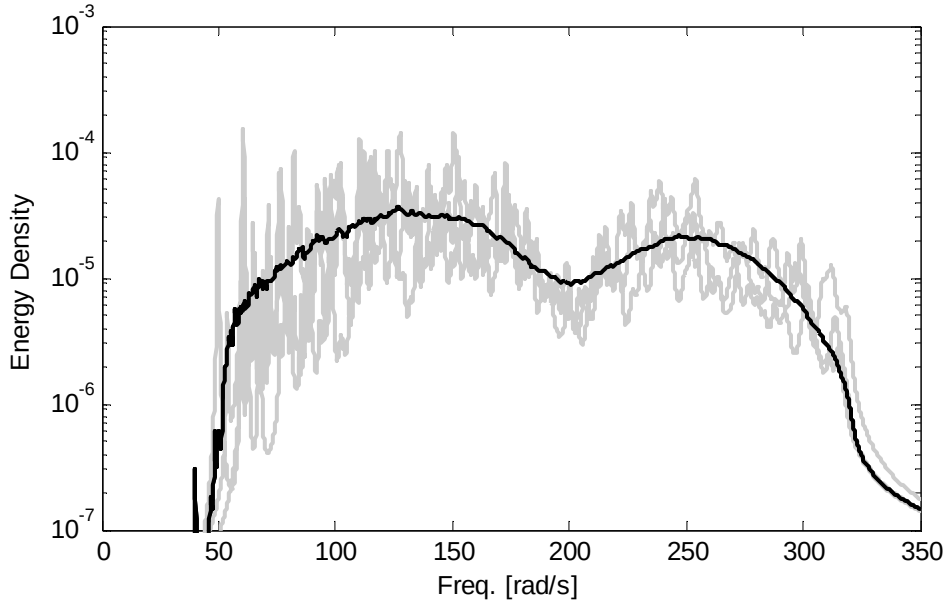

Figure D.3 – Energy density calculated considering a vector **g** as a sine with low frequency.

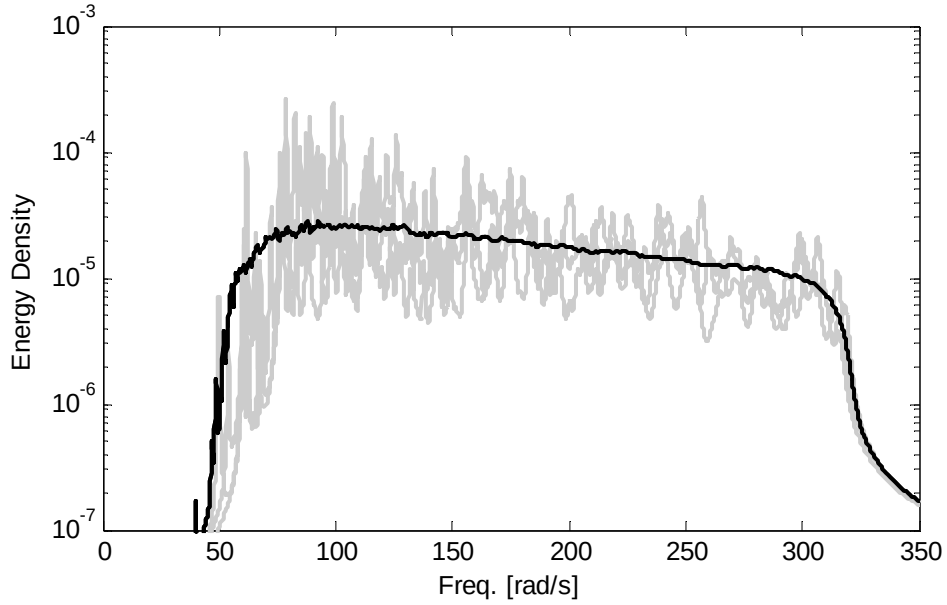

Figure D.4 – Energy density calculated considering a vector **g** as a sine with high frequency.

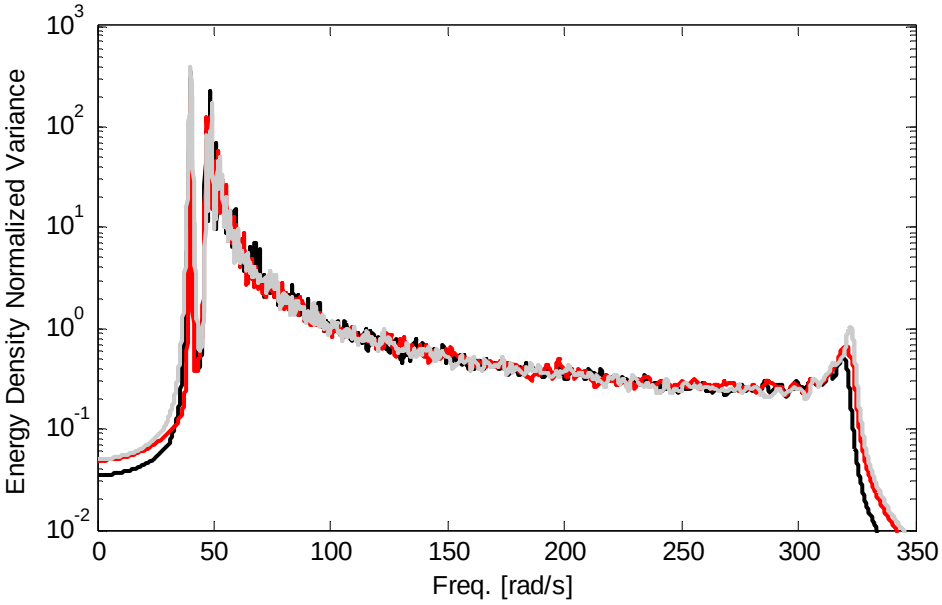

Figure D.5 – Relative energy density variance for the three vector **g** considered.

APPENDIX E

SINGLE PARAMETER FOR GOE STATISTICS

E.1 EXAMPLE OF MATLAB® CODE TO CALCULATE THE PARAMETERS

```
%%%%%%      Calculation of parameters – full and perturbation analysis
clear all;

%%%%%%      Variables -  Case C1
Ne=500;                 %Number of samples in the ensemble
N=100;                  %Size of the matrix (NxN)
det=1;                  %Type of deterministic matrix. det=1 (one sequence), det=2 (two overlapping)
a=2;                    %Variance of de diagonal terms of Aran - Group A
b=1;                    %Variance of the Off-diagonal terms of Aram - Group B
c=1;                    %Variance of the Off-diagonal terms of Aram - Group C
x0=100;                 %First natural frequency

% Varying R
R=0.1:0.1:2.5;
%R=[0.2 0.5 1 2];

%Generation of the deterministic part
if det==1
   for j=1:N
      A0(j,j)=(x0+j)^2;
   end
else
   for j=1:N/2
      A0(j,j)=(x0+j)^2;
   end
   for j=(N/2+1):N
      A0(j,j)=(x0+j-N/2)^2;
   end
end
j=(1:N)+x0;
j2=(2:N+1)+x0;
if det==1
   DF=(j2.^2-j.^2);
else
   DF(1:N/2)=(j2(1:N/2).^2-j(1:N/2).^2);
   DF(N/2+1:N)=(j2(1:N/2).^2-j(1:N/2).^2);
end

% Calculating the parameters for different levels of randomness
for r=1:length(R);
   RAN=R(r)*DF;
   %Generation of the random part and calculation of the eigenvalues
   for z=1:Ne
      for j=1:N
         for k=1:N
            if j==k
               Aran(k,j)=RAN(j)*normrnd(0,a^0.5);
            else
               Aran(k,j)=RAN(j)*normrnd(0,b^0.5);
            end
            if k<=N/2 & j>=(N/2+1)
               Aran(k,j)=RAN(j)*normrnd(0,c^0.5);
            end
```

```
            if k>N/2 & j<(N/2+1)
                Aran(k,j)=RAN(j)*normrnd(0,c^0.5);
            end
            Aran(j,k)=Aran(k,j);
        end
    end
    A=A0+Aran;
    [V,D]=eig(A);
    wn=sqrt(diag(D));
    X(z,:)=wn;
    Xv(:,:,z)=V;
    As(:,:,z)=A;
    z
    r
end

for k=1:Ne
    for j=1:N-1
        Xdf(k,j)=X(k,j+1)-X(k,j);
    end
end
Xdfm(r,:)=mean(Xdf);
Xstd(r,:)=std(X);

%Calculation of P and Q
for j=1:N
    Tp(:,:)=Xv(:,j,:);
    [U,S,V]=svd(Tp);
    M=trace(S.^2);
    count01=0;
    count02=0;
    for k=1:N
        if count02<0.9*M
            count01=count01 + 1;
            count02=count02+S(k,k)^2;
        end
    end
    Sc(:,j)=diag(S);
    P(j)=count01;
    Rr=U'*Tp;
    Rr=sort(Rr.^2);
    Rr=flipud(Rr);
    Rc(:,j)=mean(Rr,2);
    count01=0;
    count02=0;
    for n=1:Ne
        count01=0;
        count02=0;
        for k=1:N
            if count02<0.9
                count01=count01 + 1;
                count02=count02+Rr(k,n);
            end
        end
        Q(n)=count01;
    end
    MQ(j)=mean(Q);
    j
    r
end
Par_MQ(r,:)=MQ;
Par_P(r,:)=P;
K(r,:)=2*MQ-P;
```

```
    % Parameter based on perturbation analysis – Tr = 0.01
    for j=1:N
        for k=1:N
            if j==k
                VarA(k,j)=RAN(j)^2*a;
            else
                VarA(k,j)=RAN(j)^2*b;
            end
            if k<=N/2 & j>=(N/2+1)
                VarA(k,j)=RAN(j)^2*c;
            end
            if k>N/2 & j<(N/2+1)
                VarA(k,j)=RAN(j)^2*c;
            end
            VarA(j,k)=VarA(k,j);
        end
    end
    for j=1:N
        W0(j)=(x0+j)^2;
    end
    [WN1,WN2]=meshgrid(W0,W0);
    denom=(WN1-WN2).^2;
    I=eye(N);
    denom=denom+I;
    Alpha2=VarA./denom;
    Alpha2=Alpha2-diag(diag(Alpha2))+I;
    for j=1:N
        u=Alpha2(:,j);
        u(j)=0;
        M=sum(u);
        Par1(j)=M;
    end
    PAR1(r,:)=Par1;
    for j=1:N
        u=Alpha2(:,j);
        u(j)=0;
        us=sort(u,'descend');
        c1=0;
        for k=1:N
            if c1==0
                if us(k)<0.01
                    c1=k-1;
                end
            end
        end
        P1(j)=c1;
    end
    PP1(r,:)=P1;
end
save pert_an_new_varying_R_Ne500_N100 Xdfm Xstd K Par_MQ Par_P PAR1;
```